

An Investigation of Haptic Assisted Robotic Manipulating and Planning for High Accuracy Control

Mutian Li

This Thesis is submitted to the Department of Design,
Manufacture and Engineering Management, University of
Strathclyde, for the degree of Doctor of Philosophy.

COPYRIGHT STATEMENT

The copyright of this thesis belongs to the author under the terms of the United Kingdom Copyright Acts as qualified by the University of Strathclyde Regulation 3.50. Due acknowledgement must always be made of the use of any material contained in, or derived from, this thesis.

AUTHOR'S DECLARATION

This thesis is the result of the author's original research. It has been composed by the author and has not been previously submitted for examination which has led to the award of a degree.

Signed

Date

Mutian Li

31.May.2019

Acknowledgement

First of all, I would like to express my sincere appreciation to my supervisor, Professor Xiutian Yan. Since the first day when I arrived in Glasgow and started my MPhil study, Professor Yan has been really helpful and supportive to me on my research and life. Thanks to Professor Yan, I had great opportunities attending conferences, participating in research projects, collaborating with researchers and companies which are precious experiences in my PhD study.

Also I'm grateful to my colleagues in my lab and the department of Design, Manufacture and Engineering Management, especially to Dr. Cocuzza Silvio, Dr. Hao Lu and Dr. Karen Donaldso, who have helped me a lot in my research projects and experiments. Many important ideas that contribute to my thesis are inspired by our daily conversation and discussion.

Family is my most powerful motivation. I want to thank my parents, grandparents and all my family members in China, for their endless love and support. I miss them so much and feel sorry that I didn't spend much time with them for the last few years, just I hope they can be proud of what I have achieved.

Finally I appreciate all my lovely friends in Glasgow, including Kunlan Huang, Hao Wu, Xiaoyu Liu, Zhiyuan Yu, Cong Niu, Yankang Tian, Quanren Zeng, Jie Zhao, Lin Zhang, Senyong Chen, Jianan Shen, Ye Yuan, Yuanhan Mo, Xin Huang, Wenli Hu and Rone Gil. Because of them my life in Scotland has been indeed colourful and memorable.

Publications

Cocuzza, S., Li, M. and Yan, X. (2016) Published. 'Soft and Minimum Reactions Robotic Capture of Non-cooperative Spacecrafts'. *67th International Astronautical Congress 2016*, 2016. pp.3748.

Li, M., Yan, X. (2019) Accepted. 'Haptic Assisted Virtual Tele-operation of Robotic Manipulator for Smooth Space Debris Capturing '. *International Journal of Astronautics and Aeronautical Engineering*

Abstract

This research investigation advances the understanding of force feedback with the aim to achieve better human interaction with a haptic system for a diverse range of application requirements. Human-Machine interactive systems are required in various manipulation tasks, where a higher level of precision and accuracy than normal human capabilities is necessary. These systems also require human intelligence in the control loop to manage complex challenges typically found in extreme environments such as nuclear, space, underwater and mining. In these environments, visual information may not always be available or of substandard quality. The touch sensation, in terms of haptic perception, includes tactile and kinesthetic sensations. These sensations help the user understand an object's material properties in the environment as well as their body position and movement. Therefore, it is suggested that haptic force feedback can be introduced to provide assistance where a high level of accuracy of human manipulation is required. The knowledge gaps for the design of multitask haptic assisted systems are identified and concluded through a literature review. A comparison table is produced to demonstrate the functionalities and inadequacies of existing systems in dealing with the required functions. There are knowledge gaps in system design, for example, regarding haptic systems in space environments. There also exists a lack of systems in manufacturing where existing robotic systems can be easily adopted for haptic control applications.

A design methodology is proposed to support the design of a haptic assisted system that integrates professional knowledge and experience with different types of haptic virtual fixtures in manipulating and planning tasks. For this design methodology, a general Haptic Assisted Robotic Manipulating and Planning system (HARMP) is proposed and investigated. This planning system provides a common haptic interface and haptic assistance for multiple applications such as for robotic planning and manipulating tasks. A system architecture is proposed and constructed with components including hardware (Haptic user interaction system) and software

(Haptic modelling environment). The system specification template is built with geometric modelling, force modelling, force rendering, environment modelling and an integrated knowledge library. The haptic virtual fixtures are classified into three categories: telepresence, virtual constraints and guidance. In three case studies, the task requirements are analysed to identify the specifications necessary along with the virtual fixtures so they can be assigned to modify the HARMP system accordingly. A method to utilise haptic guidance in space robotic manipulation for capturing tasks is proposed. Also, a concept and implementation to enhance the HARMP design model in enabling bilateral haptic interaction is proposed and implemented as a haptic coupler which enables novel use of haptic system in both directions. This proposed HARMP is validated through three design case studies and the HARMP system has then been proven to be effective in three different types of applications namely, dental, space and manufacturing. It is anticipated that HARMP system could be equally applicable in other applications.

The contribution to knowledge reflects this wide range of activities in broad haptic interactions, including literature review, new design methodology development and validation of the proposed methodology through three case studies and finally the novel haptic systems developed through these case studies. A novel and generic design methodology, HARMP, for haptic system design is proposed, fully developed and evaluated, incorporating virtual fixtures for high accuracy manipulating and planning tasks. The HARMP methodology can be used to clarify the design process and design activity flow in order to generate necessary system specifications and components for the final haptic system for a given design problem.

Key words: Haptic System Design, Design Methodology, Haptic dental planning, Space Robotic Haptic Control, Robotic Control, Virtual Fixtures

Contents

1	Chapter 1: Introduction	1
1.1	Motivation.....	1
1.1.1	Overview of Autonomous Operations and Needs for Human Intervention....	1
1.1.2	Overall Challenges in Autonomous Robotic Systems	2
1.1.3	Autonomous Systems Advantages and Limitations.....	3
1.1.4	Motivation.....	3
1.2	Research Aim and Hypothesis.....	4
1.2.1	Research Hypothesis.....	4
1.2.2	Research Questions.....	5
1.2.3	Research Aim	5
1.2.4	Research Objectives.....	6
1.3	Research Methodology.....	6
1.3.1	Literature Review.....	7
1.3.2	Computer Supported Mechatronic System Design Tools.....	7
1.3.3	Lab Based Experimental Facilities.....	8
1.3.4	Research Problem	8
1.3.5	Solution	8
1.3.6	Evaluation.....	8
1.3.7	Thesis Writing	8
1.4	Thesis Structure	8
1.5	Chapter Summary	10
2	Chapter 2. Literature review of Haptics and Applications.....	11
2.1	Introduction	11
2.2	Haptic Technologies.....	11
2.2.1	Origin of Haptics.....	11
2.2.2	Haptic Interface in Virtual Reality	13
2.2.3	Haptic Interaction	14
2.2.4	Haptic Devices.....	16
2.2.5	Haptic Applications	19
2.3	A Review in Surgical Training and Planning	20
2.3.1	Mandible Surgical Planning without Haptics	20

2.3.2	Haptic Modelling of Bone Cutting Simulation.....	20
2.3.3	Force Model of Bone Cutting and Sawing with Different Tools.....	21
2.3.4	Dental Implant	22
2.3.5	Dental Surgical Simulators and Evaluation	23
2.3.6	Haptic in Maxillofacial Surgery Simulation	24
2.4	Literature Review of Haptic Technologies in Space Robotic Path Planning and Tele-Operation	25
2.4.1	Introduction	25
2.4.2	Redundant Space Robot Arm Path Planning.....	26
2.4.3	Least Squares (LS) Based IK Solution.....	27
2.4.4	Current Literature in Motion Planning with Haptic	29
2.5	Knowledge gap.....	35
2.5.1	Discussion of the Dental Review	35
2.5.2	Discussion of Space Path Planning and Haptic Manipulation.....	38
3	Chapter 3: Review of the Design Process of Mechatronic Systems.....	42
3.1	Introduction	42
3.2	Design Process	42
3.3	Design Process Model.....	43
3.4	Design Concept Methodology for Mechatronic Systems	45
3.4.1	V-Model.....	47
3.4.2	Complex System Engineering(CSE)	48
3.5	Digital Twin	49
3.6	Conclusion.....	50
4	Chapter 4: HARMP Design Methodology.....	51
4.1	Introduction	51
4.2	Haptic Design Process and Application of HARMP Methodology.....	52
4.2.1	Task Clarification	53
4.2.2	Conceptual Design	53
4.2.3	Embodiment Design.....	54
4.2.4	Force Modelling	54
4.2.5	Function Design Process	56
4.3	System Validation	57
4.3.1	Evaluation.....	58
4.3.2	Evaluation methods	60
4.4	Conclusion.....	60

5	Chapter 5: Dental Surgery Haptic System Development Simulation.....	62
5.1	Introduction	62
5.2	System Requirements and Specification.....	62
5.3	HARMP Modelling for Dental Surgery	64
5.3.1	Concept Design	64
5.3.2	Embodied Design	72
5.3.3	Geometric Modelling	74
5.3.4	Force Modelling	79
5.3.5	Virtual Constraints	96
5.4	Experimental Method	97
5.4.1	Data Collection.....	98
5.5	Results, Findings and Discussions	99
5.5.1	Model I.....	99
5.5.2	Model II.....	107
5.6	Discussion of the Result	109
5.7	Conclusion.....	111
6	Chapter 6: Haptic Design Case Study in Space Robotic Path Planning and Tele-Operation.....	112
6.1	Introduction	112
6.2	System Requirements and Specifications for Test Scenarios	113
6.3	HARMP Modelling for Space Robotics.....	116
6.3.1	System Architecture.....	116
6.4	Concept Design	117
6.4.1	Geometric Modelling	117
6.5	Embodied Design	118
6.5.1	Manipulation of a Haptic Space Robotic Model	121
6.5.2	Workspace Mapping	122
6.6	Kinematic and trajectory analysis	123
6.6.1	Manipulator Kinematics.....	123
6.6.2	Inverse Kinematics	125
6.6.3	Mapping between Device and Virtual Robot.....	127
6.7	Force Modelling for Haptic Rendering.....	129
6.7.1	Telepresence	130
6.7.2	Constraints	133
6.7.3	Guidance	134

6.7.4	Dynamic Control.....	137
6.8	Reaction Control Solution	140
6.8.1	Least-Squares-Based Reaction Control Solution.....	141
6.8.2	Capture Methods and Simulated Result	143
6.8.3	Integration of the Reaction Control Solution in HARMP System.....	154
6.9	Evaluation	157
6.9.1	Objectives.....	157
6.9.2	Experiment Setup.....	158
6.10	Results, Findings and Discussions	159
6.10.1	Task 1	159
6.10.2	Task 2	164
6.10.3	Discussion of Results.....	172
6.11	Conclusions	179
7	Chapter 7: Industrial Trial of Haptic Robot Control System.....	180
7.1	Introduction	180
7.2	System Requirements and Specification.....	181
7.3	HARMP Modelling for Teleoperation of a Industrial Robot.....	183
7.4	Embodied Design	184
7.4.1	System Architecture.....	185
7.5	System Setup.....	189
7.5.1	Hardware Setup	189
7.5.2	Haptic Device	189
7.5.3	Industrial Robot.....	189
7.5.4	Haptic Controller and its PC.....	190
7.5.5	Robot Controlling PC.....	190
7.5.6	IO's/ Sensing in the Environment	191
7.5.7	Network Connection	192
7.5.8	Hardware System Structure of Bilateral Robot Control.....	192
7.5.9	Software Setup.....	193
7.5.10	Windows/ OpenHaptics	193
7.5.11	Beckhoff TwinCAT 3 XAE	194
7.6	Implementation of the Virtual Interface.....	197
7.6.1	Geometric Modelling	198
7.6.2	Kinematics Solutions	199

7.6.3	Mapping of Coordinate Systems	202
7.7	Haptic Modelling.....	203
7.7.1	Telepresence	203
7.7.2	Constraints	204
7.7.3	Artificial Constraints and Guidance.....	206
7.8	Robotic Control System.....	206
7.8.1	Control logic Flow	207
7.8.2	Bilateral Position/Velocity Control.....	208
7.9	Experiment Setup.....	210
7.10	Experimental Results	211
7.11	Chapter Summary	216
8	Chapter 8 Discussion of the Results.....	217
8.1	Introduction	217
8.2	Evaluation of Research Undertaken	219
8.3	Chapter Summary	223
9	Chapter 9 Conclusion, Limitations and Future Work.....	224
9.1	Introduction	224
9.2	Conclusion.....	224
9.3	Contributions to Knowledge	226
9.4	Limitations.....	228
9.5	Future Work.....	231
10	Reference	233
11	Appendix	241
Appendix 1. 1	3D Design of Space Station Model.....	241
Appendix 1. 2	Assembly Drawing Robotic System.....	242
Appendix 1. 3	Mechanic Analysis.....	244

Figures

Figure 1-1 Research methodology	7
Figure 2-1 Feature of haptic interface in user-computer interaction (Heyward 2004) a) Conventional human computer interaction, b) New Haptic human and system interaction	13
Figure 2-2 Haptic interaction with real and virtual environments (J. C. Craig, 1999).....	15
Figure 3-1 Design process models (Pahl <i>et al.</i> , 2013) (Dym and Little, 2000)	44
Figure 3-2 Design process model (French 1999).....	45
Figure 3-3 Yan’s mechatronic system design concept (X. T. Yan and Zante, 2010).....	46
Figure 3-4 Interrelated relationship in a mechatronic system.	47
Figure 3-5 V-Model	48
Figure 3-6 Tiv Model (Melville,Yan and Gu, 2016).....	49
Figure 4-1 HARMP design model	51
Figure 4-2 Schematic structure of a virtual haptic robotic path planning system.....	56
Figure 4-3 The method of validation	58
Figure 5-1 Proposed HARMP system architecture.....	65
Figure 5-2 Phantom Desktop (Geomagic - Touch X).....	66
Figure 5-3 Base joints and gimbal joints of Phantom Desktop	67
Figure 5-4 Structure of Haptic Library API	69
Figure 5-5 Structure of Haptic Device API.....	69
Figure 5-6 Structure of QuickHaptics, HDAPI and HLAPI	70
Figure 5-7 Structure of proposed haptic interface building method.....	70
Figure 5-8 Proxy method.....	72
Figure 5-9 Panoramic radiograph. (Troulis, 2002)	73
Figure 5-10 Demonstration of cutting area (Troulis, 2002)	74
Figure 5-11 Cutting path on the mapped mandible	74
Figure 5-12 Cutting on mandible in 3DS Max	76
Figure 5-13 Three bone segments	77
Figure 5-14 Cutting procedure in the HARMP haptic environment developed through its interface.....	78
Figure 5-15 Contact analysis between two spheres -Hertz contact model	80
Figure 5-16 Contact analysis between sphere and a plane	80
Figure 5-17 Cutting area partition for haptic modelling	81
Figure 5-18 Chosen cutting tools for modeling (Stryker, 2010).....	82
Figure 5-19 Calculated force along cutting path.....	84
Figure 5-20 Fitted regression model	84
Figure 5-21 Scaled down force model I	85
Figure 5-22 Plot of force during the whole cutting path with smooth lines.....	88
Figure 5-23 Cutting force for first half of area 24	89
Figure 5-24 Regression model for first half of area 24	90
Figure 5-25 Regression model for first half of area 22	91
Figure 5-26 Regression model for first half of area 15	91
Figure 5-27 Scale down Force model I	93
Figure 5-28 Cutting force model II	94
Figure 5-29 Evaluation method for Case Study 1	98

Figure 5-30 Experimental setup for the dental surgery simulation.....	99
Figure 5-31 Calculated Force during cutting. (a graphic update (b compute force update	101
Figure 5-32 Device forces on x, y, z axes.....	102
Figure 5-33 Device torques on x, y, z axes.....	103
Figure 5-34 Planned cutting path.....	103
Figure 5-35 Planned cutting path versus real cutting path with constraint	104
Figure 5-36 Planned cutting path versus real cutting path with/without constraint.....	105
Figure 5-37 Planned cutting path versus real cutting path with constraint, no force on y axis	106
Figure 5-38 Planned cutting path versus real cutting path with/without constraint, no force on y axis.....	107
Figure 5-39 Calculated Force during cutting.....	107
Figure 5-40 Device force on y axis	108
Figure 5-41 Planned cutting path versus constrained Cutting path with Cutting force Model I/II.....	109
Figure 6-1 Experimental set-up of a three degrees of freedom robotic system	118
Figure 6-2 Robotic arm model in 3DS Studio Max. a) base, b) first link, c) second link, d) end effector.....	119
Figure 6-3 Imported robotic model in haptic interface	121
Figure 6-4 Workspace frame of a Phantom haptic device.....	122
Figure 6-5 planar 3R manipulator	124
Figure 6-6 Robotic model being manipulated via the haptic interface	129
Figure 6-7 Model of ISS in HARMF interface	131
Figure 6-8 Repulsion force to avoid singularities.....	134
Figure 6-9 Typical impedance control.....	139
Figure 6-10 Modified impedance model for velocity control.....	140
Figure 6-11 Stroboscopic view of robot motion (top), and reaction torque (bottom). Parametric trajectory 1.....	145
Figure 6-12 Simulation results. a)Curvilinear abscissa, b) First derivative of curvilinear abscissa, c) Second derivative of curvilinear abscissa, d) Capture error. Parametric trajectory 1	146
Figure 6-13 a) Joint angles, b) Joint velocities, c) Joint accelerations. Parametric trajectory 1	146
Figure 6-14 Stroboscopic view of robot motion (top), reaction torque (bottom). Parametric trajectory 2.....	147
Figure 6-15 a)Curvilinear abscissa, b) First derivative of curvilinear abscissa, c) Second derivative of curvilinear abscissa, d)Capture error. Parametric trajectory 2	148
Figure 6-16 a) Joint angles, b) Joint velocities, b) Joint accelerations. Parametric trajectory 2	149
Figure 6-17 Stroboscopic view of robot motion (top), reaction torque (bottom). Free shape trajectory1.....	150
Figure 6-18 a) Curvilinear, b) First derivative of curvilinear abscissa, c) Second derivative of curvilinear abscissa, d) Capture error. Free shape trajectory 1.....	151
Figure 6-19 a) Joint angles, b) Joint velocities, c) Joint accelerations. Free shape trajectory 1	152

Figure 6-20 Stroboscopic view of robot motion (top), reaction torque (bottom) Free shape trajectory 2.....	152
Figure 6-21 a)Curvilinear abscissa, b)First derivative of curvilinear abscissa, c) Second derivative of curvilinear abscissa, d) Capture error. Free shape trajectory 2.....	153
Figure 6-22 a) Joint angles, b) Joint velocities, c) Joint accelerations. Free shape trajectory 2.	154
Figure 6-23 Updated evaluation methods for Case Study 2	159
Figure 6-24 Initial position of manipulator and target	160
Figure 6-25 Velocity error between the end effector and the target.....	160
Figure 6-26 Distance between the end effector and the target	161
Figure 6-27 Reaction torque to the base	161
Figure 6-28 Joint angles	162
Figure 6-29 Calculated guidance force during operation	163
Figure 6-30 Actuated guidance force after rendering during operation	163
Figure 6-31 Comparison of Velocity errors	164
Figure 6-32 Comparison of distances.....	164
Figure 6-33 Velocity error between the end effector and the target with dynamic guidance	166
Figure 6-34 Position error between the end effector and the target with dynamic guidance	166
Figure 6-35 Reaction torque transferred the base	167
Figure 6-36 Joint angles	167
Figure 6-37 Calculated guidance force for dynamic guidance methods.....	168
Figure 6-38 Actuated guidance force after rendering for dynamic guidance methods	168
Figure 6-39 Comparison of velocity error with/without dynamic guidance	169
Figure 6-40 Comparison of position with/without dynamic guidance	169
Figure 6-41 Comparison of velocity errors	170
Figure 6-42 Comparison of position errors.....	171
Figure 6-43 Comparison of travelled distance until reaching the target.....	171
Figure 6-44 Calculated force with APF methods.....	172
Figure 6-45 Actuated force after rendering with APF methods	172
Figure 6-46 The means of times used to reach the target at first time (when the distance=0), with shown standard derivation.....	175
Figure 6-47 The means of travelled distances before reaching the target with shown standard derivation.....	175
Figure 6-48 The means of velocity errors at the point of first reaching the target with shown standard derivation.....	176
Figure 6-49 The MSE(mean squared error) of the relative velocity and position in 1000ms after reaching the target.....	177
Figure 6-50 The MSE (mean squared error) of the relative velocity in 1000ms after reaching the target	177
Figure 6-51 The MSE (mean squared error) of the relative position in 1000ms after reaching the target	178
Figure 7-1. Control architecture for virtual robot teleoperation.....	185
Figure 7-2 Two port model for virtual bilateral teleoperation	186
Figure 7-3. Modified bilateral control model	187

Figure 7-4. Staubli TS80 SCARA robot	190
Figure 7-5. Beckhoff Industrial PC and IO's	191
Figure 7-6 Overall HARMP hardware structure	193
Figure 7-7 TwinCAT and ADS structure of communication in HARMP system.....	195
Figure 7-8 TwinCAT3 on Microsoft Visual Studio.....	197
Figure 7-9 Imported TS80 CAD model in 3DS Max.....	198
Figure 7-10 Geometric model in haptic interface	199
Figure 7-11 Two links planar manipulator	201
Figure 7-12 Comparison between coordinates of Phantom Desktop and TS80 SCARA	202
Figure 7-13 Working envelope of TS80 SCARA robot	205
Figure 7-14 Control logic flow	207
Figure 7-15. Bilateral position/velocity control loop	209
Figure 7-16 Updated evaluation method for Case Study 3.	211
Figure 7-17 Experiment set up during tele operation	212
Figure 7-18 Virtual and real position with haptic bilateral control.....	212
Figure 7-19 Position error with haptic bilateral control	213
Figure 7-20 Bilateral Force during the manipulation.....	213
Figure 7-21 Virtual and real position without bilateral haptic control	214
Figure 7-22 Position error without bilateral haptic control.....	215
Figure 7-23 Constraint force without bilateral haptic control.....	215

Tables

Table 2-1 Comparison table of the key performance of haptic devices	18
Table 2-2 Knowledge gap in mandible surgical planning.....	36
Table 2-3 Knowledge gap in space path planning and haptic manipulation task.....	39
Table 4-1 Haptic design process	52
Table 5-1 Specification template	64
Table 5-2 Specifications parameters of Phantom Desktop. (Geomagic)	66
Table 5-3 Material properties along the selected cut	81
Table 5-4 Cutting force calculation parameter values.....	83
Table 5-5 Cutting force calculation for position 24	86
Table 5-6 Cutting force calculation for position 22	87
Table 5-7 Cutting force calculation for position 15	87
Table 5-8 Experiment set for the dental surgery simulation	98
Table 5-9 Data collection	99
Table 6-1 Updated specification template.....	115
Table 6-2 Links parameters.....	124
Table 6-3 Experiment set for the space robotic path planning and teleoperation	158
Table 7-1 Updated specification template.....	183
Table 7-2 Link parameters	200
Table 7-3 Experiment set for the robotic manufacturing manipulations	210
Table 8-1 Final system specification	222

List of Acronyms

HARMP: Haptic Assisted Robotic Manipulating and Planning System

IK: Inverse Kinematics

LS: Least Square Solution

DOF: Degree of Freedom

HLAPI: Haptic Library Application Programming Interface

HDAPI: Haptic Device Application Programming Interface

APF: Artificial Potential Field

Chapter 1: Introduction

1.1 Motivation

1.1.1 Overview of Autonomous Operations and Needs for Human Intervention

Autonomous robotic systems have been advancing in design and ability to provide assistance to humans in various tasks, since their conception as early as the 1940s. Initially, they were designed for industrial applications such as manufacturing, part assembly and mass production. Autonomous robotic systems can offer several advantages to the performance of a task. They have the ability to work at high speed and also they can be reliable over long periods of working time, which can be important factors to tasks that are repetitive. They are also able to provide a high level of precision and accuracy that human operators are not always able to deliver. As a result, the use of autonomous robotic systems can significantly increase the productivity and quality in manufacturing, along with potentially reducing the labour costs.

As robotic intelligence progresses through research, their enhanced flexibility and capabilities allow autonomous robotic systems to be integrated into human life with increasingly important roles (Wong et al., 2018). One scenario where the use of autonomous robotics can be very beneficial is in environments of an extreme nature. These extreme environments can be challenging or even hazardous for human operators to work in due to extreme conditions of temperature, air pressure, oxygen or even radiations level (Fahrner, Job and Werner, 2001). Various types of autonomous robotic systems have been designed and manufactured for space missions (Orbit service, space exploration), mining and earthquake rescue, and the maintenance and operation of nuclear plants. The deployment of autonomous robotic systems in such extreme environments can help to reduce the risk to human operators or to accomplish missions that are impossible for a human to achieve.

Autonomous robotic systems have also been designed for medical practice. . An

important application of autonomous medical robotics is the ability to perform surgery remotely in a controlled manner without the need for the surgeon to be present. Use of autonomous robotics in this scenario could lead to multiple lives being persevered. Currently, in some branches of medicine, these robotic systems are already being used for assistance in surgeries. An example of this is in joint replacement surgeries where the use of the robotic assisted systems can optimize the positioning of implants placement with higher accuracy (Elson et al., 2015). Use of these systems can also assist with surgical training and surgical planning to provide more dependable and reliable surgical practices.

1.1.2 Overall Challenges in Autonomous Robotic Systems

Whilst the use of autonomous robotics systems has illustrated that they have great potential to improve and contribute to many situations and lives there are still exist several challenges that they must overcome. Due to their nature, the working environment that an autonomous system is used, as mentioned previously, can often be extreme. In such an environment, there exist several unknown and unpredictable factors. It is important to carefully assess such an environment and that appropriate and thorough planning is conducted before final decisions are made regarding the systems operation. The success of an operation can be highly dependable on the performance of each sensor and how they are integrated as an entire sensing system. This can be a challenge in extreme environments as the conditions can be such that there are poor light conditions, extreme temperatures or high-level radiation.

Another challenge for autonomous robotic systems is being able to operate in situation with high levels of complexity. Robot intelligence is required for task planning and decision making in order to achieve tasks autonomously. As previously mentioned, currently there exist robotic systems that are capable of performing, with high accuracy, some surgical procedures such as implant positioning. However, due to the significance of the situation and potential consequences, it still remains that these scenarios are challenging for the robotic system to conduct such complex

surgery. Professional medical knowledge and extensive experience is necessary to deal with unexpected and emergency situations.

Autonomous robotic systems can encounter challenges in industrial applications. In industrial factories, for example, the reliability of the system could be compromised due to its reliance, from initial design requirements, on certain operating conditions, such as specific lighting and moisture levels. Under such operating conditions, the system may not function correctly should any of the initial requirements change. Therefore, the challenge in the industrial/commercial working environment is for the system to remain reliable with high success rate with variances of parts and change of environmental conditions. In addition to this, for high-level delicate and accurate manipulation operations, force control is necessary which requires both hardware integration and software control algorithms.

1.1.3 Autonomous Systems Advantages and Limitations

Conclusively, in comparison to human operators, autonomous robotic systems can provide several advantages such as fast, precise and reliable outputs. They are also able to work safely in remote areas or in extreme environments. However, they also have limitations such as complex sensor integration design and environment recognition. In tasks that require human experience to deal with complex situations, such as major surgery, notable progress has been made in integrating such autonomous systems. However, significant research and design is required to allow these systems to operate alone. The knowledge and experience of a surgeon cannot yet be replaced with autonomous systems. Additionally, regarding ethics and the law, all autonomous systems require an operator to have full responsibility for the control of vehicles and aircraft that have a robotic component to their operating system.

1.1.4 Motivation

As previously mentioned autonomous robotic systems have several challenges they must overcome. Due to these, Human-Machine interactive systems are necessary in

manipulation tasks that require a higher level than that of an experienced human precision and accuracy, as well as human intelligence and reaction in a control loop (Abbott, Marayong and Okamura, 2007).

As an integration of both robotic and human capabilities, Human-Machine interactive systems can overcome some of the aforementioned challenges. . However, the performance of the system in manipulation tasks can still be limited by the human user's capability. In typical Human-Computer interactions the visual and acoustic sensations are commonly used as communication channels, while the human's sense of touch also plays an essential role in communication. The touch sensation or in terms of haptic perception, includes tactile and kinesthetic sensations that help people understand the object material properties in the environment as well as their body position and movement. Therefore, it is suggested that haptic force feedback can be introduced as assistance where high level of accuracy of human manipulation is required. Haptic assistance can be utilized as simulation and constraints for training, telepresence of the scene and guidance of path for tele-manipulation.

Also, it is necessary to develop a design method for haptic assisted systems that integrate professional knowledge and experience with different types of haptic virtual fixtures in manipulating and planning tasks.

This work is motivated by the previously discussed challenges and investigates a novel solution to advance human-robotic/mechatronic interactions by proposing a novel approach to designing haptically controlled robotic solutions to challenging operations. The aim is to illustrate that this approach is effective and efficient in dealing with challenges faced in many engineering problems.

1.2 Research Aim and Hypothesis

1.2.1 Research Hypothesis

The hypothesis for this research is the design of a haptic system, following a suitable design process model, can significantly improve manipulation operations in

challenging environments. This hypothesis can be divided into two counterparts. Firstly, “A general design model of a haptic system with virtual fixtures for high accuracy manipulation and planning tasks can provide useful and informative instruction for design and building of such haptic systems and secondly, “The designed haptic system can improve the manipulation performance, e.g. accuracy control and trajectory path control in challenging environments.”

1.2.2 Research Questions

To identify a general solution to the challenges discussed it is necessary to recognise the requirements important to find such a solution. Through addressing these requirements, it will be possible to contribute new knowledge to the haptic human and robotic interactions. The following requirements have been identified for this research.

1. What necessary features and functions need to be considered while designing a general haptic system for robotic manipulating and planning tasks?
2. How is this necessary expertise and knowledge required by the specific task obtained and how are they integrated into the haptic system?
3. How are the types of available haptic virtual fixtures classified and how are they assigned to different tasks according to the task requirements?
4. How do we evaluate the usability of haptic assistance provided and compare the performance to other methods?

1.2.3 Research Aim

The aim of this research is to devise a general design methodology to support the design and building of haptic systems used to control manipulation operations in challenging environments. Furthermore, and the research will validate the design methodology through diverse system design and modelling, and a Haptic Assisted Robotic Manipulating and Planning system (HARMP) that can help users gain the experience and provide haptic assistance to improve performance in surgical and robotic manipulation tasks.

1.2.4 Research Objectives

To achieve the research aim of enabling new types of human robotic interaction, the following objectives have been identified:

1. To develop a general design methodology for haptic systems with virtual fixtures for high accuracy manipulating and planning tasks clarifying the design flow and necessary system components and specifications.
2. To build a Haptic Assisted Robotic Manipulating and Planning system (HARMP) that provides haptic interfaces and haptic assistances for robotic planning and manipulating tasks.
3. To classify the types of available haptic virtual fixtures, including telepresence, constraints and guidance, and assign them to different tasks according to the task requirements.
4. To validate the HARMP system design in realistic robot control tasks in remote environments, integrating with industrial hardware and sensing systems for environment modelling.
5. To develop an evaluation method to analyse and assess the usability of haptic assistance provided and the performance of the system.

1.3 Research Methodology

The research methodology used in this study is derived from Duffy's methodology (Duffy and O'Donnell, 1999). Duffy's methodology was developed in the CAD Centre at the University of Strathclyde as a general guide to conducting research work. The research methodology shown in Figure 1-1 adapts phases and elements based on Duffy's methodology. Further explanations are derived from Rehman's (Rehman, 2006).

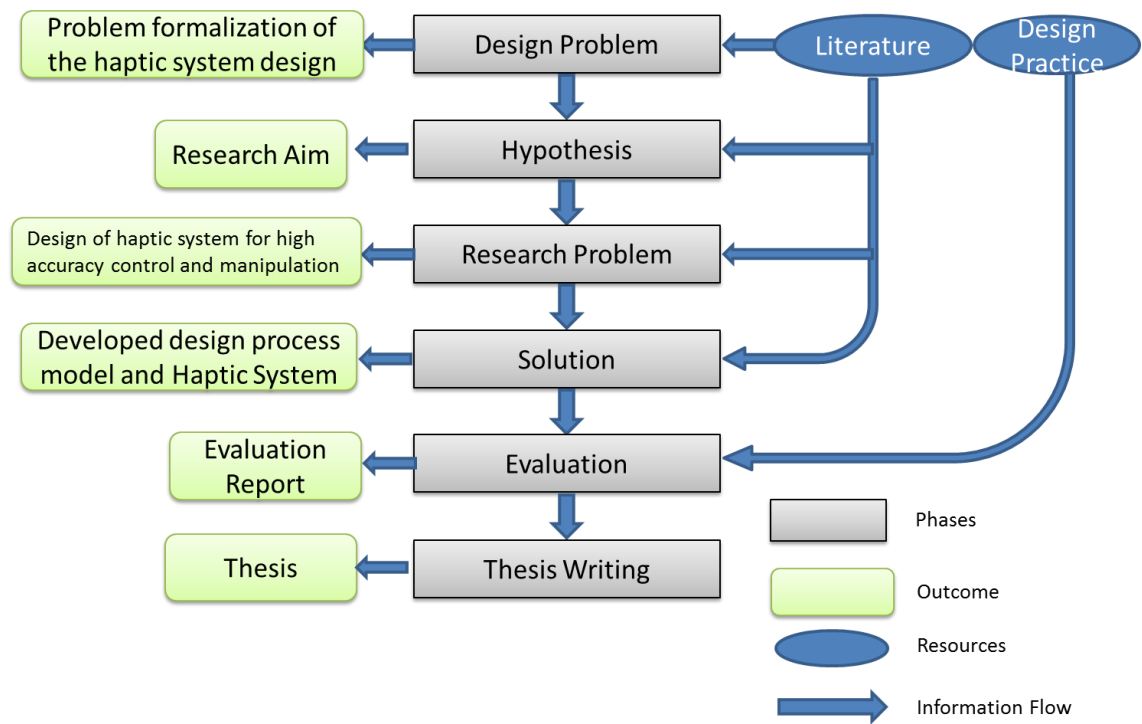


Figure 1-1 Research methodology

1.3.1 Literature Review

Literature reviews are the resources and foundations that are used to support any research work. For this research, in order to identify the design problem, form a hypothesis, identify the research specifications, and to develop the solution, an extensive literature review has been conducted. The literature review includes a general overview of the theoretical design process of haptic systems and human robot or machine interactions. The literature review also includes haptic applications in delicate manipulation tasks found in surgical procedures, space robotic human robot interactions and manufacturing systems interactions. The purpose of the review is to identify areas where knowledge gaps may exist in the development of haptic assistive interaction systems for interactions with robots in environments where, if possible, full autonomy proves to be challenging.

1.3.2 Computer Supported Mechatronic System Design Tools

Throughout the research, a range of computer tools are required to enable the understanding of the human robot haptic interactions. These tools have also been

used to develop technical solutions for a given application.

1.3.3 Lab Based Experimental Facilities

For generated computer solutions, it is critically important to validate these solutions in order to be confident of their performance in real applications. Laboratory experimental facilities play an important role to assess the feasibility and suitability of these solutions with technical analysis. Data acquisition tools have also been used to capture necessary data in order to quantitatively assess the performance of the prototype systems.

1.3.4 Research Problem

The research problem focuses on how to develop a design process model of a haptic system for high accuracy control and manipulation, and what functions and features should be considered.

1.3.5 Solution

The solution is produced and formulated to resolve the given research problems. The solution is achieved by developing a design process model for high accuracy haptic control and also a Haptic Assisted Robotic Manipulating and Planning System (HARMP), which is derived from the design process.

1.3.6 Evaluation

The proposed solution is evaluated by conducting case studies and industrial trials. The advantages, weaknesses and potential improvements are identified throughout the solution evaluation.

1.3.7 Thesis Writing

The research outputs and contributions are documented throughout this thesis and other research journal publications.

1.4 Thesis Structure

The structure of the thesis:

1. Chapter 1: Introduction

The overview of haptic systems and motivation for this research is introduced. Research aim, hypothesis, questions and objectives are presented.

2. Chapter 2: Literature Review of Haptics and Applications

The relevant literature to haptic systems and its applications are reviewed to identify any potential gaps in knowledge for further research.

3. Chapter 3: Review of Design Process of Mechatronic System

The design methods and research methodologies for engineering design are discussed and selected for the proposed work.

4. Chapter 4: HARMP Design Methodology

A design methodology for haptic systems with virtual fixtures for high accuracy manipulating and planning tasks is devised. System validation and evaluation methods are presented. The aim for this design methodology is to achieve research objective 1.

5. Chapter 5: Dental Surgery Haptic System Development Simulation

An initial design for the HARMP system is produced and modified for case study 1: Dental surgery simulation. The aim for this development simulation is to achieve research objective 2.

6. Chapter 6: Haptic Design Case Study in Space Robotic Path Planning and Tele-Operation

The HARMP system is modified for case study 2: Haptic design in space robotic path planning and tele-operation. Haptic virtual fixtures are utilized to provide assistance in space manipulation tasks which are used to investigate research objective 3&5.

7. Chapter 7: Industrial Trial of Haptic Robot Control System

The HARMP system is modified and validated for case study 3: haptic control of a realistic commercial robot. Experiments have been conducted to evaluate the performance of the system. This case study investigates objective 4&5.

8. Chapter 8: Discussion of the Results

The experimental results of three case studies are analysed and discussed. Evaluation methods are also assessed

9. Chapter 9: Conclusion, Limitation and Future Works

The conducted research work is concluded. Design and capability limitations and future works are presented.

1.5 Chapter Summary

This chapter provides an overview of autonomous systems where their advantages and limitations are introduced. The requirements of haptic systems and the motivation for this research are also analysed. Finally, the research aim, hypothesis, specification questions and objectives are also presented. A research methodology is also devised for this research work. Finally, a structure of this thesis is given.

Chapter 2. Literature review of Haptics and Applications

2.1 Introduction

A literature review summarises and provides critical evaluation and direction for future work to the proposed research investigation. In this chapter, the history and philosophy of haptic and sense of touch are discussed, such as state of the art haptic interfaces, haptic interaction and current haptic devices both in literature and in the market. Their potential to be utilized in several applications such as gaming, engineering design and surgical simulations is also discussed. In order to acquire knowledge of haptic system design, two typical applications where haptic technology can play an important role were chosen. These scenarios were surgical planning and robot manipulation where in both situations require professional knowledge and experience of the operator, as well as delicate and precise control during operational phases.

Firstly, state of art in haptics for surgical planning and training are considered, including the development of virtual surgical simulation, current methods and approaches in different surgical applications. Specifically, the haptic simulation of maxillofacial deformity surgery is investigated. Secondly, a literature review of haptics in space robotic path planning and tele-operation is conducted. Control methods, inverse kinematics and path planning in space robotic manipulating are investigated. The use of haptic technology for force and torque in motion planning and guidance is also summarised. To conclude, the common features required for both systems are discussed. The common features required for both systems are concluded. Finally, knowledge gaps are identified in both applications in order to design a haptic system that can safely provide higher accuracy and efficiency for a user.

2.2 Haptic Technologies

2.2.1 Origin of Haptics

The term “haptic” refers to the interaction between a human and environment

through the sense of touch. There has been a long history of the idea that human sensation can be rooted in the specific body organs, i.e. skin. In ancient India, the sense of touch was regarded among the five human sensations, including touch, sight, hearing, smell and taste, and each of these sensations is related to one of five elements in Indian philosophy (Muller, 1951). For example, the sense of touch is related to the element of wind. The sense of touch, or in the term of “feeling”, is accomplished by grasping using fingers through the skin.

The utilization of this sense of touch also dates back to ancient China, where it played a significant role in pulse diagnostics in traditional Chinese medicine (Hsu and Sima, 2010). Experienced doctors diagnosed patients by putting one or more fingers, usually the index or middle finger, on the wrist of the patients to feel their pulse. Chinese doctors believed that certain diseases could be diagnosed through this tactile perception of the pulse as the human body’s condition can be indicated by the motion of blood flow and the heartbeat.

Similarly, in ancient Greece, the relationship of human senses and physical organs were studied by philosophers. In Aristotelian’s view, the sense of touch should be related to the heart, instead of the skin. This sensation is linked to the organ inside the human body rather than the outside “shield”. Aristotelian described the sense of touch as a palpable sensation. Therefore Aristotelian believed that the sense of touch connects people more closely to the environment, compared to the other four sensations, because the properties of the materials in the environment are also palpable (Beare, 1906).

The first noted experiment that systematically studied the sense of touch was conducted by the German physiologist Ernst Heinrich Weber (Bück-Rich, 1970). Throughout the experiment he investigated the relationship between the sensations and the related nerve through electrical stimulation. Along with the work conducted by Gustaf Blix and Alfred Goldscheider, it was suggested that the sense of touch can be interpreted as sensations that consist of several aspects including the pain, temperature and pressure perception of the human “skin sense”. Several

years later, the word “haptic” was first introduced to describe the science of this kind of sense of touch by Max Dessoir, a German scientist (Grunwald, 2008). In 1990s, haptic technology developed and advanced in what might be termed the “haptic age” (Grunwald, 2008). Due to the fundamental concepts and principals that these pioneering philosophers and scientists developed it is possible to design and advance haptic technology today.

2.2.2 Haptic Interface in Virtual Reality

The importance of haptic sensation for human beings in knowing and understanding the world are studied and investigated. And one of the first ideas that sense of touch can be used as a communication method, in addition to the means of auditory and visual sensations was introduced by Sherrick (Sherrick, 1985). It was suggested that the complex combinations of simple patterns can extend the capacity of signal channel in information streaming. This can be utilized in the communication between the human and machine/computer.

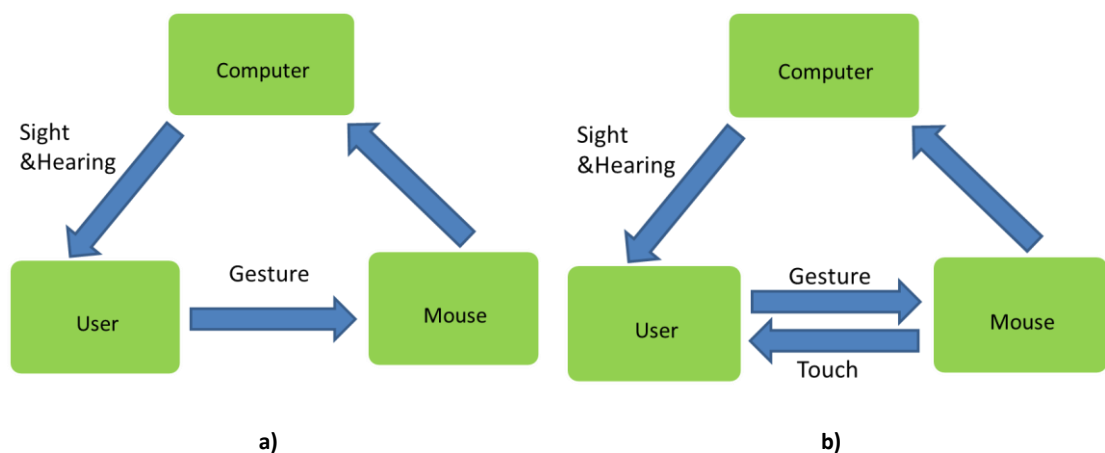


Figure 2-1 Feature of haptic interface in user-computer interaction (Heyward 2004) a) Conventional human computer interaction, b) New Haptic human and system interaction

The typical Human-Computer interface only allows a user to manipulate a mouse and keyboard as input to the computer to get sight and hearing feedback from the computer (Vincent *et al.*, 2004). In this type of interaction, the capabilities of the human are not utilized to full advantage, hence introducing haptic feedback to the interaction can address this limitation. The term “haptic display” contributes another feedback signal from the mouse to the user, which allows the tactile

interaction between the user and computer. As shown in Figure 2-1, the communication through the mouse is unidirectional while the information exchange with haptic features is bidirectional.

The haptic interface generates the synthetic stimulation of the touch and kinesthetic signals to human sensation. It can also allow user to participate and then act in the virtual environment. As suggested by philosophers and scientists, the sensation of touch is more sensitive and closer to the environment compared to sight and hearing, therefore it is also more difficult to be synthesized. Firstly, the sight and hearing sensation are generated through a specific human organ, eye or ear respectively. The sensation of touch can be related to the entire body, which makes it more difficult to define a specific receiver for the haptic interface. Secondly, since the sensation of touch is familiar and more sensitive, it requires an higher updating rate of the signal to satisfy the user compared to the video and audio (Vincent *et al.*, 2004). Currently, the most commonly used computer monitors are 60 Hz or even 144 Hz which are adequate to satisfy the user, while such a requirement for the haptic interface is at least 1000 Hz.

2.2.3 Haptic Interaction

The haptic interface provides a programmable tool using the sense of touch for intuitive and faster interaction between human and machine. The haptic interaction utilizes the practical physics fundamentals as the subject of dynamics (Ogata, 1978) which involves mechanical variables and signals including force, torque, stiffness and mass. These mechanical signals are not only generated from the environment, but they may also come from parts of the user's body that interact with the environment. It is essential to have thorough understanding of the related physics and mechanics to investigate how to contribute to human haptic perception using different mechanical and haptic signals. The haptic interaction is usually achieved by stimulating the tactile or kinesthetic channels of a user.

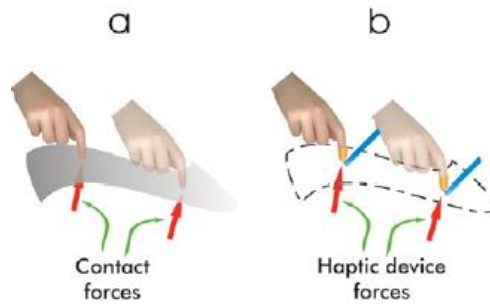


Figure 2-2 Haptic interaction with real and virtual environments (J. C. Craig, 1999)

Generally, tactile interaction is subjected to the surface of skin and related tissues. It includes the sensations of pressure, temperature, pain, vibration, texture and other material properties. For example, the haptic perception of the material can be created by controlling the mechanical signals of friction, softness, wetness and temperature. As shown in Figure 2-2, when the user touches a surface, i.e. a piece of paper, the perception of texture of the material can be acquired by rubbing it using the finger tips (J. C. Craig, 1999). Such sensation experiences can be simulated in the virtual environment by providing similar properties of variables to the user in this process. These include frictional forces, softness as well as the temperature that may be experienced by the user on a real piece of paper.

Another important type of haptic interaction utilizes kinesthetic sensations. Kinesthetic sensation relates to the gestures and movements of one or more parts of human body. These include the body's position and velocity controlled through the force by muscles. Different from the tactile sensation, the receptors for the kinesthetic sensation can be located not only in skins but also in muscles, joints, skeletons and even tendons (Vincent *et al.*, 2004). The haptic interaction using kinesthetic sensation can help a user feel the shape of objects and other encountered forces in a virtual environment. It can also provide assistance for operations that require delicate manipulations. For example as shown in Figure 2-2, if a user tries to push down on a virtual surface using finger tips, the haptic device can generate a mechanical variable (encountered force) upward indicating the surface and defining the shape of the virtual object.

By combining the tactile and kinesthetic sensations a comprehensive haptic interaction can be designed. Utilizing tactile sensation can help a user feel the texture, vibrations and other material properties of a virtual object, whilst the kinesthetic sensations help to define the virtual shape and objects as well as providing assistance for manipulation and operations in the virtual environment.

2.2.4 Haptic Devices

As for haptic devices, there are many different designs for different uses, varying from large industrial robotic manipulator to portable desktop devices.

Generally, the haptic device should provide the following haptic information (Adams and Hannaford, 2002):

1. The resistance over virtual shapes.
2. The roughness of virtual textures.
3. The mass of virtual objects.







Haptic devices have been investigated and developed since 1980s. The exoskeleton type is one approach concept formulated by Burdea and Zhuang (Burdea and Zhuang, 1991). This type of product includes hand gloves and a skeleton with force feedback. There are several actuators attached to the user's hand or other parts of body that can detect the movement and gesture of users' hand and mapping it to a virtual interface or a remote robotic hand. The force conducted in the environment can be sent back to a user through the skeleton. This allows more delicate control and force simulation where high DOF end-effectors are involved. These kinds of devices can be used in master-slave manipulators and tele-operation. Another type of haptic device has a tool handling feature which normally has a pen shaped grip (Iwata, 1993). The user can hold and manipulate the grip in the 3D space with the familiarity of holding a pen. Additionally, the actuators in the device's joints can provide a combination of both force and torque at the tip of the pen, i.e. similar to finger tips. Different from exoskeleton type device, the tool handling type device cannot specifically simulate force feedback on each finger. However, it illustrates

advantages in virtual design and point manipulation tasks which utilise more kinesthetic sensations as previously mentioned.

The current haptic devices available in the market include 1. Sensable, 2. Haption, 3. Cyberglove. Some of the haptic devices are listed and compared in Table 2-1.

The tool handling haptic device has six Degrees of Freedom (DOF) and 3-6 DOF of force feedback. Due to their different sizes and uses they can provide maximum force from 5N to 42N. The desktop version of the tool handling tool is portable and is designed for 3D modelling, medical and industrial training. There are large versions that can provide greater torque and forces which are suitable for master-slave teleoperations. Also for some large tool handling type devices several changeable end effectors are available to allow users to achieve more functions with tasks that have more diverse requirements. Currently, exoskeleton products are predominately manufactured by the company CyperGloves. The CyberGrasp is designed for grasping computer-generated objects. Its actuators can provide up to 12N of force feedback on each finger with the help of its force control unit. There also exist products that combine an exoskeleton and tool handling devices together that are capable of firming grasping and manipulation tasks in the virtual space. However, such products can be very expensive and large in size.

Table 2-1 Comparison table of the key performance of haptic devices

Type	Pictures	Name of the systems	Maximum force	Suitability of the configuration for human operations	DOF movement/ Force
Tool-handling		Novint Falcon (Novint, 2007)	8.9N	Game	3/3
		Geomagic - Touch X (Geomagic, 2018b)	7.9N	3D modeling, surgical training, virtual assembly	6/3
		Haption - Virtuose 6D Desktop (Haption, 2018a)	10N	Medical training Industrial training	6/6
		Haption - Virtuose 6D TAO (Haption, 2018b)	42N	Teleoperation Master-Slave	7/6
Exoskelton		CyberGlove CyberGrasp (CyberGlove, 2018b)	12N per finger	Grasp computer-generated objects.	5
Combined		CyberGlove CyberForce (CyberGlove, 2018a)	8.8N	Grasp and manipulate with computer-generated objects	5 on fingers 3 on hand

2.2.5 Haptic Applications

Haptic applications have been developed for many varying applications. The first commercial haptic device was introduced in the gaming industry (Adams and Hannaford, 2002), which was a joystick with force feedback that can assist the user in driving and piloting games. Using a haptic system in a gaming application can improve the user's feeling of realism whilst exploring them into an immersive virtual-reality environment.

Research has also have been conducted for people in the rehabilitation of physical, sensory or mental disabilities (Schultheis and Rizzo, 2001). As an alternative of a visual channel, haptic feedback can help blind people explore in an unknown environment by mapping the spaces cognitively into haptic and audio information (Lahav and Mioduser, 2008).

CAD designers can also benefit from the use of haptic devices. Here, it allows the user to be able to review every detail of their product with their hands before the products are manufactured (Nahvi *et al.*, 1998). Also, the six DOF haptic devices allow designers to easily target and manipulate the parts in 3D CAD software. However, it can be a more complicated operation compared to working with a traditional mouse.

Another advanced application of haptics is surgical simulation. Surgical operations require experienced surgeons not only for their knowledge and understanding of the surgery process, but also for their ability to deal with real situations that are expected or unexpected. Therefore, it is important in the training procedure of surgical students to provide them with an interface that can accurately simulate the real conditions in the surgery with graphical and haptic information (Baumann, Clavel and Ieee, 1998). Mako robotic-arm assisted surgery systems with haptic features have proven to provide a more accurate and precise implant placement with less pain in the uni knee arthroplasty compared to manual procedures (Bell *et al.*, 2016).

2.3 A Review in Surgical Training and Planning

Surgical procedures are complex and training of student doctors to master these procedures are challenging. A factor which can cause many challenges and issues is the ability for a surgeon to estimate the correct amount force required to make a cut, especially for hard tissues (Aggarwal and Darzi, 2009).

Haptic feedback can provide a force feedback sensation for a surgeon and therefore it is an important role in surgical planning operations and training (Coles, Meglan and John, 2011) (Basdogan *et al.*, 2007).

Solely computer based surgical simulation systems have been designed and produced, however they cannot provide true haptic feedback for a given surgical case. Haptic systems are used in open surgery where visualization is not possible (Hu *et al.*, 2006).

The purpose of this section is to investigate haptic modelling and address the challenges that occur when they systems are used with hard tissues, in particular maxillofacial deformity surgical procedures.

2.3.1 Mandible Surgical Planning without Haptics

A 3D planning system based on computed tomographic (CT) data was presented by Troulis *et al* (Troulis *et al.*, 2002). In this work, a three-dimensional CT scan of the craniofacial skeleton forms an information database. The software developed in the Harvard Surgical Planning Laboratory was modified for the craniofacial skeleton. A 'cutting tool' is used to segment the mandible and the segments are moved to their predicted positions. A 'collision tool', alerts the operator of skeletal interferences. This procedure made the foundation for mandible modelling. However, the concept of a haptic system was not yet introduced.

2.3.2 Haptic Modelling of Bone Cutting Simulation

To produce a mandible surgical haptic interface, the simulation of bone dissection is very important as it is a key procedure for many kinds of surgeries. Agus *et al*

proposed a bone cutting model with both visual and haptic implementation using volumetric representation (Agus *et al.*, 2003). This is based on McNeely's work of voxel based haptic rendering, which has proven to be effective in force feedback modelling of rigid bodies (McNeely *et al.*, 1999). Agus et al built volumetric models from the MRI and 3D CT scan of patients. The burring area was represented with volumetric data that can simulate the friction force and elastic reaction. The forces were calculated using Hertz contact for burr position. The densities of voxels in the contact area were decreased to represent the bone erosion. However, this method requires high performance of the processor and memory of the computer due to its large computational requirements.

Wang et al devised a method for constructing a cutting simulation using a triangle mesh (D. X. Wang *et al.*, 2003) which was integrated with a haptic device into the system. The tooth model proposed by Wang was constructed by multilayer points scan using laser scanner and reconstructed to form a triangle meshed model and polygon model. A contact force model was proposed to describe the cutting process. Three different types of tools, the physical tool, the virtual tool, and the cutting tool were introduced to perform the force computation and material removal. In 2005 Wang improved the system by proposing the vertex deformation in the procedure of material removal (D Wang *et al.*, 2005). The method updated the triangle mesh near the cutting section to reflect the shape of the cutting tool. Also, the cutting procedure was regarded as the transition of three statuses, separation, contact, and cutting. In this case a virtual model of contact force was built for the force computation.

2.3.3 Force Model of Bone Cutting and Sawing with Different Tools

Arbabtafti et al used force analysis in haptic simulation of bone machining (Arbabtafti *et al.*, 2011) where a force model was introduced as a bone milling tool by calculating the tangential cutting force. A voxelized force model was designed for haptic simulation that considered the size and speed of the spindle and the rendering algorithm. Compared to a frictionless point based model that implements

a spring force acting perpendicular to the surface of the bone, and the multipoint approach in which the spherical tool is represented by a number of sample points over the tool surface, more force analyses were considered. As a result, this approach makes their model computationally more expensive. Considering the low rate haptic rendering now, their stability still needs to be improved.

In 2012, another physics based model of bone machining was designed by Wang et al (Q Wang *et al.*, 2012b). This model considered impact mechanics to model the bone cutting process. Other previous models have been created which used similar theories to model the cutting (Agus *et al.*, 2003). Wang proposed that the speed of the drill and saw tools would be an important factor to consider when modelling the forces felt during the bone machining process. Haptic forces and torques generated on the motor driven tools were computed using impulse based dynamics. Using these values mathematical models for bone sawing, cutting and burring were generated. This use of impulse based dynamics for calculating the cutting forces as the tools rotated at high speeds is a contrast to Arbabtafti's model (Arbabtafti *et al.*, 2011) which considered spindle speeds but simply averaged the forces rather than applying the accurate forces felt for every degree of the tool angular rotation.

2.3.4 Dental Implant

A novel system for dental implant surgery was proposed in 2006 by Kusumoto et al (Kusumoto *et al.*, 2006). This system shares some similarities with previously mentioned models (D. X. Wang *et al.*, 2003) (Agus *et al.*, 2003), where the 3D jawbone model was constructed from CT images. However, as this model was for dental implant procedure, the bone model was drilled with holes for the implant insertion. Afterwards, a surgical template was milled by CAM (computer control milling machine) before being fitted to the bone model. To calculate the drilling force, a software named VRDTS was used. After inputting the jawbone model into the software, a virtual drilling can be applied and the sensed virtual force can be measured. The detected force was then used to build the force model.

2.3.5 Dental Surgical Simulators and Evaluation

Dental simulators have been investigated as integrated application tool using visual and haptic features for training purpose. The research of these simulators not only focuses on the techniques and methods for simulating the physical properties, but also investigates how to gain the required knowledge and to conduct the evaluation for the surgical procedures. The evaluation of the performance in dental surgical procedures is challenging (Quinn *et al.*, 2003) (Jasinevicius *et al.*, 2004).

PerioSim is an integrated simulator which has been designed for periodontal. (Luciano, Banerjee and DeFanti, 2009). The PerioSim simulates several operation procedures in periodontal surgeries, focusing on probing differences of tooth related tissues. It also carries out a score based statistical analysis for qualitative evaluation (Steinberg *et al.*, 2007). Hap-Tel is a prototype of a dental simulator designed in collaboration with the dental school of Kings College London (Tse *et al.*, 2010). An evaluation method is introduced by experts identifying the key factors to considerate based on the needs of dental training. Moog Simodont is a commercial product developed for dental simulations and robotic surgery (Moog, 2018)

An important method to evaluate the usefulness and effectiveness of the dental simulator is to compare the results with traditional dental training courses. Researchers in the Netherlands conducted an experiment with Simodont system to study if the skills gained from training with haptic assisted systems can be transferred to the real world. 28 students participated in the experiments were divided into 3 groups, trained with Phantom devices, with the Simodont system and with the traditional training. The performance was monitored and recorded before and after the training. The results illustrated that the performance of the students in all groups have improved knowledge and skills after the training regardless what training methods they were using. Therefore it's concluded that the Simodont system can help trainees gain the skills that are applicable in reality (Bakker *et al.*, 2010).

As an influential researcher in the area, D. X. Wang et al developed an intergated

dental simulator with haptic assistance called iDental (D. X. Wang *et al.*, 2012a)). The simulator aims to help students gain the necessary knowledge of the procedures for Periodontics surgeries. For the evaluation of the effectiveness of the simulator, a new method is developed concerning the construct validity. The term 'construct validity' is a concept introduced as an assessment tool in clinical education by Norman and Neufeld (Norman and Neufeld, 1985). A score based on construct validity can show the performance and skills of the participant. Therefore, D. X. Wang invited two groups of participants, both experts and training students, to conduct experiments with the simulator. The construct validity based score is used to illustrate the difference between their performance. This way the usability and reality of applying the simulator assessment in real life can be verified.

2.3.6 Haptic in Maxillofacial Surgery Simulation

An early proposed design for an orthognathic surgery simulation using a haptic device was made in 2004 (Sohmura *et al.*, 2004). The simulator of maxillofacial surgery for jaw deformity was developed with the tactile perception provided by a haptic device. CT images of the patients were used to build the 3D model in virtual reality interface. In the simulation of the surgical procedure, the virtual ramus and maxilla were separated and rearranged. Another simulator called Virtual Reality maxillofacial surgery (VR-MFS) was constructed by Wu *et al.* (Wu *et al.*, 2014). The haptic device was manipulated by the user for surgical procedure in the virtual interface, and the force model was calculated from regression equations. A 3D stereo visual effect was implemented in the system to provide an immersive experience. In this way, the visual and tactile sensations were integrated in order to improve the reality of the simulator.

A novel haptic model (XT Yan *et al.*, 2012) was built that a user can use as a virtual cutting tool to cut a slice of maxillofacial bone off. When the tool attaches to the slice of bone that needs to be cut, a slice of the same thickness can be mimicked with the cutting tool and the tool can be moved and dragged until the piece of bone is no longer attached to the main part. This simulates the cutting process as a

removing procedure of a targeted area. Although this model and the haptic feedback is not as complete as that from a triangle mesh and voxel model however, it is far more computationally efficient and has less time lag. As a result, the user experience has been improved. Therefore, this simulation method of the cutting procedure is used for further investigation in this research. However, the way in which the material properties of the bone have been modelled in this method may produce some challenges in some situation. Although mechanical properties have been considered, for example the cutting coefficient is calculated using Young's modulus and Poisson's Ratio, the values used for these properties are assumed and considered constant. In reality, these properties would vary throughout the various tissues within a bone and also from one patient to another. Schwartz et al argued that the direction of maximum stiffness, cortical thickness, cortical density and elastic properties for the dentate human mandible demonstrate unique regional variation. This model considers the mandible to be one component with consistent Young's Modulus and Poisons Ratio which is unrealistic and inaccurate for real life situations which therefore creates a less realistic force feedback for any given simulation.

2.4 Literature Review of Haptic Technologies in Space Robotic Path Planning and Tele-Operation

2.4.1 Introduction

Space robotic path planning and tele-operation require delicate and precise control. Space exploration is of great interest to humanity. Humans are compelled to explore the unknown. Space exploration can lead to a deeper understanding of the Universe and solar system, lending to scientific and technological advances. For many decades space exploration has caused divide and competition between certain countries (Lindberg, Longman and Zedd, 1990). Robotic systems play an important role in space missions. One significant way that robotic systems can improve and advance space missions is to reduce the hazard to astronauts from extreme temperatures and harsh radiation (Dubowsky, Torres and Ieee, 1991). Certain robotic systems can also reduce the cost of a space mission as they can be

less expensive than an Extra Vehicular Activity (EVA) system.

The typical space robotic applications include equipment transportation around a space station, providing service and maintenance to the instruments and payloads that are attached to the payload. As mentioned previously, astronauts can greatly benefit from the use of robotic systems in space. These can include capturing approaching targets, refuelling and maintenance of the satellites and capturing payload or space debris.

It is important to minimize the impacting force when capturing objects. This requires the end-effector of the robot to reach the same position and velocity as the target at the point of capture. A necessary requirement as, otherwise, damage to the robotic system or the target object could occur. It could also cause the target object to be pushed away or cause the disturbance to the base spacecraft.

In these working space scenarios, there exist more potential issues and challenges that need to be considered compared to those applications on Earth. One of the most important issues is to reduce the disturbance to the base while moving the manipulator. Although the position and attitude of the spacecraft can be controlled by the reaction jets, the use of this limiting fuel will reduce the lifetime of the system. Therefore, it is necessary to investigate path planning methods to minimize this disturbance to the spacecraft.

2.4.2 Redundant Space Robot Arm Path Planning

2.4.2.1 A Review in Space Robotic Path Planning

As previously mentioned, reduced reactions to the base result in higher energy efficiency and longer working life (Dubowsky and Papadopoulos, 1993). In order to solve the inverse kinematics of this problem two approaches have been taken to find a solution. Firstly, the kinematic approach, to minimize the disturbance to the spacecraft attitude according to the momentum conservation law. Secondly, the dynamic approach, aiming to minimize the torques and reaction forces to the spacecraft base.

2.4.2.2 The Local Minimization of the Spacecraft Attitude Disturbance Exploiting the Momentum and Angular Momentum Conservation Laws

A method to analyse the redundant robotic system in free flying mode was presented (Nenchev, Umetani and Yoshida, 1992). The analysis was based on fundamental momentum conservation laws and inverse kinematics is considered in order to make the end-effector follow the redefined path. Solutions have been given based on three different expressions of the manipulator: the inertia matrix, the Jacobian matrix and generalized Jacobian. The test cases have been defined as the spacecraft attitude control while path tracking the end-effector. Finally, a result that yields zero disturbances to the spacecraft attitude in the test case has been achieved.

In 2001 a closed-loop IK algorithms for redundant free floating manipulator was presented (Caccavale and Siciliano, 2001). Generalized Jacobian was used to solve the closed-loop IK for the tasks of space robotic system. In addition, to solve the problem of presenting both attitude of spacecraft and orientation of end-effector, unit quaternion, a non-singularity representation was used. Case studies with a six joints manipulator on a spacecraft were developed.

An on board experiment of an free-floating robot has been successfully conducted by Yoshida (Yoshida, 2003). It highlighted a manipulator control method using the concept of Jacobian matrix, which has been introduced and developed in the past year. In the experiments two modes were compared: the free-flying situation with attitude control system turned on and the free-floating robot without the attitude control system. As result, the free floating situation proved to be more suitable in the approaching phase due to its higher accuracy of the positioning of the end-effector.

2.4.3 Least Squares (LS) Based IK Solution

Recently an IK solution, based on Least Squares, to locally minimize the reaction from redundant manipulators to the spacecraft was proposed (Cocuzza, Pretto and Debei, 2012). The solution was tested experimentally on a 2D fixed robot although

it is also applicable to generally any 3D free floating robotic arm. The test robot has three degree-of-freedom, plus one degree of redundancy. To simulate the microgravity environment in space the robot was suspended by air bearings and fixed on the ground by a dynamometer to measure the force and torques transferring to the ground (Cocuzza *et al.*, 2005).

This IK solution is desirable for the following reasons. Firstly, the solution can take the physical and mechanical constraints of the robot, in terms of joints angle, velocity and acceleration into the algorithm of solution directly (Cocuzza, Pretto and Debei, 2012) (Y. N. Zhang, Wang and Xia, 2003) and still be able to avoid algorithm instabilities (O'Neil, 2002) (J. Park *et al.*, 2002). Secondly, when taking into account the constraints and limits the result is applicable to real-time solutions using recursive algorithm (Zhu and Li, 2007), solutions for Quadratic Programming Problem (QPP), which is more generally constrained (K. C. Park *et al.*, 1998) (Cheng, Chen and Sun, 1994) (Y. N. Zhang and Ma, 2007) (Xu and Wang, 2007) and solutions using neural network algorithms (Y. N. Zhang and Wang, 2002) (Y. Zhang, Ge and Lee, 2004) (Xia, Feng and Wang, 2005).

A solution for manipulators with multi DOF was proposed in 2011 (Cocuzza, Chiaradia and Debei, 2011) (Chiaradia, Cocuzza and Debei, 2011). While the concept of Zero Reaction Workspace (ZRW) being proposed (Cocuzza, Pretto and Angrilli, 2008b), a study using operational parameters which can maximize the ZRW of a space manipulator with multi-DOF was presented. A method using redundant manipulator to capture a non-collaborative target in space is proposed by means of (a) reactionless motion from the space manipulator, (b) the optimal control method of the path of end-effector, (c) Kalman filtering method that reduces measurement error of position, velocity and acceleration between manipulator and the target (Cocuzza, Cuccato and Debei, 2013). Moreover, the algorithm optimization for the proposed solution can also be applied to minimize the contact force and achieve kinematic control for rovers and climbing robots (Pretto *et al.*, 2008) (Artusi *et al.*, 2011).

A study of non-collaborative target capturing has been proposed by Cocuzza et al (Cocuzza, Li and Yan, 2016). Two novel methods for capturing a target with a redundant robot were proposed and compared. Null reaction torque is ensured to transfer to the spacecraft base. This result is advantageous compared to other state of the art capture methods, in which the capture and reaction minimization problems are separately handled and the integration of them is complicated.

2.4.4 Current Literature in Motion Planning with Haptic

Once the inverse kinematic and dynamic of the robotic system is solved, the next step is to find a method to assist the manipulation haptically. Similar motion planning methods have been developed not only for robotic manipulation but also to provide assistance to different interactive tasks such as hand writing, driving, and surgical training.

2.4.4.1 Spring Damper Model

A robotic Chinese handwriting “teacher” using a six DOF haptic device was invented in 2002 (Teo *et al.*, 2002). When considering the structure of a typical commercial haptic device such as Phantom, the way that the user holds the haptic device is very similar to holding a regular writing pen which makes it perfect for simulating handwriting. While being manipulated by the teacher for virtual writing, the trajectory and path of teacher were recorded. A virtual spring damping model would then be attached to make the learner follow the teacher’s path. The system has proven to be able to improve performance of beginners of the device.

A haptic guidance system for vehicle control was built in 2001 by Steele and Gillespie (Steele and Gillespie, 2001). Here, users were required to follow a straight path in the centre of a road and avoid the obstacles whilst driving a vehicle. Force feedback was provided to inform user of the desired path and obstacles and a visual display of the obstacles and path were shown due to the demand of user. As a result, compared to driving without force feedback, the haptic assistance largely reduced the user’s demand in visual display.

In these examples the main purpose of providing haptic assistance is for motion based training where the user can practice an operation following a determined path repeatedly. Also, the movements are relatively slow, therefore, a simple spring damper model with high stiffness is adequate for the guiding task.

2.4.4.2 Planning with Potential Field

For real time robotic control and manipulation tasks, a simple spring damper model may be useful for telepresence of obstacles or objects in an environment. However, they are not adequate for the task of path planning. For robotic path planning problems, applying an artificial potential field has long been utilized as a solving method. One of the earliest investigations into this method was introduced by Khatib (Khatib, 1986) where potential fields were assigned in real space. An attraction potential was set at the target position that acted on the Point Subject to Potential (PSP), which was placed at the end effector of the manipulator. Moreover, repulsion potentials were set around obstacles with PSPs placed on robot links and as a result, the target point will become an attraction pole to the end effector, whilst the obstacles perform as repulsion objects to the robotic parts. In this way, a free path can be obtained to the target position. Since this method further advances have been made, Newman and Hogan focused on impedance control of the manipulator using dynamic potential fields (Newman and Hogan, 1987). This method advanced the potential field method from path planner to motion controller.

Efforts also have been made to solve the local minima problem in potential field (Okutomi and Mori, 1986) (Warren, 1989). These investigations focused on manipulator path planning using potential field before the 'haptic age'. Hence, the haptic or force feedback had not yet been integrated into the method. The potential field method, itself, also has some limitations. The building of potential field requires the full modelling of an environment, meaning that all the obstacles information must be available at the time of planning. Also, since the whole environment is represented as a potential field, the end effector might move into

local minima and be trapped there instead of reaching the final destination. However, despite these limitations, the potential field method still forms an important foundation for later manipulation methods using haptic force feedback.

2.4.4.3 Virtual Fixture

To integrate haptic technology into the manipulating tasks, a more specific term 'Virtual Fixture' was introduced to describe this integration. The virtual fixture is defined as the position and force signals, generated by software, that are applied to the human user to improve the safety and accuracy in robotic manipulation tasks (Abbott, Marayong and Okamura, 2007). The term was first noted by Rosenberg (Rosenberg, 1993), at which time most other researches involving telepresence and remote manipulation focused on improving fidelity of interaction between user and environment to improve the user's performance. Rosenberg, however, wanted to investigate the possible benefit of adding virtual fixture as an abstract perceptual tool into the interface. He made a metaphor comparing virtual fixture with a ruler. If given a task of drawing a straight line without a ruler, the human operator will require focus of the vision system, precise control of hand motion and interaction between them in real time throughout the whole procedure. However, if the user was given a ruler the task seems much easier. The task is still achieved by the human user, however with a high probability of taking less and a better overall performance. The mental processing ability of the user can be saved to be used in other situations or emergencies in the task. According to the uses of virtual fixture, it can be classified into two different types: the guidance virtual fixture (Kuang *et al.*, 2004) and forbidden region virtual fixture (Payandeh and Stanisic, 2002). As the name suggests, the guidance virtual fixture helps a user follow a planned path, while forbidden region virtual fixture keeps the user out of a strictly constrained area. This classification was later updated to the term 'regional and guidance' active constraints from the outcome of a survey in virtual fixtures (Bowyer, Davies and Baena, 2014). The guidance active constraints, or guidance virtual fixture, may include two more specific terms: the attraction and repulsion active constraints. The attraction active constraints drive the user towards the constraints, whilst the

repulsion active constraints drive users away from the constraints. Bowyer also classified the constraint types according to literature, including point, linear, parametric curve, plan, parametric surface, or even polygonal mesh. Regardless of the different types, uses or classifications of virtual fixtures or active constraints, the methods to deploy them in the interface are essential either with potential fields or spring damper models. Attraction potential fields are used to achieve attraction guidance constraints and the strict regional constraints are formed by spring damper models. For the modelling of an obstacle in manipulating and path planning tasks, repulsion potential fields are placed around the obstacle to achieve the repulsion guidance constraints. When contact with a surface is made or even upon continuous moving into an obstacle, spring damper models are used to show regional constraints. Different methods utilizing virtual fixtures in manipulating applications have been developed since then. A vision based virtual fixtures generating system for robotic teleoperation was presented by Selvaggio et al (Selvaggio *et al.*, 2016). Stereo cameras are used to provide accurate environment information which is essential to build the potential fields. Turro was one of the first researchers to apply the virtual fixture in robotic manipulation (Turro *et al.*, 2001). He assigned the virtual constraints to specific robotic geometry constraints, such as robot's joints limits, workspace limits and singularities. Constrained movement such as following a curve or surface was also implemented with potential field. A six DOF haptic rendering for teleoperation was introduced by He and Chen (He and Chen, 2008). The six joints of a virtual robot were mapped and coupled to a six DOF haptic device, rather than three DOF. Path following tasks were also accomplished with virtual constraints. However, the path following control in these researches was not dynamic. These virtual fixtures can only guide the user following the desired path constrained by position but not by velocity which means that it is not adequate for manipulation tasks that require control of velocity during the path such as object capturing.

2.4.4.4 Control Method

In a teleoperation task, the user controls a haptic device as a master robot and a

real or virtual slave robot will move in the environment following the command. The robots used in the system can be classified into two different types: impedance or admittance (Adams and Hannaford, 1999). Impedance and admittance were originally concepts to describe the relationship between voltage and current, however they have been integrated into robotic control methods to describe the dynamic relationship between manipulator and the environment (Hogan, 1985). Hogan described the motion of manipulator as a result of energy transfer. The energy in the system was classified into two different types: effort (force/ torque) and flow (velocity). The system that takes effort as input and transfers to the flow is defined as admittance. The impedance system takes flow as input and transfers to the effort. The impedance robot is back drivable, such as the typical haptic device. The admittance type robot is a non back-drivable such as a normal industrial robot without force/torque sensors at the actuator.

2.4.4.5 Look Ahead Methods

To improve the performance of haptic guidance in dynamic tasks, a predictive guidance method was presented by Forsyth and MacLean (Forsyth and MacLean, 2006). Forsyth questioned how strong the guidance should be or how much is necessary. If the guidance force is too dictatorial giving no compromise to the operation from user then there is no point on bringing the human user into the control loop. Forsyth suggested that in a haptic cueing motion control, both the performance and user's preference should be respected to ensure the absolute control from a user. Also, to improve the usability of the haptic guidance, these guidance fixtures should be gradually introduced instead of abruptly. To achieve these goals, a look-ahead algorithm was used adding to the ordinary potential field method in a one DOF guided steer driving scenario. The current position and velocity of the vehicle were used to calculate the predictive position in the following period of time. If the predictive points are out of the planned path then guidance force will be introduced to make a desired change in direction in advance. In this way, the user can experience the gradually changing guidance force and avoiding the sudden and strong force change that could be dangerous in a high speed driving

control situation.

Although this predictive method was introduced in a one DOF steered control scenario, it inspired other for researchers in the field of haptic guidance in robotic manipulation. A haptic path planning for assembly task adopting this method is was design by Ladeveze et al (Ladeveze,Fourquet and Puel, 2010). Path planning algorithms such as the A star method were used to determine the path for a specific assembly task, and then a “following zone” was assigned along the calculated path. While entering the following zone, a predictive control was applied by deploying a calculated mean of attraction force to reach the successive target points. If the system detects that the user rejects the given path by a specific manner, the current force guidance will be ceased and an alternative path solution will be calculated. This allows the complete control from the user.

2.4.4.6 Task in Space Environment

For the use of a haptic system in space related tasks and research, many inspiring contributions have been conducted by NASA (National Aeronautics and Space Administration), ESA (European Space Agency) and DLR (German Aerospace Center) (Artigas and Hirzinger, 2016). Most focus on the teleoperation of space telerobot using force feedback. One of the researchers investigated the bilateral control of a robotic system for on-orbit servicing (Artigas *et al.*, 2016). Latency was considered in the bilateral controller to overcome delays in communications. Here, the robotic system was set to free floating mode for simulation in space environment. The force feedback was utilized to achieve delicate bilateral control of the slave robot. However, other haptic virtual fixtures such as constraints or guidance were not considered in these teleoperation tasks.

A haptic experimental kit called Haptics-1 was developed by ESA (A Schiele, 2015) (A. Schiele *et al.*, 2016a). Haptics-1 is a one DOF joystick controller with force feedback. It was launched to the International Space Station (ISS) in 2014. Working with NASA and astronauts, various sets of experiments have been conducted on the Earth and in orbit, such as feeling and exploring the virtual shape and objects in

haptic interface. The purpose of the research was to study how astronauts react to haptic force feedback, including tactile force and vibrations, in micro-gravity space environment comparing to that on Earth. Later, an extension of this work was developed by ESA called Haptics-2 (Krueger and Schiele, 2015) (A. Schiele *et al.*, 2016b). Two similar haptic joystick models were connected, one on-board the ISS and one on Earth. The two models were controlled by an astronaut in orbit and an expert in Netherland respectively. The sensation of this experiment resulted in the astronaut and expert on Earth feeling like they were shaking hands with each other. This research aimed to study the astronaut reaction to the feeling of force that comes from thousands of miles away.

Exoskeleton is another approach. Two prototypes of wearable exoskeleton systems with haptic features have been developed by ESA (Rebelo *et al.*, 2014) (A. Schiele, Hirzinger and Ieee, 2011). The Space Exoskeleton Controller (SPOC) and X-Arm-2 Exoskeleton are master haptic devices that can reflect the force feedback to user's right arm. They have between 8 and 14 actuated joints to achieve bilateral teleoperations in human-robotic space exploration tasks.

2.5 Knowledge gap

2.5.1 Discussion of the Dental Review

A thorough investigation of haptic applications in medical fields reveals the knowledge gap identified in Table 2-2.

Table 2-2 Knowledge gap in mandible surgical planning

	Researches	Modelling of tooth	Modelling of jaw bone	Force modelling	Computing efficiency	Selection of tools	Force constraints /guidance	Consider the properties of material	Record the procedure	Use in maxillofacial deformity operations	Evaluation method
Bone Cutting	McNeely			x							
	Agus	x		x		x					
	D Wang	x	x	x	x	x					
	D. X. Wang <i>et al.</i> , 2003	x	x	x	x						
	D Wang <i>et al.</i> , 2005										
Dental Implant	Kusumoto		x	x	x	x					
	Arbabafti	x	x	x	x	x					
	Q Wang <i>et al.</i> , 2012b	x		x		o					

Dental Simulators	PerioSim	x		x					x		x
	Hap-Tel	x		x			o		x		x
	Simodont	x		x			o		x		x
	iDental	x		x			o				x
Maxillofacial	Troulis		x							x	
	Sohmura		x	o						x	
	Wu		x	o						x	
	Yan		x	x	x					x	

o: proposed but not implemented/partly implemented

x: proposed and implemented

Many inspiring works have been conducted in the study of haptic surgical planning systems including the 3D modelling of a jaw bone, visual solution of the material removal and force calculation. However, further development of these methods is necessary to successfully meet all the requirements needed for surgical procedures, particularly for maxillofacial deformity surgical planning with haptics.

From the above table it can be seen that the properties of bones in specific area, specifically for maxillofacial surgery, is not considered in current approaches. Also, the compromise between the quality of the model and the efficiency of computing still needs to be improved. Force guidance features should be integrated into the system to assist the user to follow the desired cutting path. This can be achieved using virtual constrains.

Finally, for a planning system, the monitoring and recording of the procedure, the collecting and analysis of the result data are also important functions. These features will be used to achieve one of the key purposes of the planning system, evaluation of the operation, to give feedback and improve the performance. Only in this way a planning system can be completely built.

Above all, there has been no research undertaken to design a haptic planning and training system for dental surgical students to learn how to work with complex operations and to be trained to master hand skills before operating on real patients.

2.5.2 Discussion of Space Path Planning and Haptic Manipulation

A thorough investigation of haptic applications in space path planning and haptic manipulation task reveals the knowledge gap identified in Table 2-3

Table 2-3 Knowledge gap in space path planning and haptic manipulation task

Type of systems	Authors		Virtual fixtures						
Features		Haptic	Telepresence	Constraints	Guidance	Predictive	Dynamic control	Bilateral control	Space environment
Non robotic	Teo	x		x					
	Steele	x		x					
	Forsyth	x				x	x		
Potential field	Khatib								
	Newman								
	Okutomi								
Haptic	Rosenberg	x	x		x				
	Kuang	x			x				
	Payandeh	x			x				

	Bowyer	x	x	x	x				
	Selvaggio	x	x	x	x				
	Turra	x	x	x	x				
	He	x	x	x	x				
	Abbott	x		x	x		x		
	Ladeveze	x		x	x	x	x		
	Artigas	x	x				x	X	x
	Schiele, 2015	x	x	x					x
	Krueger	x	x	x				x	x
	Rebelo	x	x	x				x	x
	Schiele, 2011	x	x	x				x	x

For the path planning in specific spacecraft capturing task, a least square based inverse kinematics solution was presented (Cocuzza, Li and Yan, 2016). A redundant robot was used to capture the non-collaborative objects while transferring null torque reaction to the base station. It shows great performance with respect to some of the existing state of art devices available.

Haptic assisted methods in human-machine interactive manipulation tasks are concluded. Different terms such as virtual fixture, haptic guidance and active constraints are used to describe the use of haptic in telepresence and teleoperation scenarios. Regardless of what terms are called or used, two basic models exist: potential field and spring damper are always utilized for the implementation of the force modelling. However, to provide a clear and helpful instruction for the haptic system design, a systemic classification of these haptic assistants should be built according to their natural properties and usages.

Finally, for the haptic control of a space robot in capturing tasks, current methods using haptic guidance still need to be improved. The nature of the capturing task requires the end effector reaching the target position at desired velocity in a limited time and distance which increases the difficulties encountered in the dynamic control. The space environment brings new challenges. There are more limits and constraints on joints velocities and the force/torque should be considered in control methods. In addition, the balance point between 'dictatorial and suggestive' of the haptic guidance should also be found for the good performance.

Chapter 3: Review of the Design Process of Mechatronic Systems

3.1 Introduction

In this chapter, the design methods and research methodologies for engineering design are discussed and then selected for this investigation. Firstly, French's conceptual design for engineers is presented (French, 1985), followed by a methodology for mechatronic design developed by Yan and Zante (X. T. Yan and Zante, 2010). Based on these models, a comparison has been made, and then a suitable methodology for research questions, research aims, and objectives of this investigation was determined. This methodology was adopted throughout the entire process of the research, from concept design, system development, experiments and onto the final evaluation.

3.2 Design Process

The term "design" can be either a noun or verb, referring to a process of "Plan or Decide upon the look and functioning of (a building, garment, or other object), by making a detailed drawing of it" (Oxford, 2018). The meaning of design and design process have been defined and interpreted by different researchers according to their research background in the past.

One of the descriptions of design process is given by Archer (Archer, 1971). Archer described design as a process of generating ideas of a product or system and forming the idea in embodied expressions. Roozenburg, Eekels and Hurst described design as a process of design solution generating in order to satisfy the requirements of the customer and solve the problems (Roozenburg and Eekels, 1995) (Hurst, 1999). In this process the use of computer aided design systems are considered by analysing the activities of problem solving. Suh, described design as a process of generating a solution in terms of processes, products and systems to meet the needs and satisfactions of clients (Suh, 1990). The functional requirements are mapped in the functional domain and the design parameters are properly

selected in the physical domain. These descriptions can be summarised as a solution generating and selecting process to satisfy the customer requirements. Therefore, in this investigation the design process should generate solutions by mapping the haptic functional requirements and parameters of design requirements in the form of an embodiment system. Hence, the design process models containing a detailed solution and function creation will be discussed and proposed.

3.3 Design Process Model

Several design process models for engineering systems has been introduced in order to improve the understanding and application for the engineering design. Three of these design process models of the main contributions are shown in Figure 3-1 (Pahl *et al.*, 2013) (Dym and Little, 2000) and

Figure 3-2 (French, 1985). These contributions of design process models provide a foundation for the engineering design with systematic phases and approaches. Several different stage phases in the design flow and design outputs are interpreted in these design process models. For example, a classic design concept model for engineering can be found in the book written by French (French, 1985). A block diagram in

Figure 3-2 shows this design process. In French's model, design starts from a need followed by conceptual design, embodiment of schemes and detailing which ends with the output such as working drawings that allow design to be validated. The term scheme in this process refers to products that are made during the conceptual design stage. It should be noted that there is no "evaluation" block in this design process, as it is believed by the author that evaluation should be conducted consistently during the whole procedure, instead of being regarded as a final stage.

Although the specific design flow in different design process models may have different terms and interpretations, there are basically four stage phases that can be found in all design process models: Task specification, Conceptual design, Embodiment design and Detail design.

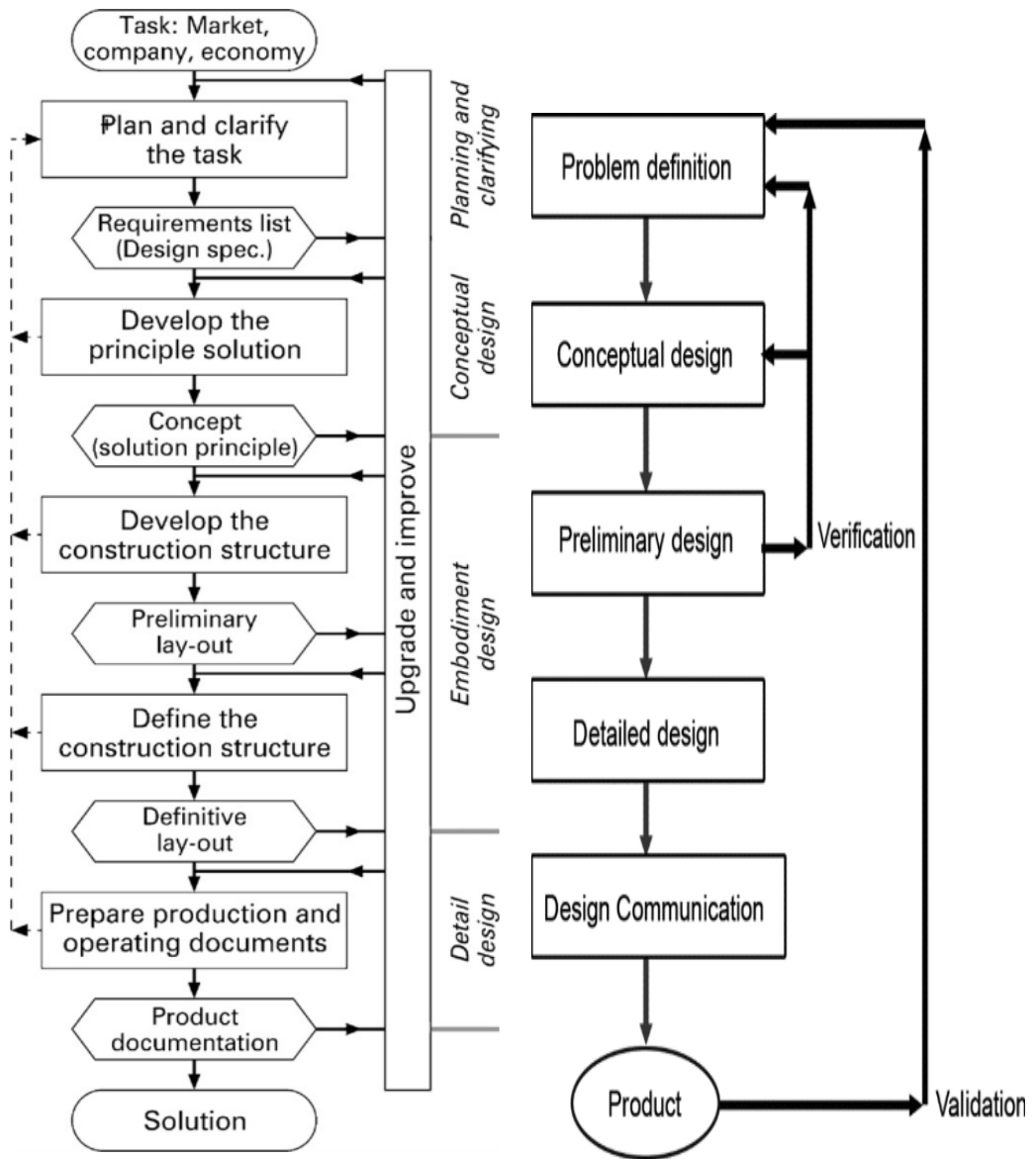


Figure 3-1 Design process models (Pahl *et al.*, 2013) (Dym and Little, 2000)

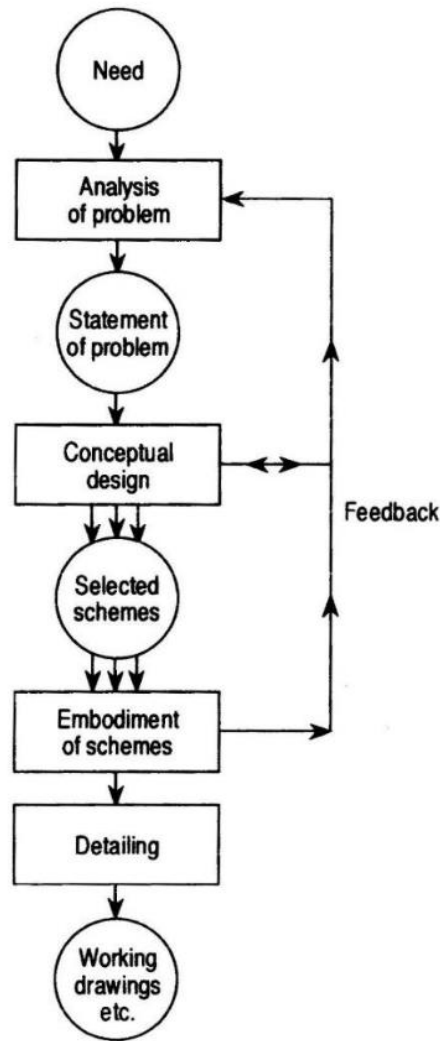


Figure 3-2 Design process model (French 1999)

3.4 Design Concept Methodology for Mechatronic Systems

A model of a design process for a mechatronic system has been proposed as shown in Figure 3-3 by Yan and Zante (X. T. Yan and Zante, 2010). Based on French’s model, the specific needs for a mechatronic system design are addressed in this model. Furthermore, this model also introduces the principles of current engineering design using knowledge of lifecycle mechatronic systems to support the concepts. Thus, the model can provide a comprehensive solution to a specific given design problem in a mechatronic system. There are three key stages including:

1. Market research.
2. Conceptual design.

3. Embodiment/detail design.

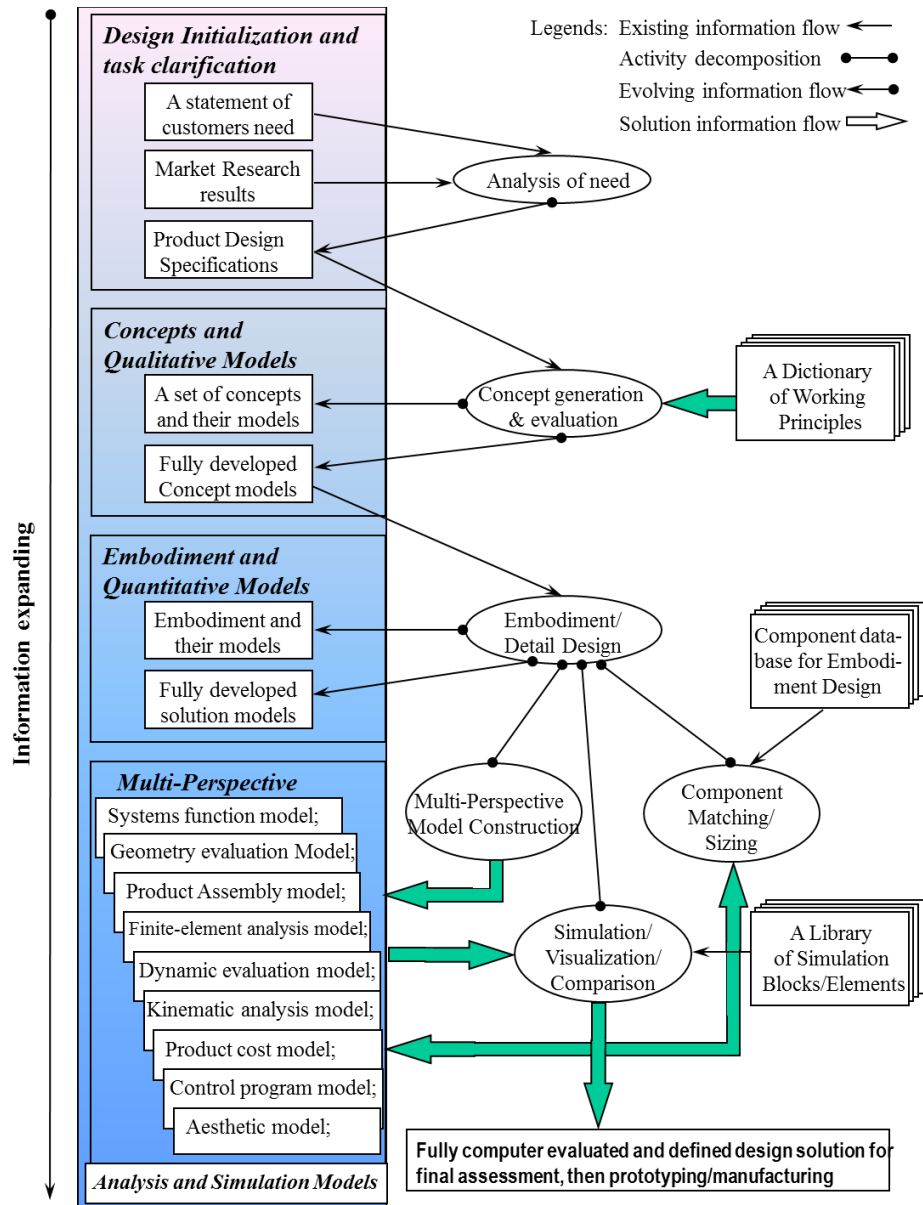


Figure 3-3 Yan's mechatronic system design concept (X. T. Yan and Zante, 2010).

The Market research stage analyses the need and requirement of the product, it also clarifies the initial task. Conceptual design stage develops the concept and qualitative model. The final stage, embodiment design, not only generates the detailed and quantitative model but also performs the simulation of the product through several mechatronic techniques and tools.

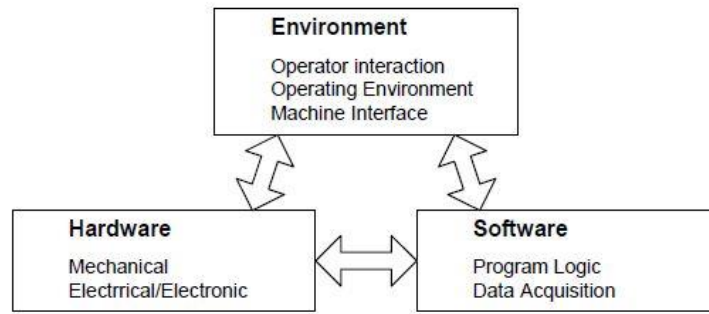


Figure 3-4 Interrelated relationship in a mechatronic system.

Figure 3-4 shows the interrelationship of hardware, the software and environment in a mechatronic system. The name of “mechatronic”, which is a combination of “mechanical” and “electronic”, suggests that it is an interdisciplinary system integrated in nature. Therefore, to develop a design concept for a mechatronic system, it requires the understanding of the user, function requirements, control system and interaction of different systems and their subsystems. Haptic systems, which are investigated in this study, is a perfect example of a mechatronic system. It acquires forces from the interaction between the human and the environment, it calculates forces and updates the geometric model through the software. It then applies this force and movement onto the hardware. Therefore, this design process model for mechatronic systems is adopted as a design concept methodology for this investigation.

3.4.1 V-Model

A design methodology for mechatronic systems in the form of “V-Model” is illustrated in Figure 3-5 (Tamre and Sell, 2005). The V-Model was first introduced as a process model for software development (Bröhl, 1995). The model has been developed as a design guideline for mechatronic systems by German Association of Engineers (VDI), aiming to provide a systemic method for cross domain design in mechatronic systems. One of the features of this V-Model is the ability to distinguish between system design and system integration. The lifecycle of design starts with requirement specification, which results in a specification of the desired behaviour and functions of the design product or system. It continues to the system

design, which includes mechanical, electrical and electronic engineering in the system architecture. Lastly, the system integration is carried out with continuous performance checks to validate and verify the resultant system's properties with those that were desired at the beginning.

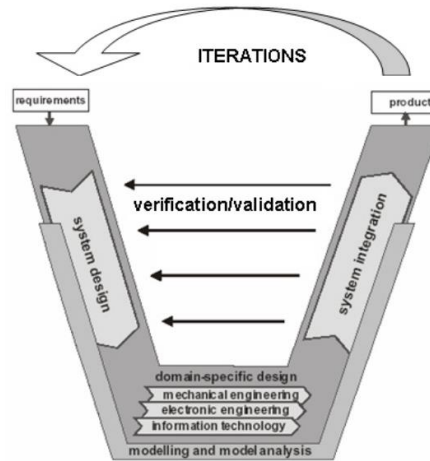


Figure 3-5 V-Model

3.4.2 Complex System Engineering(CSE)

In 2017 a Tiv Model was developed as design methodology for Complex System Engineering (CSE) as shown in Figure 3-6 (Melville, Yan and Gu, 2016). The aim of the Tiv Model is to provide more efficient and effective design guidelines for researchers and engineers in the design of complex systems such as those encountered in the aerospace and satellite industry. In the complex system engineering, designers often experience a lack of information resources to obtain the necessary knowledge. Therefore, the Tiv model suggests a multi-disciplinary knowledge base of the required knowledge and information for the mechatronic systems. It also follows then, that tracking and documenting the necessary knowledge is an important step in the design process.

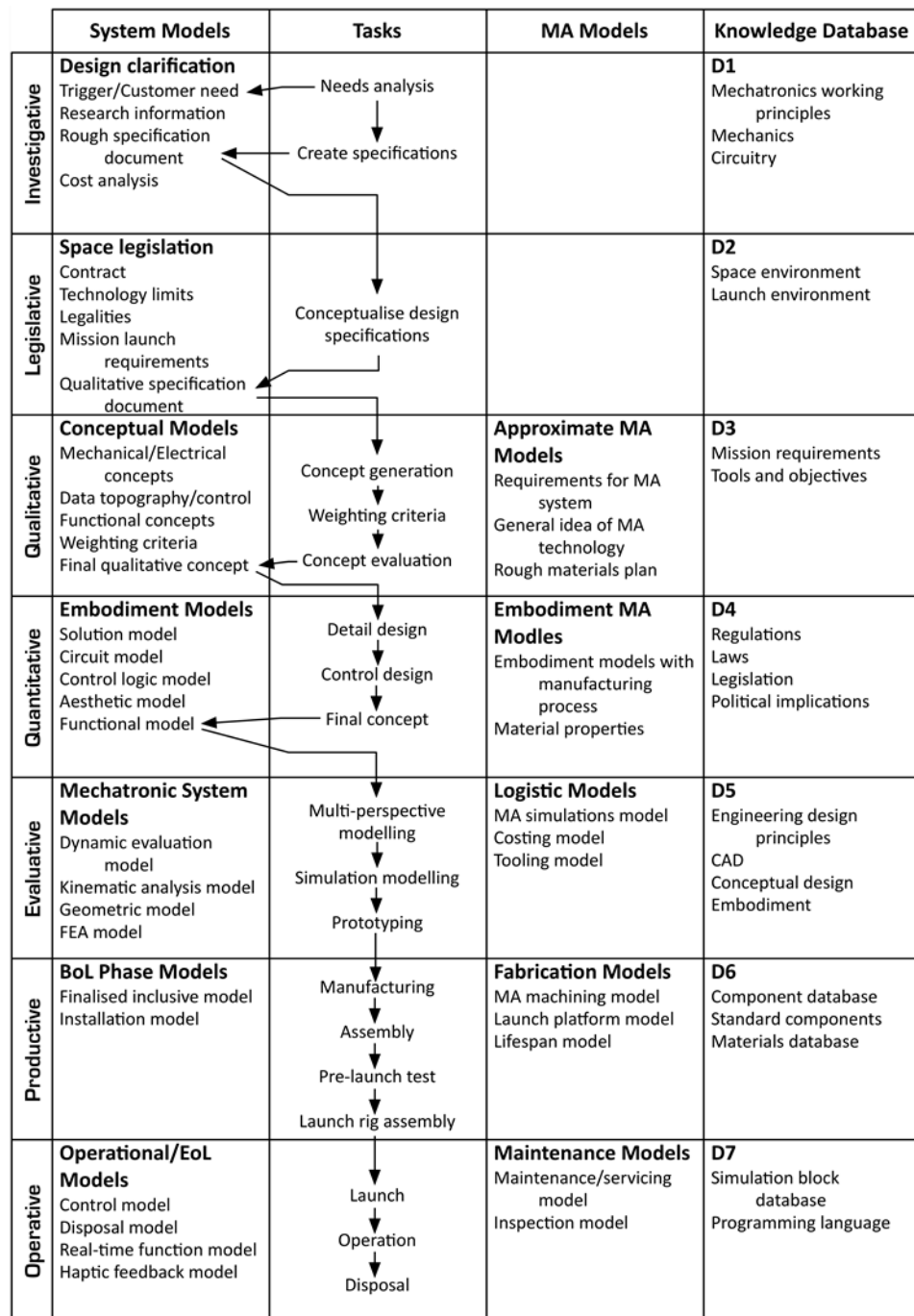


Figure 3-6 Tiv Model (Melville, Yan and Gu, 2016)

3.5 Digital Twin

A concept of “Digital Twin” was introduced in mechatronic system design as a simulation phase to handle its complexity (Boschert and Rosen, 2016). The term was first proposed by NASA in its future roadmap for technology that indicated the challenging directions for modelling and simulation (Shafto *et al.*, 2012). It was

defined as a simulation of a system, usually a vehicle or an aircraft, integrated with the available physical models, sensor information, etc., in order to mirror its physical twin. In mechatronic design, the simulation phase is becoming a core system functionality to support the operation along the life cycle. And the Digital Twin designed with principal structures can optimize the mechatronic systems and products during the development and operation.

3.6 Conclusion

In this chapter, the design concepts and research methodologies are reviewed and discussed. Firstly, the definitions and interpretations of the design process given by different researchers and approaches are introduced and summarised. Then several contributors to the design process models for engineering system are compared. Although the design process models from different researchers vary in details, there are generally four phases in common: Task specification, Concept design, Embodiment design and Detail design. Finally, the design concepts and functionalities specifically developed for mechatronic systems are introduced and compared. It is clear from the review that most of the design process models are intended for general engineering design, whereas some models such as the V-model are more specifically intended for mechatronic systems. And the term Digital Twin is used in simulation phase that supports the mechatronic design in whole life cycle. There is, however, no comprehensive design process model specifically designed for human haptic interaction system design, which can provide an interdisciplinary instruction for researchers and designers. Chapter 4 describes a proposed design process model specifically for haptic system design.

Chapter 4: HARMP Design Methodology

4.1 Introduction

In this chapter, a design methodology is proposed for a Haptic Assisted Robotic Manipulating and Planning (HARMP) system. The design process model is developed based on Yan’s model, previously discussed in Chapter 3, for mechatronic system design.

To meet the specific requirements of haptic systems in this study, a design concept methodology for mechatronic systems with haptic functionality has been developed as shown in Figure 4-1.

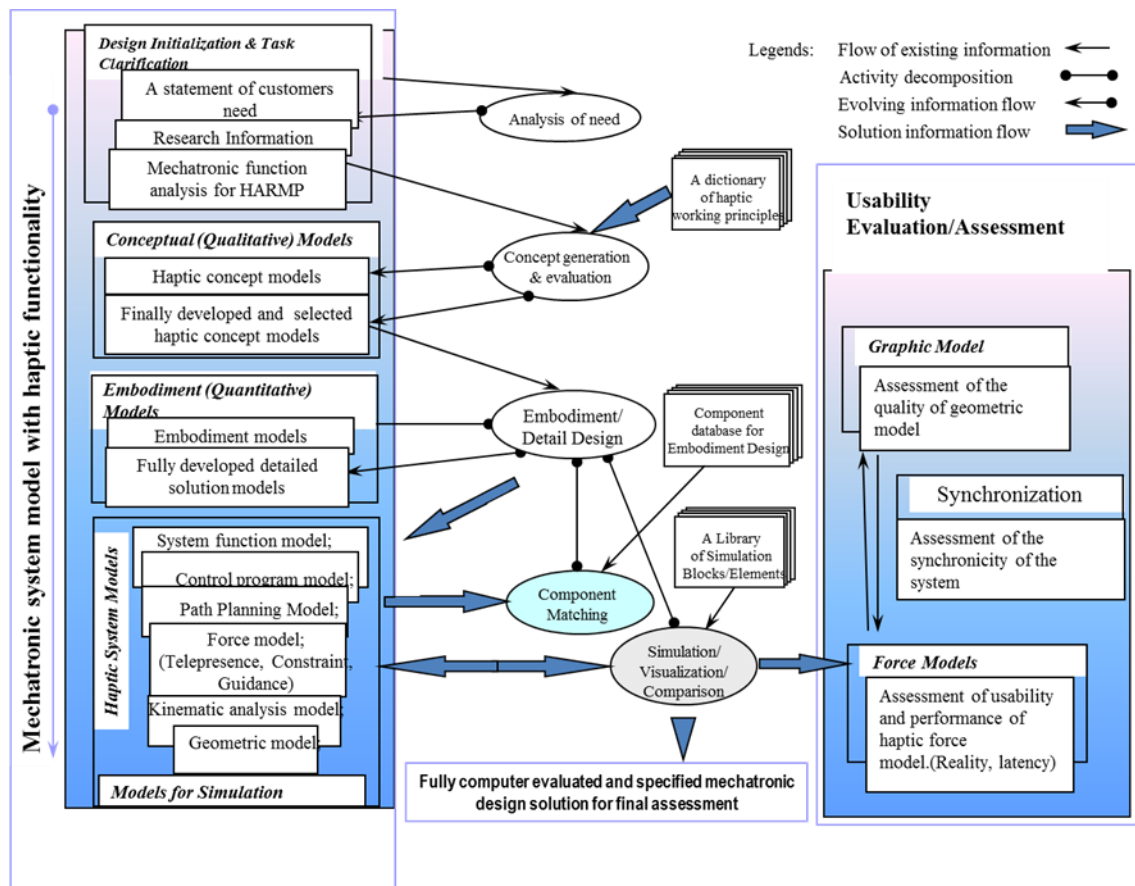


Figure 4-1 HARMP design model

Force modelling has been added as one of the mechatronic system models with haptic functionality, which is required based on the principles of haptic systems. Path planning models, which will use force models, is considered a key function of the

system. Final evaluation and assessment of the usability of the system is also included. As two key models in the haptic system, the geometric model and force model in the final product need to be evaluated.

This methodology, as illustrated in Figure 4-1, shows instruction of the design and evaluation process of a haptic mechatronic system. It should be considered in each step of this investigation thoroughly.

4.2 Haptic Design Process and Application of HARMP Methodology

Table 4-1 Haptic design process

Models	Tasks
Task clarification Inspiration, research review	Analysis of needs Requirements and specifications
Conceptual models Mechanical/Electrical/Haptic concepts Functional concepts	Essential problem abstracting Haptic function structure generation Work principle implementation Concept generation Concept evaluation
Embodiment Models Detailed functional models Software development model	Embodiment requirement identification Main functions identification Preliminary layout development and selection Detailed function design formation Control methods adoption
HARMP system models Control program model Path Planning model Force model Kinematics solution model Geometric model	Initial interface building System implementation Simulation testing
Operational models Models deployment	System validation Usability evaluation

As shown in Table 4-1, a Haptic design process and methodology for HARMP has been implemented. Tasks for each stage of the design process are specified and clarified. An operational model has been added to deploy the design models, validate the system and evaluate the performance.

4.2.1 Task Clarification

The hypothesis for this research is “Design of a haptic system, following a suitable design process model, can significantly improve manipulation operations in challenging environments”. Therefore, the tasks can be classified into different categories due to the nature of the requirements for their procedures, as any given task can contain one or more different task types. The first type of task is for virtual modelling, which is the most basic requirement for such haptic applications. In this type of task, the haptic assistance is supposed to help a user build haptic perception to understand the shape of object and their locations in the virtual space. This is the first step for almost every manipulating and planning tasks. There are also tasks for training purposes. For example, this can be the simulated training of a surgical procedure or simply teaching for handwriting. Haptic assistance in these tasks is supposed to help a user meet task requirements that strictly follow a desired path and pattern during the operation. The third type is the path planning during manipulation, which can be virtual assembly or teleoperation of a manipulator to reach a target. Users can have better understanding of the sequence and desired movement for the tasks with the help of haptic assistance. In these types of tasks, the haptic assistance is expected to be suggestive instead of strict.

4.2.2 Conceptual Design

In the conceptual design of the haptic design process, the first task is to abstract the essential design problem. This is concluded from the task clarification phase. The essential and primary requirements are identified from the full list of requirements. Thereafter, the function structure is built with haptic features according to these requirements. These functions can be reduced to sub-functions for less complexity. The working principle for the designed haptic system needs to be generated, which may be adopted from mechanical, electrical and haptic concepts. Therefore, a knowledge base and dictionary of these concepts are necessary to support the selection of the working principles. Finally, the working principle for haptic system design is confirmed, the haptic concept model is generated and evaluated.

4.2.3 Embodiment Design

The next phase is the embodiment design. The working principles and function structures are selected in the conceptual design phase before the design concepts can be confirmed. In the embodiment design phase of the haptic system design, the critical requirements and constraints for the embodiment design first need to be identified. These can be the determining requirements and limitations of the available hardware, such as which commercial haptic device is suitable for the haptic system. Finally, the initial layout needs to be finalised, one of which that is able to fulfil the main functions selected from the function structures. The main functions include training and manipulating with the provision of haptic assistance. The preliminary layout, including detailed function design, can be configured and selected according to its compliance with the embodiment requirements and constraints. The preliminary layout for remaining functions can be developed. Finally, the detailed layout and function design can be developed, confirmed and evaluated.

4.2.4 Force Modelling

Force modelling is an essential and critical part in the haptic system design. As concluded from the literature discussed in Chapter 2, different terms such virtual fixture (Rosenberg, 1993), (Abbott, Marayong and Okamura, 2007), haptic guidance (Turro *et al.*, 2001) and active constraints (Bowyer, Davies and Baena, 2014) are used to describe the integration of haptics in telepresence and teleoperation scenarios. A design method for haptic interaction, proposed by MacLEAn, (MacLean, 2008) suggested the use of precise force for position control, as well as guidance force for training and remote collaboration purposes. Therefore, to provide an instruction for the haptic system design, a systemic classification of these haptic assistants is constructed according to their nature, properties and uses shown in the following.

1. Telepresence: a) Shape b) Force model.
2. Constrains: a) Natural constraints b) Artificial constraints.

3. Guidance: a) Attraction b) Repulsion.

Three categories are concluded according to uses, which are: 1) Telepresence; 2) Constraints; 3) Guidance. Telepresence reconstructs and mimics the force encounters with the environment, including the shape rendering of objects or obstacles, collision detection and other force generated by environment, i.e., cutting or frictional force. Constraints are defined as hard guidance that the user must obey and follow, including natural constraints and artificial constraints. Natural constraints are the constraints that are defined by the structure and mechanism of the robotic manipulator, such as working space and joints limits. Artificial constraints are set according to the requirements of a specific task, such as following a desired curve path in a training system. The guidance is defined as a suggestive haptic assistant provided for the user, as opposed to absolute hard constraints, this type of haptic guidance can be attraction or repulsion. The attraction guidance can lead the user following a desired path, while repulsion guidance can be used to drive the user away from potential obstacles, trap area or singularities.

This instruction of force modelling can be useful in a haptic system design. Available haptic assistants can be selected for different objectives according to the requirements and specifications of the tasks.

4.2.5 Function Design Process

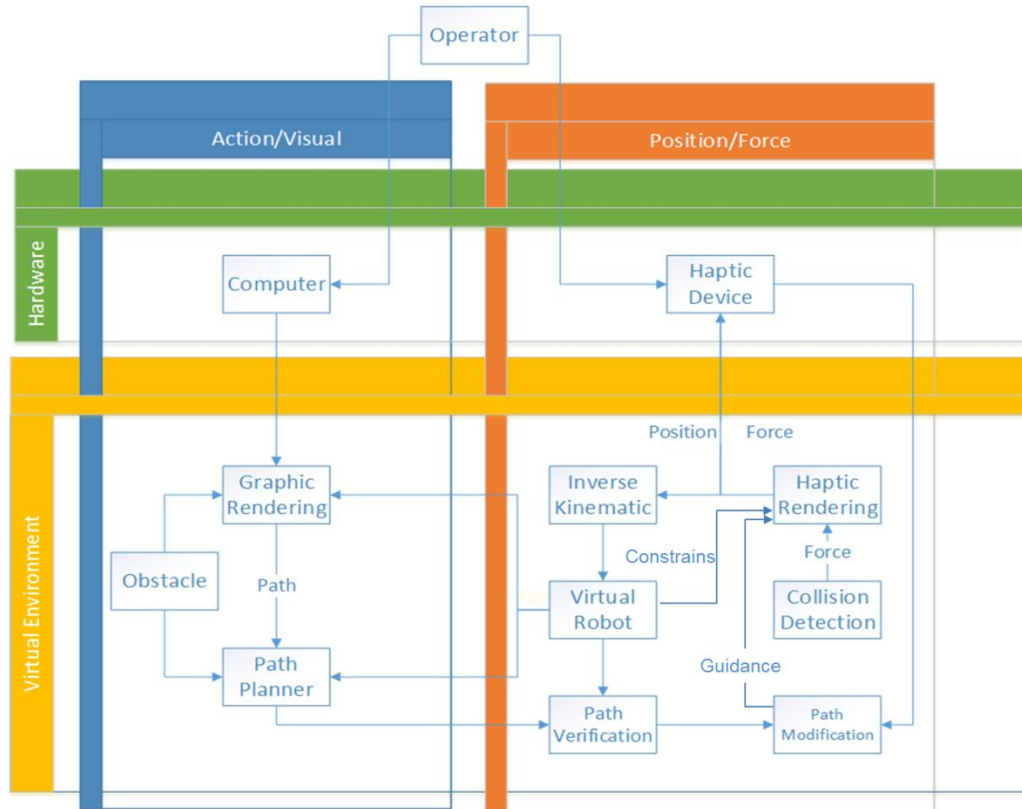


Figure 4-2 Schematic structure of a virtual haptic robotic path planning system

To formulate the functions in the HARMP system model, schematic structures for specific functions need to be developed. Figure 4-2 is an example. Figure 4-2 is a schematic structure of a haptic path planning system for robotics inspired on He's model (He and Chen, 2008). Here the hardware includes a computer and haptic device. Virtual environment of the haptic interface achieves graphical and haptic rendering of the model. Operators manipulate the haptic device, which gives the position into virtual interface to calculate the inverse kinematic of the robot and modify the path. This information will be used to verify the path, detect any possible collision and then update the geometric model. If the virtual robot reaches constraints, such as workspace or joints limits, this virtual constraint signal will be sent back to the device. If a collision is detected or the path is rejected, a calculated force will be sent back to the haptic device which can be felt by the user. The guidance force generated by the path modification scheme (attraction or repulsion) will be presented on the device as a haptic cue for a user to follow. This schematic

structure gives a control instruction to design a specific function in the HARMP system model.

4.3 System Validation

To build and validate the system model, three case studies are conducted in this research as shown in Figure 4-3. The first case study is to design a HARMP system for a dental surgery simulation. Surgical simulations provide a planning and training tool for trainees and surgeons. The first simulation application considered is for maxillofacial deformity surgery. The objective of this case study is to confirm the process of need analysis, concept design and embodied design, and initial building of the HARMP system. The haptic interface where the 3D model can be graphically and haptically rendered is introduced. The second case is to design a tele-operation system of a virtual robotic system which can achieve several different tasks. Based on the model built in the first case study, robotic kinematics is added into the system. A more complete force model is implemented to apply the virtual constraints and guidance assistance for path planning and dynamic control. The objective of this study is to confirm the modification of HARMP system, to build and validate the detailed and complicated force model. The third case is an experimental case study. The control model built in the second case is used to control a real industrial robot. Force information in the real environment is sent back to the user for the assistance of path planning. The objective of this study is to validate the design of a complete system, evaluate the usability and performance of the HARMP system.

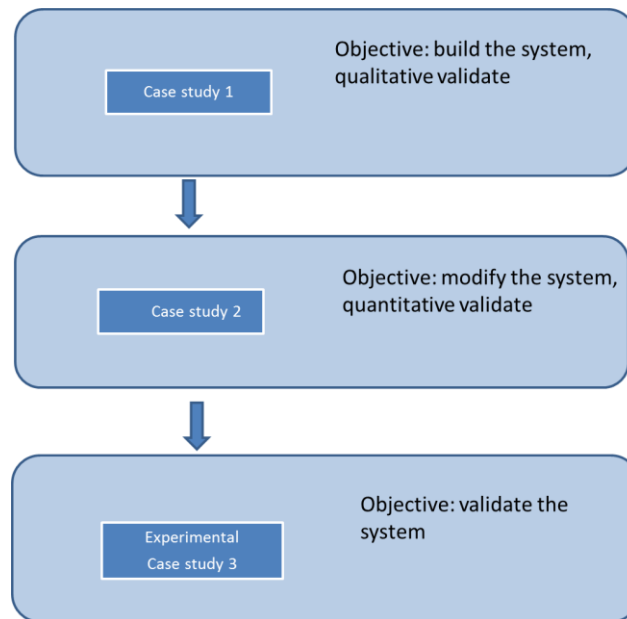


Figure 4-3 The method of validation

4.3.1 Evaluation

In French's design model (French, 1985) it is suggested that evaluation should be conducted constantly during the entire design process. After each stage of the validation in each of the three case studies the evaluation of the performance and usability of the system need to be conducted. Therefore, an evaluation methodology is required for the assessment of the HARMP system. The aim of the evaluation process of a system design is to answer the following three questions (Gediga, Hamborg and Düntsch, 2002):

1. "How good is it?"

This question aims to verify the qualities of the system and usability of the system functions.

2. "Which is better?"

This part is aimed to compare the developed system with the alternative systems or approaches to solve the given task and requirements and decide the best fitting one.

3. "What are weaknesses?"

This question is to identify the weakness of the system and find suggestions and developments for future work.

As for the evaluation criteria, the usability of the system refers to the user's experience regarding a defined task including efficiency, effectiveness and satisfaction. The resultant data are collected and classified into following criteria (Hix and Hartson, 1993):

Quantitative: Numerical data showing the result of system performance.

Qualitative: Non-numerical data such as list of suggestions and improvement that can be made for the development of the system.

In order to evaluate the usability of the HARMP system and the efficiency, effectiveness and satisfaction of its functions, the data in the above criteria need to be collected. Considering the main components in HARMP system, geometric model, force model and force rendering, the data to be collected for the evaluation of the HARMP system are identified and classified as the following:

Qualitative:

1. The quality of geometric model.
2. The reality of geometric model.
3. Reality of haptic rendering of the objects.
4. Usability of the haptic guidance.
5. Reality of the operation.

Quantitative:

1. Real time computed force.
2. Actual applied force/torque.
3. Usability of the virtual constraints.
4. Performance of the haptic guidance.

5. Position and speed error during operation.

6. Latency.

4.3.2 Evaluation methods

For evaluating the design methodology, due to the complexity and the time required for a full evaluation, it is proposed to use three case studies to validate the methodology. For the three systems designed, depending on the type of the systems, a suitable evolution methodology has been selected. Specifically, for surgical haptic planning systems, it is more appropriate to use the subjective evaluation method to assess its suitability by asking potential users to evaluate the system.

4.4 Conclusion

In this chapter, a mechatronic system model with haptic functions is derived based on Yan's mechatronic system design concept (X. T. Yan and Zante, 2010). This leads to the implementation of a haptic design process and methodology for HARMP system. All the research in following chapters will be guided by the methodology shown in Figure 4-1. Two case studies have been conducted. The first one investigates the design of a haptic system for training and planning of dental deformity surgery. A haptic interface is built, where geometric and force models are imported and implemented. The system is then qualitatively validated by comparing to surgical reality. This study tests the usability of the HARMP system design methodology and provides a basic platform for the following studies. The second case study targets the path planning and tele-operation of space robotic systems. In addition to the previous haptic interface, a path planning model is included. The system can then be quantitatively validated in regard to the accuracy of position and velocity in specific tasks.

After two case studies, an experimental case study is investigated. In the first two case studies, the operation and manipulation are conducted in the virtual environment. In the third case study, the control system used in the second case is

modified to control a virtual industrial SCARA robot model. In addition, a real SCARA robot is controlled by the manipulator, coupling with the virtual one. Therefore, the interaction between user and the real environment is constructed and studied. The usability of the system is evaluated.

Chapter 5: Dental Surgery Haptic System Development Simulation

5.1 Introduction

In this chapter, a haptic modelling approach for dental surgical operations is investigated. Here, high resolutions are required for the force feedback. In particular, the research focuses on maxillofacial deformity operations. The main aim of the research is to increase the realism of a computer model based simulation system that allows the dental students and surgeons to feel like they are conducting a real dental surgery procedure. A generic set of jaw bone models have been developed and have been validated by collaborating researchers from the Glasgow Dental School. The model can be customized and obtained for each specific patient. A chosen model can be used to control the force feedback generated by a haptic device to give a realistic force feedback representation and experience for the user of the system, which meets the requirements of the selected dental operations. The simulation forces are calculated based on the properties of bones, cutting tools used and the position of the cut. Using a haptic device as a controller, a user can perform relevant operations such as cutting procedures and manipulation of bone segments from the virtual jaw bone model. The haptic system generates the corresponding force feedback to the user as in reality. The validation and feedback experiments have been conducted to assess the effectiveness of the system in providing.

5.2 System Requirements and Specification

The success and accuracy of the maxillofacial deformity surgeries depends on good planning and analysis, which can be based on different diagnostic information.

Thus, the system built from these investigations is expected to meeting the following requirements:

Graphically:

1. Showing detailed 3D jaw bone model of patient before the surgery.
2. Update the 3D model in real time during the surgery, showing the cutting procedure.
3. Predict the result, showing the predictive 3D model after the correction.

Haptically:

1. Make user feel the presence of the object of target jaw bone, can touch to feel the detail, drag or rotate using the haptic device.
2. Simulate the force applied to the user during the cutting procedure.
3. Lead user through the planned path.

User needs:

1. Input data dicom.
2. Maximum feedback force: 10 N.
3. Required degree of freedom.

Table 5-1 Specification template

Specification category	Category attributes	Design parameter
Geometric model	Manipulation target	Jawbone mode: Input Dicom data from patient
		Cut into pieces during surgical procedure
	Manipulator Cursor	Cutting tool Showing the point of cut
Force modelling	Telepresence	Touch of Jaw bone
		Cutting force
	Constraints	Natural constraint
		Artificial constraint: Following cutting path
Force rendering	Force scaling	Scale matching Scale resolution
	Force actuation	Actuating force model on Haptic device
Environment modelling	Lighting condition	Lighting modeling in Haptic interface
Integrated knowledge library	Task procedure planner	Surgical planning and training procedure

5.3 HARMP Modelling for Dental Surgery

5.3.1 Concept Design

In order to achieve haptic modelling and planning of maxillofacial surgery, the Haptic Assisted Robotic Planning system has been built to meet the requirements. The planning procedures include viewing the 3D model of patient, running a simulation of the cutting process, evaluating the result and providing a planning and training environment using haptic devices. The architecture of the system includes a haptic device, in this case a Phantom Desktop, a haptic modelling interface where 3D models could be imported and located and a force engine to provide the force feedback to 1) simulate the cutting procedure; 2) to guide the user through the planned path.

5.3.1.1 Building of the Haptic Interface

In Chapter 3, the interrelationship between hardware, software and environment in

a mechatronic system is illustrated in Figure 3-4 (X. T. Yan and Zante, 2010). These three parts are critical in the design of a mechatronic system. Therefore, the hardware, software and environment will be identified and selected for the building of the interface of the HARMP system, illustrated in Figure 5-1.

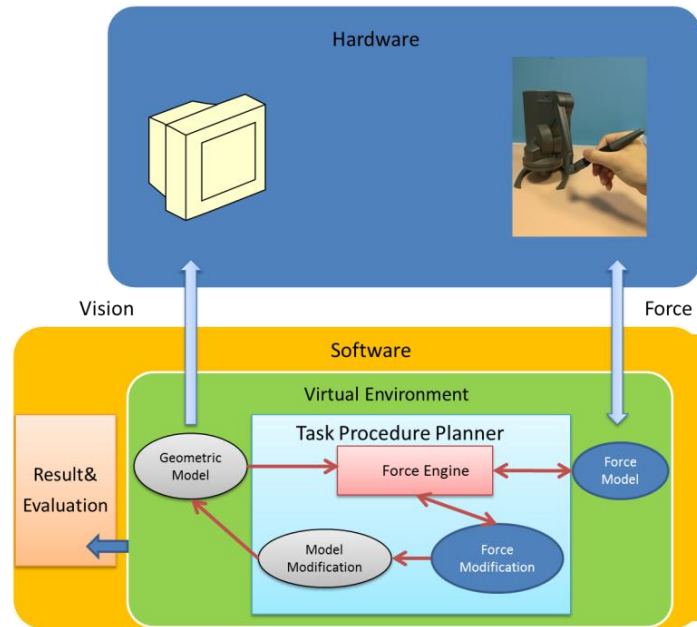


Figure 5-1 Proposed HARMP system architecture

5.3.1.2 Hardware

A computer and a haptic device form the hardware part of a simple haptic system.

5.3.1.3 Haptic Device

Types and models of haptic devices in the market are discussed Chapter 2. Phantom Desktop (Current Geomagic - Touch X) is used in this study as shown in Figure 5-2. Phantom Desktop is an affordable haptic device provided by 3D Systems.



Figure 5-2 Phantom Desktop (Geomagic - Touch X)

Table 5-2 Specifications parameters of Phantom Desktop. (Geomagic)

Workspace (mm)	160 (W) x 120 (H) x 120 (D)
Maximum output force (N)	7.9
Stiffness (N/mm)	Axis x: 1.86 Axis y: 2.35 Axis z: 1.48
Force Feedback (3 DOF)	x, y, z
Position input (6 DOF)	x, y, z, roll, pitch, yaw

The Phantom Desktop specifications are shown in Table 5-2. The maximum output force is 7.9N, the movement is six DOF including the position in Cartesian system by x, y, and z axes and orientation by roll, pitch and yaw joints. However, the force feedback it is able to provide is three DOF, only on x, y and z axes.

As shown in Figure 5-3, the base joints include Joint 1, 2 and 3. There is one motor built into each joint. Therefore, force and torque can be applied on each joint as a result of the output from motors, this can be achieved by the user through functions that control the current of the motors. In addition, digital encoders built into the joints give relative position information. Combining these three joints, forces on x, y, z axes can be applied and the position in Cartesian coordinates can be read.

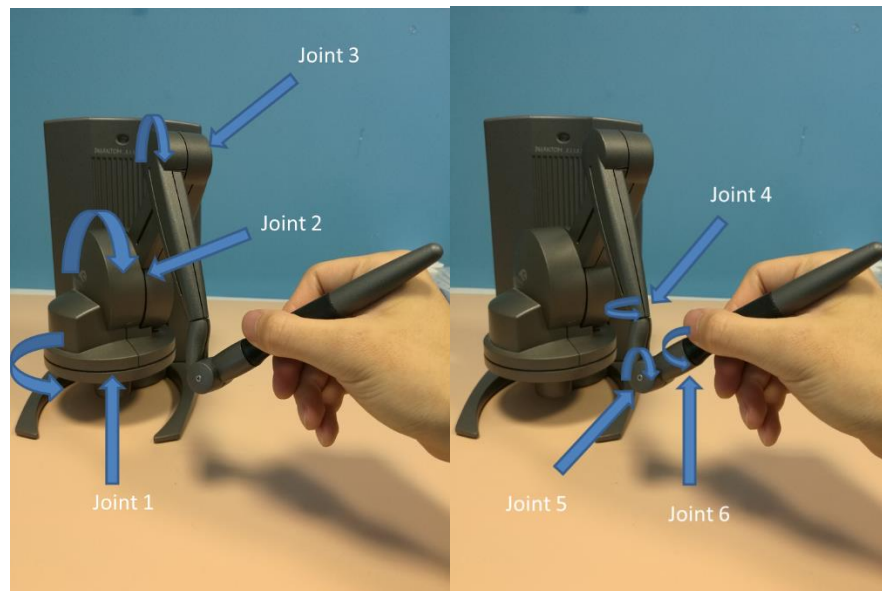


Figure 5-3 Base joints and gimbal joints of Phantom Desktop

Gimbal joints of Phantom Desktop include Joint 4, 5, and 6, which contribute to Yaw, Pitch and Roll of the system. In each joint a linear potentiometer is built to detect relative movement. Combining these three joints the orientation in the space can be applied and read. Since there is no motor built in these three joints, force and torque can't be applied which results in only three DOF of force feedback being provided by this device.

5.3.1.4 Computer

A powerful computer is needed in the system as large computational requirements are necessary to deal with geometric and force modelling and to communicate with the haptic device. In this study, a Dell Latitude E5540 with Intel i7-4500 and 16 GB RAM is used. The system is 64-bit Windows 7 Professional, which is compatible for most engineering software necessary for this investigation. The graphics card is NVidia GeForce GT 720M.

5.3.1.5 Virtual Environment

5.3.1.5.1. OpenHaptics

Along with the Geomagic haptic device, the OpenHaptics tool kit is introduced by

the same company (Geomagic, 2018a). It provides fundamental functions and components required to create a haptic environment. The implementation of the geometric part in the environment is based on OpenGL (Open Graphic Library).

OpenGL includes various libraries and functions. It's a cross platform API commonly used in applications to create computer graphics. It provides a group of simple shapes such as points, lines and squares. Some basic 3D object such as spheres and cubes can also be created. However, for the creation of more complex models, like a teapot, a set of simpler shapes and meshes need to be used and functions are called for construction. In OpenHaptics toolkit, OpenGL is used for defining geometric models and implementing algorithms for haptic rendering. The result shown on the screen is the 2D representation in OpenGL world.

The OpenHaptics toolkit itself mainly includes three APIs: the QuickHaptics API, the Haptic Device API (HDAPI) and the Haptic Library API (HLAPI). Also, utilities, Phantom Device Drivers (PDD) and example code are provided.

QuickHaptics, a pre-built micro API, is introduced in OpenHaptics 3.2. The idea is to provide an easier and faster way for user to build haptic programs or modify the existing program with the features of haptics. Some geometric models and default parameters are already integrated which helps reduce the length and complexity of code for users who may not be familiar with OpenGL or haptics.

The Haptic Device API (HDAPI) provides a low-level control of the haptic device as shown in Figure 5-4 and Figure 5-5. The forces are rendered and sent directly by HDAPI. This requires a good understanding of force modelling. Also, it creates scheduler call-back for the haptic device which allows commands to be entered in a servo loop to be performed.

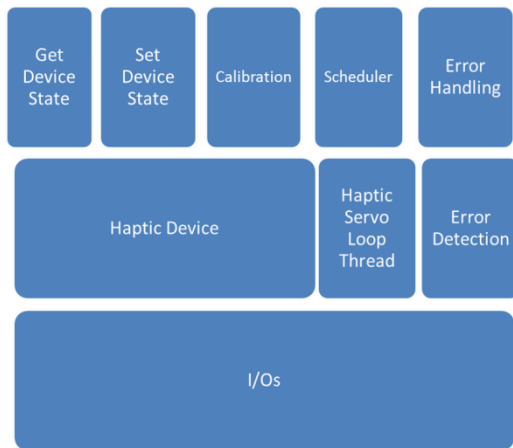


Figure 5-4 Structure of Haptic Library API

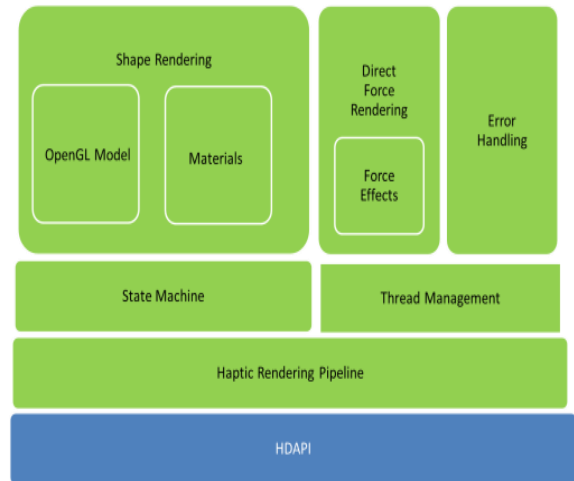


Figure 5-5 Structure of Haptic Device API

The Haptic Library API (HLAPI), as shown in Figure 5-4 is on the top of HDAPI, providing a high level rendering for haptic scenes. Users who are familiar with OpenGL can reuse the existing codes to render the haptic scenes. Haptic features such as friction and stiffness are assigned to materials of the graphic objects, instead of having to be calculated through force equations by the users themselves.

5.3.1.6 Relationship between QuickHaptics, HDAPI and HLAPI

As shown in Figure 5-6, the QuickHaptics is an integrated tool provided for users with in-built functions and a force/ graphic model. It reduces the amount of code needed in high level. Code is then “translated” in low level so that it can be suitably read and managed by HD/HL APIs, then the program can run on the HD/ HL functions.

5.3.1.7 Method Used in This Study

In this study, HD and HL APIs are mainly used for the construction of the haptic interface. QuickHaptics was not used for this investigation. HDAPI was chosen due to the complex and delicate force models that are necessary for in this study. Force equations can only be sent directly to the haptic device through HDAPI, similar to the reason why HLAPI is also suitable. Various types of geometric models need to be displayed, some of which are imported from complex medical scan models, while

others are built in CAD software with large amount of details. These models can only be handled by HLAPI. Therefore, a combination of HD and HL APIs for the development of haptic interface are used in this study as shown in Figure 5-7.

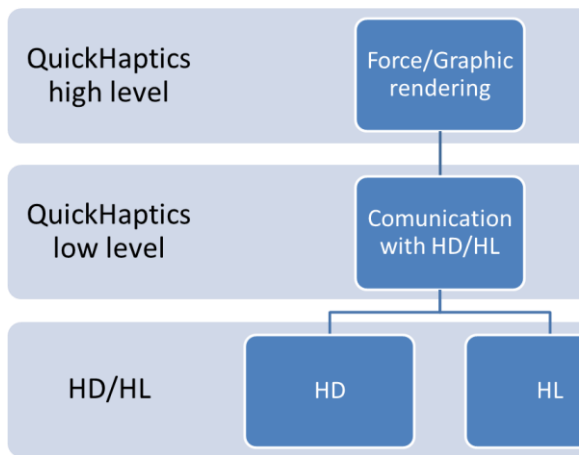


Figure 5-6 Structure of QuickHaptics, HDAPI and HLAPI

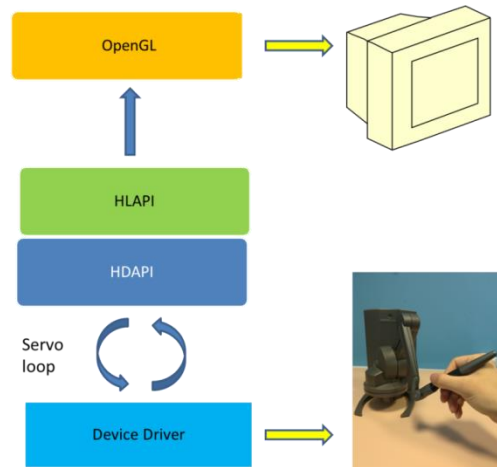


Figure 5-7 Structure of proposed haptic interface building method

5.3.1.8 Software

5.3.1.8.1. Microsoft Visual Studio 2013

The OpenHaptics toolkit is implemented in C++. The developer environment of Microsoft Visual Studio needs to be configured. The Microsoft Visual Studio 2013 is used in this study as the main programming, coding and debugging tool.

5.3.1.8.2. Engineering CAD Software

PTC Creo (ProE) software is chosen for this investigation to design and build the CAD model for the system. The Creo Parametric is a 3D CAD software widely used in design and engineering industry. It has features such as parametric design, part modelling and assembly simulation. The parametric feature allows united design for different parts. As long as the relationship between the assembled parts is assigned, if the parameter of one part needs to be changed, other related parts and features will change accordingly. Therefore, this software is perfectly suitable for part modelling of geometric system in this study.

5.3.1.8.3. CAD Rendering Software

Autodesk 3DS Max is CAD software for 3D modelling and rendering. Comparing to the PTC Creo, 3DS Max focuses more on the quality and realism of rendering. The model rendering in 3DS Max is a shell, not as a solid part like in Creo.

5.3.1.9 Force Model

To build and render the geometric models, HLAPI is used since it utilizes OpenGL functions as mentioned before. Similar to OpenGL, HLAPI is also based on the state machine. The states include the material information of the model, rendering setting, and the status of haptic device including position and rotation.

In HLAPI there are mainly two ways to generate force feedback: shape rendering and force effects. These are also methods for force modelling in this HARMF system. Shape rendering allows users to feel the geometry of objects. The haptic engine can calculate the force and send it to the haptic device to simulate the touch on the surface of objects. As mentioned earlier, OpenGL provides several primitives including points, lines and squares. In addition, geometry stored in vertex arrays can also be presented. This makes it possible to import existing geometric models into the system. These models can be medical models from CT scans or part models created from CAD software.

The force effect rendering is more customizable, compared to the shape rendering. It allows a user to design and customize force models. This includes classic force models such as spring forces and friction forces to simulate specific force effects. Also, it allows force modelling for more complicated tasks, such as the simulation of a cutting force or the assistance of navigation in robotics path planning. These will be discussed in the following case studies.

For shape rendering, a proxy method, as shown in Figure 5-8, is used. A proxy point is created near to the real haptic device position. When the device position is not in contact with any object, the proxy point is at the same position with the device.

When the device position is moved to come into contact with an object surface or continues to penetrate inside of the object, the proxy point will remain exactly outside of the surface, without contact or going inside the object. A spring-damper model is used to demonstrate the force between proxy and haptic device position. The spring force depends on the distance between the two points, and the damper force depends on the velocity of the device position. The further the device point goes into the object, the larger force will be applied, while the proxy point shown in the graph stays outside the surface. In this way, the force model for the simulation of the touch and contact of an object surface is built.

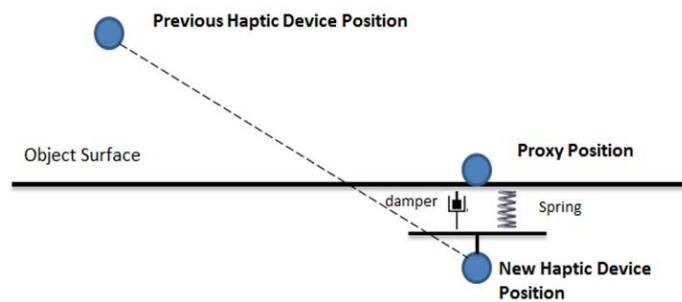


Figure 5-8 Proxy method

5.3.2 Embodied Design

5.3.2.1 Cutting Procedure

For the embodied design of the HARMP system for this case study, the first task is to specify the procedure for maxillofacial deformity operations. A 3D surgical planning system has been developed by Troulis et al (Troulis *et al.*, 2002). Although haptics was not introduced in Troulis's study, Troulis built and modified a craniofacial skeleton model, measured it for planning, virtually cut it with a cutting tool and repositioned the bones accordingly. The model was provided from a CT scan of a patient with hemifacial macrosomia (HFM). Here, a seven-year-old boy was presented with several facial asymmetries, which was confirmed as mandibular deformity by a panoramic radiograph.



Figure 5-9 Panoramic radiograph. (Troulis, 2002)

From the above panoramic radiograph of the patient's mandible, Figure 5-9, it can be seen that there is a 25mm difference between ramus heights. The first step of treatment is the analysis of clinical examinations, radiograph and models. Afterwards, a mandible osteotomy is conducted to surgically cut the planned area. While under anaesthesia, the patient's mandibular ramus is exposed following the intraoral incision, then the osteotomy is created in the anterior and posterior. Next, a distraction device is planted under the mandible's inferior border, fixed to bones by bicortical screws. Lastly, the corticotomy is completed and the wound is closed. After a period of 48 days the distractor can be removed, while the shorter mandible is lengthened to correct the different heights between the ramus.

The procedure of this mandible osteotomy involves bone repositioning and cutting forces. Therefore, it was decided to focus on the haptic simulation of this mandible osteotomy for this case study.

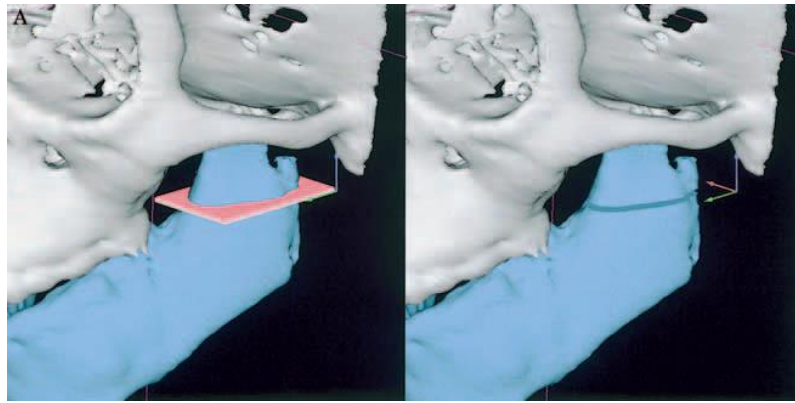


Figure 5-10 Demonstration of cutting area (Troulis, 2002)

Figure 5-10 shows the simulated cutting on the desired position of the patient's mandible (Troulis *et al.*, 2002). This gives an example and indication of the position of cutting procedure. In order to further specify the position for geometric modelling and force calculation, a study of mandible regional variation is referenced (Schwartz-Dabney and Dechow, 2002) (Schwartz-Dabney and Dechow, 2003). Schwartz mapped 31 areas on the mandible, each of which has specific properties including stiffness, density and elastic properties. These properties can be used when calculating the cutting force for the simulation.

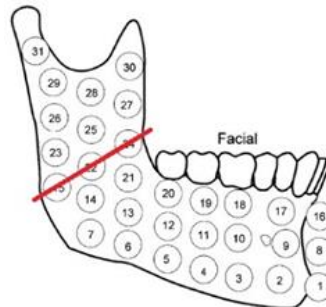


Figure 5-11 Cutting path on the mapped mandible

Combining Troulis's cutting model and Schwartz's mapped mandible, a cutting path going through three of areas is decided and allocated. This cutting path is shown in Figure 5-11, as such the cutting procedure for the simulation is ready for geometric and force modelling.

5.3.3 Geometric Modelling

The geometric modelling of the HARMP system is based on OpenHaptics which

adopts functions from OpenGL, as explained previously. These functions include the ability to read geometric models imported from different file types such as STL and OBJ, which makes it possible to utilize most types of professional medical images and models. Also, tools used in surgical processes can be specifically modelled by CAD software and imported to the system in addition to the surgical simulation. In OpenGL it is also able to create basic primitives such as lines and balls, which can be used as indications and hints during surgical training or planning. Therefore, these features make the HARMP system compatible and extendable for medical and surgical applications.

For the geometric modelling for simulations of surgical training and planning, the ideal 3D mandible model should be built for the patient specifically. This model can be created according to the personalized data acquired from the patient and imported to the HARMP system for the haptic rendering. Thereafter, the force model during cutting is established and can be applied along with the geometric model in the HARMP system. The creation of the 3D mandible model used for this case study will be introduced in the following section.

In Chapter 2 it was concluded that the novel slice model (XT Yan *et al.*, 2012) is more computationally efficient compared to the voxel or mesh cutting model. Considering the update rate of OpenHaptics and the haptic device, this model is adopted in this case study in order to ensure the responsiveness of the system. Therefore, a piece of bone slice should be created on the planned cutting path, contacting with another two bone segments. This slice of bone on the mandible can be removed by the operator during the simulated cutting procedure. In this way, the system can provide a clear view of the removal process.

To build these bone segments, a whole mandible model of the patient should firstly be created. This model can be acquired by CT scans on the specific patient's mandible. The CT scanned data contains the personalized information of the mandible, stored in one of the medical formats. In this case study, with assistance and support from Glasgow Dental School, a scanned model of a human skull stored

in raw Dicom file was created and obtained. Dicom is a standard for digital imaging and communication in medicine which is widely used by hospitals and doctors.

Dicom files consist of a group of CT scanned images. Therefore, the next step is to transfer the Dicom file to a 3D format that can be imported and edited by the CAD software. The model then can be modified in other CAD software for further purposes. The Autodesk 3DS Max is chosen to import and edit the CAD model.

Next, a piece of bone slice was to be cut on the planned area to create the three parts, this was done by a cutting tool in 3DS Max. According to the Schwartz's mapped mandible model, cutting through areas and the cutting path were mapped to the 3D mandible model. Two cuts were made using the cut and slice tool as shown in Figure 5-12. The distance between two cuts was defined by the thickness of the cutting tool. In this case, an oscillating tool with a thickness of 0.38mm (Stryker, 2010) was chosen for the simulation.

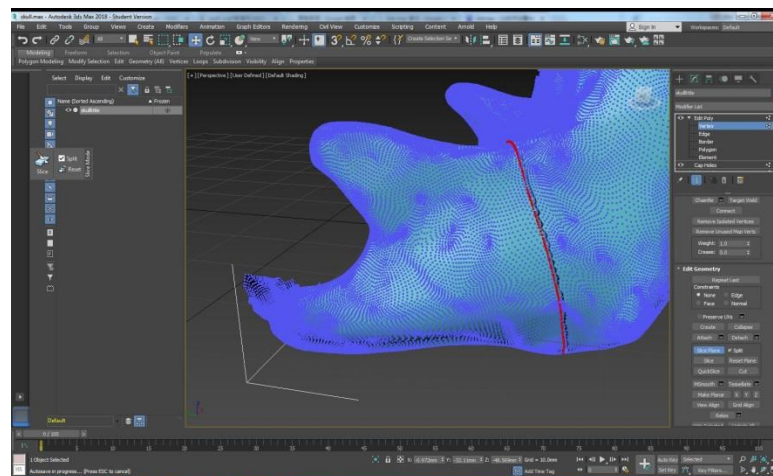


Figure 5-12 Cutting on mandible in 3DS Max

The parts were isolated from the others, and all three parts were saved separately as shown in Figure 5-13. The cap hole tool was used on each part to cap the holes created by the cutting. Finally, the mandible models were exported to .obj format, ready for integration into the haptic interface. A file containing material information of the model is also created for each part.

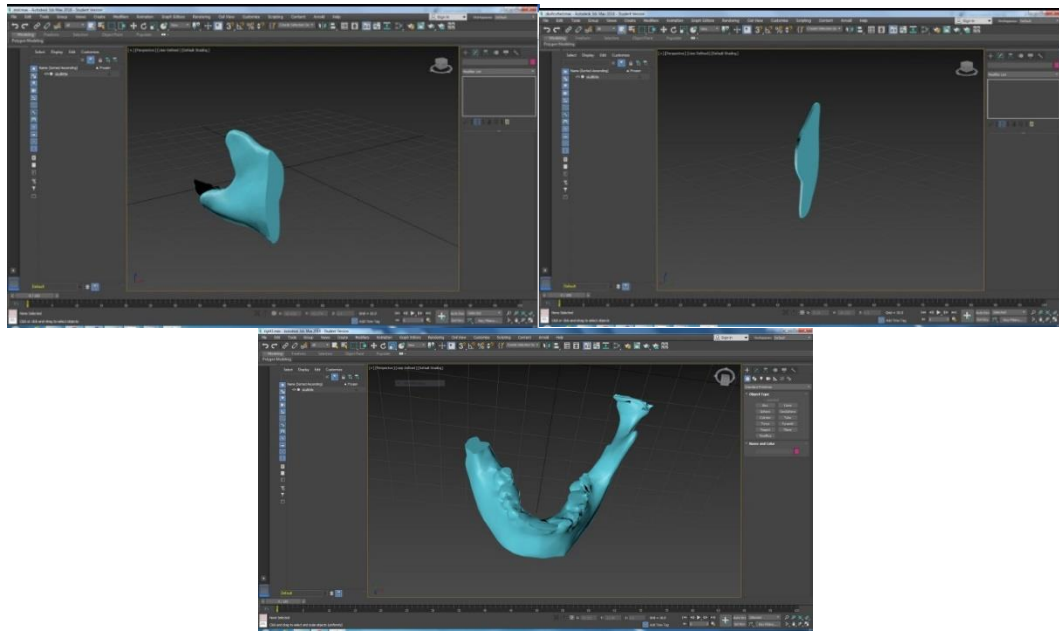


Figure 5-13 Three bone segments

The following task is to add the 3D models into the haptic interface and to rebuild the mandible in a haptic environment. As mentioned before, OpenGL is able to read geometric models in .obj files. In this case, three models saved in obj files were imported to OpenHaptics by calling the OpenGL function `glmReadOBJ()`. This built the shape representations of the three parts. In order to make the models haptic, a structure of draggable object was built. This structure contains shape representation in HLAPI and transforms information including the position and orientation. The object represented in this structure can be seen, felt, touched, and manipulated by a user. Three parts were saved as vectors of this `draggableobject`, before their positions and orientations are adjusted to form a whole mandible by calling of functions. In this way, the whole mandible model was rebuilt in a haptic interface.

Parts in the haptic interface can be felt, touched and manipulated by the cursor representing the haptic device. In the simulated surgical process of this case study, only the middle part should be able to be dragged and manipulated. Also, the movement of the cut part should be constrained to follow the planned cutting path. The transform function which implements the change of position and orientation is

called only when the middle object is selected by the user through the haptic device. Also, the movement of the selected part is constrained on the Y axis to simulate the cutting procedure. The geometric modelling of the surgical simulation in haptic interface is shown in Figure 5-14. The force model during the cutting will be analysed and built in the next section.

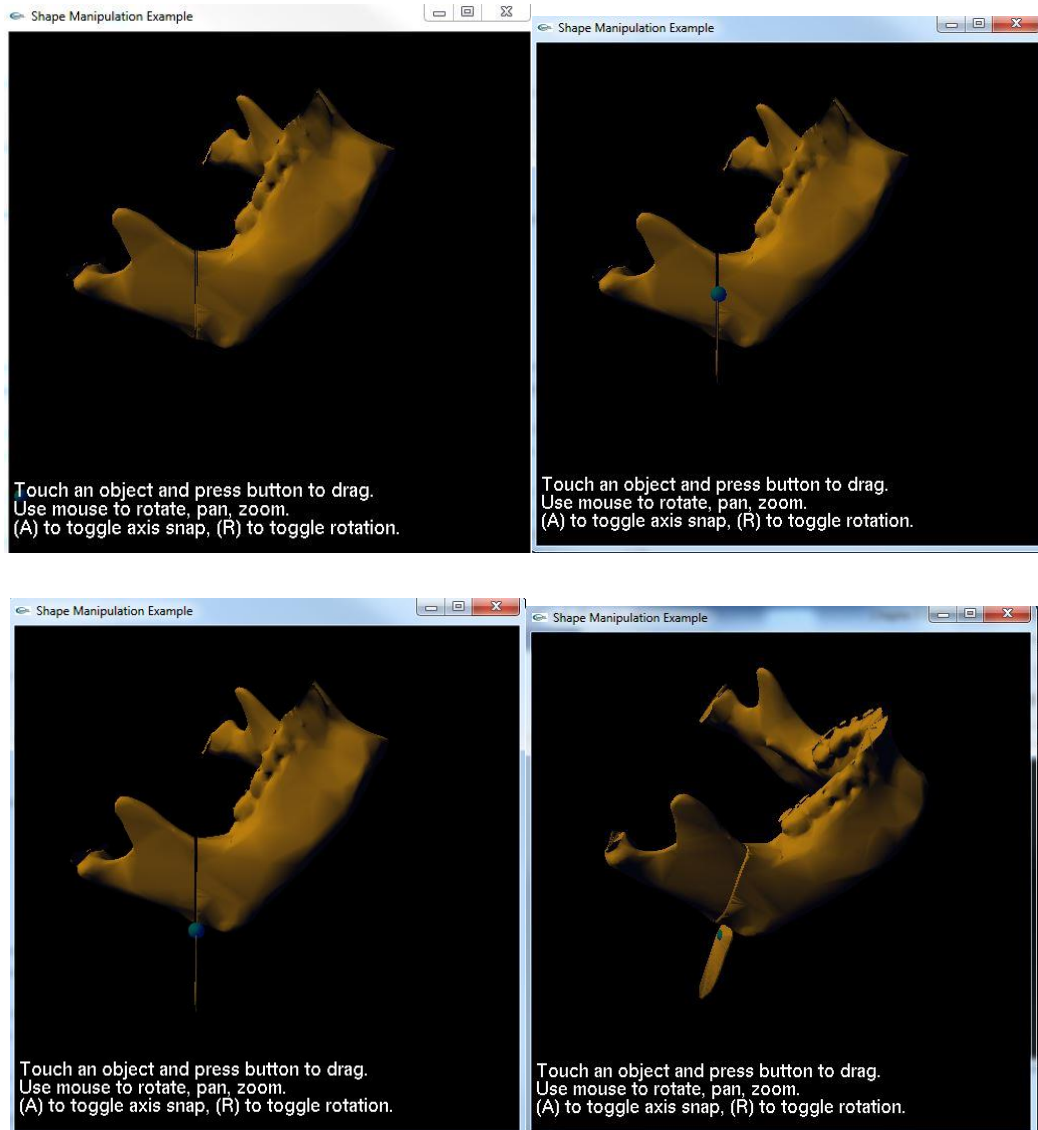


Figure 5-14 Cutting procedure in the HARMP haptic environment developed through its interface

5.3.4 Force Modelling

5.3.4.1 Telepresence

5.3.4.1.1. Modelling of Bone Tissues and Their Contact with Cutting

Tools

To build the force model during the cutting procedure, the material properties on the cutting path need to be investigated. According to Schwartz-Dabney (Schwartz-Dabney and Dechow, 2002), “The direction of maximum stiffness, cortical thickness, cortical density, and elastic properties for the dentate human mandible demonstrate unique regional variation”. Ten mandibles of human adults were analysed in the study. The mandible was mapped into 31 areas with different properties. A cutting path going through three of these areas is shown in Figure 5-11.

To study the physical simulation during cutting procedure, researchers have mainly focused on two types of models. The first model studies the metal cutting and chip formatting, taking into more consideration the feed rates and parameters of cutting rather than the properties of the material. Whilst another type considers the contact mechanics. This type of solution uses impact mechanics to construct a cutting procedure model, considering the material properties of the entire mandible. For this study, a contact model is used taking into account the contact mechanics between the cutting tool and the mandible. This allows real-time computing performance when developing haptic feedback for the user. Although the proposed model compromises the complexity of cutting mechanism, it can still be used to demonstrate the procedure of cutting and to study the relationship between force modelling and force rendering.

To conduct the physics analysis during cutting procedure, Hertz’s equation is used, which studies the contact mechanics. Hertz’s equation studies a contact relationship between any elastic bodies that can be used to find contact areas and indentation depths for simple geometries (Agus *et al.*, 2003) (Smart, 2013). Due to

these features, Hertz's equation is therefore used to calculate the force in the impact model during the bone cutting processing.

Contact between two spheres shown in Figure 5-15 based on the Hertz equation (Budynas and Nisbett, 2010).

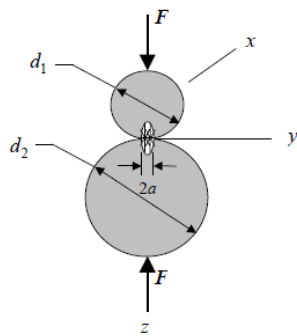


Figure 5-15 Contact analysis between two spheres - Hertz contact model

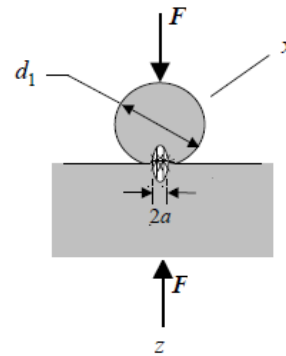


Figure 5-16 Contact analysis between sphere and a plane

$$a = K_a \sqrt[3]{F} \quad \text{Eq. 1}$$

$$K_a = \left[\frac{3}{8} \frac{(1-\nu_1^2)/E_1 + (1-\nu_2^2)/E_2}{(1/d_1) + (1/d_2)} \right]^{1/3} \quad \text{Eq. 2}$$

Where, a is radius of circle which represents area of the contacts, E_1 , E_2 are the elastic moduli and ν_1 , ν_2 are the Poisson's ratios of each body. F is the required impact force.

In this case, the equation can be modified to study contact between a sphere and a non-elastic plane as shown in Figure 5-16, where it can assumed that $d_2 = \infty$

Hence, the simplified equation is:

$$K_a = \left[\frac{3}{8} \frac{(1-\nu_1^2)/E_1 + (1-\nu_2^2)/E_2}{(1/d_1)} \right]^{1/3} \quad \text{Eq. 3}$$

A diagram produced from Budynas and Nisbett's research illustrates the elastic moduli and Poisson's ratio properties of each area on the mandible. Based on this, it is possible to have the values of ν_2 and E_2 in the cutting path shown Table 5-3.

Table 5-3 Material properties along the selected cut

Position	Young's Modulus (GPa)	Poisson's Ratio
24	19.3	0.28
22	18.6	0.3
15	17	0.23

Based on these values, elastic moduli E_2 and the Poisson's ratios ν_2 of the mandible can be derived from the table to describe the selected cutting path shown in Figure 5-17. If a different cutting path has been selected, a separate set of data tables need to be derived and used instead.

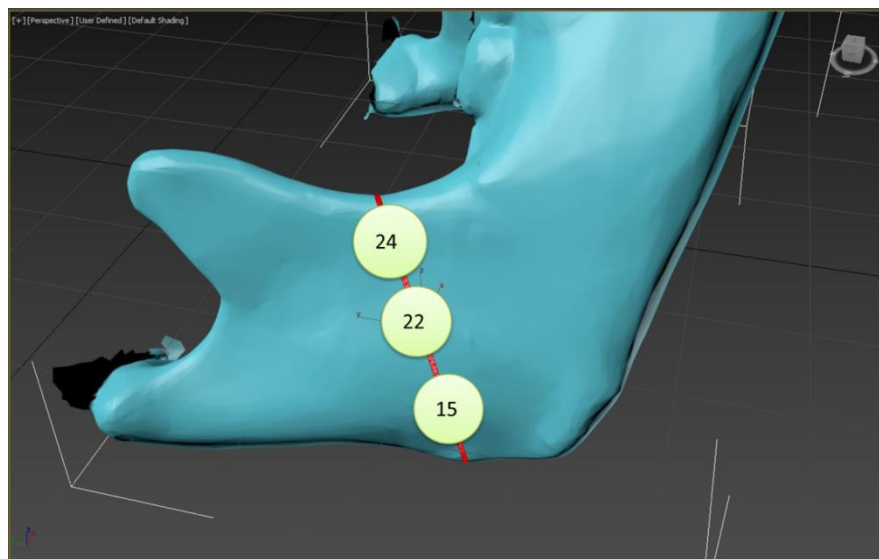


Figure 5-17 Cutting area partition for haptic modelling

In order to calculate the impact force using the Hertz equation, the parameters need to be determined. Thus, the necessary and correct cutting tool needs to be decided upon to obtain the material properties ν_1 and E_1 , as well as the value d_1 , which is determined by the size of the tool, and the value of a can be estimated. An oscillating cutting tool manufactured from steel was selected for this study based on a tool already used in surgery, as shown in Figure 5-18. The tool has options to vary the thickness and diameter. For the purpose of this model, an oscillating tool was selected which had a diameter of 11.5mm and a thickness of 0.38mm with a speed of 5000 to 10000 rpm from an available tool specification (Stryker, 2018). Therefore, d_1 in the equation is assigned to 11.5mm. According to the material

properties of the selected oscillating saw, the elastic moduli E_1 is set to 2.03 GPa, and the Poisson's ratio of the tool ν_1 is set to 0.295.

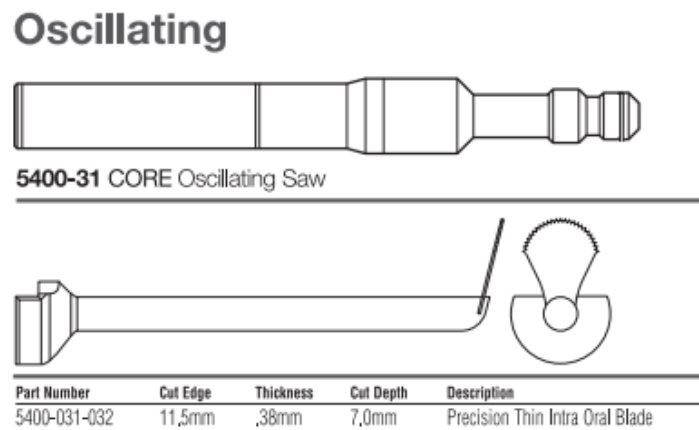


Figure 5-18 Chosen cutting tools for modeling (Stryker, 2010)

5.3.4.1.2. Force Calculation

According to the Schwartz model previously mentioned, the material properties of the bone on the cutting path changes in different areas. In order to calculate the force and build the simulation model of the cutting procedure, the real positions on the cutting path need to be assigned. Thus, it is important to decide the depth of the mandible where the cut is conducted. According to a human mandible study, the average length of adult human mandible is 3.2 cm (Balcikonyte, Balciuniene and Alekna, 2003). By measuring the height of mandible and the length of cutting path on the mandible model in 3DS Max, it was found that the length of cutting path is 3.6 cm. Thus, to build the primary model in this study, 3.6 cm was used as the depth of cutting in the system. In the future planning system, this dimension needs to be determined by the real CT scanned images of the specific patient to allow higher accuracy.

Based on the selected cutting section and data from Table 5-3, two different methods of force calculation have been developed. The first one assumes that the force value calculated using properties in the area applies to the centre of that area.

The second one considers the relationship between the cutting depth and the tooth on the cutting tool involved. These two force models were derived and modified to cope with the limitation of the haptic device, and rebuilt in a haptic environment. In this way the force modelling in HARMP system was validated and tested.

5.3.4.1.3. Force Model I

In the first model, three areas were equally assigned on the cutting path with a depth of 3.6cm. The centres of three areas have been identified on the cutting path. The radius of the contact area, a , was set to half of the thickness of the cutting tool, which is 0.19mm. Therefore, all values needed in the force calculation equation were given and the cutting force for each position along the cutting plane can be calculated as shown in the following Table 5-4.

Cutting force is calculated by using the following equations:

$$K_a = \left[\frac{3(1-\nu_1^2)/E_1 + (1-\nu_2^2)/E_2}{(1/d_1)} \right]^{1/3} \quad Eq. 3$$

$$F = \left(\frac{a}{K_a} \right)^3 \quad Eq. 4$$

Table 5-4 Cutting force calculation parameter values

Position	Young's Modulus (GPa)	Poisson's Ratio	Depth(m)	Force(N)
24	19.3	0.28	0.006	30.44
22	18.6	0.3	0.018	29.772
15	17	0.23	0.03	26.416

It was also assumed that at the start and end points of the cutting path, the contact force is 0. This gives five samples of forces versus depths of cut which are shown in Figure 5-19. The unit of force is N (Newtons) and the unit of depth is m (meters) in the graph.

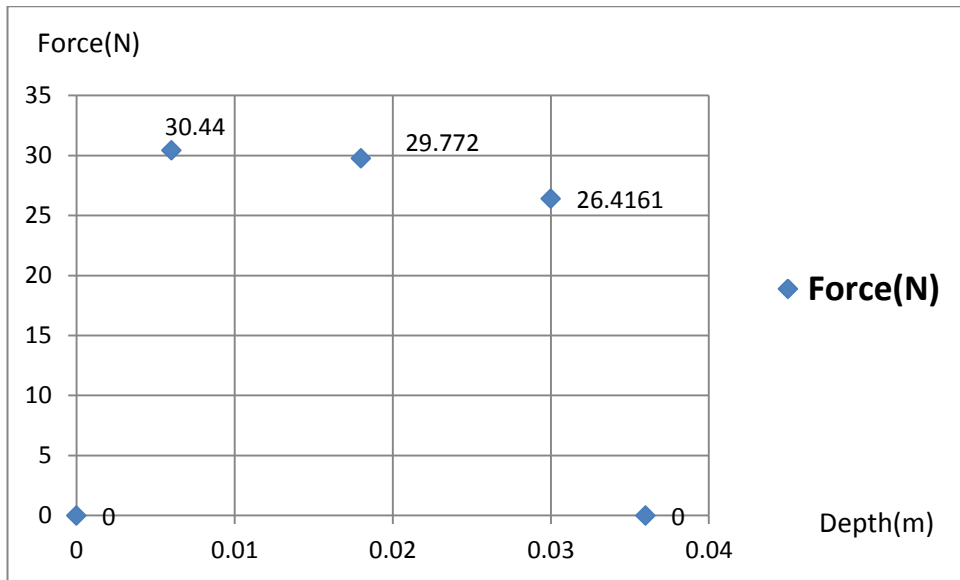


Figure 5-19 Calculated force along cutting path

A regression analysis was conducted on the sampled forces versus the depths using statistical software Minitab. A fitted regression model has been calculated and fitted using the 4th order of the input. The coefficients of the terms have been determined and a regression equation is given as shown in Figure 5-20.

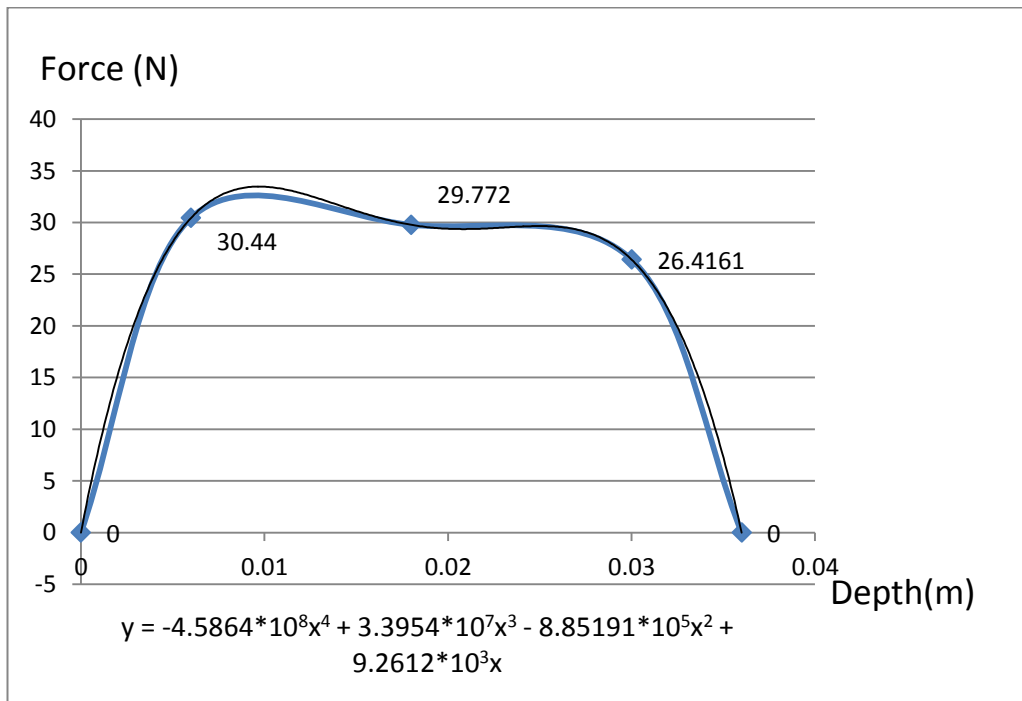


Figure 5-20 Fitted regression model

The function of force during the cutting procedure is given:

$$y = -4.5864 \times 10^8 x^4 + 3.3954 \times 10^7 x^3 - 8.85191 \times 10^5 x^2 + 9.2612 \times 10^3 x$$

Eq. 5

where x represents the cutting depth between 0 to 0.036m and y is the corresponding applied force.

The local maximum of this model is 33.47N at $x = 0.97$. However, the haptic device Phantom Desktop was used in this study. The maximum output force that can be provided is 7.9N. It is further suggested that the continuous output force should not exceed 7N. Therefore, to apply the force model into the haptic interface in HARMF system, the force equation needs to be scale down due to the limitation of the selected haptic device. Thus, a ratio of 0.2 was applied on the original equation to ensure that the maximum force during the cutting procedure is under 7N.

The modified function of force during the cutting procedure is:

$$y = -9.1728 \times 10^7 x^4 + 6.7908 \times 10^6 x^3 - 1.77038 \times 10^5 x^2 + 1.85224 \times 10^3 x$$

Eq. 6

The plot of this scale down model is shown as the following Figure 5-21.

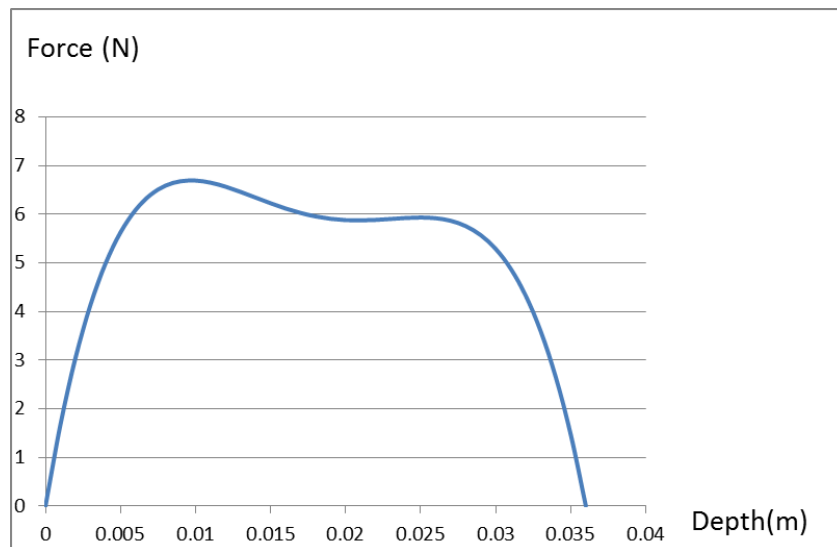


Figure 5-21 Scaled down force model I

The force model I is ready to be implemented in the haptic interface.

5.3.4.1.4. Force Model II

The second force model uses a different approach. The limitations due to the cutting depth of the tool were considered. The maximum cut depth of the tool is 7.0mm. Therefore, in the cutting path with length of 12mm in one area, it was necessary for two stages of cutting to be conducted. The cutting force in one area was also specified according to the depth, referring to Eq. 4, the value a was determined by the number of teeth engaged during cutting and the, estimated, small contact between the cutting tool tip with 1% of the cutter pitch size contact. The number of engaging teeth can be estimated by the contact arc length through different depths.

The cutting force was calculated using the following equation and the input values shown in Table 5-5:

$$F = \left(\frac{a}{K_a}\right)^3 \quad \text{Eq. 4}$$

Table 5-5 Cutting force calculation for position 24

Depth (m)	Possible contact arc length (m)	Number of tooth engaged	a value	Ka	Force F (n)
0	0	0	0	6.08511E-05	0
0.001	0.006884683	8	6.6E-05	6.08511E-05	1.25791239
0.002	0.009893999	12	9.9E-05	6.08511E-05	4.24545434
0.003	0.012329414	15	0.00012	6.08511E-05	8.29190301
0.004	0.01450774	17	0.00014	6.08511E-05	12.0705539
0.005	0.016559872	20	0.00016	6.08511E-05	19.6548812
0.006	0.018564315	22	0.00018	6.08511E-05	26.1606469
0.007	0.006884683	8	6.6E-05	6.08511E-05	1.25791239
0.008	0.009893999	12	9.9E-05	6.08511E-05	4.24545434
0.009	0.012329414	15	0.00012	6.08511E-05	8.29190301
0.01	0.01450774	17	0.00014	6.08511E-05	12.0705539
0.011	0.016559872	20	0.00016	6.08511E-05	19.6548812
0.012	0.018564315	22	0.00018	6.08511E-05	26.1606469

Similarly the cutting force for area 22 and 15 can be calculated and results are shown in Table 5-6, and Table 5-7 respectively. These results form a flexible haptic

model for different region of cutting and the corresponding forces were applied to provide realistic force feedback for either planning or training.

Table 5-6 Cutting force calculation for position 22

Depth (m)	Possible contact arc length (m)	Number of teeth engaged	a value	Ka	Force F (n)
0	0	0	0	6.13032E-05	0
0.001	0.006884683	8	6.6E-05	6.13032E-05	1.23028191
0.002	0.009893999	12	9.9E-05	6.13032E-05	4.15220147
0.003	0.012329414	15	0.00012	6.13032E-05	8.10976850
0.004	0.01450774	17	0.00014	6.13032E-05	11.8054200
0.005	0.016559872	20	0.00016	6.13032E-05	19.2231549
0.006	0.018564315	22	0.00018	6.13032E-05	25.5860192
0.007	0.006884683	8	6.6E-05	6.13032E-05	1.23028191
0.008	0.009893999	12	9.9E-05	6.13032E-05	4.15220147
0.009	0.012329414	15	0.00012	6.13032E-05	8.10976850
0.01	0.01450774	17	0.00014	6.13032E-05	11.8054200
0.011	0.016559872	20	0.00016	6.13032E-05	19.2231549
0.012	0.018564315	22	0.00018	6.13032E-05	25.5860192

Table 5-7 Cutting force calculation for position 15

Depth (m)	Possible contact arc length (m)	Number of teeth engaged	a value	Ka	Force F (n)
0	0	0	0	6.37966E-05	0
0.001	0.006884683	8	6.6E-05	6.37966E-05	1.09159933
0.002	0.009893999	12	9.9E-05	6.37966E-05	3.68414774
0.003	0.012329414	15	0.00012	6.37966E-05	7.19560106
0.004	0.01450774	17	0.00014	6.37966E-05	10.4746631
0.005	0.016559872	20	0.00016	6.37966E-05	17.0562395
0.006	0.018564315	22	0.00018	6.37966E-05	22.7018548
0.007	0.006884683	8	6.6E-05	6.37966E-05	1.09159933
0.008	0.009893999	12	9.9E-05	6.37966E-05	3.68414774
0.009	0.012329414	15	0.00012	6.37966E-05	7.19560106
0.01	0.01450774	17	0.00014	6.37966E-05	10.4746631
0.011	0.016559872	20	0.00016	6.37966E-05	17.0562395
0.012	0.018564315	22	0.00018	6.37966E-05	22.7018548

The force along the cutting path was plotted against the depth of the cut as shown

in Figure 5-22, according to the values given in Table 5-5, Table 5-6 and Table 5-7. The lines between the connecting sample points have been smoothed. It illustrates that in this force model the cutting force gradually increases until the maximum cutting depth then starts again at the next cycle. The sudden changes in cutting force mean that the selected cutting tool reaches its maximum depth before entering the next cutting stage.

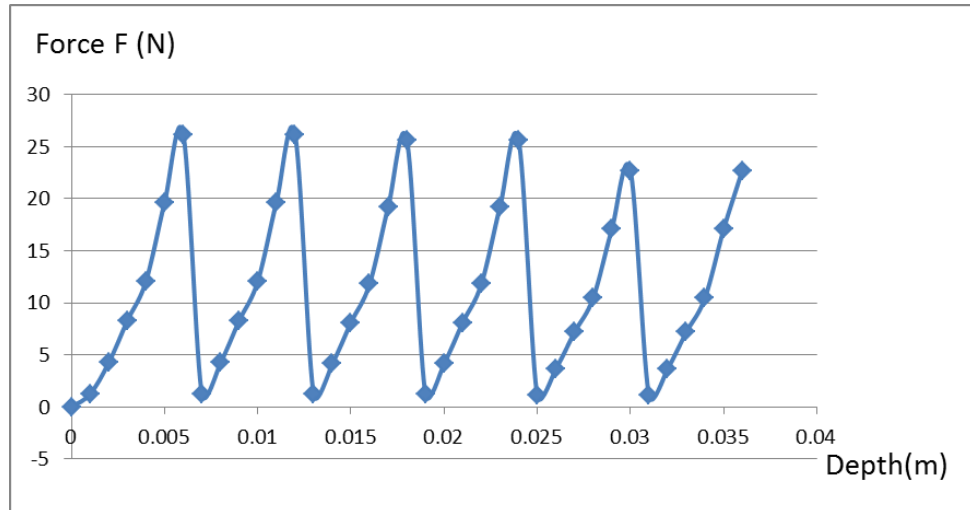


Figure 5-22 Plot of force during the whole cutting path with smooth lines

In order to build a force model for a haptic interface, the force equations need to be concluded. Therefore, the first half of each stage were selected and analysed. The cutting force in first half of the procedure on area 24 was plotted in Figure 5-23.

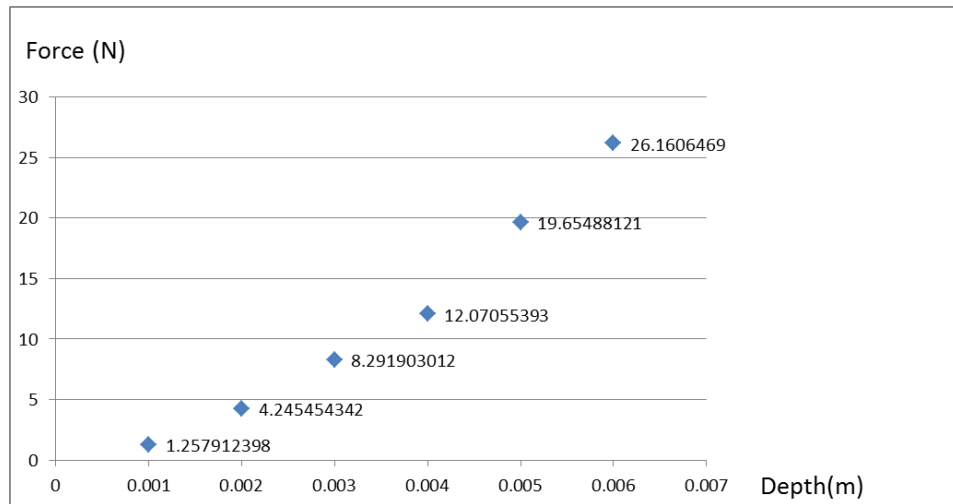


Figure 5-23 Cutting force for first half of area 24

As shown in Table 5-5, the calculated force along the second half of the procedure is identical to the first half. Again, a regression analyse was conducted on the sampled data and a force equation versus the depth was built as shown in Figure 5-24.

The force equation of the cutting force in the first half of the procedure on area 24 is given as:

$$y = 579614x^2 + 918.78x \quad \text{Eq. 7}$$

where x is the cutting depth (m) and y is the responding cutting force (N).

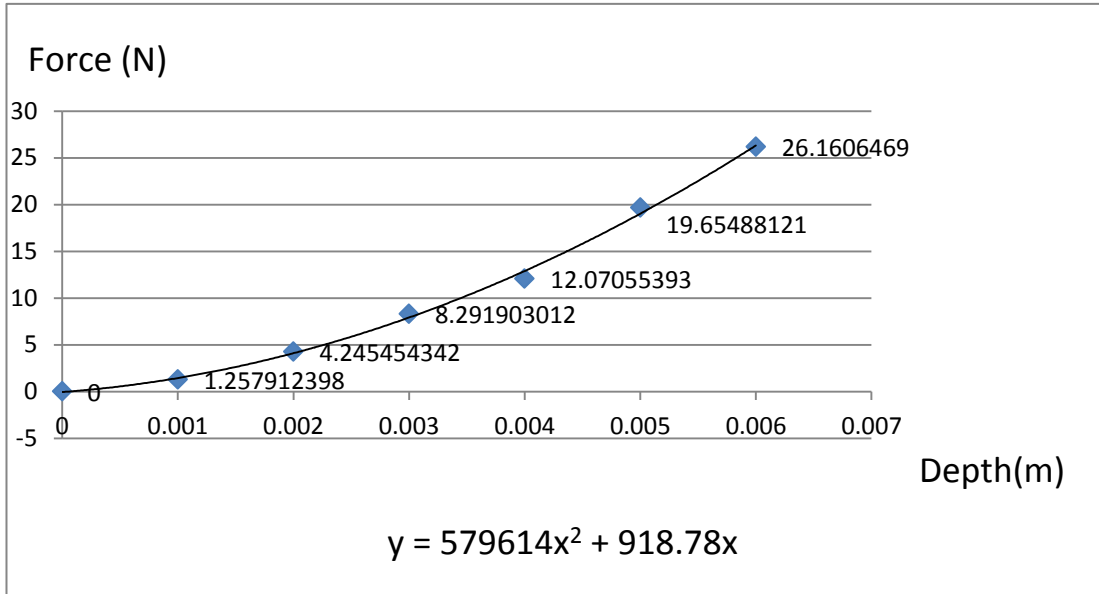


Figure 5-24 Regression model for first half of area 24

Similarly, the regression model for area 22 and 15 were also created as shown in Figure 5-25 and Figure 5-26.

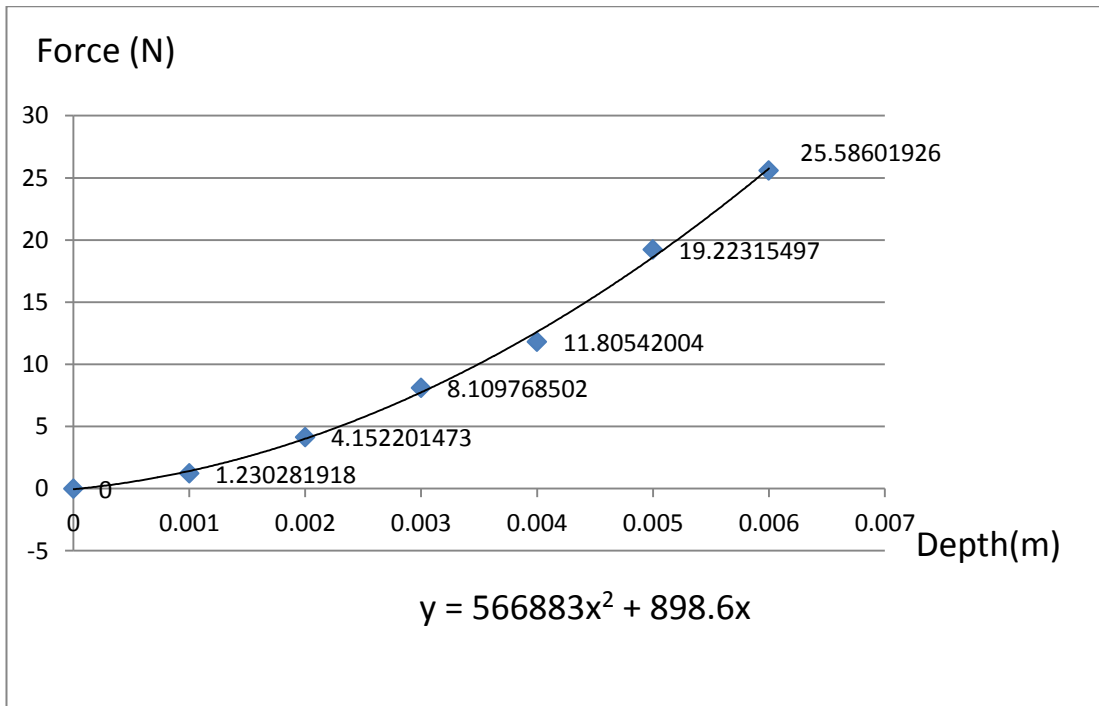


Figure 5-25 Regression model for first half of area 22

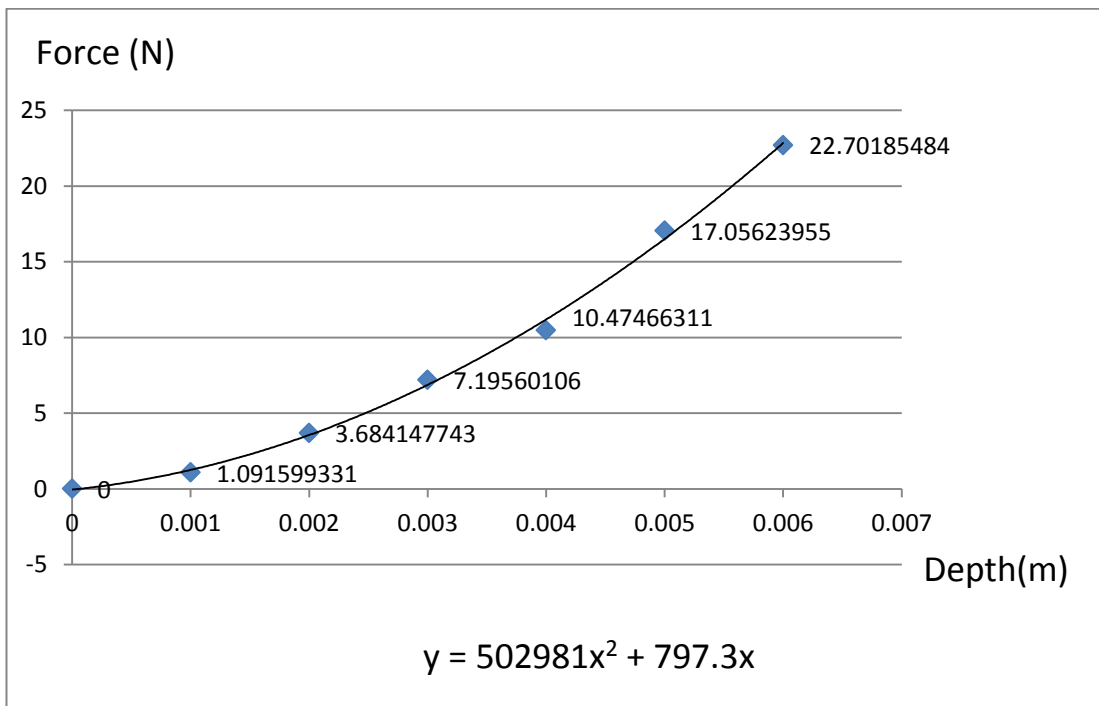


Figure 5-26 Regression model for first half of area 15

The force equation of cutting force in first half of the procedure on area 22 is:

$$y = 566883x^2 + 898.6x \quad \text{Eq. 8}$$

The force equation for area 15 is:

$$y = 502981x^2 + 797.3x \quad \text{Eq. 9}$$

where x is the cutting depth (m) and y is the responding cutting force (N).

5.3.4.2 Rendering of the Force Models in the Haptic Interface

The next step is to integrate the generated force models into the haptic interface.

5.3.4.2.1. Scale Factor

For Model I, the local maximum of this model is 33.47N at $x= 0.97$. However, as introduced in the specification of the haptic device Phantom Desktop used in this study, the maximum output force can be provided is 7.9N. It was further suggested that the continuous output force should not exceed 7N. Therefore, to apply the force model into the haptic interface in HARMF system, the force equation needs to be scaled due to the limitations of the selected haptic device. Thus, a ratio of 0.2 was applied to the original equation to ensure that the maximum force during the cutting procedure is under 7N.

The modified function of force during the cutting procedure is:

$$y = -9.1728 \times 10^7 x^4 + 6.7908 \times 10^6 x^3 - 1.77038 \times 10^5 x^2 + 1.85224 \times 10^3 x \quad \text{Eq. 10}$$

The plot of this scaled model is shown as Figure 5-27.

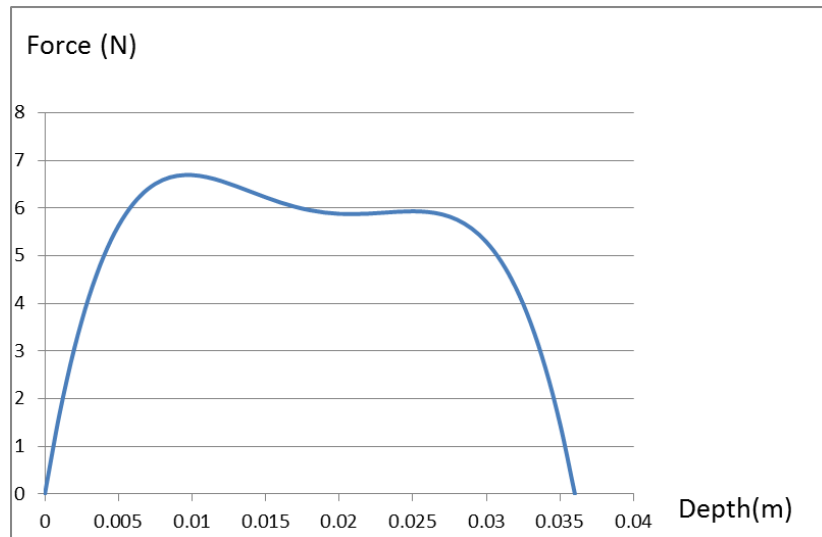


Figure 5-27 Scale down Force model I

Force model I shown in Figure 5-27 is ready to be implemented in the haptic interface.

In order to meet the requirements of the maximum output force that can be provided by the haptic device, the force Model II needs to be scaled. Again, a ratio of 0.2 was chosen to apply on the force equations. The cutting force for the entire cutting path can be concluded as:

$$\begin{aligned}
 y = & 115923x^2 + 183.756x & x \in (0, 0.006] \\
 & 115923(x - 0.006)^2 + 183.756(x - 0.006) & x \in (0.006, 0.012] \\
 & 113377(x - 0.012)^2 + 179.72(x - 0.012) & x \in (0.012, 0.018] \\
 & 113377(x - 0.018)^2 + 179.72(x - 0.018) & x \in (0.018, 0.024] \\
 & 100596(x - 0.024)^2 + 159.46(x - 0.024) & x \in (0.024, 0.03] \\
 & 100596(x - 0.03)^2 + 159.46(x - 0.03) & x \in (0.03, 0.036]
 \end{aligned}$$

Therefore, the cutting force in Model II can be seen in Figure 5-28. Force Model II is prepared for the haptic rendering. Similar to the plot of force shown in Figure 5-22, the sudden changes in cutting force mean that the selected cutting tool reaches its

maximum depth before entering the next cutting stage.

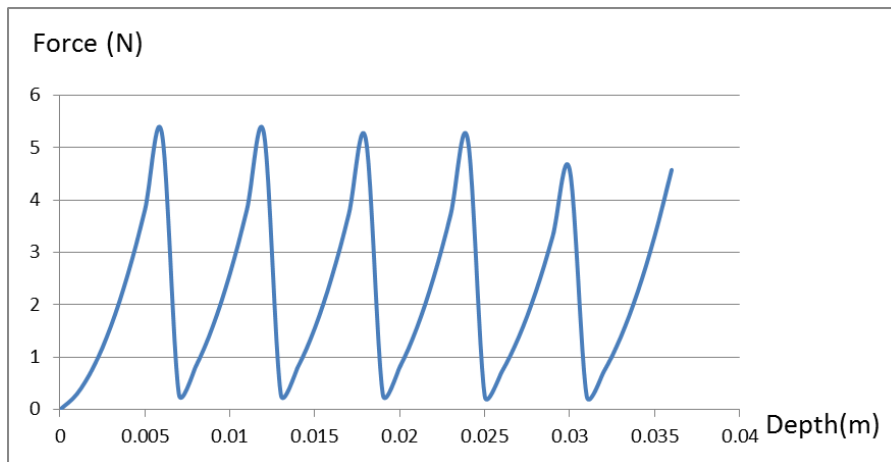


Figure 5-28 Cutting force model II

5.3.4.2.2. Force Actuation

As previously mentioned, the geometric model was built in the haptic interface as the representation of the cutting process. When the middle part of the bone slice is selected by the cursor, it can be dragged down out of the mandible as a result of removal. Therefore, the force models should also be incorporated into the system during this operation. The haptic rendering of the geometry happens to all three parts of bone models, whilst the generated force equations only apply to the middle slice.

The force equations illustrate the relationship between two factors: the cutting depth and the output force. To integrate the force equations, these two factors need to be specified in our haptic interface. The total cutting depth of 3.6 cm was assigned from the top to the bottom of the slice. Since the cutting tool was represented by the cursor, the real time cutting depth during the operation can be described as the change of the cursor's position from start of cutting on the y-axis.

To get the correct position for cursor, or any objects, in the haptic interface, several functions need to be called. In OpenHaptics the position information is saved in the

type `hduVector3Dd`, which contains either three parameters or a vector array in `HDdouble` representing the *x*, *y* and *z*. The current proxy position is saved in `HL_PROXY_POSITION`, an enum type in haptic library. HL function `hlGetDoublev()` can be called to transfer the proxy position from `HL_PROXY_POSITION` to `hduVector3Dd`. The change of the proxy position can be acquired by calculating the difference between the current position and that at the beginning. The second element in this delta position is the change in the *y*-axis. In the building of the graphical model, this change of the cursor's position in the *Y* axis is applied to the part being dragged by calling the function `hduMatrix::createTranslation()`. In this way, the bone slice can be visually dragged and moved along with the cursor. In the building of the force model, this delta in *Y* is used to calculate the cutting depth. Since this change in *y*-axis is acquired in workspace coordinates of the haptic interface, it is then rescaled to fit our force equations.

The next step is to specify the output force. The description of forces in the HARMP system is a 3-element array in `HDdouble`, representing the force in *x*, *y* and *z* directions. This is due to the three DOF output force of the Phantom Desktop, the haptic device used in the study. A `HLCALLBACK` function needs to be built and integrated to compute the output force. In this case study, the force equations are built in this function. The custom force effect can be achieved by calling the HL function `hlCallback(HL_EFFECT_COMPUTE_FORCE, (HLcallbackProc) computeForce, &pointMass)`, where `HL_EFFECT_COMPUTE_FORCE` is a `HLenum` type, `computeForce` is the `HLCALLBACK` function and `pointMass` is the userdata. In the function `computeForce()`, `Force(1)` represents the force on the *Y* axis, and *d* is the rescaled cutting depth. Then the force models are constructed:

Model I:

$$Force(1) = -9.1728 \times 10^7 d^4 + 6.7908 \times 10^6 d^3 - 1.77038 \times 10^5 d^2 + 1.85224 \times 10^3 d$$

Model II:

$$\begin{aligned}
 \text{Force (1)} &= 115923d^2 + 183.756d & d \in [0, 0.006] \\
 &115923(d - 0.006)^2 + 183.756(d - 0.006) & d \in (0.006, 0.012] \\
 &113377 (d - 0.012)^2 + 179.72 (d - 0.012) & d \in (0.012, 0.018] \\
 &113377 (d - 0.018)^2 + 179.72 (d - 0.018) & d \in (0.018, 0.024] \\
 &100596 (d - 0.024)^2 + 159.46 (d - 0.024) & d \in (0.024, 0.03] \\
 &100596 (d - 0.03)^2 + 159.46 (d - 0.03) & d \in (0.03, 0.036]
 \end{aligned}$$

5.3.5 Virtual Constraints

Path planning is another feature that can assist the user during the surgical procedure. While the graphical model of the dragged slice only moves along the y-axis, the haptic device should also be guided to move only along the y-axis as well. This procedure can be regarded as a force constrained manipulation task.

A control framework for constrained tasks was introduced by Craig (J. J. Craig, 2005). These tasks include the control of motion constrained by the contact with surfaces or special force requirement. In this framework, a manipulation task is specified into different subtasks, which can be defined by mainly two different sets of constrains. The first set of constraints is called Natural Constraints, which represents the contact with the specific geometric properties in the environment such as contacting with a stationary surface. The second set is the Artificial Constraints that can specify the planned motions or special force applications.

In this case study, both sets of constraints apply. While being manipulated by the user, the middle slice of bone is still contacting with the surfaces of the two other parts. This sets the natural constrains for the motion. In addition, the motion in the z direction should also follow the desired path during the cutting procedure. This provides a force requirement for artificial constraints. Therefore, as a result a set of

virtual constraints on the x and z axes can prevent the user going out of the planned cutting path. Two virtual surfaces were created on both the xy and yz planes, by having the cursor in the middle.

To build the virtual constraints effect into the haptic interface in this investigation, the function `computeForce()` was used again. Delta x and delta z were acquired by calculating the difference between the current proxy position and the proxy position at the start. Two spring-damper models were built to form virtual walls on each direction. One spring-damper model on the x-axis takes two factors, the difference between delta x and x position of the surface, and the velocity of the cursor on x-axis. A high value for stiffness was chosen for the constraints. A 1mm position difference will cause a constraint force to increase to 1N to restrict the users operation. By constructing four virtual walls surrounding the cursor, the cursor was then constrained to follow the planned cutting path in y-axis.

5.4 Experimental Method

A set of experiments were undertaken to assess the haptic feedback provided by the HARMP system. The experimental environment was set in the robotics laboratory as shown in Figure 5-30. The Phantom Desktop was manipulated by the user on a desk. A monitor on the desk shows the geometric model during the cutting procedure. The experimental procedure is shown in Table 5-8. For each force model, two simulated surgical procedures were conducted. The first procedure was conducted with the virtual constraints on the x and z planes, while the second procedure was set without constraints as a comparison. It should be noted that the user should have some basic experience with the use of haptic devices. The reality and quality of geometric and force models were evaluated by the user.

Table 5-8 Experiment set for the dental surgery simulation

	Force Model I	Force Model II
Experiment 1	With constraints on X,Z	With constraints on X,Z
Experiment 2	Without constraints on X,Z	Without constraints on X,Z

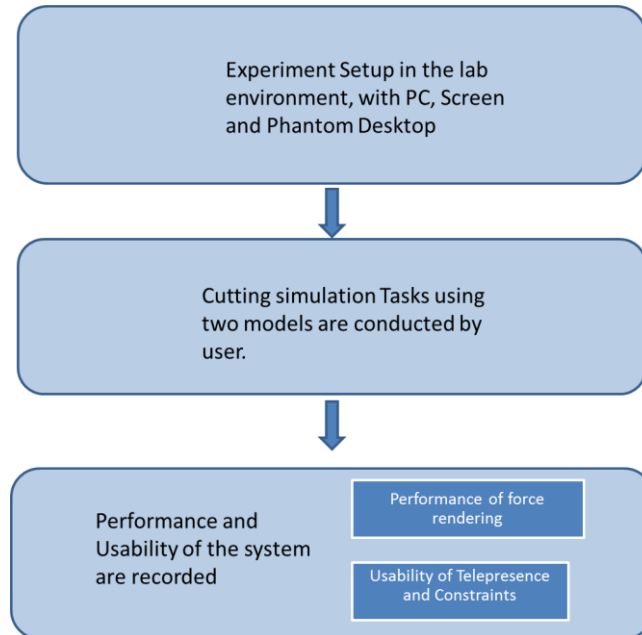


Figure 5-29 Evaluation method for Case Study 1

5.4.1 Data Collection

5.4.1.1 Objective Data

While the simulation was conducted, the calculated force, output force applied on the haptic device and position data were also recorded and output for analysis. The output force can be obtained by calling the function `hlCacheGetDoublev()` to get `HL_DEVICE_FORCE`. This `HL_DEVICE_FORCE` is a 3D vector representing the last force sent to the haptic device. On each frame, the calculated force and real output force are slightly different due to the ability of haptic device. All generated data during the experiments are saved in a TXT file. This was achieved by the read/write to FILE functions in C++ programs. This data file can be output to other software such as Excel and Minitab for further data analysis. The data collection plan is shown in Table 5-9.

Table 5-9 Data collection

Force model	Reality of telepresence
	Usability of constraints
Force rendering	Stability



Figure 5-30 Experimental setup for the dental surgery simulation

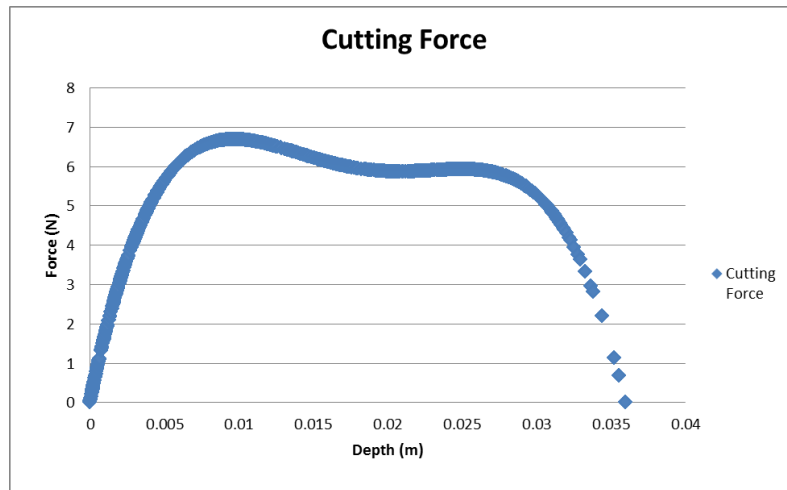
5.5 Results, Findings and Discussions

5.5.1 Model I

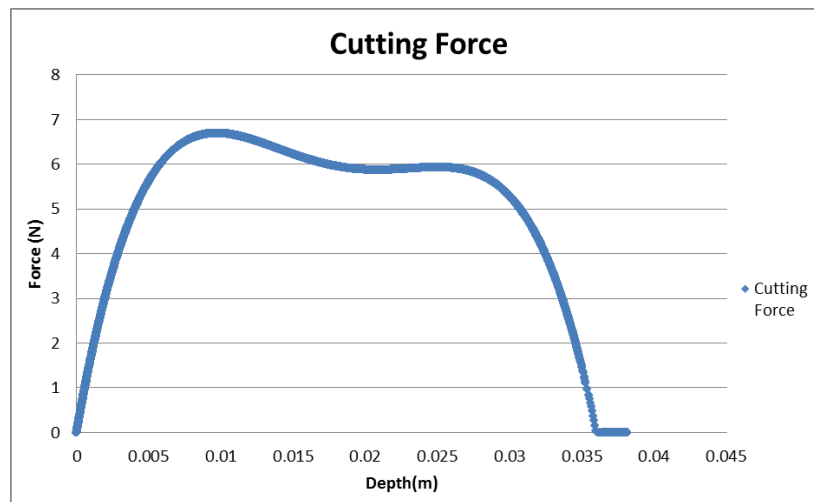
For force model I, ten repetitions of experiments were conducted for both with and without constraints on the x, z planes. The data was collected and analysed.

Figure 5-31 illustrates the calculated cutting force against the cutting depth on each frame in experiment 1 with constraints. 13484 sets of data are collected. Compared to the desired calculated force model, the calculated force was a general good fit into the model. The depth of the cut was calculated from the change of proxy position during the cutting. Two methods of obtaining this proxy position change were compared. The first method is to adopt the proxy position change that is used to apply the transform of objects in graphic update function. The second method is to call the HL_PROXY_POSITION again in the computeForce() function. As can be seen in Figure 5-31(a), the data at the end stage of cut are becoming discrete,

insufficiently sampled comparing to the rest. After analysing the raw data, it was concluded that this was a result of the rapid changing rate of the applied force and the insufficient update rate from the haptic device. The rapid changing rate of the force could lead to a high velocity of the end effector, making it harder to be precisely controlled by the user. Analysing Figure 5-31(b), it is found that the force function `hlCallback(HL_EFFECT_COMPUTE_FORCE, (HLcallbackProc) computeForce)` has a higher frequency compared to the other functions called in the main loop. The Phantom Desktop used in this study has a 1k Hz update rate. By calling `HD_INSTANTANEOUS_UPDATE_RATE` to check instantaneous update rate in real time, it is found that the function `computeForce()` runs at frequencies that vary between 950Hz-1050Hz. Therefore, it illustrates a better performance hence it has been identified as the method of the force modelling in this investigation



(a)



(b)

Figure 5-31 Calculated Force during cutting. (a graphic update (b compute force update

Figure 5-32 and Figure 5-33 show the output force and torque on the haptic device including the constraint force on x and z planes. This data was collected by calling functions to obtain the current `HL_DEVICE_FORCE`, `HD_CURRENT_JOINT_TORQUE`. `HL_DEVICE_FORCE` represents the device force at the current frame, which is found to be the last force sent to the device. Therefore, there is a system latency of one frame, approximately 0.001s, which is acceptable for the performance of haptic simulation. However, these force and torque parameters cannot be read in the `computeForce()` function due to the limitation of `HLAPI` and `HDAPI`. As a result, the data was collected in the main loop which has a lower update rate than the force

rendering. Therefore, the data collected has lower sample rate. However, this does not adversely affect the performance of the haptic simulation. The real applied force and torque are sent through the computeForce() that has adequate update rate.

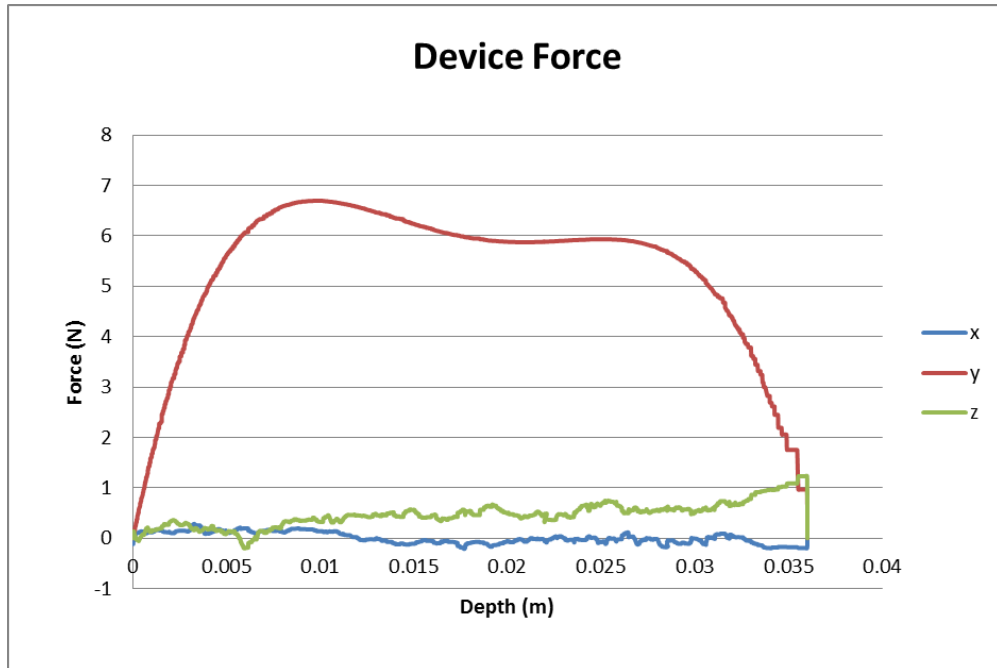


Figure 5-32 Device forces on x, y, z axes

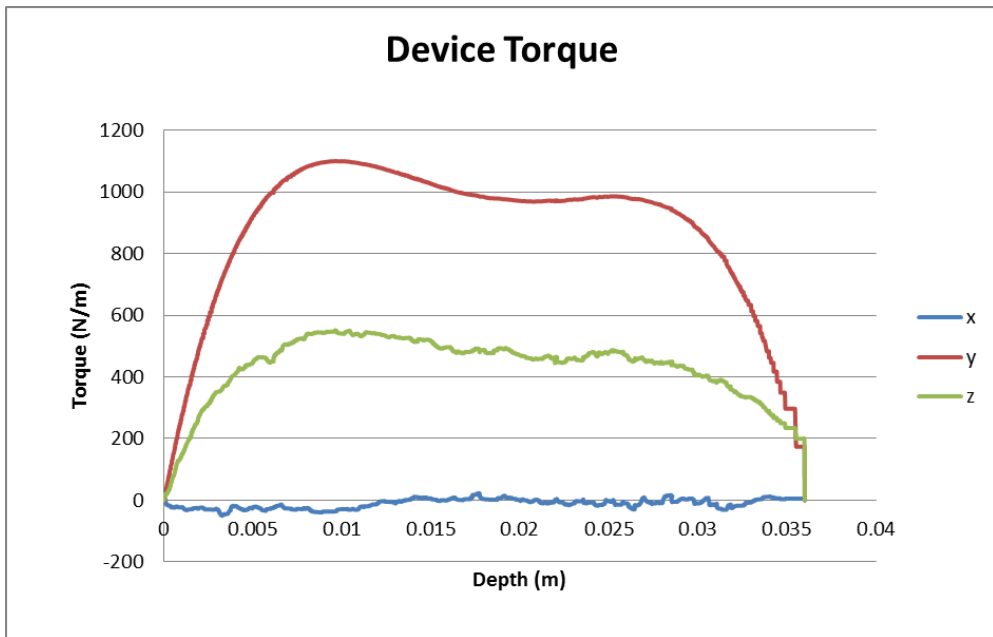


Figure 5-33 Device torques on x, y, z axes

5.5.1.1 Constraints

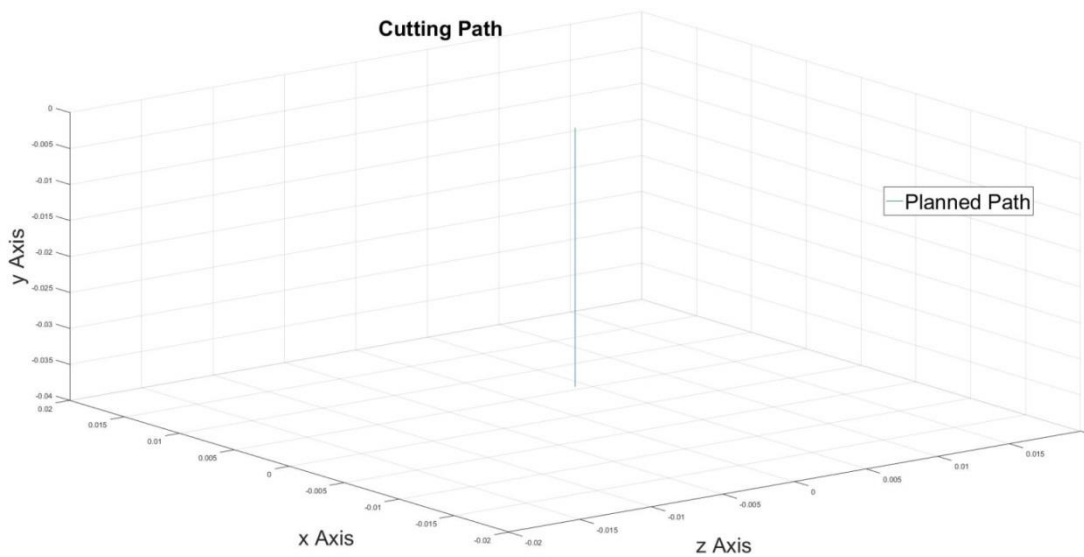


Figure 5-34 Planned cutting path

Figure 5-34 shows the planned cutting path in three dimensions plotted in Matlab. To ensure the reality of the figure, the x, y and z axes are equally scaled. As can be seen from the planned cutting path, while the cutting depth on the y-axis changes from 0 to 0.036, there should, ideally, not be any movement on x or z axis. This is due to the implementation of the algorithm developed for this function. Figure 5-35 illustrates the position data collected during the cutting procedure with constraint

on x and z axes. Referring to Figure 5-35, the real cutting path starts to follow the planned path at the beginning, while the error on z-axis increases at the end of cutting procedure. This means the provided haptic constraints does help a user follow the desired path however the effectiveness is gradually decreasing.

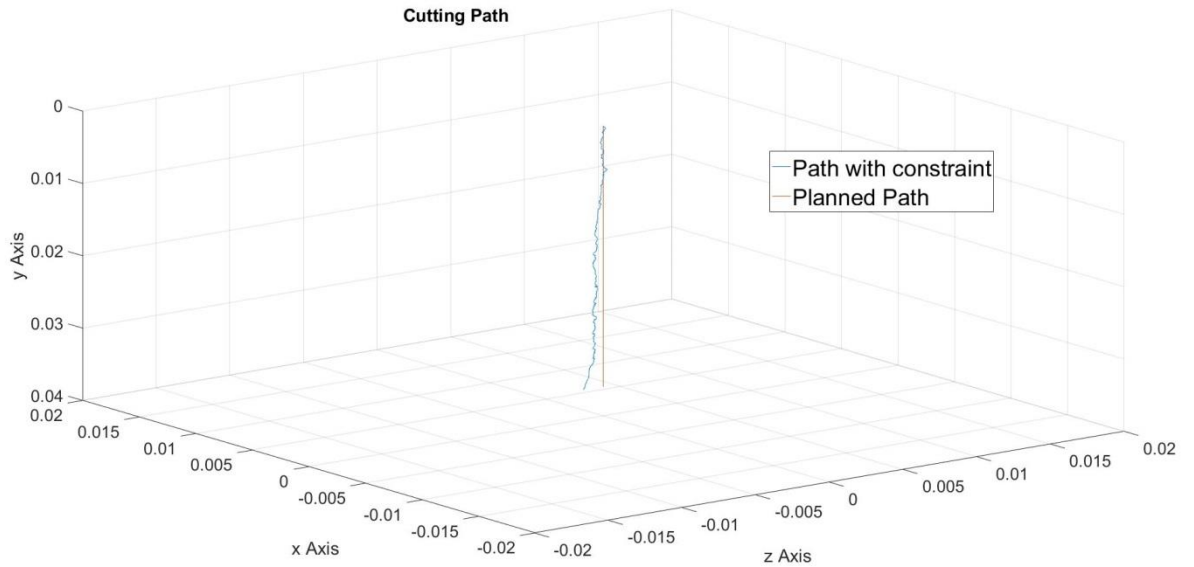


Figure 5-35 Planned cutting path versus real cutting path with constraint

Figure 5-36 shows the position data collected during the cutting procedure without constraints on the x or z axis. As can be seen from the figure, the real path without constraint shows larger errors from the desired path. Compared to the cutting path with haptic constraints, this error is significant in both x and z axis, which means that the user has less precision control of the virtual cutting tool during the cutting procedure.

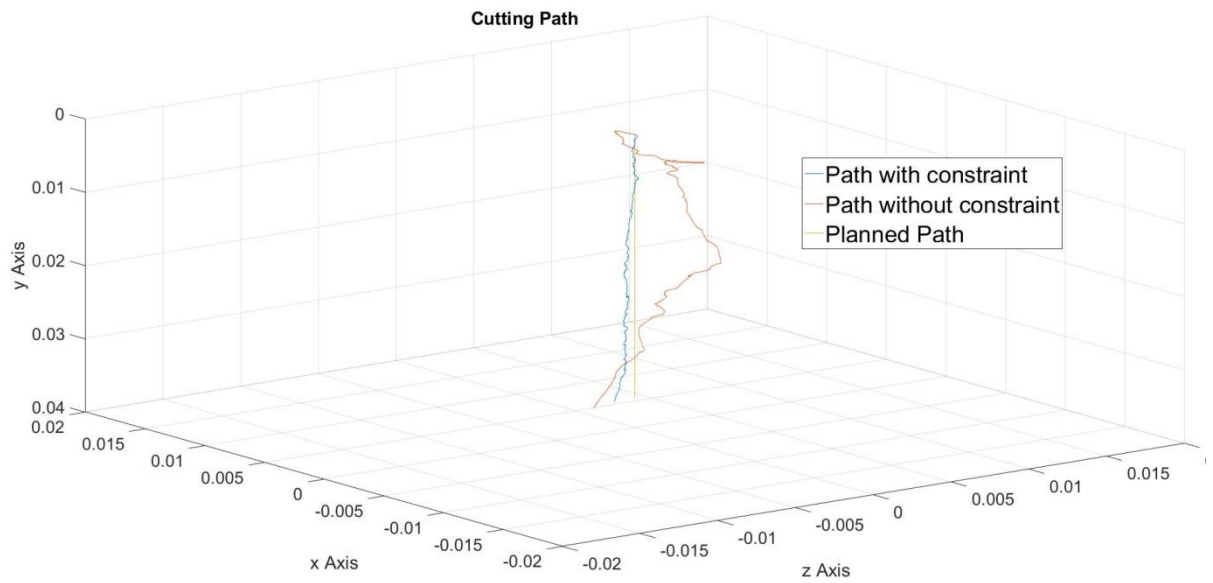


Figure 5-36 Planned cutting path versus real cutting path with/without constraint

To study the performance of the virtual constraints, an experiment with only constraint forces on x and z axes and without cutting force on the y-axis is undertaken as a comparison. Figure 5-37 shows position data collected during the cutting procedure with constraint on x and z axes without cutting force on the y-axis. The cutting path with only force of constraint on the x and z axes is almost a perfect fit for the planned path. This shows a user's precision control with the assistant of haptic constraints.

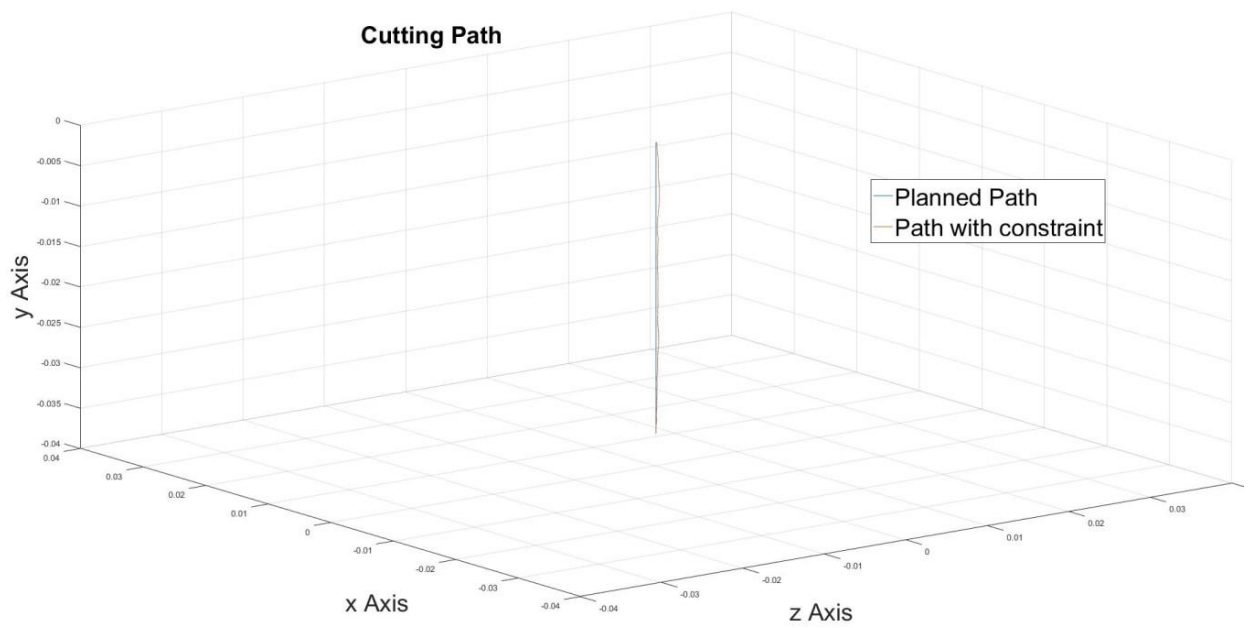


Figure 5-37 Planned cutting path versus real cutting path with constraint, no force on y axis

Figure 5-38 the position data collected during the cutting procedure without constraints on the x and z axes and with no cutting force on y-axis. The cutting path without any constraints shows larger errors compared to the desired path and the path with haptic constraints provided.

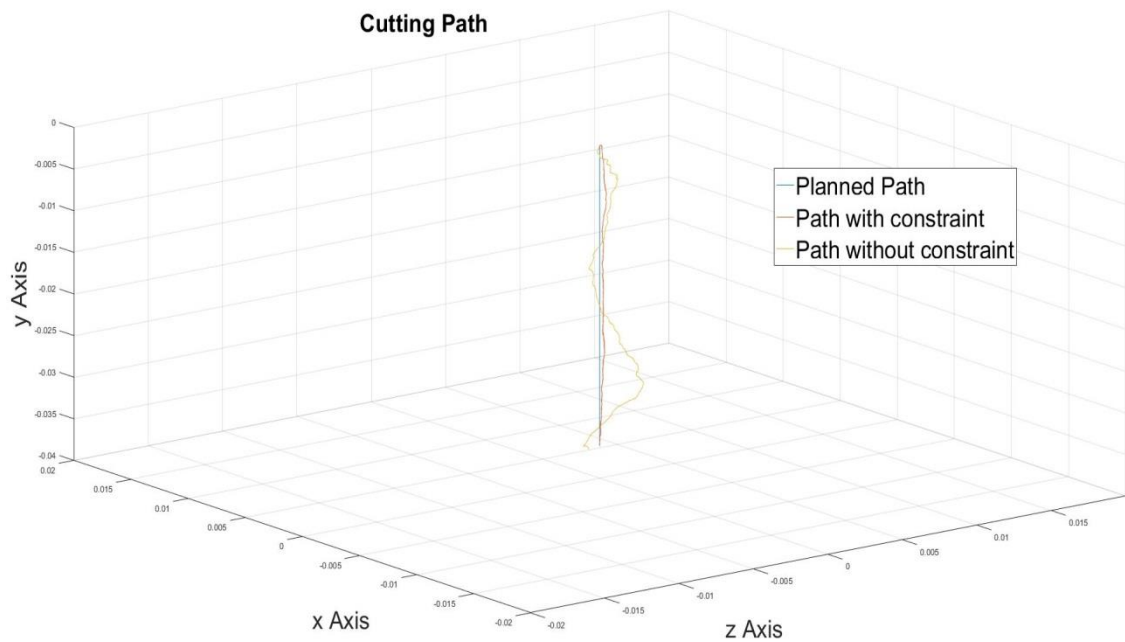


Figure 5-38 Planned cutting path versus real cutting path with/without constraint, no force on y axis

5.5.2 Model II

Similarly, for the force model II ten experiments are undertaken for both with and without constraints on the x and z axes. The data is collected and analysed.

Figure 5-39 shows the calculated force during the cutting procedure. As can be seen from the graphical data, most of the plotted forces are continuous and the change is smooth and is only discontinuous at the beginning of the second half of the first stage of the procedure. This shows the calculated force versus cutting depth is ideally smooth and continuous.

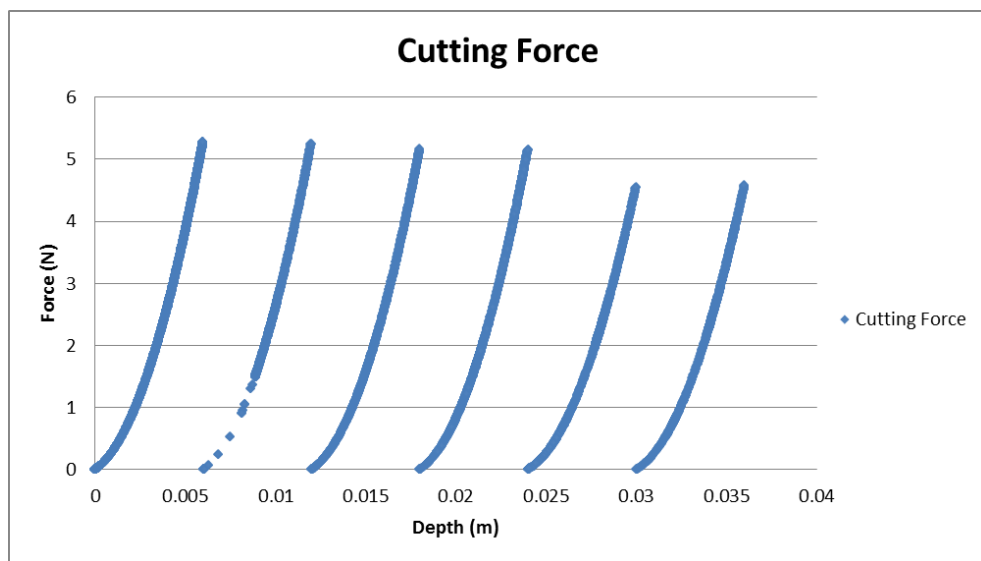


Figure 5-39 Calculated Force during cutting

Figure 5-40 shows the output force on the haptic device during the cutting procedure. As can be seen from the figure, the realistic output force is also continuous at the beginning. But just after the first half of first stage of the procedure, the plot suddenly becomes significantly abrupt and discrete. Compared to the calculated force plot, the real output force is much more discontinuous and unstable, showing difficulties in precision control.

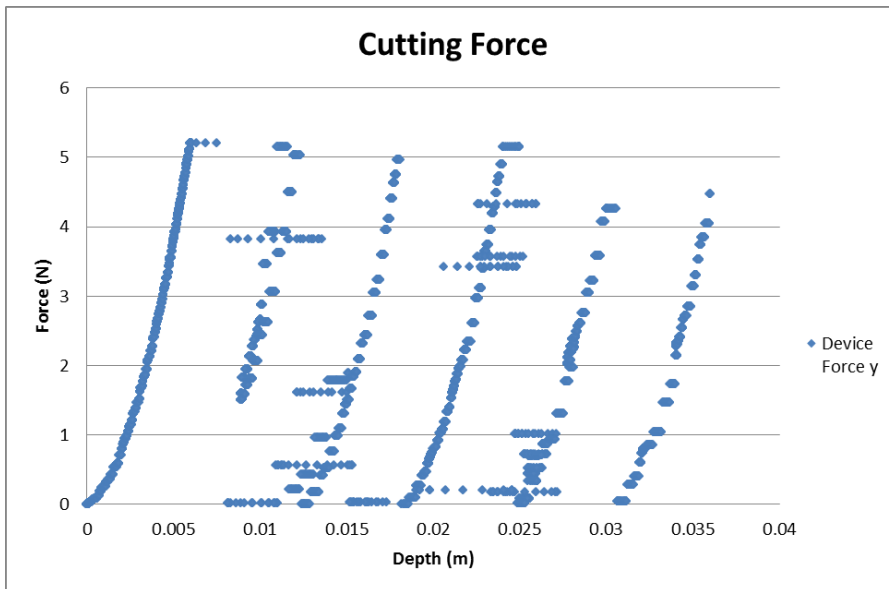


Figure 5-40 Device force on y axis

Figure 5-41 shows comparisons of the planned cutting path, the path with virtual constraints, and with cutting force in Model I and Model II. As can be seen from the graph, even with the haptic constraint on the x and z axes, the cutting path using force Model II obviously failed to follow the planned path. The errors are significant compared to the path with constraints in Model I. This shows that the user has poor position control of the cutting tool with this cutting force model.

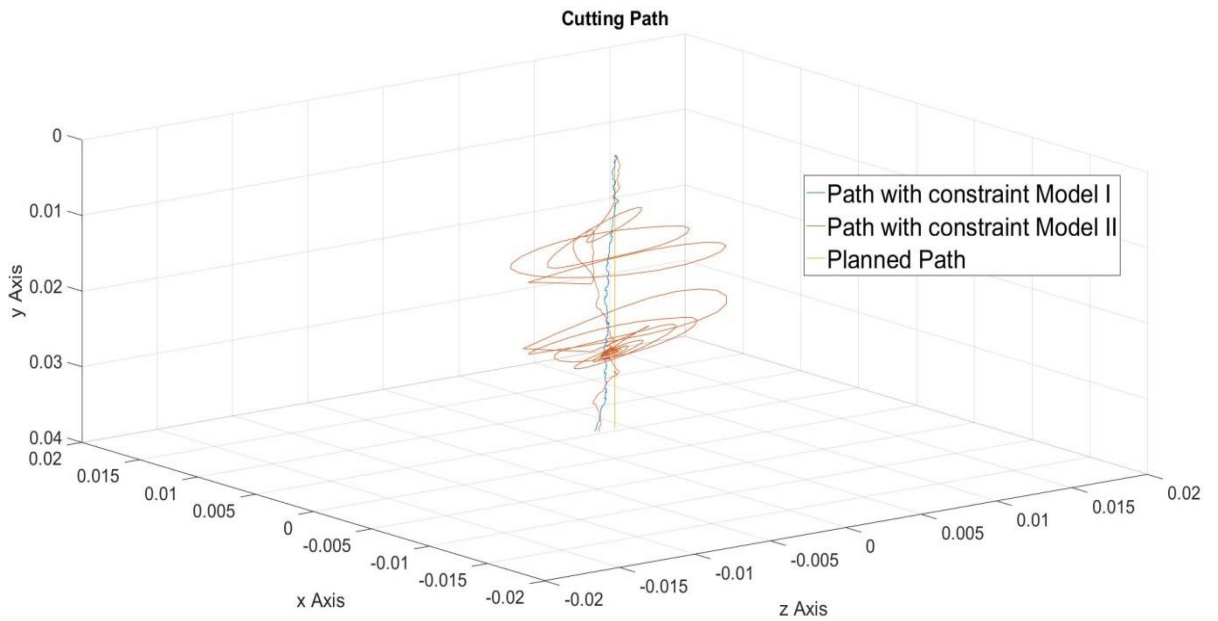


Figure 5-41 Planned cutting path versus constrained Cutting path with Cutting force Model I/II

5.6 Discussion of the Result

5.6.1.1 Virtual Constraints

In Figure 5-35 it can be seen that at the beginning of the cut, the cutting path with constraints follows the desired path. However, the position error on z-axis increases during the cutting and at the end of procedure. This increase in position error is also shown by the device force on the z-axis in Figure 5-32. The maximum position error reaches 1.2 mm, at the end, causing a 1.33N constraint force being applied on the z-axis. By analyses of the data, there was found to be three main reasons that this occurred.

Firstly, while the cutting force that is applied on the y-axis becomes relatively large, the constrained force cue on other axes becomes less significant so that it is not noticed by a user.

Secondly, the rapidly changing rate of the force at the end of the cutting could lead to a high velocity of the end effector, making it harder to be precisely controlled by a user.

Thirdly, it may be caused by users' operation of the haptic device. When users try to

drag the device down and if they encounter a large force, users may tend to drag the device towards them to maintain the control. This explains why the position error on the z-axis is larger than the position error on the x-axis. In order to improve the performance of the constraint model, it is necessary to find a better balance between the high stiffness of the constraint and the stability of the system. However, significant advantages and improvements are readily seen by the use of virtual constraints as compared to the cutting path in the unconstrained process shown in Figure 5-36. This shows that the haptic constraint can be useful and helpful in dental surgical simulations and training.

5.6.1.2 Force Rendering

As can be seen in Figure 5-39 the second half of first stage of the procedure shows discreteness at the beginning, while other parts illustrate acceptable performance. This is caused by the sudden change in the cutting force between the end of first half (5.3N) and the beginning of the second half (0N). The sudden change of force will make it more difficult for a user to maintain control, which can lead to a higher velocity causing insufficient sampling on any given part of path. This instability can be better shown by the device force illustrated in Figure 5-40. Although, the calculated force during the cutting generally fits the force model. The output force from the haptic device on the y-axis demonstrated discrete behaviour and failed to handle the calculated force in many regions. Despite the issues of low sampling rate mentioned earlier, it still shows the instability caused by the discontinuous force function adversely affects the performance of the haptic device in the system.

This instability also appears on the applied constraint forces on x and z-axis. While a user makes movement on the x and z axes during the cutting, the haptic device fails to provide proper constrained forces accordingly to guide the user through the desired path. The comparison between the paths with constraint in Model I and Model II are shown in Figure 5-41. Although the force functions on the x-axis and z-axis are continuous, the instability on the y-axis also affects the force applied on the other two axes, making the constraint function unviable.

By comparing the performance during the cutting between Model I and Model II, it can be concluded that to ensure the performance and stability of the haptic system, the deployed force model has to be continuous and the force should increase or decrease only gradually. If the force model has to be discrete or discontinuous due to the specific task requirement, modification must be made to provide a usable and helpful haptic surgical training system that a user can control.

5.7 Conclusion

In this chapter, a method for simulating a dental deformity surgery using haptic technology is presented. A composite skull model, which reproduces both the bony structures and the dentition with a high degree of accuracy, was constructed by creating an STL file from the Dicom slice images through the CT scans. Next, a mathematical model was developed and incorporated into a haptic simulation of dental deformity surgery. The haptic model was built and deployed to provide virtual constraints to assist a user to follow the desired path. Research techniques were used to identify the required values for the mathematical model and to gain an understanding of the surgical procedure. Finally, sets of experiments were conducted to evaluate the design and performance of the system for validation.

Through applying the generic haptic system design methodology, this chapter shows the contribution of applying the generic design methodology in tackling the specific medical problem. Haptic rendering force models have been developed and demonstrated in the chapter. The proposed model can be used to demonstrate the procedure of cutting and to study the relationship between force modelling and force rendering which provides a useful simulation tool in interacting with a virtual skull model of a patient.

Chapter 6: Haptic Design Case Study in Space Robotic Path Planning and Tele-Operation

6.1 Introduction

In this chapter, the design methodology of the HARMP system is adopted for the design of a space robotics application and the methodology is evaluated to assess its suitability in this particular sector. Specifically, the path planning and tele-operation of a virtual space robotic system is considered and studied. Based on use case scenarios, the critical system requirements are investigated and identified within the boundary for the purpose of this study to assess graphical representation and haptic modelling. In order to represent these scenarios, CAD modelling of the space robotic system is developed to provide a base geometric representation for the haptic system. The aim of this modelling is to produce a realistic force-feedback for enhanced interaction during human and space robotic system interaction. These CAD models and haptic models collectively should meet the design requirements. Based on the geometric representation, a full kinematic model of the space robotic arm is developed, including forward kinematics and inverse kinematics. Forward kinematics is used to manipulate the robot with the use of the haptic controller, through a haptic user interface in this case a Phantom device, which is able to drive and determine how the remote site robot moves.

Inverse kinematics is derived to provide different capabilities. In this mode of operation, typically an end point with a set of orientation requirements are specified in simple cases to specify paths for the robot to achieve. In more complex applications, a spatial path trajectory is defined to specify how the robotic arm is to move in order to pass all these points on the trajectory with acceptable accuracy in terms of position (x,y,z) and orientation (dx,dy,dz) . From the given path specification, motion planning equations based on the robotic configuration are solved for the robotic manipulator to meet the path specifications.

Building on the previous geometric and kinematic models, haptic models are

required to represent the behaviour of interaction between the remote-site robots with its environment. The interaction is managed by a haptic controller which is normally supported by visual information of the environment in which the remote-site robot is operating. Haptic models are built and implemented for telepresence, as well as virtual constraints and guidance in position and dynamic control of a robotic system. For the space capturing tasks, two novel methods are proposed and compared for capturing a non-collaborative target with a redundant robot whilst transferring a null reaction torque to the base spacecraft. These methods offer many advantages with respect to current state of the art capture methods. Both methods have shown a good performance and in both cases the manipulator is able to reach the target with the desired end-effector velocity and with a null reaction torque transferred to the base spacecraft.

6.2 System Requirements and Specifications for Test Scenarios

The robotic system is designed to capture a target in space exploration in situations such as space debris removal. It is therefore necessary to provide a simulation and planning system to manipulate a space robotic arm, in order to achieve different tasks including approaching and capturing targets. The design methodology from Chapter 4 is utilised for this case study. The robotic system needs to meet following requirements:

Graphically the modelling system must:

1. Provide a user interface for a user to define such a robotic system in terms of its configuration, structure and behaviour.
2. Enable a realistic working environment for realistic geometric and visual representations of the actual environment.
3. Allow 3D model representation of the robotic system created by typical CAD systems to be imported into the modelling system.
4. While a user manipulates the haptic controller through a user interface, e.g. haptic arm or joystick, the robotic arm should move accordingly with kinematic

constraints and solutions, to ensure that minimum reactions are transferred to the base.

5. Provide visual information of the related objects in the tasks, such as the target or obstacles.

Haptically, the modelling system must

1. Make a user feel the presence of the robotic arm through inertia based force feedback or collision force when there is a such collision between the remote-site robot and its environment.
2. While a user manipulates the arm, provide an inertial force to prevent a user moving it rapidly as if there were no constraints in the physical world.
3. Send force feedback to the user if the arm is engaged with any obstacles in terms of collision or physical contacts intended.
4. In dealing with the task of capturing a target, guide the user to traverse and complete the task through an optimum path.

Table 6-1 Updated specification template

Specification category	Category attributes	Design parameter
Geometric model	Manipulation target	Robotic system model: Built and imported from CAD model
		Modification: Kinematics are solved while being manipulated
	Manipulator cursor	Indicating the supposed end effector position
Force model	Telepresence	Touch of target objects
		Frictional forces
	Constraints	Natural constraint: Joints limit
		Artificial constraint: Singularities Forbidden areas
	Guidance	Attraction: Towards target Dynamic control
		Repulsion: Avoid obstacles
Force rendering	Force scaling	Scale matching Scale resolution
	Threshold	Force threshold
	Force actuation	Actuating force model on Haptic device Stability
Environment model	Lighting condition	Showing the lighting condition in space environment
	Gravity	Simulate the gravity condition in space environment
	Working scenario	Other objects in working scenario i.e. target and obstacles
Task procedure planner	Integrated knowledge library	Inverse kinematics solution of manipulator to minimize reaction torque in space manipulation

6.3 HARMP Modelling for Space Robotics

In order to meet the system requirements and apply the general haptic system development methodology proposed in this study, generalised functional modules have been identified and hence reserved for these applications. Modifications have been made to the original HARMP system to tailor it to this specific application, and a review of this will be undertaken with a view to improve the methodology. Similar to the interface for dental surgery, the system architecture includes a Phantom Desktop as the haptic device, a haptic interface where a user can manipulate the robotic arm to achieve different tasks and a force engine that can 1) help a user detect the objects and obstacles, and 2) guide the user to achieve the specific tasks. Diverging from the dental model, the model of robotic arms used in the system needs to be designed to meet space task requirements and then created using CAD software. In addition, the inverse kinematic solution needs to be included in the system. This solution will allow a minimum reaction transfer to the base station while the arm is being manipulated in the space mission even with new types of constraints that come with being in a micro-gravitational environment. Finally, as a result of the environment change between Earth and space, the force engine requires modification to simulate the environment of space.

These changes and modifications are detailed in the following sections.

6.3.1 System Architecture

Building on the generic haptic system defined in Chapter 5, for the space environment, a customized system haptic architecture is developed.

As previously mentioned in Chapter 4, the system architecture for haptic space robotic tele-manipulation systems is shown in Figure 4-2. An operator manipulates the haptic device, which provides a position to the virtual interface to calculate the inverse kinematics of the robot and modify its path. This information is used to verify the path, detect any possible collisions and then update the geometric model. If the virtual robot reaches constraint boundaries, such as workspace or joints

limits, these virtual constraints are detected and sent back to the device. If a collision is detected or the path is rejected, calculated forces are also sent back to drive the haptic device which can be felt by the user. The guidance forces generated by path modification schemes (attraction or repulsion) are presented on the device as a haptic cue for a user to follow. This system architecture provides a structure on which to design a specific function in the HARMP system model.

6.4 Concept Design

Conceptual design of space robots is limited by the microgravity environment or planetary environments, which is a specialist area of research in itself. This research focuses on the design of a conceptual space robot for in-orbit servicing and maintenance and therefore the concepts need to meet the requirements identified in Table 6-1.

6.4.1 Geometric Modelling

6.4.1.1 CAD Software

PTC Creo is one of the software systems chosen to design and build the CAD model for the system. The Creo Parametric is a 3D CAD software widely used in industrial design and engineering. It has features such as parametric design, part modelling and assembly simulation. The parametric feature allows unified design for different parts, if the dimensional relationships between various parameters of a component are established and further relationships among the assembled parts are also assigned. Once these parametric relationships are established for a design, if the parameter of one part needs to be changed, other related parts and features will change accordingly. Therefore, this software is perfectly suited for part modelling of graphical system in this case study as it will enable a parametric model to be created for a potential group of space robotic systems for varied or different tasks.

The design requirements and known attributes of this new space robotic system are as follows:

1. The system is used to reach and capture a payload. The robotic arm manipulator

is installed on a space station.

2. After capturing and docking the payload to its end-effector, the robotic arm then manipulates the payload to transfer it to the space station.
3. When the task is completed, the robotic arm should park alongside the space station. The rest arm should be able to minimize its size compared to that when it is working.
4. The weight of a space robotic system should be carefully considered at design to ensure the energy efficiency.

6.5 Embodied Design

A conceptual scenario for a space robotic system working on a space station is described above. To focus on a kinematics algorithm and haptic feedback during manipulating and path planning of the robotic arm, the CAD model used in the haptic interface is redesigned accordingly (due to the lack of access to such a real operational system). A scaled version of such a large scale robotic system is more appropriate for use in this investigation. In a study of reaction control shown in Figure 6-1, a robotic arm model was built and the base was fixed to study Inverse Kinematic solutions (Cocuzza, Pretto and Angrilli, 2008a).

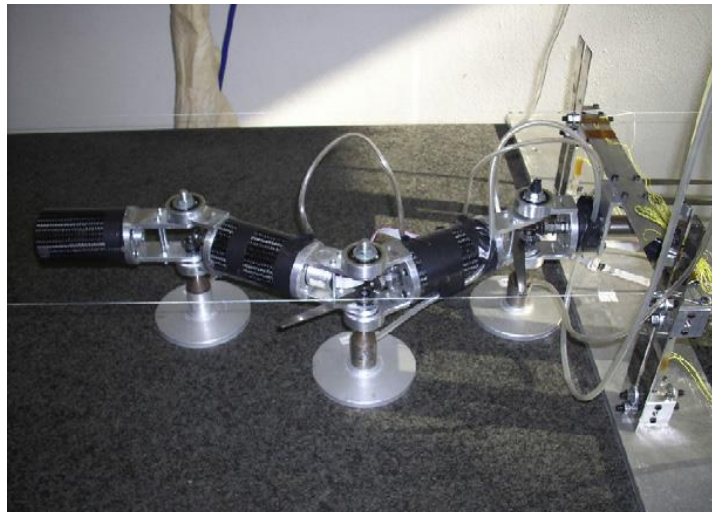
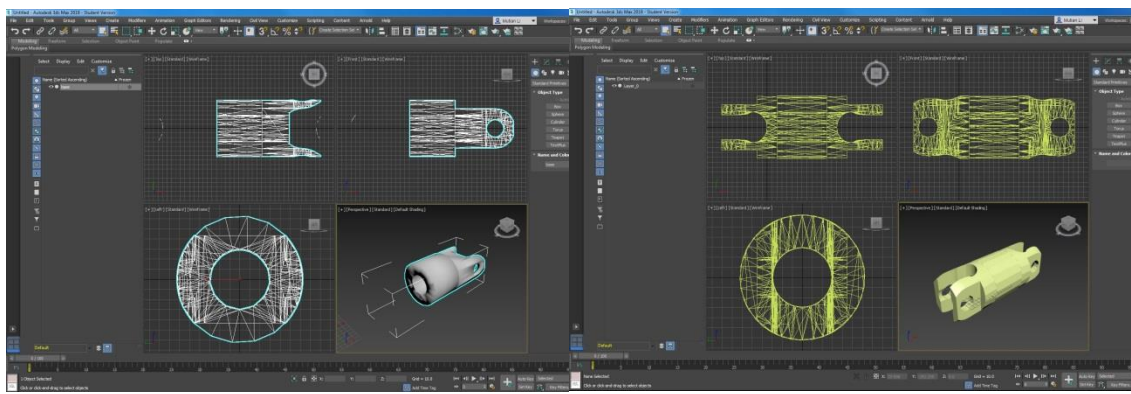


Figure 6-1 Experimental set-up of a three degrees of freedom robotic system

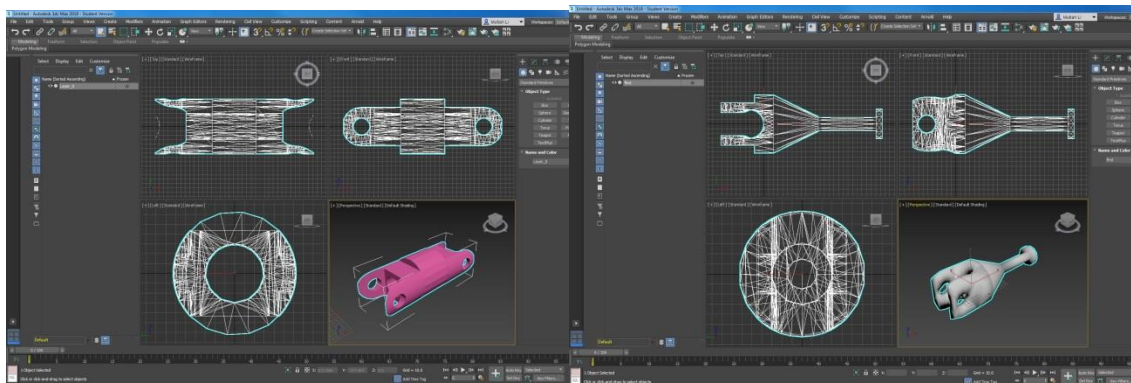
The length of each arm is: 0.176m, 0.176m, 0.1375m. The detailed parameters of

the 3D models are determined by the arm used in this experiment. Four parts of the arm are designed with the CAD software Creo: first the base and then the first, the second links, and lastly, the end effector. The base part serves as a mounting tool which connects the arms and the spacecraft as it would, for instance, on the space station. The first and second links as well as the end effector form a space robotic arm with four DOF. A multifunctional end effector is designed and attached at the end of the second link. This is representative of an arm that can be used to achieve missions such as refuelling, screw fixing or object capturing. After implementing the CAD model in Creo as shown in Figure 6-2, they are imported into 3DS Max for final modification.



a)

b)



c)

d)

Figure 6-2 Robotic arm model in 3DS Studio Max. a) base, b) first link, c) second link, d) end effector

As discussed in Chapter 5, the HARMP interface can take .obj file as geometric 3D model. Thus, these robotic models in 3DS Max need to be exported to .obj files that can be read and imported into the HARMP system. 3DS Max provides powerful exporting function available to a variety of data types. Polygon is selected as the

face type for the generation of the 3D model.

Two files are generated for each part, one is the .obj file which contains the coordinates of the vertices of all features of the robotic modelled parts. The other one contains the material information of the parts.

These files can be read and imported to the HARMF interface by calling several functions. The first step is to build the geometric models. In OpenHaptics, function `glmReadOBJ()` can be called to read the OBJ file and then the model object can be created and saved. Four parts of robotic arm models are imported, saved in an array structure `draggableobject`. The positions and rotations of each of the models can be adjusted due to the kinematics requirement. Function `hduMatrix::createRotation()` can be used to rotate the model over a specified axis, while the function `hduMatrix::createTranslation()` applies any change of position in x, y or z direction.

Finally, the processed models saved in the 'Draggableobject' array are visualised in the haptic interface. Geometric models can be created by calling function `glCallList()`. These models can then be haptically built by calling `hlBeginShape()` followed by `glCallList()`. In this way, models are graphically modelled with precise geometric representation of the robotic arms and these geometrical models are also haptically modelled and rendered in such a way that can be detected through the force feedback. The final designed models in the haptic interface are shown in the window as seen in Figure 6-3.

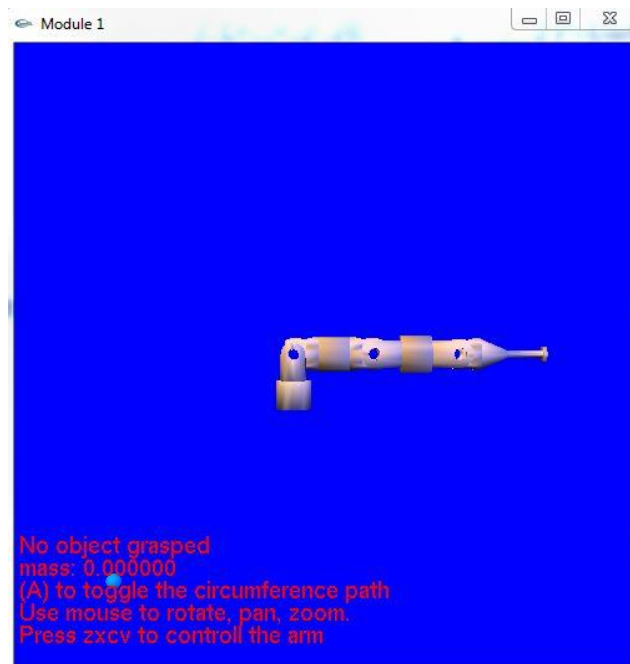


Figure 6-3 Imported robotic model in haptic interface

6.5.1 Manipulation of a Haptic Space Robotic Model

The next step is to find a method to manipulate this virtual robotic arm with the haptic device. The haptic device used in this study is the Phantom Desktop, with six DOF movements and three DOF force feedback. It can manipulate an object through joint translation and rotation. Similar to a mouse, a cursor can be shown on the screen as an indication of the input coordinate. The difference is that the cursor of a traditional mouse operates in 2D with coordinates only on the x and y axes, while the cursor of the haptic device is 3D, with an additional coordinate in the z-axis.

This 3D coordinate input by the haptic device can be set as the target in the position control of the four DOF space robotic arms. The other three DOF of the manipulator can be used to control the orientations of the specific arm if necessary, depending on the required task.

To achieve this manipulation of the robotic system, the following two questions need to be investigated: 1) How to set the frame workspace for robotic arms according to the workspace of the haptic device? 2) How to solve the inverse

kinematics problem of the arms while manipulated by the haptic space?

6.5.2 Workspace Mapping



Figure 6-4 Workspace frame of a Phantom haptic device.

A haptic interface may be selected or designed in many different ways and it is important to establish the mapping between the remote-site robotic coordinate system to the haptic input device coordinate system. This will allow the required movements to be mapped from the user input side to the remote-site robotic side. According to the programming guide for OpenHaptics, the workspace frame of a Phantom haptic device is shown in Figure 6-4. It is specified in an ordinary Cartesian system. The positive axis x is pointing to the right by default, the positive axis y is pointing up, while the positive axis z is pointing out to the front plane, towards the user.

For a robotic system, a frame refers to a pair of position and orientation representations. Normally, it is built by four vectors: one vector represents the position information, while the rotation matrix is described by the other three.

Therefore, in order to manipulate the robotic system in OpenHaptics workspace, the graphic frame shown in Figure 6-4 is also set as the reference frame of the robotic system. Then the position vector consists of x , y and z in a Cartesian coordinate system.

The next step is to map the workspace of Phantom haptic device to the workspace of graphic view in geometric representation. To define this mapping, the working dimensions of the haptic device are first considered. The physical workspaces of most haptic devices are not uniform for all its dimensions. For example, the Phantom Desktop used in this study has a workspace of 160 (W) \times 120 (H) \times 120 (D) mm. Directly mapping the device workspace by multiplying a scale matrix will lead to the non-uniform translation of the proxy. Therefore, for the uniform mapping to the scene, several convenient mapping methods are provided by HLAPI. By calling the function `hluFitWorkspace()` with parameter projection matrix which describe the volume of graphic scene, the device workspace can be mapped uniformly to meet the application's requirement.

6.6 Kinematic and trajectory analysis

6.6.1 Manipulator Kinematics

Kinematics studies the motion of the robotic manipulator, including position, velocity and acceleration. In this section, the position of the manipulator will be considered in static situation, while the velocity, acceleration and dynamics will be considered in later sections. The geometry of a manipulator can be complex, therefore different frames should be affixed to each part of mechanism. The relationship between the frames can be described and the position/orientation of the end effector can be calculated by solving functions of joint variables.

To describe the robot kinematics, a convention called Denavit—Hartenberg notation is normally used (Denavit and Hartenberg, 1955). Four quantities are given to each link, two are used to describe the current link: link length and link twist. The other two are for relationships with the connecting link: link offset and joint angle.

For example, in the case of revolute joint, there is one joint variable, joint angle, while the other three are link parameters that are fixed. Frames are allocated to the links. \hat{Z} axis of the frame is assigned coincident with the joint axis. \hat{X} axis is assigned pointing along the perpendicular from joint(i) to joint (i+1). Therefore, the four parameters are defined as (J. J. Craig, 2005):

link length $a_i =$ the distance from \hat{Z}_i to \hat{Z}_{i+1}

link twist $\alpha_i =$ the angle from \hat{Z}_i to \hat{Z}_{i+1}

link offset $d_i =$ the distance from \hat{X}_{i-1} to \hat{X}_i

joint angle $\theta_i =$ the angle from \hat{X}_{i-1} to \hat{X}_i

The robotic model used in this case study has three revolute joints, which is usually called a 3R manipulator as shown in Figure 6-5. For the planar 3R manipulator in this case study, the parameters are shown in Table 6-2:

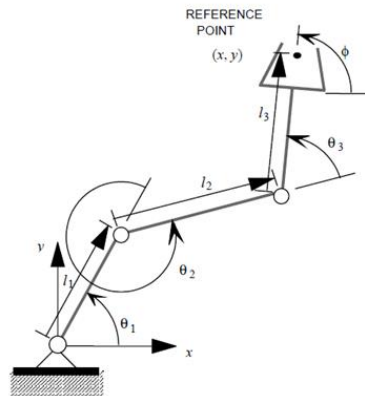


Figure 6-5 planar 3R manipulator

Table 6-2 Links parameters

i	a_{i-1} (m)	α_{i-1}	d_i (m)	θ_i
1	0	0	0	θ_1
2	0.176	0	0	θ_2
3	0.176	0	0	θ_3
4	0.1375	0	0	0

In order to determine the movement of end effector and each link, the

homogeneous transform matrix of the arms needs to be specified with above four parameters. To form a transform from frame 4 to frame 0, the kinematic problem is broken down to four sub problems of homogeneous transform matrix for each link that:

$$\begin{aligned}
{}^0_1T &= \begin{bmatrix} \cos\theta_1 & -\sin\theta_1 & 0 & 0 \\ \sin\theta_1 & \cos\theta_1 & 0 & 0 \\ 0 & 0 & 1 & 0 \\ 0 & 0 & 0 & 1 \end{bmatrix} \\
{}^1_2T &= \begin{bmatrix} \cos\theta_2 & -\sin\theta_2 & 0 & 0.176 \\ \sin\theta_2 & \cos\theta_2 & 0 & 0 \\ 0 & 0 & 1 & 0 \\ 0 & 0 & 0 & 1 \end{bmatrix} \\
{}^2_3T &= \begin{bmatrix} \cos\theta_3 & -\sin\theta_3 & 0 & 0.176 \\ \sin\theta_3 & \cos\theta_3 & 0 & 0 \\ 0 & 0 & 1 & 0 \\ 0 & 0 & 0 & 1 \end{bmatrix} \\
{}^3_4T &= \begin{bmatrix} 1 & 0 & 0 & 0.1375 \\ 0 & 1 & 0 & 0 \\ 0 & 0 & 1 & 0 \\ 0 & 0 & 0 & 1 \end{bmatrix}
\end{aligned}$$

The total transform matrix from frame 4 to frame 0 is determined by multiplication of these sub transformation matrixes, given by

$$\begin{aligned}
{}^0_4T &= {}^0_1T {}^1_2T {}^2_3T {}^3_4T \\
&= \\
&\begin{bmatrix} \cos(\varphi) & -\sin(\varphi) & 0 & 0.176\cos\theta_1 + 0.176\sin(\theta_1 + \theta_2) + 0.1375\cos(\varphi) \\ \sin(\varphi) & \cos(\varphi) & 0 & 0.176\sin\theta_1 + 0.176\cos(\theta_1 + \theta_2) + 0.1375\sin(\varphi) \\ 0 & 0 & 1 & 0 \\ 0 & 0 & 0 & 1 \end{bmatrix}
\end{aligned}$$

$$\text{where } \varphi = (\theta_1 + \theta_2 + \theta_3) \qquad \text{Eq. 11}$$

6.6.2 Inverse Kinematics

Once the target position is input by the haptic device, inverse kinematics needs to be solved to calculate the joint angles. Then the geometric model can be updated to show the movements of arms.

6.6.2.1 Solutions Condition

The inverse kinematic problem of a manipulator is non-linear. The number of solutions depends on the DOF of the manipulator. The existence of the solution depends on the workspace of the arms (J. J. Craig, 2005). For example, for a two-link robotic arm, the lengths of two links are L_1 and L_2 . The workspace of this manipulator is limited by a circle with radius of (L_1+L_2) as outer boundary and a circle with radius of $|L_1-L_2|$ as inner boundary. The condition of solutions depends on this workspace: 1. If the target is out of this workspace, then no solution exists. 2. If the target is right on the boundary, there is only one solution. 3. When target is within this workspace, there are two solutions to this inverse kinematic problem.

6.6.2.2 Multiple Solutions

For a robotic arm with three links, the structure of this model is similar to the geometric model built for the prototype discussed in this chapter. Although, the workspace, the position and orientation of the end effector are fixed, there are two solutions to the inverse kinematic problem, only one of the solutions needs to be selected. Based on the principle of minimum energy consumption, generally speaking, the solution with less movement is a better solution.

6.6.2.3 Geometric Solution

Basic Inverse kinematics and the joint variables and link lengths for a 3R planar manipulator is analysed as:

$$\begin{aligned}\theta_1 &= \gamma + \sigma \cos^{-1}\left(\frac{-(x'^2 + y'^2 + l_1^2 - l_2^2)}{2l_1\sqrt{x'^2 + y'^2}}\right) \\ \theta_2 &= a \tan 2\left(\frac{y' - l_1 \sin \theta_1}{l_2}, \frac{x' - l_1 \cos \theta_1}{l_2}\right) - \theta_1 \\ \theta_3 &= \varphi - \theta_1 - \theta_2\end{aligned}\tag{Eq. 12}$$

where

$$\gamma = a \tan 2\left(\frac{-y'}{\sqrt{x'^2 + y'^2}}, \frac{x'}{\sqrt{x'^2 + y'^2}}\right)$$

$$\sigma = \pm 1$$

This inverse kinematic problem is solved using a combination of algebraic and geometric method. For the 3R planar manipulator, the problem has multiple solutions. However, as can be seen from the solution, if the position and orientation of the end effector are already determined, there are only two solutions for the inverse kinematic with $\sigma=1$ or -1 . In this way the basic inverse kinematic of the manipulator can be solved in static situation. The inverse kinematic considering dynamics required in space environment is discussed in section 6.6.

6.6.3 Mapping between Device and Virtual Robot

To achieve the teleoperation of the virtual robot using the haptic device, a method to connect the frame of haptic device and the frame of the end effector must be found. Since the structure of a haptic device and the virtual robot are not identical, this connection needs to be carefully mapped. There are two main methods to achieve this mapping.

The first method is to link and map the joints of the haptic device to the virtual manipulator's joints. Specifically, the length of a link in the haptic device is measured, similarly with the length of the matching link in the virtual robotic arm. For each of these pairs, it is then possible to find the ratio of their lengths. The scale factor is calculated by dividing the length of a matching link in virtual robotic arm by the length of a link in the haptic device. The Phantom Desktop used in this study has six DOF/ (six revolute joints), while the virtual robotic model built and prototyped has four DOF (four revolute joints). Therefore, it is adequate for the control of joints of a virtual manipulator. The corresponding joints can be directly coupled or with a ratio, in this way the manipulator can be controlled by changing the joint angles of one or more device joints. This method can achieve direct control of the joints angles of a manipulator, however, without being able to precisely control the

position of links or end effector. Also, it depends on the similarities of structures between the haptic device and the manipulator. Therefore, a more universal mapping method needs to be formulated.

The second method is more universal. It links the haptic device position to the position of the end effector of manipulator. As previously explained in this chapter, the device position in work coordinates can be mapped into world coordinates of the graphical scene. This mapped device position can be used to control the position of the end effector and the movement of joint links can be solved using inverse kinematics.

To solve the inverse kinematic problem of our model, variables of position (x,y) and orientation φ of the end effector in equations need to be determined. Therefore, a hybrid method combining the above two methods is formulated and utilized. The target point (x, y) is determined by the x, y of position input from the haptic device in world coordinate. The orientation of the end-effector is determined by the roll joint of the haptic device. Lengths of three links are also available, so the joint angles can be solved for this 2D planar scenario. The next step is to extend this solution to 3D space. The z orientation of the position input from the haptic device is included in the calculation. While the target is moving in 3D space, the manipulator is rotating by the Y axis by an amount of $\arctan(z/x)$. The new target position (x, y) is now determined by $(\sqrt{x^2+z^2}, y)$.

Once all the joint angles are solved, the homogeneous transform matrix of each link can be determined by:

$${}^0T_i = {}^0T_1 {}^1T_2 \dots {}^{i-2}T_{i-1} {}^{i-1}T_i$$

The translation and rotation functions are called in the haptic interface to update each geometric part of the robotic model accordingly. The virtual robotic arm can now be manipulated to reach a target with the required orientation of the end-effector as shown in Figure 6-6.

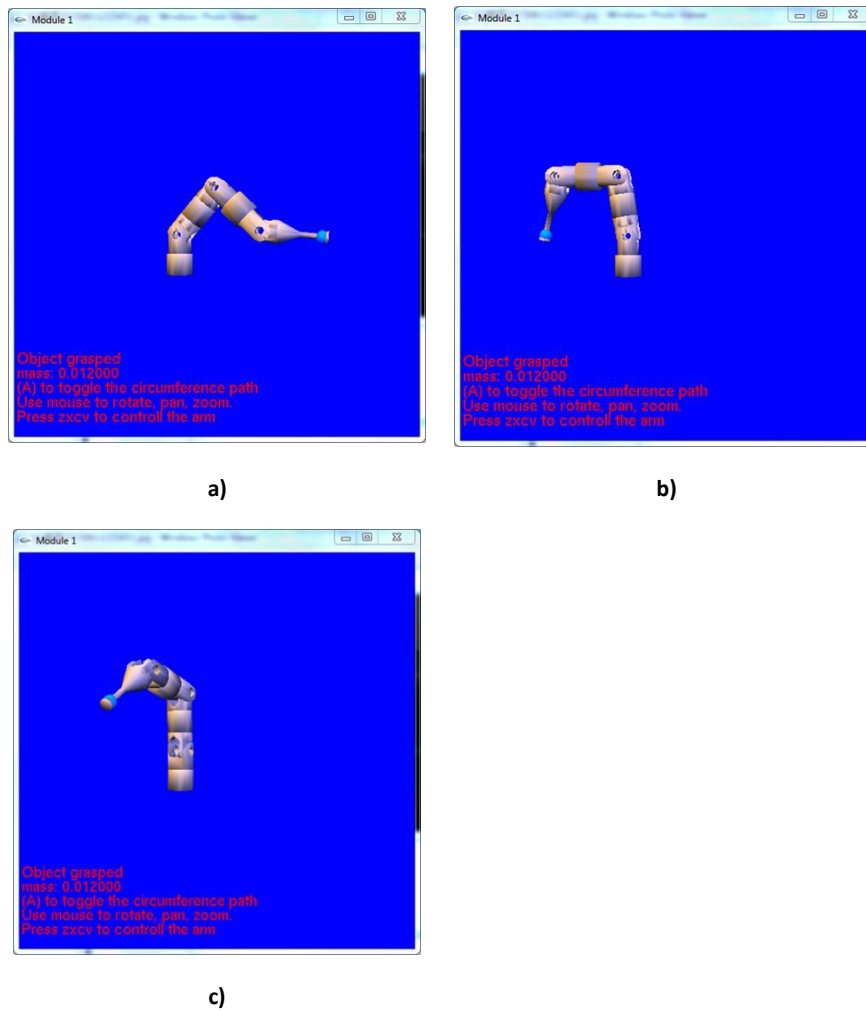


Figure 6-6 Robotic model being manipulated via the haptic interface

The geometric model for basic robotic manipulator control is complete.

6.7 Force Modelling for Haptic Rendering

Having established the relationships in terms of geometries of two sets of dimensions in the virtual world as well as the haptic input device, it is necessary to integrate the haptic features into the space robotic control system. According to the design methods of the HARMP system and the system architecture of the space robotic control, the haptic features can be designed and implemented for three objectives: telepresence, constraints, and guidance.

6.7.1 Telepresence

6.7.1.1 Haptic Presence of Object

This scenario represents space exploration in orbital environments where there may be poor or even no visual feedback, for example in a remote environment such as that surrounding the space station during the dark period. In order to achieve telepresence of a space robotic system in a space environment, the first task is to haptically feel the shape of objects. These objects can be a space station, an approaching spacecraft and expected or unexpected obstacles. This function can be implemented by shape rendering provided by HLAPI in OpenHaptics. The surface of an object can be touched and felt by the user using a proxy position method. For example, Figure 6-7 shows a virtual 3D model of the International Space Station (ISS) imported to the HARMP interface. While manipulating the space robotic arm using a haptic device, if the end effector comes in touch with the surface of the station and follows its contour, a user can feel the shape of the touched surface through the force signals sent back to the haptic device. Similarly, if any obstacles appear in the environment and are imported into the interface, they can be felt and detected by the user while manipulating the arm, providing assistance in the path planning of the manipulator. In this way, this haptic feature makes it possible for a user to detect the objects with a sense of touch in the space environment, especially during harsh visual conditions.

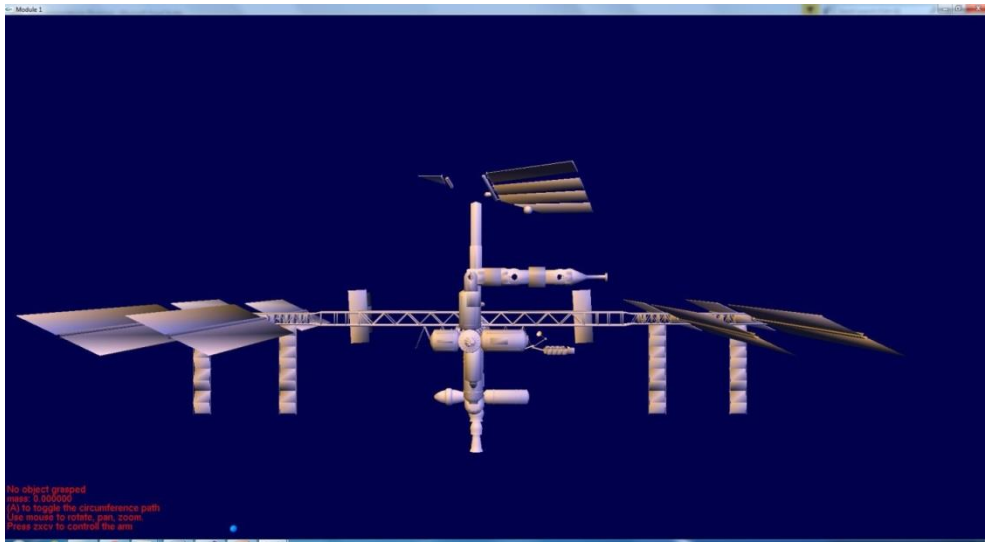


Figure 6-7 Model of ISS in HARMP interface

6.7.1.2 Micro-Gravity

Another special property relating to a space environment is the microgravity environment in which the robotic system needs to operate, which is very different compared to the normal working environment on the Earth. Normal acceleration resulting from gravity near the Earth surface is $1g$, which is equal to $9.8m/s^2$. Therefore, while designing and planning motion of a robotic system on Earth, gravity needs to be considered as an environmental force applied on the arms. However, for spacecraft such as space shuttle or space station that travel in orbit at a velocity approximately $28000km/h$, the acceleration towards the Earth is close to zero (sometimes referred to as Zero Gravity or microgravity at $10^{-0}g$) (NASA, 2009). Objects on the space station appear to be in a free floating state. To achieve the teleoperation of a space manipulator with a haptic control, this free floating state should also be considered and applied on the master controller, i.e., the haptic device as the result of telepresence. There are potentially two working scenarios of this teleoperation of the space manipulator. The first scenario is that an astronaut manipulates the haptic device inside the space station to control a robotic manipulator installed outside. In this situation, since the haptic device is also in microgravity environment, there is no extra work required for the consideration of the gravity effect in the haptic environment installed inside a space station with a

simulation. The second working scenario is that a user manipulates the master haptic device on Earth to control the manipulator in orbit. In this situation, the mass of one or more links of the haptic device can be felt by a user during the operation, instead of free floating. To solve this problem, a new simulation method is implemented, a force F is modelled and assigned to the positive y-axis pointing up, that

$$F_i = m_i g + F_{ifricition_on_joint} \quad Eq. 13$$

where i is the ' i 'th joint of the robotic manipulator, m is the mass of parts of the haptic device that come into contact with the user's hand during a manipulation. As it is in the Earth environment, it is difficult to represent the microgravity environment of the master haptic device and this will be represented and modelled in this approach as the part mass of the haptic master device. The part mass is normally quite small and therefore the gravitational force due to this is also small. A user is made aware of this approach and the small additional force due to this modelling approach. In this way, the free floating state of the remote-site robotic manipulator can be simulated on the haptic device, giving a user a better understanding of the robotic manipulation in a space environment through the sense of touch.

6.7.1.3 Friction Force

Another environmental force that might apply to the space manipulator is frictional forces. The study of friction between components with contacting surfaces and relative motion in space environment is called space tribology (Roberts, 1990). The different ranges of temperature and pressure experienced by components in space environment can be extreme, making it unfeasible to lubricate using traditional methods like liquid oils. Therefore, for the lubrication of spacecraft mechanism in space environment, thin and solid films were introduced as solution for low friction. The performance of these materials also varies due to the temperature and how long time it has been used. The behaviour of several polymers at different temperature has been studied by Gradt et al (Gradt *et al.*, 1998). Six polymers were

tested at temperatures of 8K, 77K and 300K. In the test the best performance came from the material polytetrafluorethylene (PTFE). With the use of PTFE the friction coefficient ranges from 0.04 to 0.075 under conditions of vacuum and different temperatures. Therefore, this friction force needs to be considered for the haptic control simulation.

6.7.2 Constraints

6.7.2.1 Natural Constraints

Natural constraints in haptic teleoperation are defined by the structure and mechanism of the robotic model. For the four DOF 3R manipulator used in this study, it is constrained by the links length and joints angle. Assuming the ideal joints angle limit is $(-\pi, \pi)$, then the working space of the robotic arm is a sphere with the radius of the sum of lengths of all three links, centred at the base of the manipulator. Therefore, the constraints can be deployed at the inner surface of this sphere by introducing a spring damper model with high stiffness. In this way, it can prevent the user from driving out of the work space making it unsolvable for the kinematics and the motion control of the manipulator.

6.7.2.2 Artificial Constraints

Artificial constraints in the haptic teleoperation can be defined according to the requirement of specific space tasks. The manipulation will be strictly constrained for desired path or movement. These artificial constraints may have different types and shapes, including point, line, parametric curve, plane, parametric surface, or even polygonal meshes. Again, to implement the artificial constraints, the spring damper model with high stiffness is introduced and integrated. For example, if the movement of the robotic manipulator is required to keep on a plane surface, a spring damper model can be used to form a virtual wall as a simulation of the desired surface. In this way, the artificial constraints can be used for the specific tasks. However, since the constraint is strict and dictatorial it should be carefully chosen and designed for the purpose of introducing a forbidden area. Otherwise, the guidance force should be considered which is more suggestive and allows user's

control in the control loop.

6.7.3 Guidance

6.7.3.1 Repulsion Guidance

Apart from the limit of working space, there is another critical issue for robotic motion planning that needs to be considered, namely singularities. Singularities are points where the Jacobian matrix of a manipulator becomes singular and non-invertible. Therefore, the joint angles and velocities cannot be solved for the desired path. Reaching singularities will cause the manipulator to lose certain degrees of freedom, making it uncontrollable in some directions. Generally, the position of singularity points can be classified to two categories: at a working space boundary or inside a working space. All kinds of manipulators have singularities in their working space boundaries. In this case, all the links of the manipulator are fully stretched and the end effector is almost reaching or at the working space boundary. The other case is that most manipulators have singularities inside the working space. This happens while two or even more joints are lining up. By introducing repulsion guidance force, as shown in Figure 6-8, into the control system, these singularities can be avoided while being manipulated by the user.

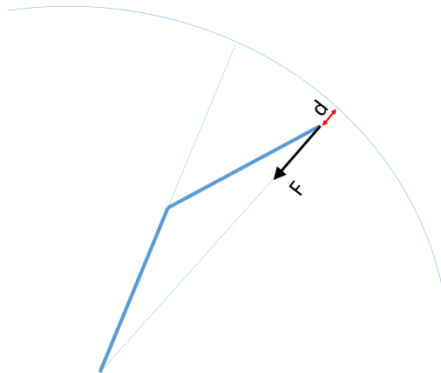


Figure 6-8 Repulsion force to avoid singularities

Another use of repulsion guidance is to predict and avoid the obstacles in advance. The telepresence of the shape of the objects is already introduced by implementing the high stiffness spring damper model. However, in many circumstances in the working scenario of the robotic manipulation, the contact or collision between the

manipulator and obstacles in the environment is strictly not allowed. With the telepresence of the obstacle it can be detected by the user but it is too late for a user to react if the contact is unwanted. Therefore, the prediction of the obstacle and avoidance in advance is necessary for the haptic control of the space manipulator.

This is where the potential field method in path planning problems can be utilized. As introduced in state of art models repulsion potentials can set around obstacles, with point subject to potential (PSPs) placed on robot links. As a result, obstacles appear to exhibit repulsion forces towards the robot. By implementing this repulsion potential method with the haptic work space on the haptic device, providing repulsion force back to the user, the potential obstacles can be detected in advance. A sphere of influence of the obstacle is introduced in the force modelling. It can be determined according to the properties of the obstacle and the manipulator, or due to specific requirement of the task. While the manipulator is outside of this sphere of influence, the motion of the manipulator is being affected. The repulsion potential field is activated while the manipulator enters the sphere of influence, and the repulsion force increases while getting closer to the obstacle. At this stage, a user can make a decision whether to go on further or begin to find an alternative path to avoid the obstacles. This repulsion guidance allows full control by user which is different from the strict constraints. This is important and necessary since the choice of motion might be compromised between safety and performance, and should be made depending on the experience of the user.

Assuming a point subject to potential is set on the end effector, and not allowed to touch the obstacle, then the repulsion potential field is:

$$U_{rep} = \begin{cases} \frac{1}{2}\eta \left(\frac{1}{D} - \frac{1}{\rho}\right)^2 & \text{if } D \leq \rho \\ 0 & \text{if } D > \rho \end{cases}$$

Where

D is the minimum distance between the end effector and the obstacle, ρ is the radius of sphere of influence, η is a constant of scaling factor for the equation.

Then while inside the sphere of influence the repulsion force is:

$$\begin{aligned}
 F_{rep} &= \\
 &= -\nabla U_{rep} \\
 &= -\nabla \left(\frac{1}{2} \eta \left(\frac{1}{D} - \frac{1}{\rho} \right)^2 \right) \\
 &= -\eta \left(\frac{1}{D} - \frac{1}{\rho} \right) \nabla \left(\frac{1}{D} - \frac{1}{\rho} \right) \\
 &= \eta \left(\frac{1}{D} - \frac{1}{\rho} \right) \left(\frac{1}{D^2} \right) \nabla D \qquad \text{Eq. 14}
 \end{aligned}$$

Where ∇D is the unit vector of the minimum distance directing from end effector to the obstacle.

To implement this repulsion potential field and force into the HARMP system, the position and geometry of the obstacles must be identified in advance. The position of the end effector can be defined as the proxy position in world space. The distance and vector between the end effector and the obstacle can be calculated. The relative repulsion force can be calculated and sent back to the haptic device with a given sphere of influence.

6.7.3.2 Attraction Guidance

The artificial potential field includes repulsion and attraction potentials. The repulsion potential is used to predict and avoid the obstacles in advance. Similarly, the attraction potential can be used in the HARMP system as attraction guidance towards the targets or as assistance for the user to follow the desired path. The attraction potential field can be described as:

$$U_{att} = \frac{1}{2} k d^2$$

Where d is the distance between the end effector and the target, k is a constant of scaling factor.

Then the attraction force is:

$$\begin{aligned} F_{att} &= -\nabla U_{att} \\ &= -\nabla\left(\frac{1}{2}kd^2\right) \\ &= -k d\nabla d \end{aligned} \tag{Eq. 15}$$

Where ∇d is the unit vector of the distance pointing from the end effector to the target.

Again, to implement this attraction potential field and force into the HARMF system, the position and geometry of the target can be identified. If the target is moving, the position can be updated during the manipulation. The position of end effector can be defined as the proxy position in world space. The distance and vector between the end effector and the obstacle can be calculated in real time. The corresponding attraction force can be calculated using Eq. 15 and sent back to the haptic device to guide the user towards the target.

6.7.4 Dynamic Control

The above method using the potential field can achieve position control of the manipulator, guide user to reach a target and avoid the obstacles. However, it does not control the velocity of the manipulator, which is not adequate for manipulation tasks that require control of velocity during the path such as object capturing. Therefore, the guidance force should also be introduced to assist the dynamic control of the manipulator.

The dynamic control in this case study focuses on achieving two goals. Firstly, it aims to control the velocity of the manipulator by providing a guidance force to the haptic device. If the user agrees with the guidance and follows the device without applying any external forces, the end effector will move with a desired velocity. If the user decides to change the position and velocity of the end effector by applying forces on the haptic device, the device will follow the user's command until the

applied forces finish. After finishing applying forces on the device, the user will be assisted to maintain the desired velocity of the end effector again. This velocity control can be used in tele-manipulation tasks such as following or capturing an object travelling with a known velocity. The position and travelling path of the target object might be unknown or inaccurate due to the limited performance of the sensing system in a harsh space environment. This is where the reaction and control by a user in real time is required. While manipulating the end effector, the relative position between end effector and the target can be controlled by the user. At the same time, the guidance force can help the user maintain a stable relative velocity, allowing the user to be able to focus on the procedure of other operations such as refuelling and capturing.

The next goal of haptic guidance in dynamic control of the manipulator is to reach both the desired position and velocity. Guidance force will be provided on the haptic device as assistance to the user. If the user agrees with the guidance and follows the device without applying any external forces, the end effector will reach a static or moving target position with a desired velocity. This dynamic control can be used in telemanipulation tasks such as capturing a target object with a known velocity and trajectory. The guidance should produce an optimum capturing path reaching the target calculated in real time considering the travel time and distance. The user can engage and take charge of the control at any time if a better solution is available, or to deal with unexpected events such as unknown obstacles. After the engagement of the user, the optimum path will be calculated again and the guidance force will be updated to continue assistance in the task. Both of these guidance methods provided for dynamic control are suggestive, still allowing full control of manipulator by the user.

6.7.4.1 Implement for Velocity Control

The haptic device used in this study uses impedance. Thus to achieve the velocity control into the HARMP system, the impedance control of the haptic controller needs to be studied and implemented. Impedance control takes forces from the

environment and outputs changes in positions. A typical impedance control is a linear second-order system expression with mass, spring, and damper shown in Figure 6-9,

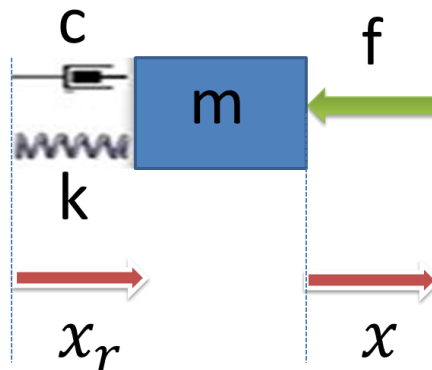


Figure 6-9 Typical impedance control

The system fits the equation:

$$m\ddot{x} + c\dot{x} + k(x - x_r) = -f \quad \text{Eq. 16}$$

Where \ddot{x} , \dot{x} and x are acceleration, velocity and position of the end effector, m is the mass, c is the damper constant and k is the stiffness of the spring. f is the external force applied on the device in the environment.

The impedance control model can be modified for velocity control in this study. The stiffness, k , in the system demonstrates the stiffness reacting to the external force applied to the device. In this case, while the user engages the control of manipulator, the haptic device will follow the user's commands to achieve force control. Therefore, a stiffness $k = 0$ is set in this case model. Including the guidance force into the system, the model in velocity control can be described in Figure 6-10:

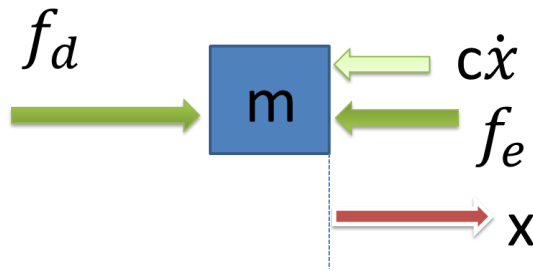


Figure 6-10 Modified impedance model for velocity control

The system is described by the equation:

$$m\ddot{x} + c\dot{x} = f_e - f_d \quad \text{Eq. 17}$$

Where m is the mass, c is the damper constant, \ddot{x} , \dot{x} are acceleration and velocity of the end effector of the device. f_d is the force applied by the actuator of the device and f_e is the environmental force applied by the environment i.e. by the user.

While being followed by the user without any interference external force, the guidance force provided to the user should be:

$$f_d = m\ddot{e} + c\dot{e} \quad \text{Eq. 18}$$

where \ddot{e} , \dot{e} is the acceleration and velocity error between the desired and actual values.

In this way the guidance force for velocity control is complete and can be integrated with the haptic device. For dynamic control of a desired velocity, position or path, the guidance force will be solved in the next section along with the dynamic analysis of the space manipulator.

6.8 Reaction Control Solution

Until now only a geometric model of the space manipulator has been created, where the static forward and inverse kinematics are solved, as well as the haptic assistance for telepresence, the virtual constraints and guidance in position and velocity control are introduced. The next task is to formulate a solution for the reaction control of the space manipulator that takes the special requirements of

dynamics in space into account.

6.8.1 Least-Squares-Based Reaction Control Solution

For a n -DOF redundant space manipulator which has k components of the end-effector pose to track, it has the degree of redundancy as defined by $r = n - k > 1$. If r equals the number of reaction torque components to be minimized, it is able to study the condition of IK solution with a zero torque. To minimize the reaction torque transferring to the base, the redundancy needs to be solved at the desired acceleration levels. Therefore, the Forward Kinematics equation can be described as:

$$\mathbf{J}\ddot{\mathbf{q}} + \dot{\mathbf{J}}\dot{\mathbf{q}} - \ddot{\mathbf{x}} = \mathbf{0} \quad \text{Eq. 19}$$

where $\ddot{\mathbf{x}}$ represents the desired acceleration of the end-effector, $\dot{\mathbf{q}}, \ddot{\mathbf{q}}$ are the joint velocities and accelerations, and $\mathbf{J}, \dot{\mathbf{J}}$ are the *Generalized Jacobian Matrix* and its time derivative of the manipulator (Umetani and Yoshida, 1989). For redundant manipulators Eq. (19) is indeterminate since $k < n$.

If a desired acceleration vector $\ddot{\mathbf{x}}$ of the end-effector is given, \mathbf{q} and $\dot{\mathbf{q}}$ at present are known, Eq. (19) can be solved by the pseudoinverse of the Generalized Jacobian Matrix:

$$\ddot{\mathbf{q}} = \mathbf{J}^\dagger(\ddot{\mathbf{x}} - \dot{\mathbf{J}}\dot{\mathbf{q}}) + (\mathbf{I} - \mathbf{J}^\dagger\mathbf{J})\ddot{\boldsymbol{\phi}} \quad \text{Eq. 20}$$

The first part on the right-hand side of the Equation represents the classical *pseudoinverse solution*, which is the particular solution that minimizes $\|\ddot{\mathbf{q}}\|$, while the second term represents the general solution of the homogeneous system $\mathbf{J}\ddot{\mathbf{q}} = \mathbf{0}$. Different $\ddot{\mathbf{q}}$ can be generated for the same $\ddot{\mathbf{x}}$ by varying the vector $\ddot{\boldsymbol{\phi}}$ arbitrarily and projecting it onto the null-space of \mathbf{J} by means of the projecting operator $(\mathbf{I} - \mathbf{J}^\dagger\mathbf{J})$, where \mathbf{I} is the identity matrix.

The *pseudoinverse solution*, which is also called *LS solution*, can be used as a reference in order to measure the performance of the solution which minimizes the reaction torque (Cocuzza *et al.*, 2007).

On the other hand, the reaction torque about the centre of mass of the spacecraft can be described as:

$$\mathbf{T} = \mathbf{M}\ddot{\mathbf{q}} + \mathbf{n} \quad \text{Eq. 21}$$

where the mass matrix \mathbf{M} depends on the joint variables of the manipulator \mathbf{q} , while the centrifugal and Coriolis term \mathbf{n} depends on both \mathbf{q} and $\dot{\mathbf{q}}$.

Then the suitable measure for the base reaction torque is represented by the quadratic cost function:

$$f(\ddot{\mathbf{q}}) = \mathbf{T}^T \mathbf{T} = \|\mathbf{T}\|^2 \quad \text{Eq. 22}$$

which depends on $\ddot{\mathbf{q}}$ only, since the current \mathbf{q} and $\dot{\mathbf{q}}$ are considered as state variables.

In this context, the following local constrained optimization problem can be defined as:

$$\begin{aligned} \text{Min } f(\ddot{\mathbf{q}}) &= \mathbf{T}^T \mathbf{T} \\ \text{subject to } \mathbf{J}\ddot{\mathbf{q}} + \dot{\mathbf{J}}\dot{\mathbf{q}} - \ddot{\mathbf{x}} &= \mathbf{0} \end{aligned} \quad \text{Eq. 23}$$

where $\ddot{\mathbf{q}}$ represents the local optimization variable.

The base reaction torque \mathbf{T} in Eq. 21 depends linearly on $\ddot{\mathbf{q}}$, since the current \mathbf{q} and $\dot{\mathbf{q}}$ are considered as state variables. Eq. 23 can therefore be interpreted as the formulation of a linear *Least Squares problem with Equality constraints* (LSE) (Cocuzza, Pretto and Angrilli, 2008a).

A closed-form solution can be found for the LSE problem by combining Eq. 20 and

Eq. 21:

$$\begin{aligned} \ddot{\mathbf{q}} = & \mathbf{J}^\dagger (\ddot{\mathbf{x}} - \dot{\mathbf{J}}\dot{\mathbf{q}}) + \\ & -[\mathbf{M}(\mathbf{I} - \mathbf{J}^\dagger \mathbf{J})]^\dagger [\mathbf{M}\mathbf{J}^\dagger (\ddot{\mathbf{x}} - \dot{\mathbf{J}}\dot{\mathbf{q}}) + \mathbf{n}] \end{aligned} \quad \text{Eq. 24}$$

The solution introduced in this section and its extension which takes into account the limits of joint acceleration, result to be suitable for real-time implementation.

A useful generalization of the constrained optimization problem of Eq. 23 can be made by introducing inequality constraints on joint accelerations:

$$\begin{aligned} \text{Min } f(\ddot{\mathbf{q}}) = & \mathbf{T}^\mathbf{T} \mathbf{T} \\ \text{subject to } & \begin{cases} \mathbf{J}\ddot{\mathbf{q}} + \dot{\mathbf{J}}\dot{\mathbf{q}} - \ddot{\mathbf{x}} = \mathbf{0} \\ \bar{\mathbf{q}}_l \leq \ddot{\mathbf{q}} \leq \bar{\mathbf{q}}_u \end{cases} \end{aligned} \quad \text{Eq. 25}$$

where $\bar{\mathbf{q}}_l, \bar{\mathbf{q}}_u$ represent the lower and upper acceleration limits respectively. The inequalities are interpreted component wise, and the joint acceleration limits may in general be different for each robot joint. This formulation leads to the minimization of the base reaction torque and to the limitation of joint accelerations under physically acceptable values. In particular, this formulation has the advantage that the avoidance of algorithmic instabilities may be automatically fulfilled.

The theory presented in this section takes into consideration the base reaction torques minimization. Nevertheless, it can be extended to the minimization of the base reaction forces and of weighted combinations of base reaction torques and forces.

6.8.2 Capture Methods and Simulated Result

For the capture of a moving target, two capturing methods are designed and compared. The procedure of capturing can be simulated in Matlab, by monitoring the value of parameters including the joint variables, end effector's position, velocity, acceleration and their errors regarding the target, as well as the reaction torque to the base. This data will be collected and analysed to evaluate the

performance of the reaction control solutions and capturing methods.

6.8.2.1 Parametric-Trajectory Reactionless Capture Method

In the first capture method, which is referred to as “Parametric-trajectory reactionless capture method”, the LSE method is used, with a parametric half circle trajectory for the end-effector.

The parametric information (radius, centre, curvilinear abscissa) are computed from the target information (initial position, direction, velocity), in such a way that the target is captured at the point of its trajectory with minimum distance with respect to the end-effector’s initial position. The end-effector trajectory is tangent to the target trajectory at the time of capture. The end-effector velocity is the same as the target velocity at the time of capture and the curvilinear abscissa is derived (by integration) from a curvilinear acceleration which is a combination of cosine functions (in order to have a sufficiently smooth curvilinear abscissa, i.e. to be continuous with continuous derivative up to the 2nd order derivative).

Two target trajectories were tested in order to show the performance and reliability of the capture method, which works for any target trajectory, with the obvious exception of the cases in which some kinematic or dynamic singularity of the manipulator is encountered (which can be avoided by using standard singularity avoidance methods).

Target trajectory 1: target approaching with a 45° angle with respect to the Ox axis of the manipulator (see for example Figure 6-11).

Target trajectory 2: target approaching with a 0° angle with respect to the Ox axis of the manipulator. (see for example Figure 6-14).

The target velocity is set to 0.1 m/s in both cases.

6.8.2.1.1 Target Trajectory 1

In Figure 6-11 a stroboscopic view of the robotic capture is presented, together with

the plot of the reaction torque (bottom), which is always null with some negligible numerical noise.

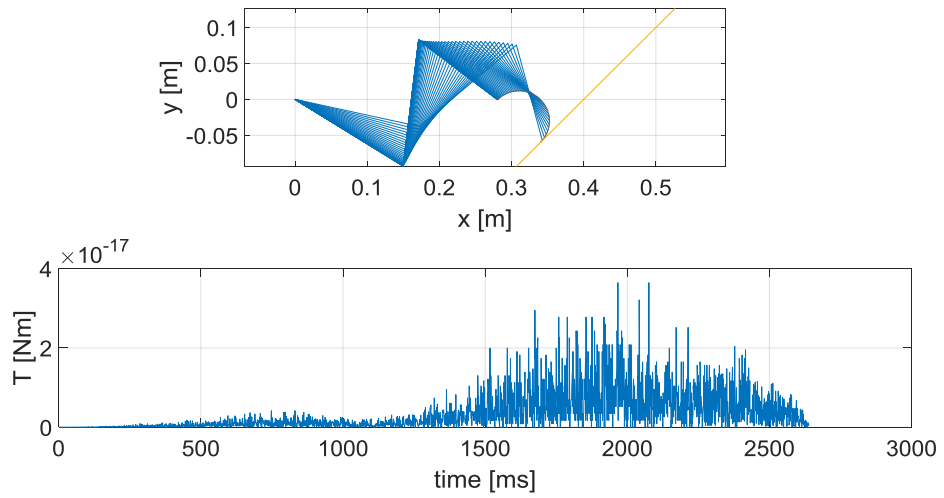


Figure 6-11 Stroboscopic view of robot motion (top), and reaction torque (bottom). Parametric trajectory 1

In Figure 6-12 the plot of the curvilinear abscissa and its first and second derivatives are presented.

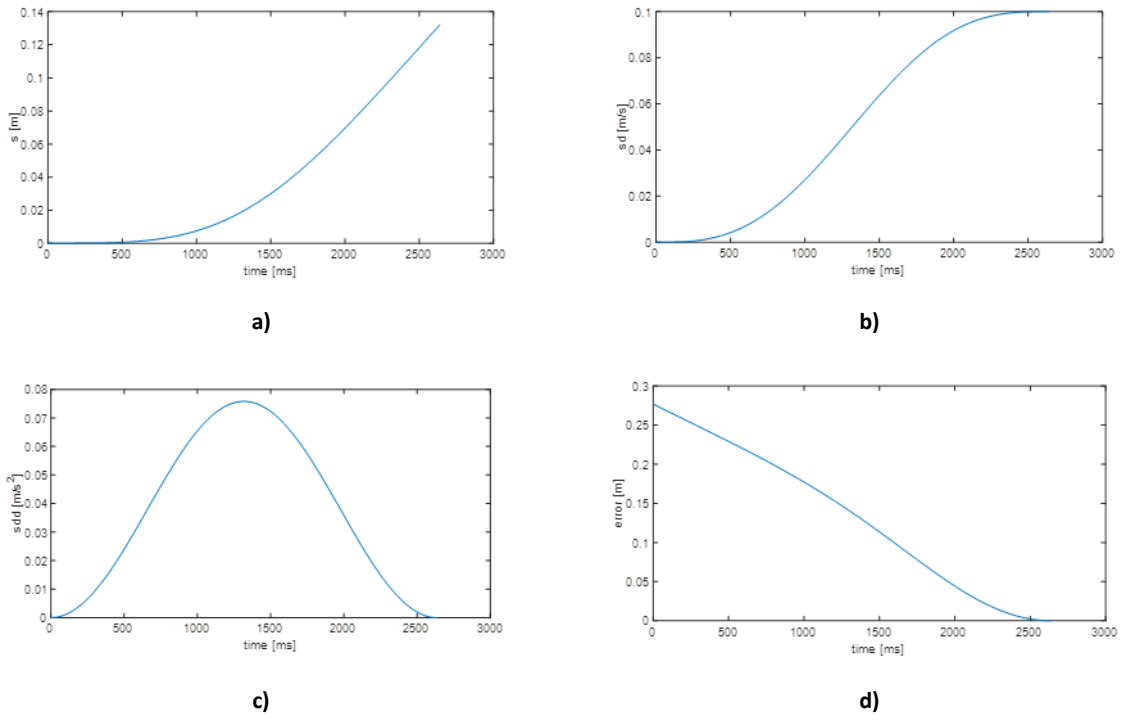


Figure 6-12 Simulation results. a) Curvilinear abscissa, b) First derivative of curvilinear abscissa, c) Second derivative of curvilinear abscissa, d) Capture error. Parametric trajectory 1

In plot of the joint angles, velocities, and accelerations are presented.

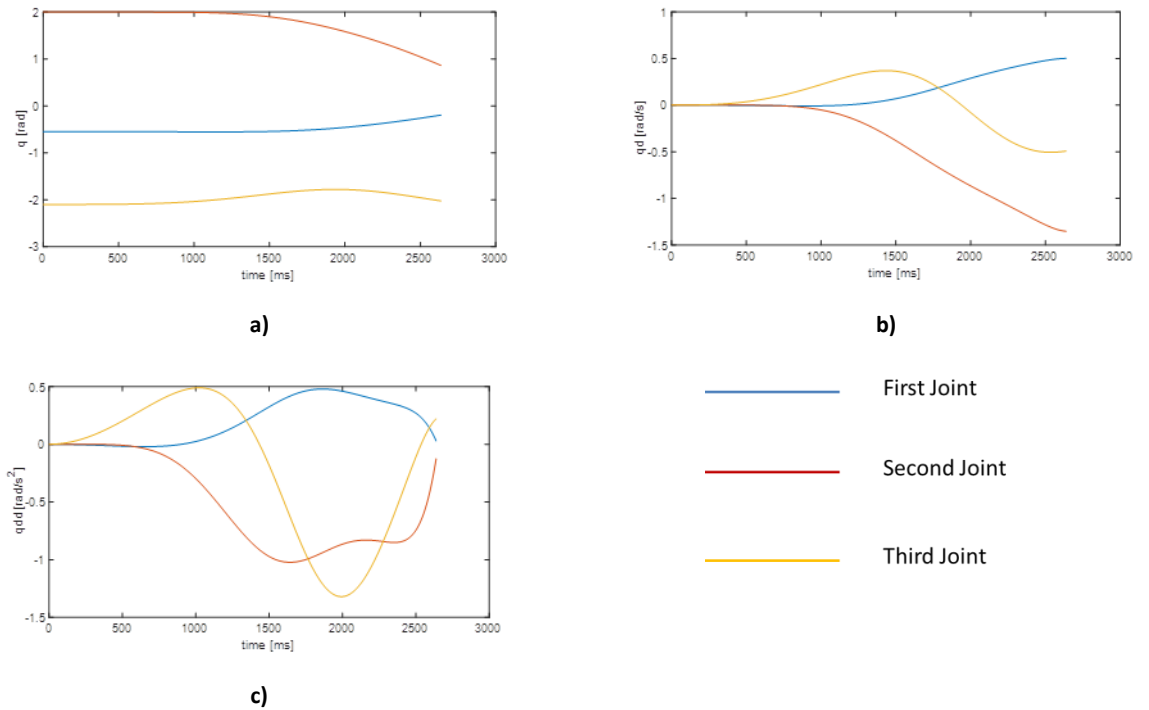


Figure 6-13 a) Joint angles, b) Joint velocities, c) Joint accelerations. Parametric trajectory 1

6.8.2.1.2. Target Trajectory 2)

In Figure 6-14 (top) a stroboscopic view of the robotic capture is presented, together with the plot of the reaction torque (bottom), which is always null with some negligible numerical noise.

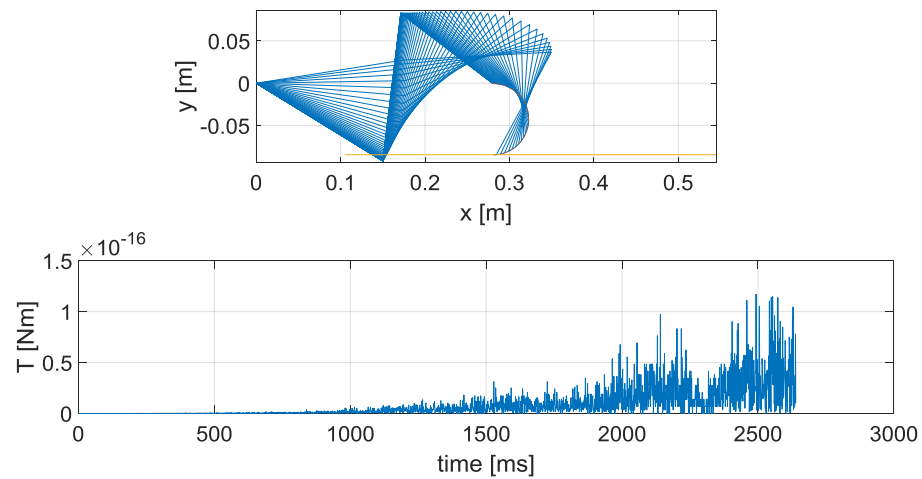
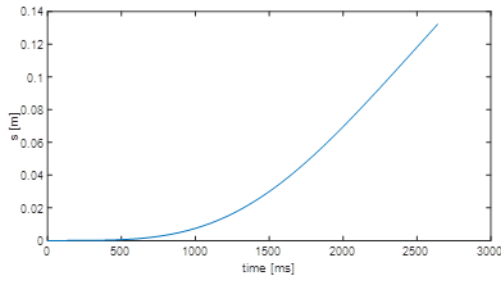
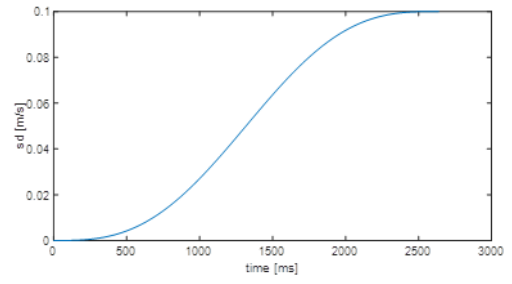


Figure 6-14 Stroboscopic view of robot motion (top), reaction torque (bottom). Parametric trajectory 2

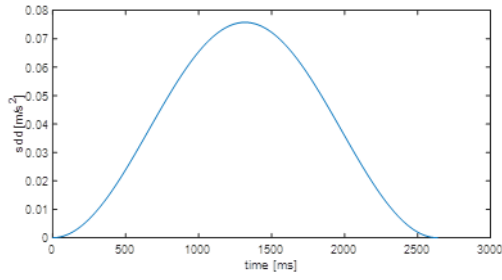
In Figure 6-15 the plot of the curvilinear abscissa and its first and second derivatives are presented.



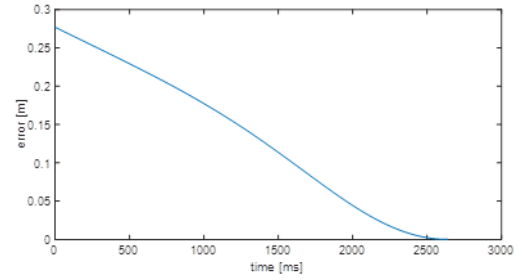
a)



b)



c)



d)

Figure 6-15 a) Curvilinear abscissa, b) First derivative of curvilinear abscissa, c) Second derivative of curvilinear abscissa, d) Capture error. Parametric trajectory 2

In Figure 6-16 the plot of the joint angles, velocities, and accelerations are presented.

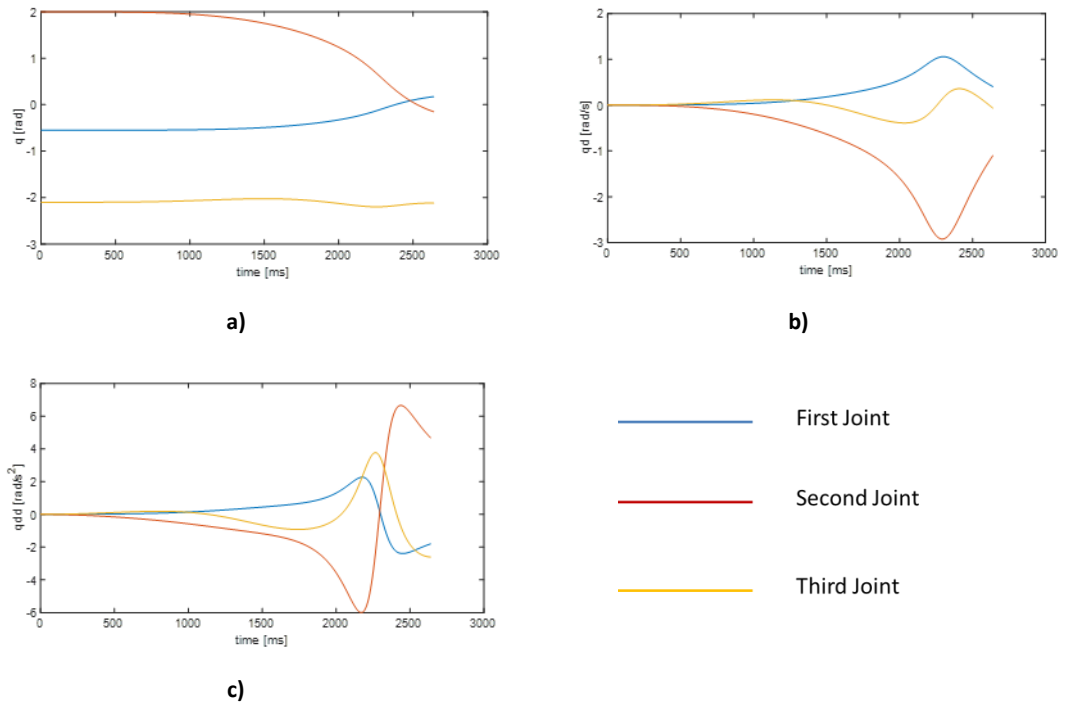


Figure 6-16 a) Joint angles, b) Joint velocities, b) Joint accelerations. Parametric trajectory 2

6.8.2.2 Free-shape-trajectory reactionless capture method

In the second capture method, which referred to as “Free-shape-trajectory reactionless capture method”, the LSE method is used. The end-effector trajectory is computed by the double integration of the \ddot{x} , where the position error (e) and velocity error (de/dt) are reduced to zero by means of two gains k_p and k_d , such that:

$$\ddot{x}_d = \ddot{x} - k_p \cdot e - k_d \cdot de/dt \quad Eq. 26$$

where \ddot{x}_d is the desired end-effector acceleration, and \ddot{x} is the current end-effector acceleration.

In this case, both the end-effector trajectory and the curvilinear abscissa are not fixed in advance (such as it was in the Parametric-trajectory reactionless capture method) but they are computed by the kinematic inversion algorithm.

Similar to the previous capture method, the same two target trajectories of the previous case will be used (with the same initial target position and velocity) to

demonstrate the capture method and in order to compare both of the results. Also, the robot model and initial configuration are the same as those used in the previous capture method.

As it can be verified in Figure 6-17 and , using the gains $k_p = 7.7$ and $k_d = 5$, the target is always reached, and in particular the speed and direction of the end-effector are equal to those of the target at the time of capture, avoiding undesired impact forces. These factors are decided as a result of sensitivity analysis conducted in an earlier study that proved to always be able to reach the target at desired speed and directions in given tasks (Cocuzza, Li and Yan, 2016).

6.8.2.2.1. Target Trajectory 1)

In Figure 6-17 (top) a stroboscopic view of the robotic capture is presented, together with the plot of the reaction torque (bottom), which is always null with some negligible numerical noise.

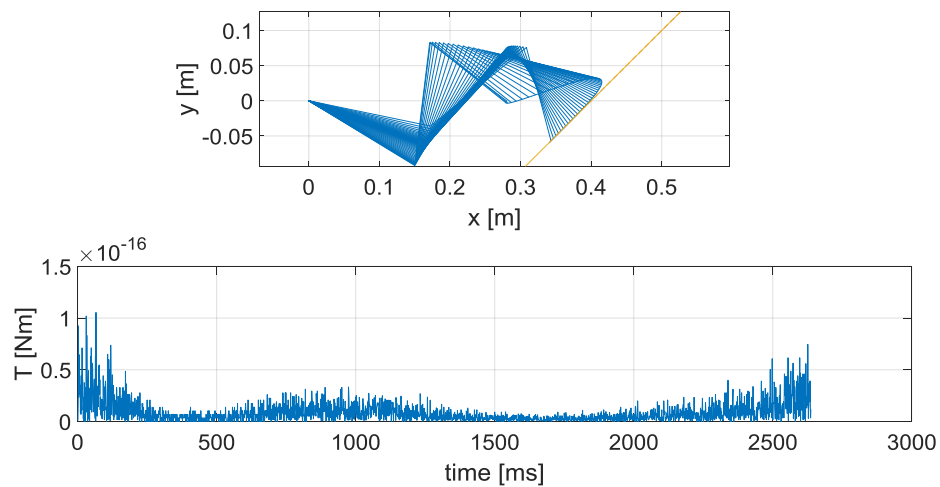
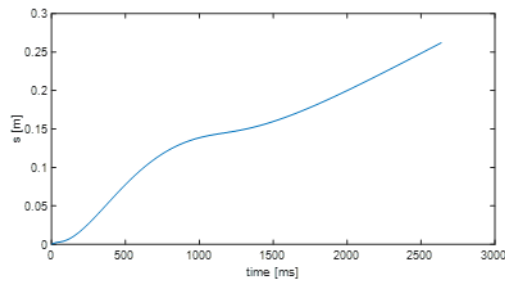
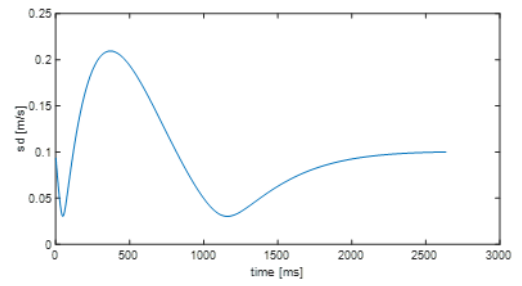


Figure 6-17 Stroboscopic view of robot motion (top), reaction torque (bottom). Free shape trajectory1

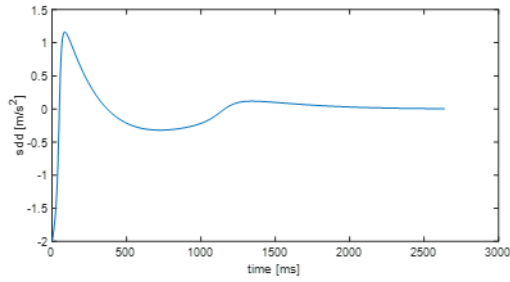
In Figure 6-18 the plot of the curvilinear abscissa and its first and second derivatives are presented.



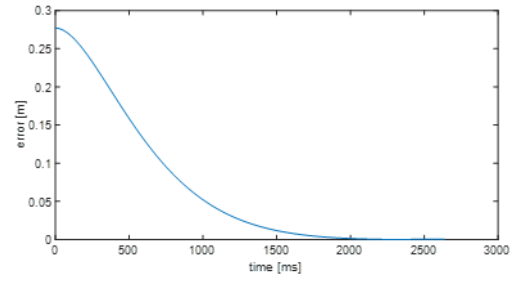
a)



b)



c)



d)

Figure 6-18 a) Curvilinear, b) First derivative of curvilinear abscissa, c) Second derivative of curvilinear abscissa, d) Capture error. Free shape trajectory 1

In Figure 6-19 the plot of the joint angles, velocities, and accelerations are presented.

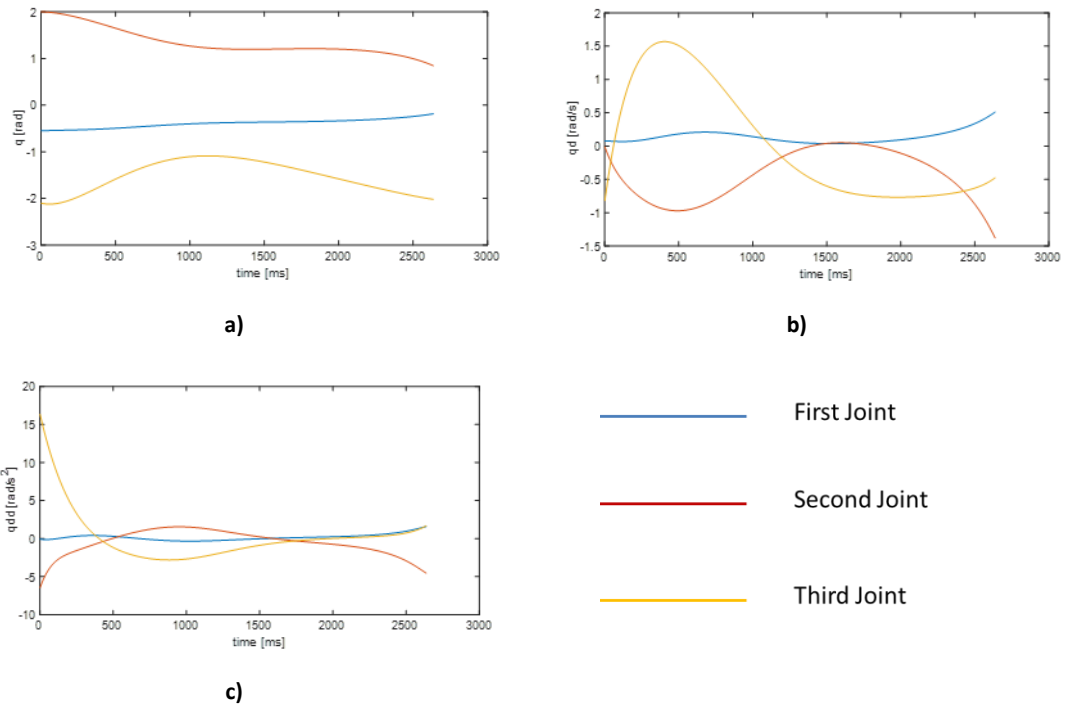


Figure 6-19 a) Joint angles, b) Joint velocities, c) Joint accelerations. Free shape trajectory 1

6.8.2.2.2. Target Trajectory 2)

In (top) a stroboscopic view of the robotic capture is presented, together with the plot of the reaction torque (bottom), which is always null with some negligible numerical noise.

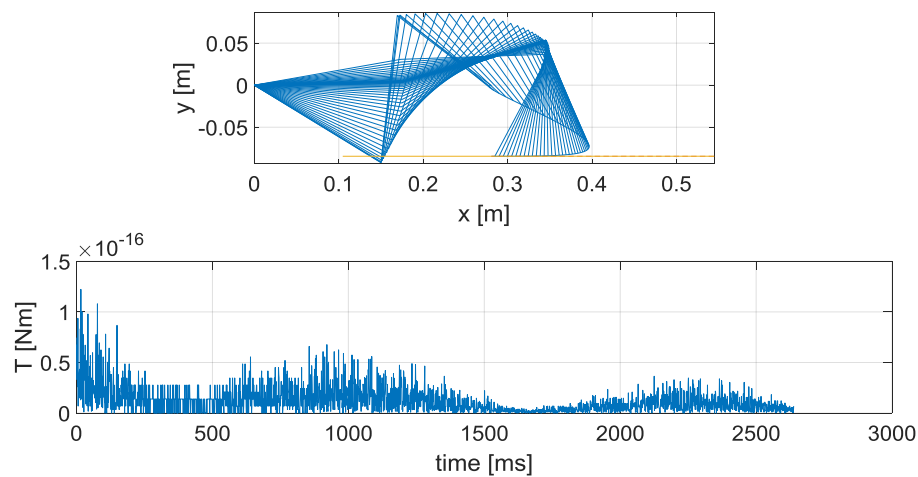


Figure 6-20 Stroboscopic view of robot motion (top), reaction torque (bottom) Free shape trajectory 2

In Figure 6-21 the plot of the curvilinear abscissa and its first and second derivatives

are presented.

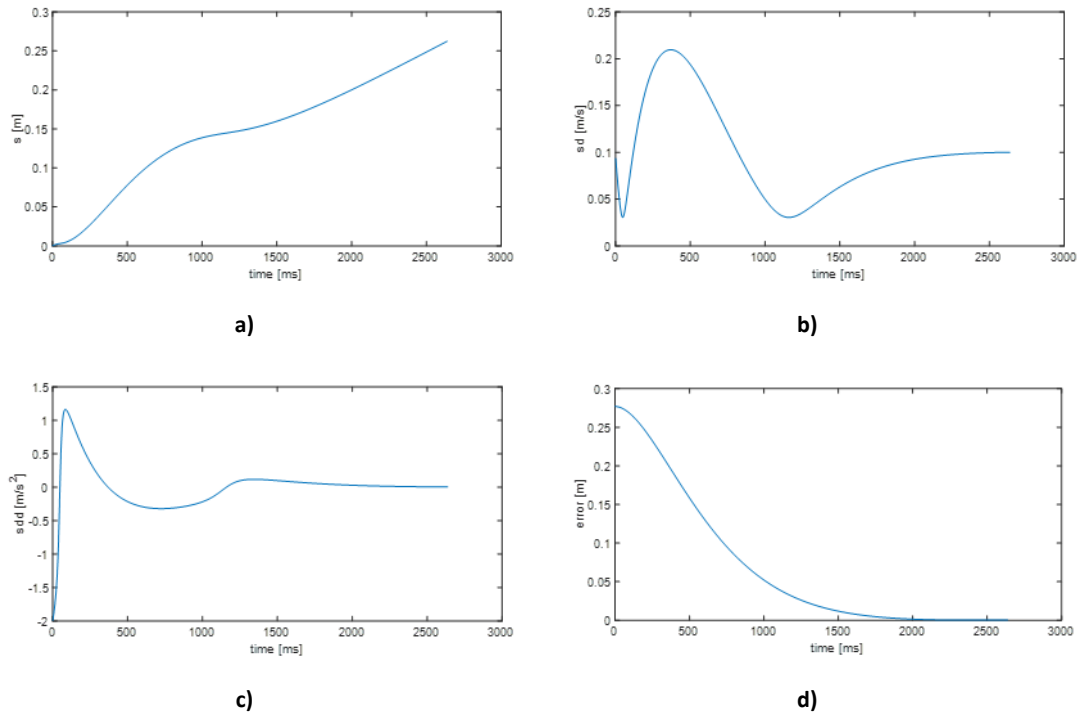


Figure 6-21 a)Curvilinear abscissa, b)First derivative of curvilinear abscissa, c) Second derivative of curvilinear abscissa, d) Capture error. Free shape trajectory 2

In Figure 6-22 the plot of the joint angles, velocities, and accelerations are presented.

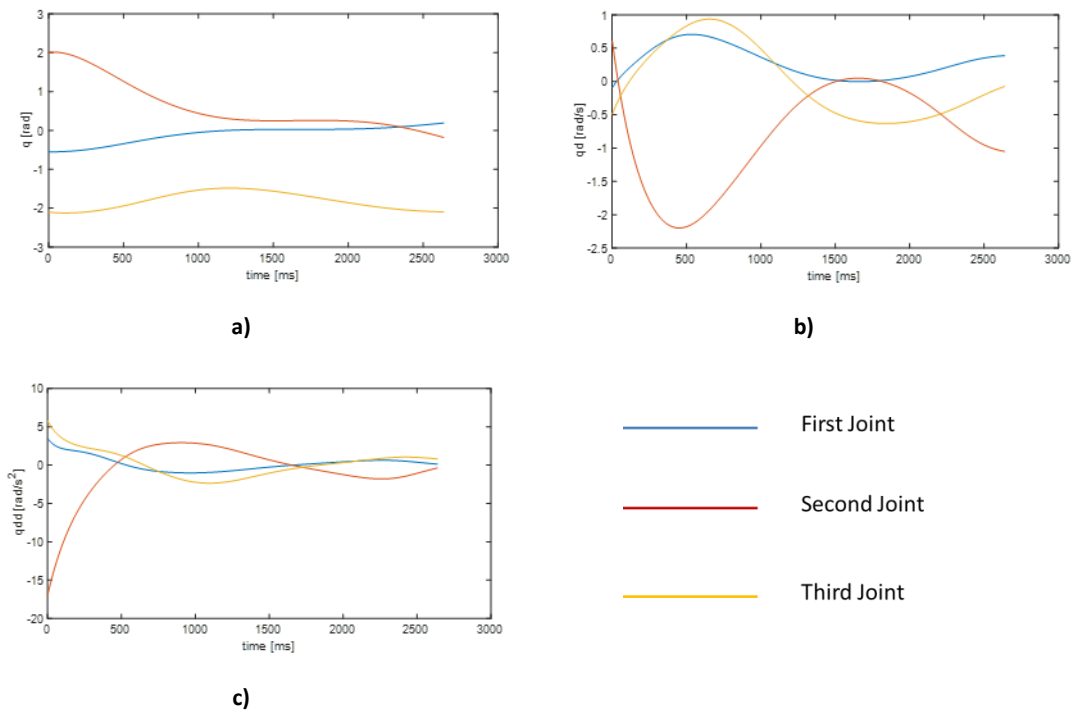


Figure 6-22 a) Joint angles, b) Joint velocities, c) Joint accelerations. Free shape trajectory 2.

6.8.2.3 Comparison of the Two Capture Methods

In the dynamic simulations, both of the presented methods demonstrate good performance and, in particular, the end-effector reaches the target with a zero relative velocity and with a tangent trajectory to one of the targets

Comparing Figure 6-15, Figure 6-18 and Figure 6-21 it can be seen that the position error converges to zero much more quickly with the Free-shape-trajectory reactionless capture and therefore the capture position is also anticipated, such as can be easily verified in the stroboscopic views. This is an important advantage, since more time is available to track the target and eventually correct positional errors.

6.8.3 Integration of the Reaction Control Solution in HARMP System

The simulation results from the Matlab program shows that the reaction control methods result in a minimization of the base reaction torque. In the capturing tasks the used methods can achieve the task successfully, reaching the target at desired velocity and direction. Therefore, the developed reaction control method and

capturing strategy are proved to be competent for the motion planning and target capturing tasks in space environment. So these reaction control solutions and capturing methods can be integrated into HARMP system for haptic teleoperation of the space manipulator.

In order to be able to use the developed reaction control solution to update the motion and kinematic of the virtual model of robotic manipulator, it was necessary to update the method of mapping between haptic devices and virtual robot. The original mapping used a hybrid method combining joint angle mapping and the end effector position mapping to solve the inverse kinematics. This is due to the multi-solution condition of the 3R manipulator used in this study. If the only solution is the position of the end effector, the solution for the joints movement cannot be determined. However, with the reaction control solution using LSE methods it is possible to determine the dynamic solution for the joints by only using the status of end effector as input. Therefore, the proxy position of the device mapped in the world space can be used directly as the desired position in the trajectory. This position updates for each frame while the haptic device is being manipulated by the user. In the Matlab simulation the Δt set for each frame is 0.001 seconds, while the update rate of the haptic device is around 1000 Hz. Therefore, by deriving the same Δt for the input desired position, the desired velocity and acceleration of the end effector are also available for the solution. By applying the LSE solution, the corresponding joints acceleration with minimum reaction torque to the base can be solved. Similarly, the joints velocity and angle can also be updated. The solved joints angle will then be updated in the geometric model in the HARMP interface by calling transform functions. As a result, while the user moves the position of haptic device, the end effector of virtual manipulator will follow the user's command while considering reaction control. The dynamic motion of the space robotic manipulator can be controlled by the user with the haptic device with minimization of the base reaction torque.

6.8.3.1 Capture Method with Haptic Guidance

The next step is to introduce the haptic guidance into the system for dynamic control together with the capture methods described. The LSE method is used, the end-effector trajectory is computed by double integration of the \ddot{x} , where the position error e and velocity error \dot{e} are reduced to zero by means of two gains k_p and k_d , such that:

$$\ddot{x}_d = \ddot{x} - k_p \cdot e - k_d \cdot de/dt \quad \text{Eq. 26}$$

where \ddot{x}_d is the desired end-effector acceleration, and \ddot{x} is the current end-effector acceleration. The impedance control of the haptic device developed earlier, only considers the velocity and acceleration in the equation.

$$f_d = m\ddot{e} + c\dot{e} \quad \text{Eq. 18}$$

Combining these two control methods will add the position error, which will also reduce the position error to achieve capturing task with impedance control of the haptic and reaction control of the manipulator.

f_d

$$\begin{aligned} &= m\ddot{e} + c\dot{e} \\ &= m(\ddot{x} - \ddot{x}_d) + c\dot{e} \\ &= m(k_p e + k_d \dot{e}) + c\dot{e} \\ &= mk_p e + (mk_d + c) \dot{e} \end{aligned} \quad \text{Eq. 27}$$

In this way the capturing method is integrated into the impedance control of the haptic device and can provide a guidance force to assist the user to reach the desired position and velocity. Therefore, it can achieve dynamic control in target capturing tasks in a space environment. The performance of the control and capturing method in the HARMP system can be recorded and evaluated.

6.8.3.2 Force Rendering

After the modelling of the dynamic guidance force, the next task is the force

rendering and actuation on the device. To render the guidance force model in this case study, the scale factor method used for telepresence force rendering in Chapter 5 does not apply. The main reason is that in this case study the difference of the calculated guidance force in each stage can be large. For example, at the beginning of the task the calculated guidance force can be relatively large due to the large initial velocity and position errors. While the end effector gets close to the target to achieve the following or capturing of an object, the guidance force can be relatively small but it is still important that the user is able to feel it. Therefore, simply scaling down the force model to meet the maximum force limit is now not a suitable solution. To solve this problem, a rendering method by introducing a force threshold is developed. By setting a fixed threshold of the force limit, if the calculated force exceeds this value the actuated guidance force on the device will remain and stop following the calculated force until it enters back to the range again. In the HDAPI for the Phantom haptic device there is a safety parameter `HD_SOFTWARE_FORCE_IMPULSE_LIMIT` defining the maximum changing rate of the force that can be applied safely, which is 4N/ms. Therefore, the threshold of the guidance force rendering in this case study is set to be 3N, 75% of the limit to ensure safety. This threshold can prevent a large and sudden change of the force at the beginning of the manipulation to increase the stability. Also, during the manipulation if the guidance force reaches 3N it can be assumed that the user has already been made aware of the suggested assistance but decided to maintain their own control. In this case there is no need for the guidance force to continue increasing.

6.9 Evaluation

6.9.1 Objectives

The objectives of the evaluation are to assess the effectiveness of the haptic assistance with dynamic guidance methods compared to other approaches such as potential field methods and with no haptic guidance. The hypothesis is that the dynamic guidance provides enhanced performance over the other approaches and

in complex space tasks such as target following and capturing objects. The evaluation results will be shown in graphical charts to demonstrate the qualitative result of the approaches and using MSE (mean squared error) performance analysis of the position and velocity errors to show the quantitative results.

6.9.2 Experiment Setup

A set of experiments were undertaken to assess the haptic feedback provided by the HARMP system. The experimental environment was established in the robotics laboratory at the University of Strathclyde. The Phantom Desktop is operated by the user on a desk and monitor on the desk displays the geometric model. The experimental procedure is shown in Table 6-3. For each space task, two simulated teleoperation procedures are conducted. The first procedure is conducted with dynamic haptic guidance, while the second procedure is set without haptic guidance for comparison. For the second task an additional experiment providing guidance using an artificial potential field method is conducted to capture the moving target. The user should at least have basic experience with the use of a haptic device. The evaluation methods are modified for this case study. The performance of the geometric and force models and the efficiency of the haptic guidance are evaluated by the user.

Table 6-3 Experiment set for the space robotic path planning and teleoperation

	Task 1. Velocity control/Target following	Task2. Velocity & Position control/ Target capturing
Experiment 1	With haptic guidance	With dynamic guidance
Experiment 2	Without haptic guidance	Without haptic guidance
Experiment 3	None	With Potential Field Method

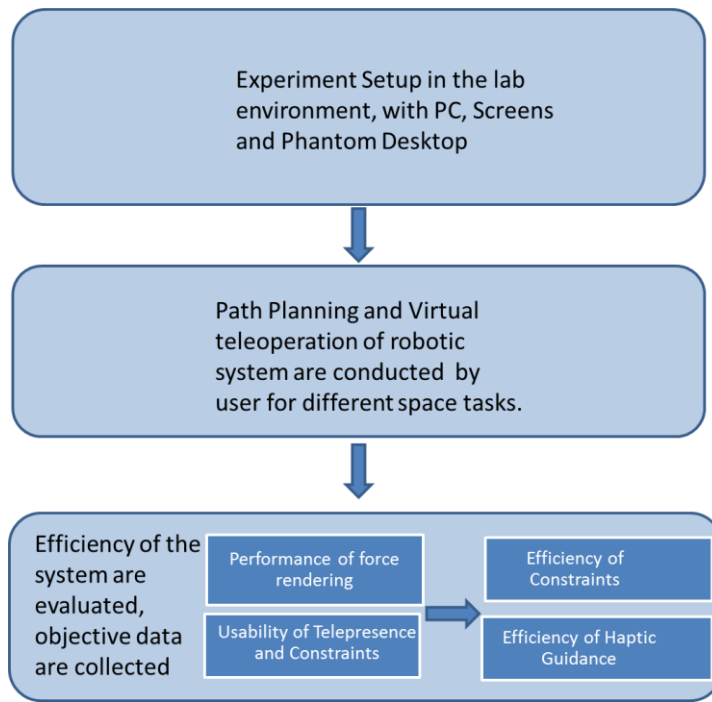


Figure 6-23 Updated evaluation methods for Case Study 2

6.10 Results, Findings and Discussions

6.10.1 Task 1

For the first task the participant is required to control the velocity of the manipulator with and without a guidance force on the haptic device. The initial conditions of the robotic manipulator and target are set identically as in the Matlab simulations. The target is traveling at the same velocity as target trajectory 2 in the simulation (0.1m/s). The participant then manipulates the haptic device trying to control the manipulator to follow the target. The desired operation is to ensure the end effector moves at the same velocity as the target, while the relative distance between the end effector and the target is controlled by the operator.

6.10.1.1 With Haptic Guidance

With the guidance model, the force is provided to achieve impedance control to maintain a stable velocity. Therefore, a PD control is integrated with the original force model and the provided force can be expressed as:

$$f_d = 10\dot{e} + 1000(\dot{e} - \dot{e}_{last}) \quad Eq. 28$$

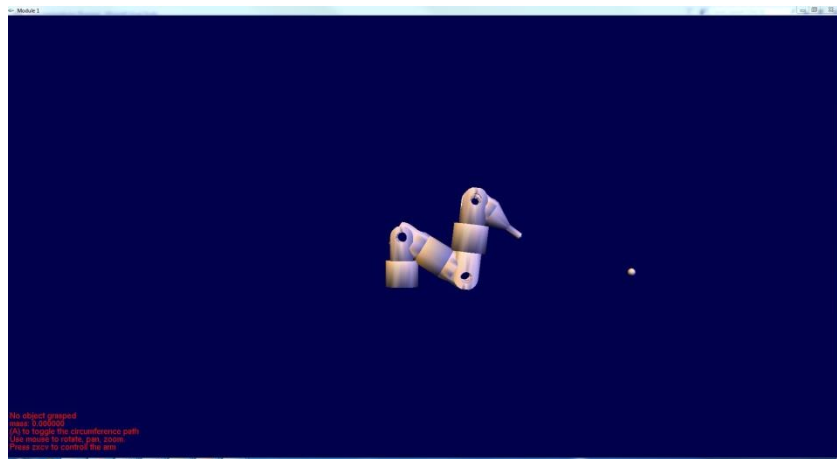


Figure 6-24 Initial position of manipulator and target

The following two figures show the plots of velocity error and distance between the end effector and the target during the manipulation. Figure 6-25 shows that the velocity error starts at 0.1m/s, temporally reduces to 0.06m/s, going back to 0.1m/s for about 2s then gradually reduce to 0.

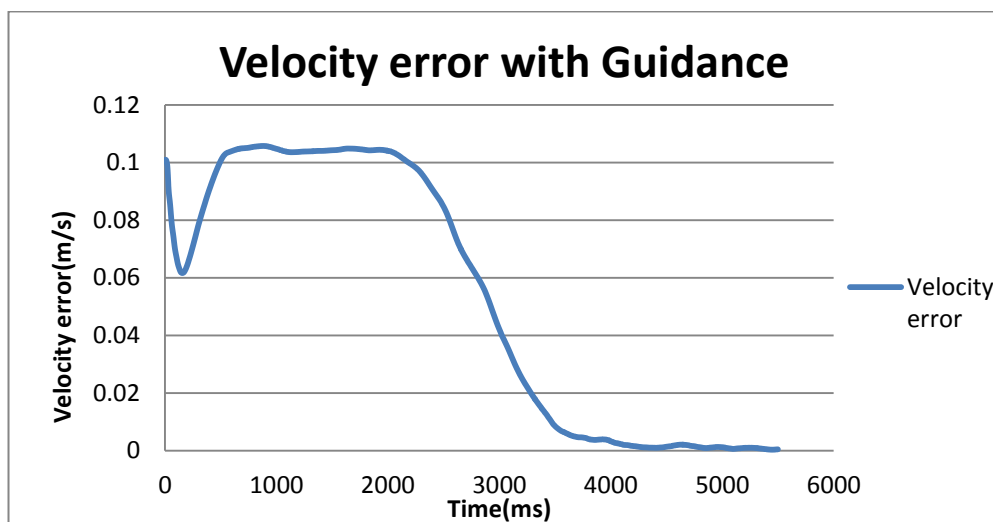


Figure 6-25 Velocity error between the end effector and the target

Figure 6-26 shows that the plot of distance between end effector and the target starts at 0.3m, then keeps reducing to a steady distant of 0.04m. The reduction of distance is at a constant rate and completed in 3 seconds. Then the distance stays at 0.04m which means the end effector is following the target at that distance.

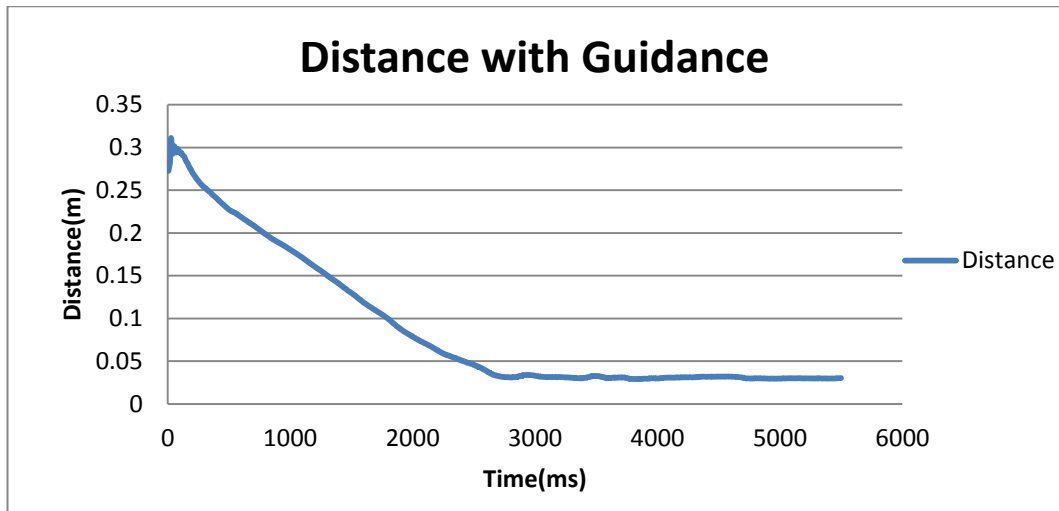


Figure 6-26 Distance between the end effector and the target

The following two figures show the reaction torque transferred to the base and the plot of the joint angles during the manipulation. Figure 6-27 shows that the reaction torque transferred to the base is always null with some negligible numerical noise.

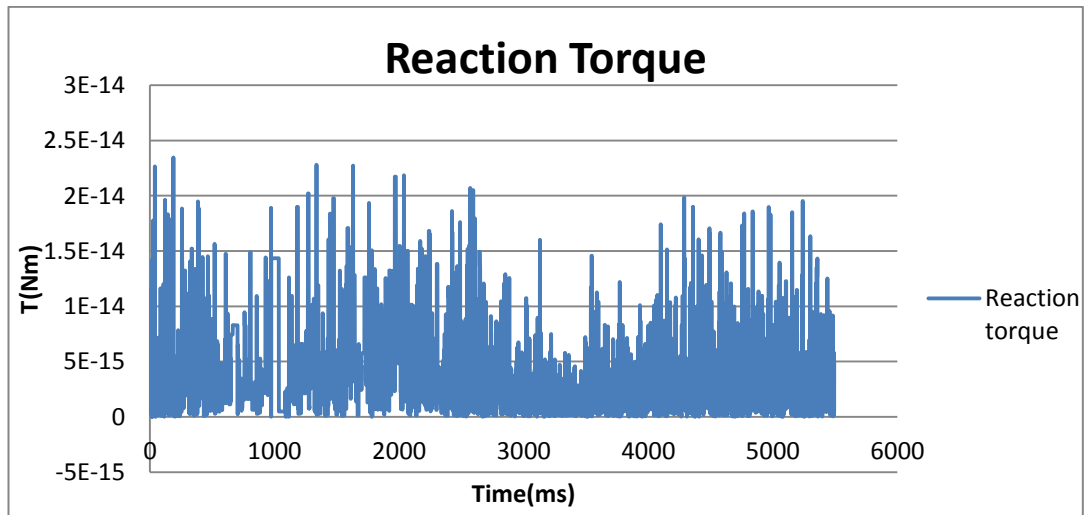


Figure 6-27 Reaction torque to the base

Figure 6-28 shows the plot of joint angles of the manipulator during the manipulation. It can be seen that the second joint angle has the largest rate change during the second half of the manipulation, while the rate change of two other joint angles are relatively less.

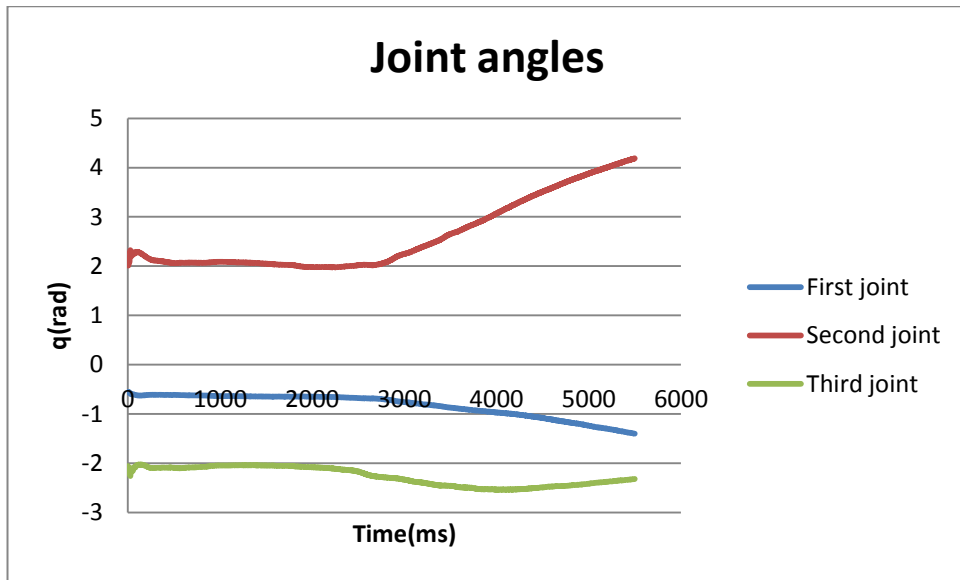


Figure 6-28 Joint angles

Figure 6-29 and Figure 6-30 show the plots of the guidance force provided on the x-axis to help the user follow the desired velocity during the operation. It can be seen that the calculated guidance force on the x-axis reaches almost 9N in one second and then gradually reduces to zero in 3.5 seconds. The real actuated guidance forces has a threshold of 3N, which means the actuated force on the device stays on a maximum force of 3N if the calculated force exceeds it.

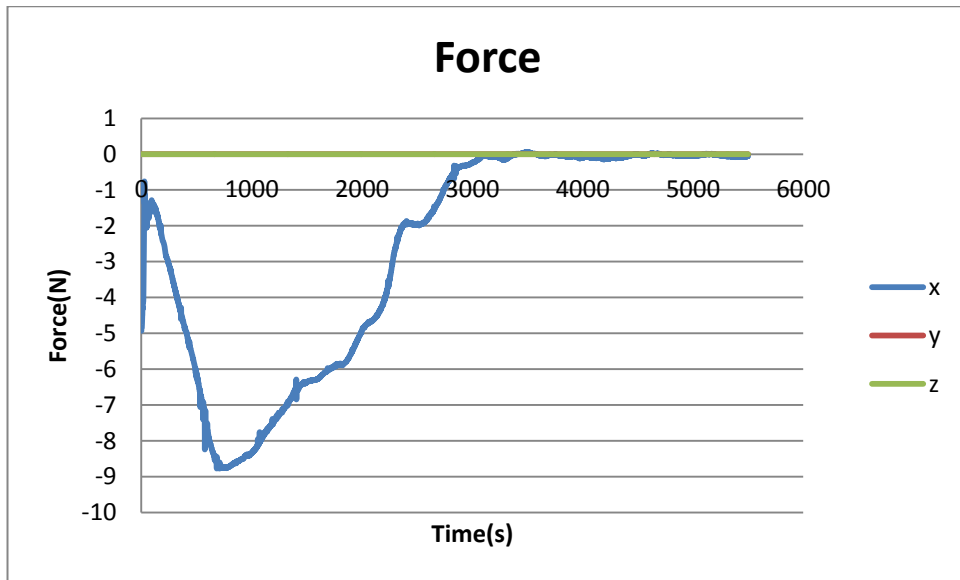


Figure 6-29 Calculated guidance force during operation

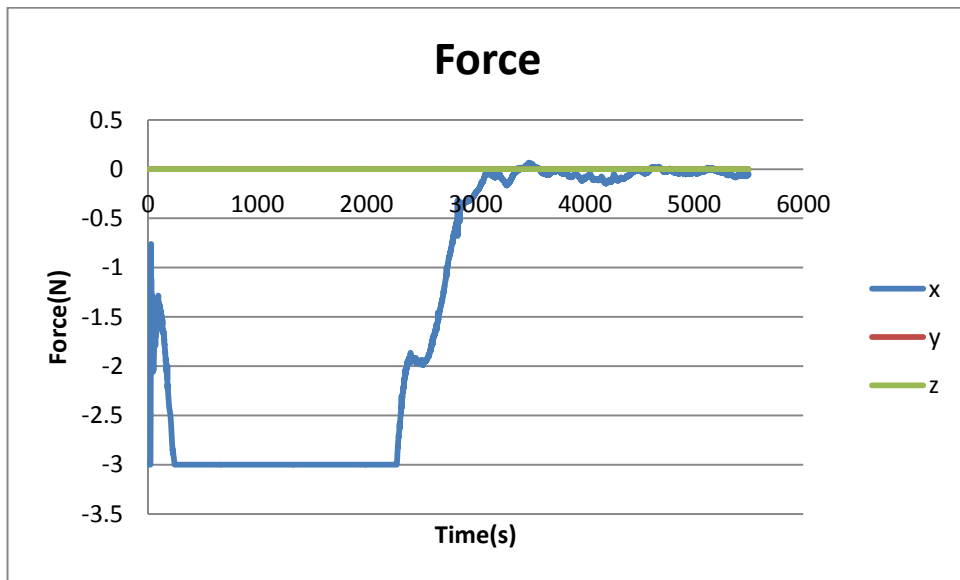


Figure 6-30 Actuated guidance force after rendering during operation

6.10.1.2 No Guidance

For comparison the participant is asked to control the velocity of the manipulator without a guidance force. The task requirements are still to follow a moving target at a constant velocity while keeping a constant distance.

The following two figures show the comparison of velocity error and the distance between the end effector and the target with and without guidance. It can be seen

from Figure 6-31 that the velocity error using both methods reduces to zero in 3 seconds, while the guidance method stays zero and no guidance method still oscillates around zero. The plot of distance in Figure 6-32 shows that both methods reduce to a steady distance in 2 seconds and there is no significant difference between them.

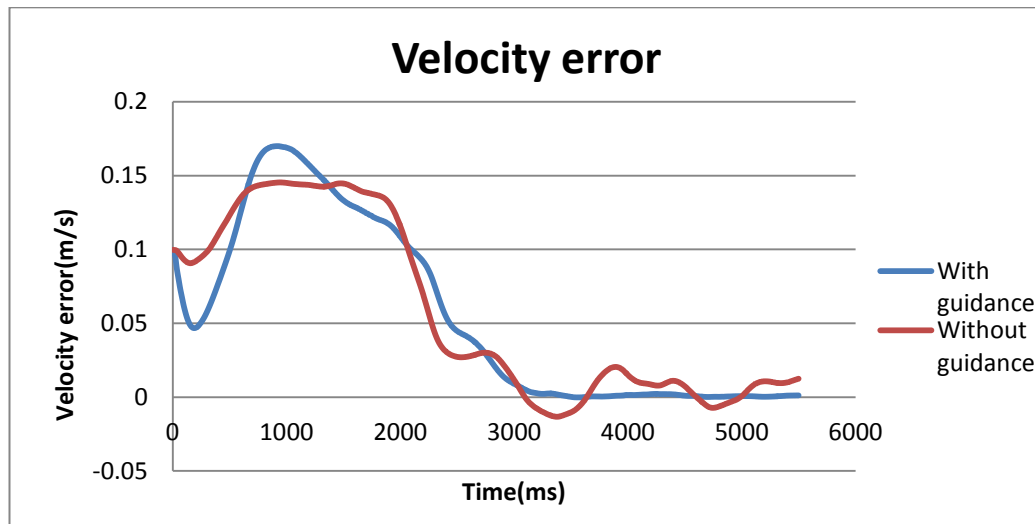


Figure 6-31 Comparison of Velocity errors

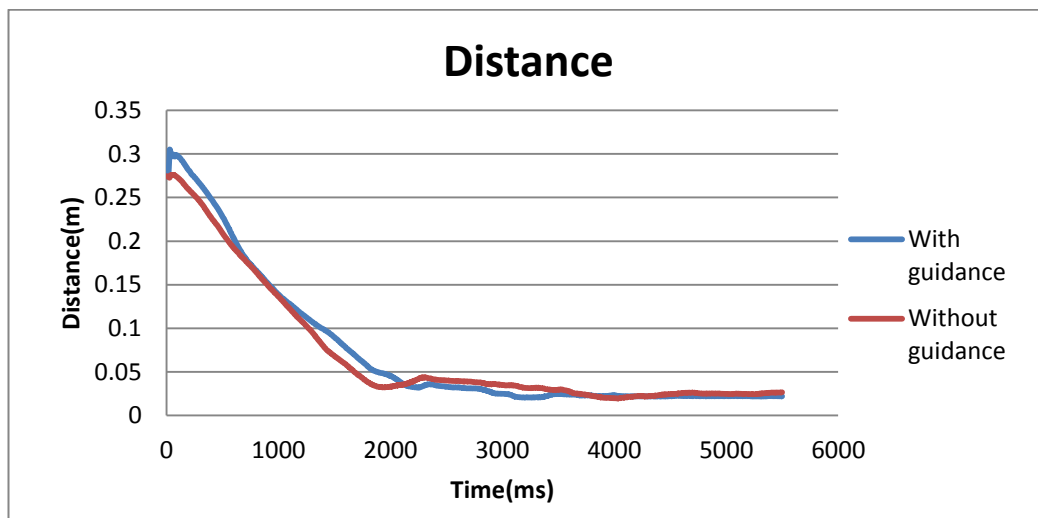


Figure 6-32 Comparison of distances

6.10.2 Task 2

The second task requires the participant to control the manipulator to reach both the desired position and velocity. This capturing task is conducted with and without the guidance force. The initial conditions of the robotic manipulator and target are

again set identically as in the Matlab simulations. The desired operation is to ensure the end effector moves at the same velocity while reaching the target to allow smooth capture.

6.10.2.1 With Dynamic Guidance

With the guidance model, the force is provided to achieve impedance control of the end effector of the manipulator. The guidance force is equated as introduced earlier:

$$f_d = mk_p e + (mk_d + c) \dot{e}$$

The following two figures show the plots of velocity error and distance between the end effector and the target during the manipulation with provided dynamic guidance. It can be seen in Figure 6-33 that the velocity error increases to 0.35m /s at the beginning, then constantly reduces to zero, and maintains this for 3.5 seconds. Figure 6-34 shows that the position error constantly reduces from 0.28m to 0 in 3 seconds.

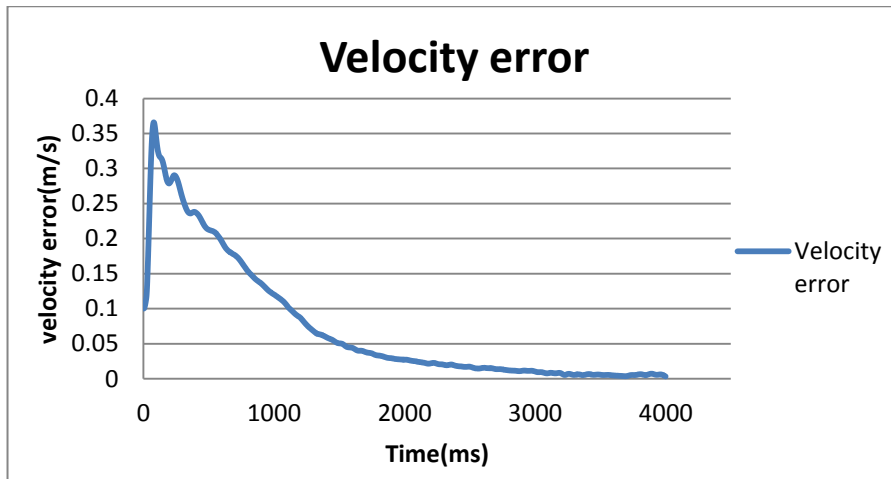


Figure 6-33 Velocity error between the end effector and the target with dynamic guidance

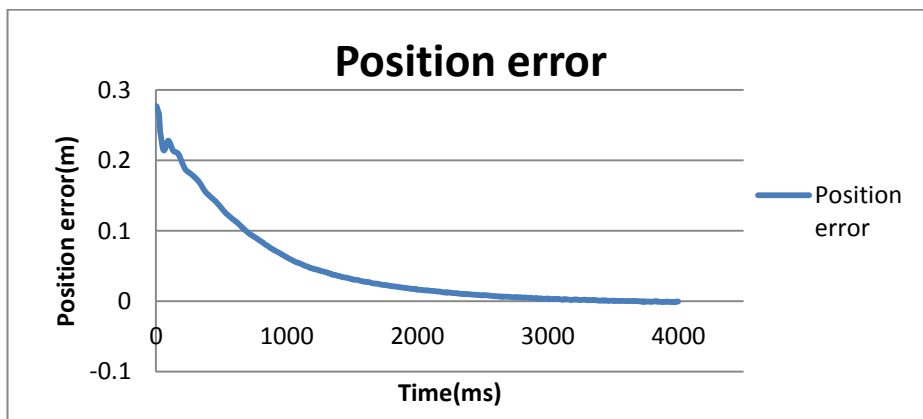


Figure 6-34 Position error between the end effector and the target with dynamic guidance

The following two figures show the reaction torque transferred to the base and the plot of the joint angles during the manipulation. Figure 6-35 shows that reaction torque transferred to the base is always null with some negligible numerical noise.

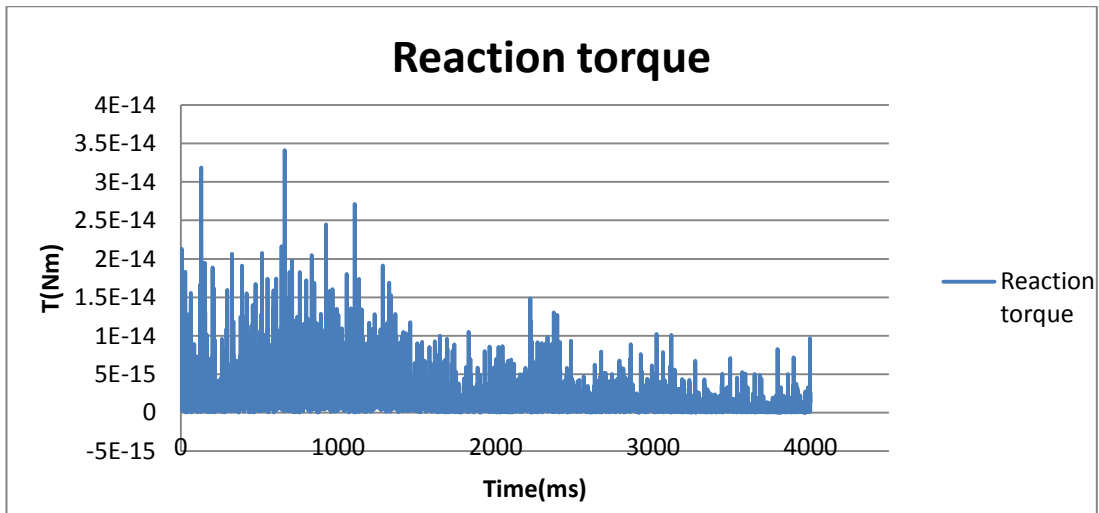


Figure 6-35 Reaction torque transferred the base

It can be seen in Figure 6-36 that the second joint angle has the largest rate change during the second half of the manipulation, while the changing rates of two other joint angles are relatively less.

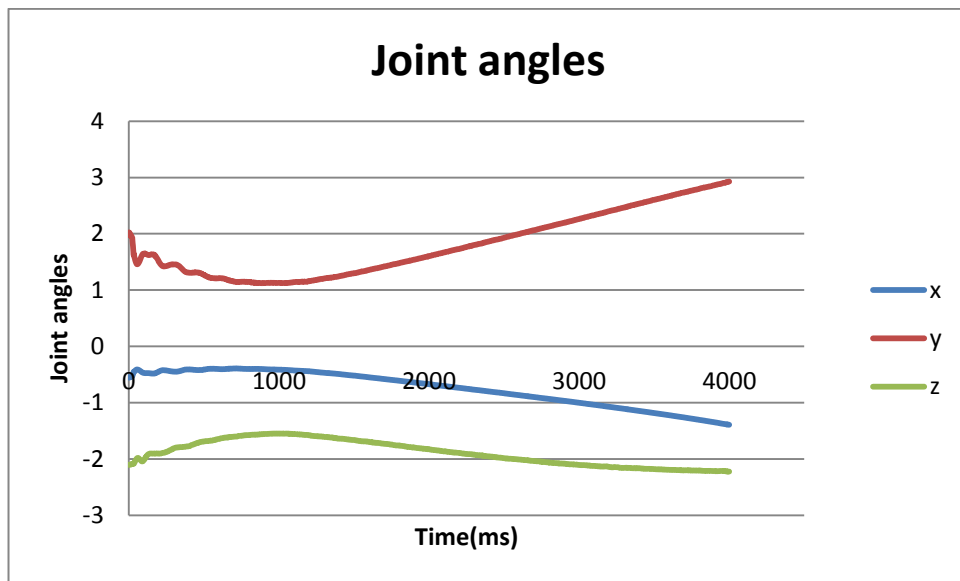


Figure 6-36 Joint angles

The following figure shows the plot of guidance force provided on the x-axis to help a user follow the desired velocity during the operation. It can be seen in Figure 6-37 that the calculated guidance force on the x-axis starts from ~ 8 N, then reduces rapidly and finally stays zero after 1.5 seconds. The calculated force on the y axis starts from 3.8N and oscillates to zero in 1.5 seconds. The plot of actuated guidance

force in Figure 6-38 shows that the maximum actuated forces on the x and y axes are constrained at 3N.

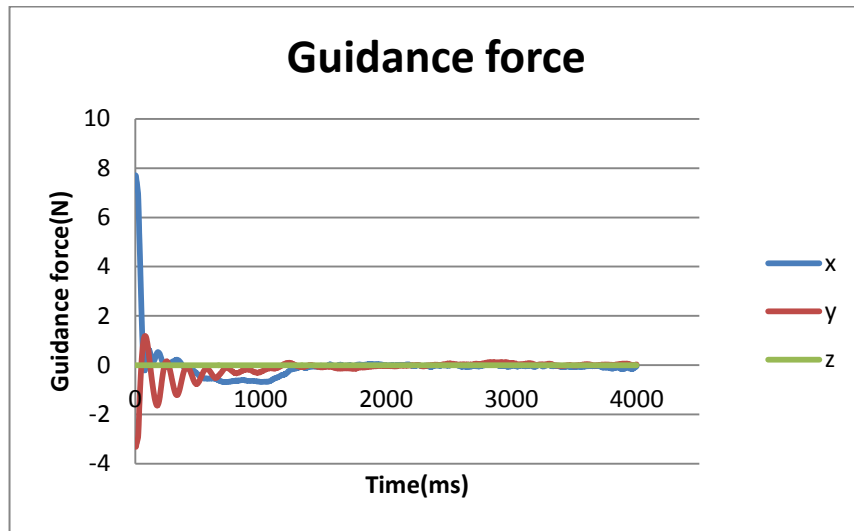


Figure 6-37 Calculated guidance force for dynamic guidance methods

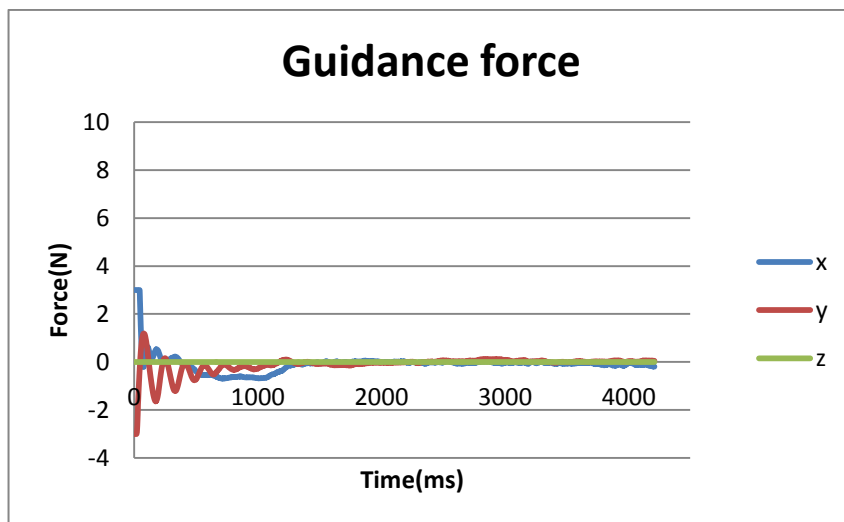


Figure 6-38 Actuated guidance force after rendering for dynamic guidance methods

6.10.2.2 No Guidance

For comparison the participant is asked to control the manipulator to reach the target without provision of a guidance force. The task is to capture the moving target at the desired velocity.

The following two figures show a comparison of the velocity error and distance between the end effector and the target with and without guidance. Figure 6-39

shows that without guidance the velocity error reduces eventually but hardly stays at zero. Figure 6-40 shows that without guidance the position error gradually reduces and finally reaches zero after 4 seconds.

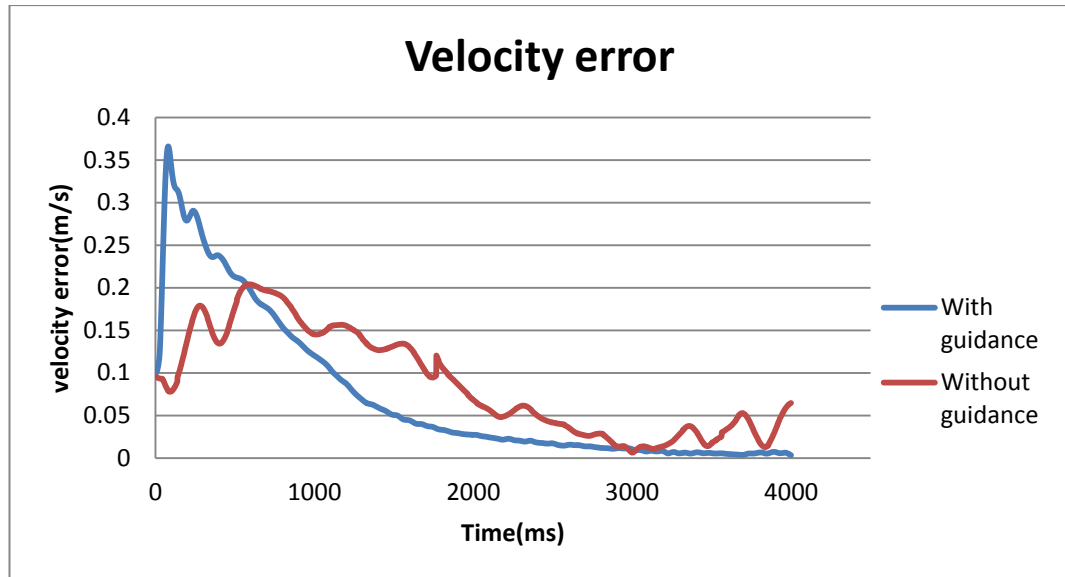


Figure 6-39 Comparison of velocity error with/without dynamic guidance

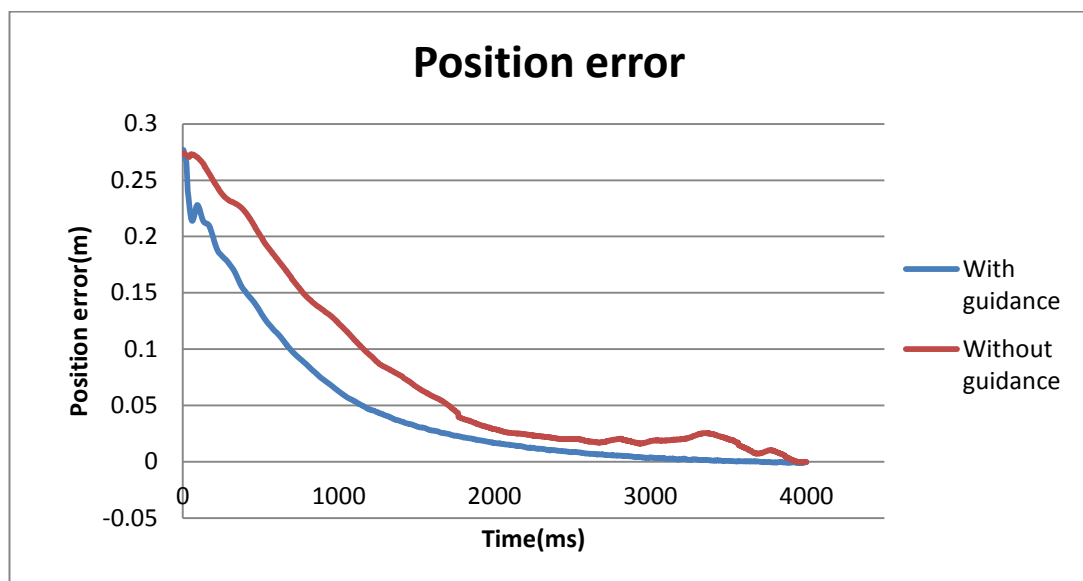


Figure 6-40 Comparison of position with/without dynamic guidance

6.10.2.3 With Artificial Potential Field (APF) Method

To study the performance of the dynamic guidance methods, other approaches need to be compared. Therefore, a traditional guidance method using artificial potential field (APF) is used for comparisons.

Again, the participant is asked to control the manipulator to reach a target with the guidance force generated by the artificial potential field (APF) method, which only depends on the distance to the target without considering the velocity difference. The task is still to capture the moving target at the desired velocity.

The following two figures show the comparisons of velocity errors and distances between the end effector and the target with 1) dynamic guidance; 2) no guidance; 3) artificial potential field force. In Figure 6-41 it can be seen that the velocity error with APF methods increase to 0.5m/s at the beginning and then reduces to zero in 2 seconds. However, it rises again and eventually comes to stay at zero after 4 seconds.

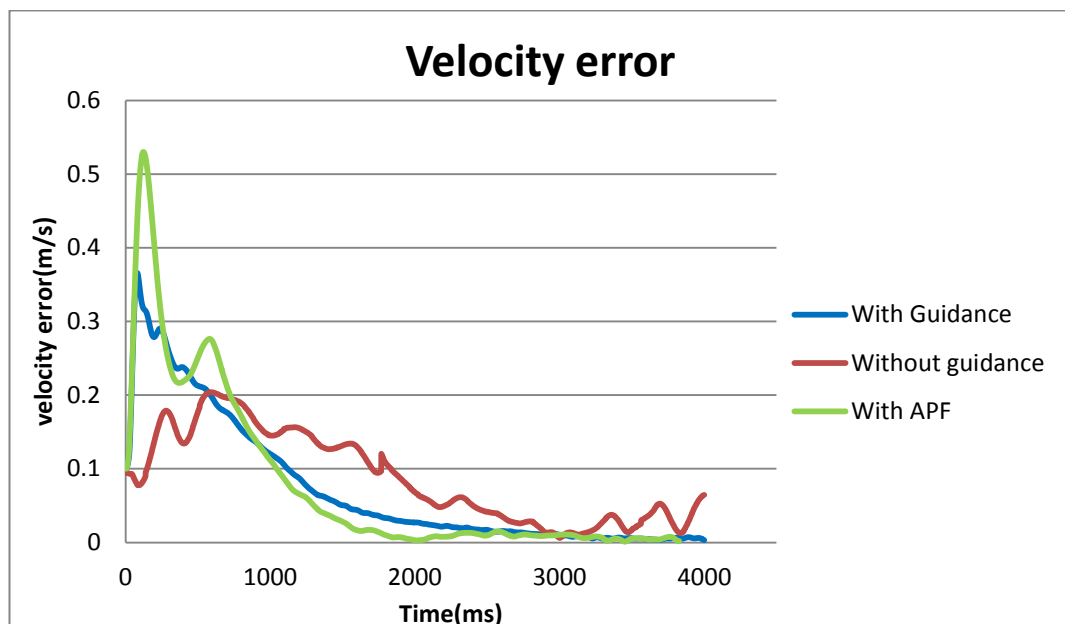


Figure 6-41 Comparison of velocity errors

In Figure 6-42 it can be seen that the position error using APF methods reduces to zero steadily in 1.5 second and stays, which is a faster time than the other two methods. In Figure 6-43 the performance with guidance and APF methods are similar, better performance than the with no guidance method until after 4 seconds they reach the same level.

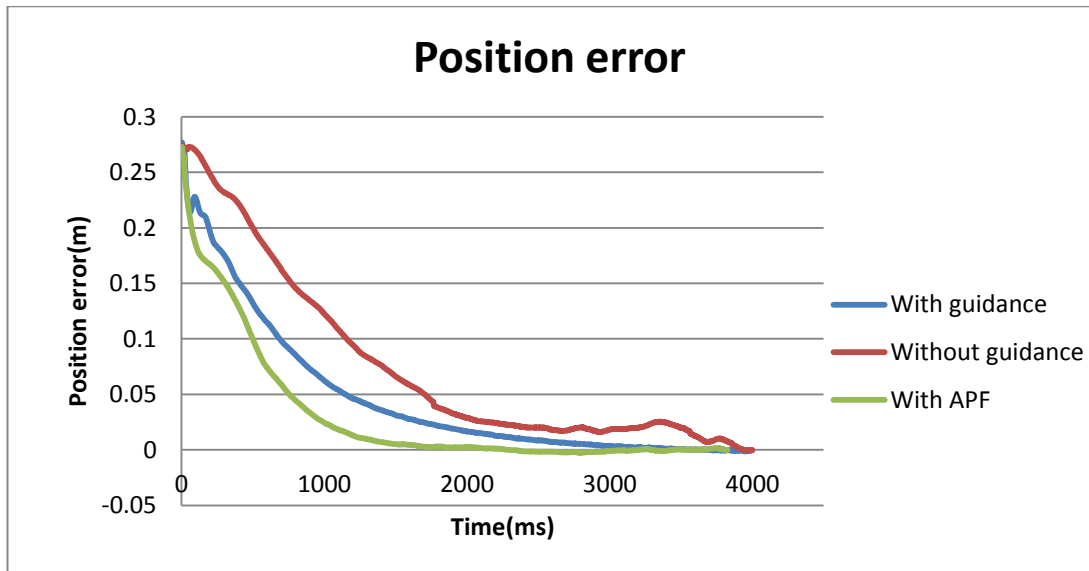


Figure 6-42 Comparison of position errors

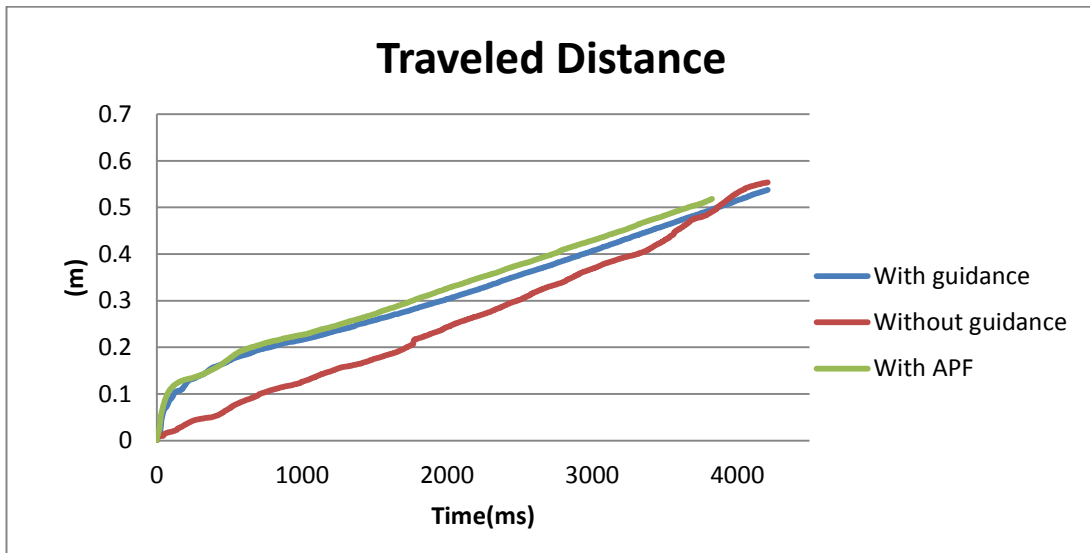


Figure 6-43 Comparison of travelled distance until reaching the target

The following figures show the plot of forces provided with the APF method during the capture task. In Figure 6-44 the calculated force on the x-axis starts from almost 10N, then reduces rapidly and finally stays zero after 2.5 seconds. The calculated force on the y-axis starts from 3.8N and reduces to zero in 2.5 seconds. The plot of actuated guidance force in Figure 6-45 shows that the maximum actuated forces on the x and y axes are constrained at 3N.

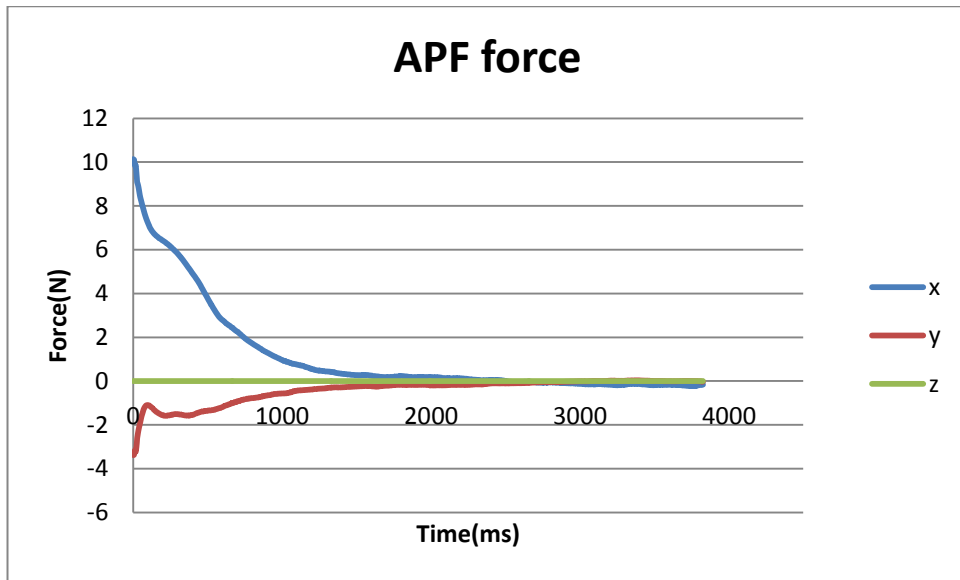


Figure 6-44 Calculated force with APF methods

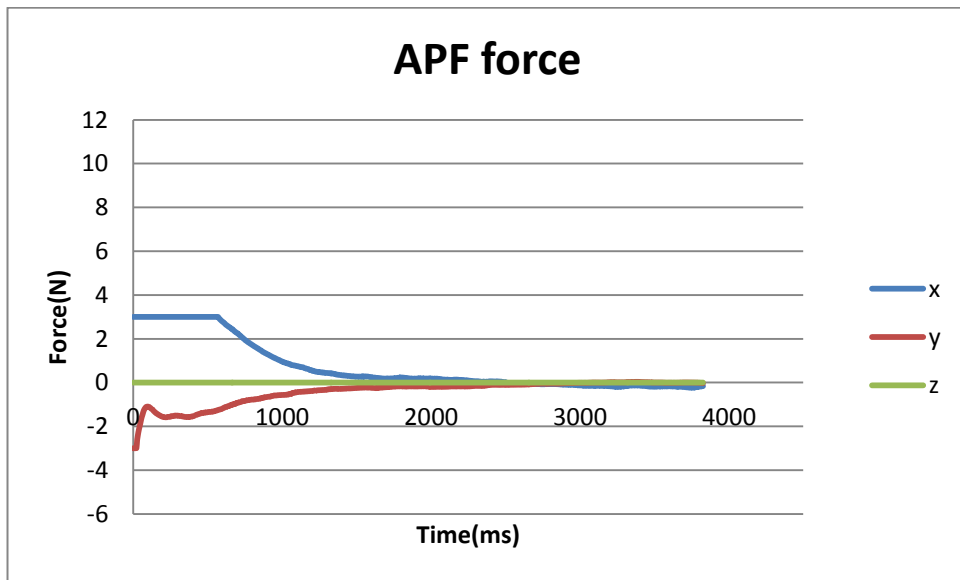


Figure 6-45 Actuated force after rendering with APF methods

6.10.3 Discussion of Results

6.10.3.1 Discussion of the Graphical Results

6.10.3.1.1 Task 1

For task 1, from Figure 6-25 and Figure 6-26, it can be seen that the user started following the dynamic guidance to reduce the relative velocity, and then tried to go against the guidance to reduce the distance to the target. After reaching a stable

distance to the target, the user starts to follow the guidance again. Figure 6-25 and Figure 6-26 show that the dynamic guidance method shows good performance and, in particular, the end-effector keeps a stable distance to the target with a near to zero relative velocity. Moreover, Figure 6-27 shows that the reaction torque transferred to the base is always close to null with some negligible numerical noise which meets the requirements for the space robotic manipulation tasks.

For comparison, Figure 6-31 and Figure 6-32 show the performance of the operation without haptic guidance. In Figure 6-32 it shows that the end effector kept a stable distance to the target, although it is out performed by the dynamic guidance method. Figure 6-31 indicates that without the dynamic guidance, it is difficult for a user to keep a stable relative velocity. In this case, the dynamic guidance method demonstrates a much better performance in target following tasks. The force plot for the potential field method in Figure 6-30 shows that the provided attraction force gradually reduces when approaching the target.

6.10.3.1.2. Task 2

For task 2, in Figure 6-33 and Figure 6-34 it can be seen that the velocity error increases at the beginning, and then drops while the relative distance keeps decreasing until reaching the target. These show the combined effect of the dynamic guidance method which takes both the position error and the velocity error into account. Figure 6-37 shows that the guidance force on the x-axis is relatively large at the beginning; this is due to the large velocity and position error to the target. While the user tries to maintain control of the manipulator to prevent it moving too fast, the guidance forces on the x-axis and y-axis gradually reduces with decreasing vibrations until reaching the target, which shows the effect of dynamic control of the manipulator. Moreover, Figure 6-35 shows that the reaction torque transferred to the base is always close to null with some negligible numerical noise which meets the requirements for the space robotic manipulation.

Figure 6-41 and Figure 6-42 show the comparison of performance between the

dynamic guidance, artificial potential field method and no guidance at all. In Figure 6-42 it can be seen that the potential field method reaches the target earlier than the dynamic guidance and the no guidance methods. However Figure 6-41 also shows that the velocity error in the potential field method does not reach zero by the time the end effector reaches the target. It reaches zero at almost the same time as the dynamic guidance methods, while the velocity error without guidance is still unstable.

6.10.3.2 Discussion of Quantitative Results

To analyse and compare the performance of different approaches, an evaluation with quantitative result is required. These quantitative results include four approaches for a space capture task: Dynamic Guidance (DG), No Guidance (NG), Artificial Potential Field (APT) and the Automatic Simulation (AS). The automatic simulation takes the result of the Free-shape-trajectory reactionless capture method simulated in Matlab in the last section. This is an ideal result automatically calculated by the design algorithm without any human operator's participation in the control loop, used to compare with the performance of the other approaches. In each method four factors are taken into account for the analysis: 1) The time taken to reach the target (when the distance=0); 2) The travelled distance before reaching the target; 3) The MSE (mean squared error) of the relative position in 1000ms after reaching the target; and 4) The MSE (mean squared error) of the relative velocity in 1000ms after reaching the target. Each factor is calculated as the mean of the data collected from three repetitions. The results are shown below.

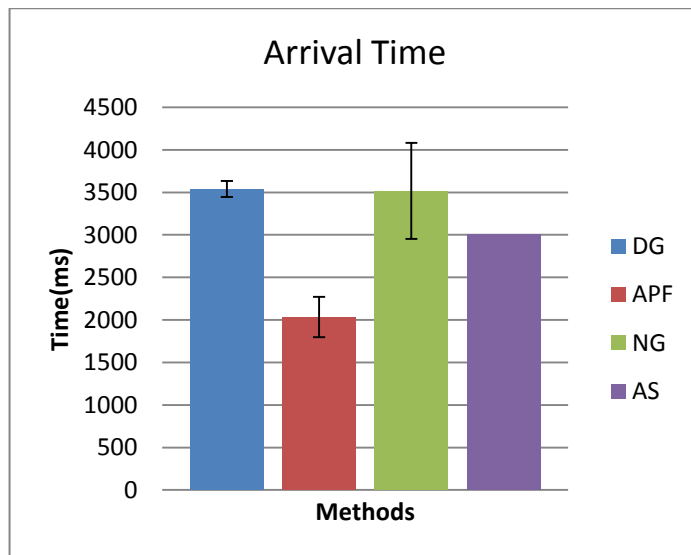


Figure 6-46 The means of times used to reach the target at first time (when the distance=0), with shown standard derivation

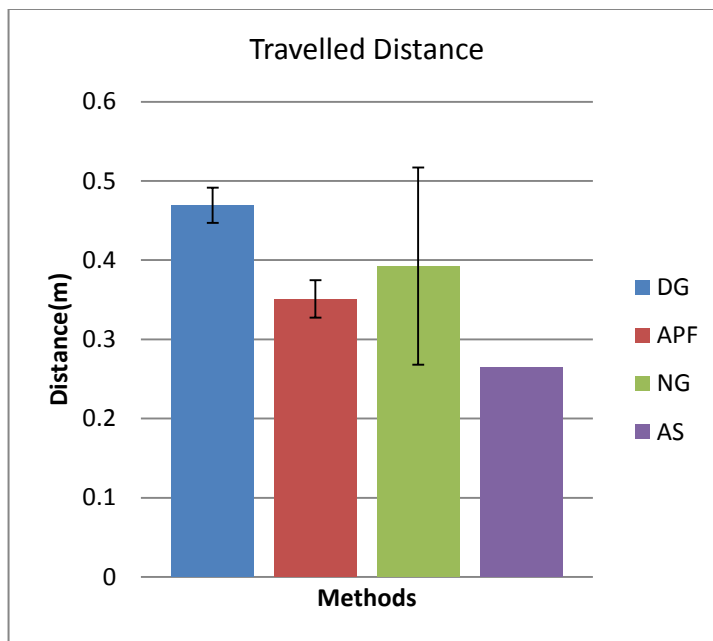


Figure 6-47 The means of travelled distances before reaching the target with shown standard derivation

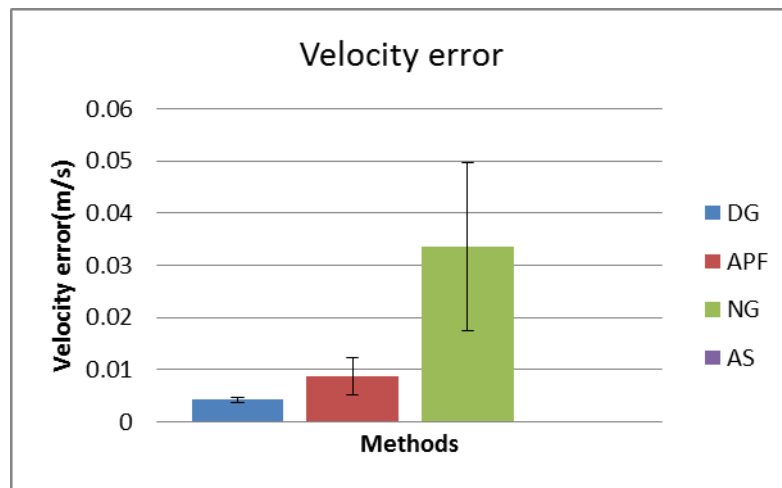


Figure 6-48 The means of velocity errors at the point of first reaching the target with shown standard derivation

Figure 6-46, Figure 6-47 and Figure 6-48 show the comparison of times, travelled distance and relative velocities at the moment of reaching the target (when distance=0), with the shown standard derivation. It can be seen that the DG method travelled the longest time and distance to reach the target, while the velocity error at the moment of reaching the target (impacting velocity) is lowest among three manipulation methods. The APF method reaches the target first, even faster the simulated result AS. However, it has roughly double the impact velocity compared to the DG, which will cause higher impact reaction. The NG method reaches the target slightly earlier than the DG, but the impact velocity is significantly higher than both the DG and APF. In addition, as can be seen from Figure 6-46, Figure 6-47 and Figure 6-48 the NG has the largest standard deviation (STDEV) which shows the instability. As a comparison the DG demonstrates much better performance for stability due to lower STDEV.

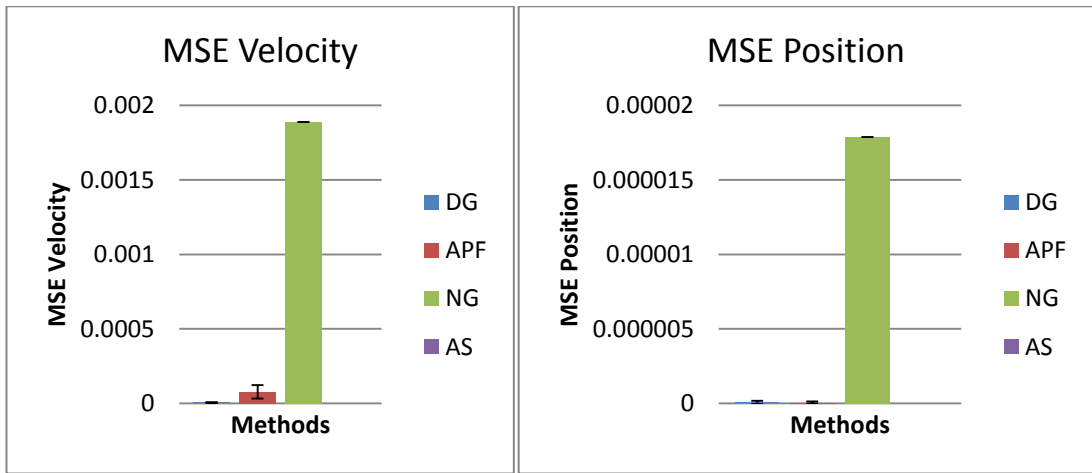


Figure 6-49 The MSE(mean squared error) of the relative velocity and position in 1000ms after reaching the target

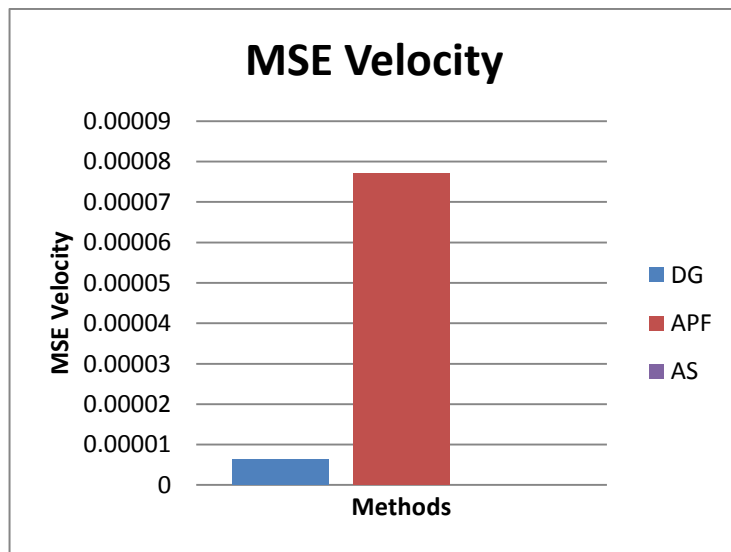


Figure 6-50 The MSE (mean squared error) of the relative velocity in 1000ms after reaching the target

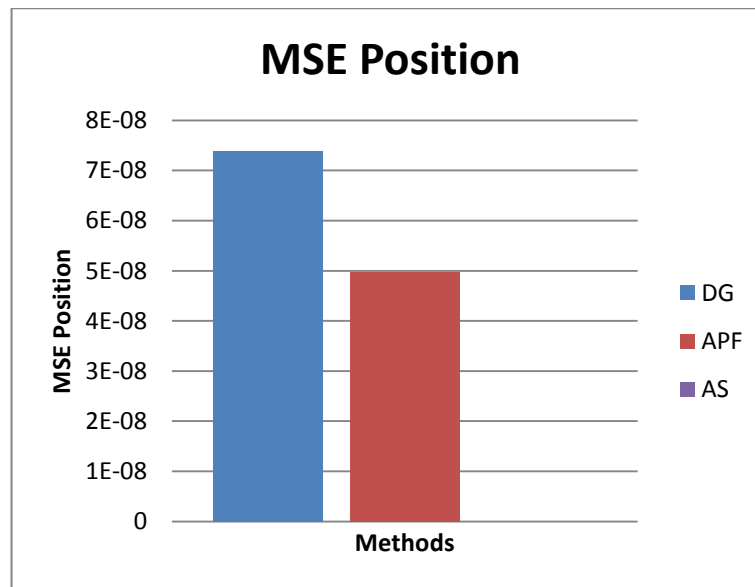


Figure 6-51 The MSE (mean squared error) of the relative position in 1000ms after reaching the target

Figure 6-49 shows the MSE (mean squared error) of the relative velocity and position in 1000ms after reaching the target. These results are good indications of the effectiveness and stability of the performance in target capturing tasks. As shown in Figure 6-50 the NG method has much larger MSEs in both position and velocity compared to the other two methods. Therefore, to compare the results of DG and APF another graph needs to be plotted without NG. Figure 6-51 shows that the MSE of velocity in 1000ms after capturing in DG method is significantly lower than in APF method, which indicates a better performance of stability. As for the MSE of position, APF shows a slightly better performance, however looking at the numeric level it can be concluded that both methods show adequate performance for position following.

In summary, the dynamic guidance method for haptic target capture shows adequate performance and advantages for the task. Compared to other guidance methods, the dynamic guidance shows better performance by resulting in a significantly lower impact velocity at the moment of capturing and maintaining a low MSE of velocity after the capturing. These are important factors defined by the task requirements. The dynamic guidance method takes a longer time and distance to reach the target, but not significantly. Also, the impact velocity and MSE of

velocity in dynamic guidance is lower than the other guidance methods but still above zero. This is due to the nature of human operating compared to an automatic machine. The haptic guidance can improve stability and precision, while the manipulation is still fully controlled by the human operator.

6.11 Conclusions

In this chapter, the HARMP system is specifically tailored and designed for the haptic control of a space robotic manipulator. A system architecture is built following the design methodology. Geometric models of the space manipulator are designed and built with CAD software. Kinematics of the manipulator is analysed. Haptic virtual fixtures including telepresence, constraints and guidance are built for the specific requirements of space teleoperation tasks.

Two novel methods are proposed and compared for capturing a non-collaborative target with a redundant robot whilst transferring a null reaction torque to the base spacecraft. They have demonstrated to be effective in modelling space robotics and developing a working haptic control of a space robotic manipulator within a microgravity environment using a system on Earth. This is a significant advantage with respect to current capture methods, in which the problem of capture and of reaction minimization are handled separately and whereby integration is complicated. In the dynamic simulations both methods have demonstrated good performance and, in particular, the end-effector reaches the target with a zero relative velocity and with a tangent trajectory to that of the target and, moreover, the reaction torque transferred to the spacecraft base is null in both cases.

The dynamic guidance method for the haptic target capture demonstrates adequate performance and advantages for the task compared to other guidance methods. It can improve stability and precision, while the manipulation is still fully controlled by the human operator. This is the most important advantage of the haptic guidance methods over automatic control, as the human operator is able to deal with emergencies and complicated situations at any time during the operation.

Chapter 7: Industrial Trial of Haptic Robot Control System

7.1 Introduction

In this chapter, the design method of the HARMP is implemented to demonstrate its application in the 'conceptual design' of a haptically controlled manufacturing system involving the haptic control of a real commercial robot. System requirements are identified for graphical and haptic modelling after analysing the market needs. Control diagrams including the master haptic controller, virtual robot and real robot are designed and developed. Firstly, a haptic teleoperation system is developed to control a virtual industrial robot. Geometric models of the industrial robot are built and kinematics are analysed. Haptic virtual fixtures are implemented for telepresence, constraints and guidance in the manipulation of the virtual robot. Communication is then established between the master haptic device and the real industrial robot. While a user is manipulating the haptic device to control the virtual robot, the real industrial robot will also act upon the commands received by the virtual robot to generate the desired motion in the physical world. This effectively achieves teleoperation of a physical robotic system through a virtual and interactive user interface for a user having a direct overview of the robot's behaviour in the virtual environment. Similar to the concept of Digital Twin, the virtual robot is built identically as the physical robot, while the virtual environment is modelled and updated based on the sensors information. In addition to the use of digital twin in simulation phase, the haptic fixtures applied on the virtual robot provides assistance for the manipulation of real robot during the operation in this study.

This teleoperation capability can be used for many manipulation tasks which require a precise and powerful industrial robot and for tasks that can only be completed with the full control of the actuators by a human operator. The haptic assistance provided during these manipulations will enable the user to detect the potential obstacles in an environment of poor visibility, to obey the constraints imposed on the robotic system by its operating environment, such as a manufacturing plant where there are other pieces of equipment that the robot

must avoid , and follow the desired trajectory. As a result, this capability will increase the safety, efficiency and usability of robotic systems in complex environments where there are many other objects either known or unknown. An example of such an environment is nuclear storage, where years of accumulating nuclear waste becomes a complex and hazardous environment to have a human directly operate robots to handle nuclear waste.

7.2 System Requirements and Specification

In order to evaluate the proposed HARMP design process model, this case study intends to determine if the methodology is applicable in a manufacturing environment for parts assembly at an industrial plant. The case scenarios of the expected system is defined as the following: The haptic system is expected to provide a simulation for planning of the teleoperation system, which drives an industrial robotic arm in achieving different tasks including approaching and then capturing targets. Thus, based on this scenario, the final haptic system needs to meet following requirements:

Graphically, the new system will

1. Provide an interface to an environment of the working scenario modelled with accurate geometric representation of objects within such a scenario environment.
2. Allow 3D models created by other CAD software systems to be imported into the system.
3. Ensure that the robotic arm should move accordingly with kinematic solution associated with its configuration structure to follow the commands and achieve specific tasks while a user manipulates the haptic robot controller.
4. Provide visual representation of the geometric information of the related objects in the tasks, such as the target to be captured for manipulation or other obstacles in the scenario environment.

From haptic perspective, the new system will need to:

1. Make the user feel the presence of the robotic arm, obstacles and forces engaged in manipulating the robotic arm in the remote environment.
2. While the user manipulates the arm, provide an inertial force to prevent a user moving too fast.
3. Build motion constraints for the robotic motion control due to task requirements, e.g. the speed of approaching a peg in a hole assembly operation, and environmental constraints, e.g. when the robotic arm is too close to an object the motion and speed of the robotic arm need to be restrained in order to avoid any potential unintended damages.
4. Provide a repulsion force to avoid the possible obstacles and forbidden areas.
5. In the manipulation tasks such as capturing target, guide the user to follow a pre-planned optimum path.

Table 7-1 Updated specification template

Specification category	Category attributes	Design parameter
Geometric model	Manipulation target	Robotic system model: Imported from CAD model
		Modification: Kinematics are solved while manipulated
	Manipulator cursor	Indicating the supposed end effector position
Force model	Telepresence	Touch of assembly tool and parts
		Frictional forces
	Constraints	Natural constraint: Joints limit
		Artificial constraint: Singularities Forbidden areas
Guidance	Attraction: Towards target Dynamic control Impedance control	
	Repulsion: Avoid obstacles	
Force rendering	Force scaling	Scale matching Scale resolution
	Force actuation	Actuating force model on haptic device
		Stability
Environment modelling	Lighting condition	Showing the lighting condition in the working environment
	Working scenario	Building objects models in the environment from the data acquired by sensing system
Integrated knowledge library	Task procedure planner	Control of industrial robot.
		Communication between systems and platforms.
		Coupling of virtual and realistic robots, monitoring and updating the environment

7.3 HARMP Modelling for Teleoperation of a Industrial Robot

In order to meet the system requirements, the HARMP design process model is followed to create a haptic system. Similar to the interface for space robotic

teleoperation, the system architecture includes a haptic input device to allow a user to interact with the virtual system, a virtual model representing the physical robot and its operational environment and also a representation of the user's interaction device, e.g. a cursor or a virtual hand or end-effector, a haptic rendering model to represent the forces generated either due to a collision or inertia, and finally a physical robotic system which is deployed to achieve the manipulation requirements. Due to the lack of access to other haptic interaction devices, plus its suitability, Phantom Desktop is considered as the haptic device for ease of use. It is, however, ideal for designing a new haptic interface device that has more consideration of the user customisation requirements and also the physical robotic configurations, which is beyond the scope of this thesis and will be discussed for future research. A haptic interface is required to enable a user to manipulate the robotic arm to achieve different tasks. A force engine can 1) help the user to calculate the relative positions of the robot and its adjacent objects and detect the objects and obstacles for potential collisions, 2) calculate the forces generated due to a collision between two objects and provide these to the user through the haptic interface, and 3) guide the user in three dimensional space to achieve the specific manipulation tasks. The model of the robotic arms used in the system needs to ideally be identical to the real physical robot to create direct and close mapping of its physical behaviour in the virtual world. For any given robot, its geometries can then be used to create a virtual model accordingly using CAD software. In addition, the inverse kinematic solution needs to be generated and included in the system, to allow teleoperation and remote control while the arm is manipulated in the execution of the planned tasks. Finally, the force engine also needs to be modified to simulate the environment in the industrial working scenario.

7.4 Embodied Design

In order to implement the above conceptual design, the HARMF design model is implemented to achieve the concept through the generation of system architecture, implementation and selection of suitable components or subsystems of the system architecture to realise the whole system into a physical prototype.

7.4.1 System Architecture

Compared to the control system developed for haptic teleoperation for the virtual space manipulator, the control algorithm for real industrial robots is more complicated. It needs to consider the complex dynamics of the real robot, set up communication between systems and deal with possible latency in the system as a whole.

Figure 7-1 shows the control diagram of the haptic teleoperation for the virtual manipulator in the HARMP system. A user holds the end effector of the haptic device and manipulates it by moving around, this movement will result in the change of device position in the workspace. After mapping the device position to the worldspace of the graphical interface, the position can be used as the target position to command the virtual robot. The virtual robot will then follow the command to undertake the motion accordingly with consideration of the kinematics and dynamic solution. The interaction between the virtual robot and virtual environment, such as coming in contact with obstacles, will result in position changes back to the virtual robot as well as haptic force feedback. This haptic force feedback generated in the virtual environment, along with the haptic fixtures for constraints and guidance, will be sent back to the haptic device. Finally, this haptic force feedback will be felt by the human operator as an assist tool in telemanipulation and path planning.

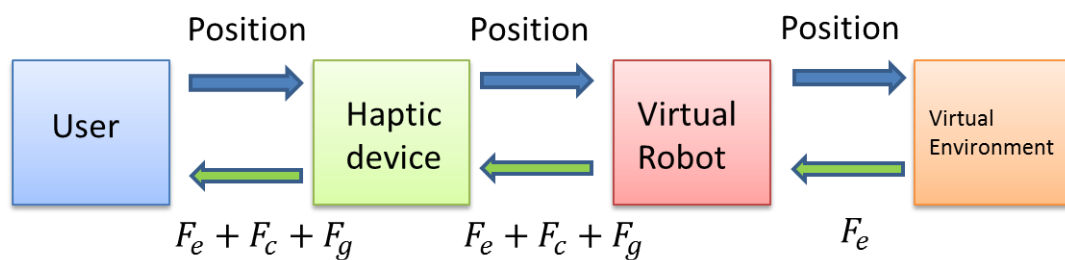


Figure 7-1. Control architecture for virtual robot teleoperation

A simulation control model for virtual teleoperation control was proposed by Adams and Hannaford (Adams and Hannaford, 1999). It is developed from the two port model for bilateral teleoperation (Hannaford, 1989) (Anderson and Spong,

1992). The model is built to demonstrate how the energy exchanges inside the system between human, manipulator and environment. As explained in the literature review, the energy in the system is classified into two types: effort (force/torque) and flow (velocity/angular velocity). In this study, these concepts are adopted to study the relationship between the effort and flow within a haptic system in this case study. In this study, for the system that takes one or multiple efforts as input and transfer to the flows, it is defined as an admittance system. The impedance system is defined as taking one or multiple flows as inputs and transfer to the efforts.

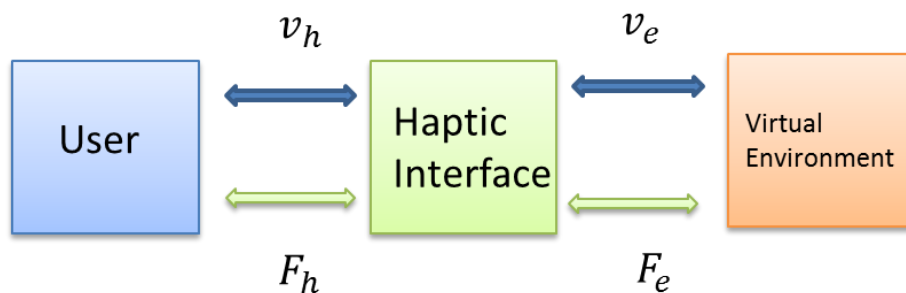


Figure 7-2 Two port model for virtual bilateral teleoperation

For a stable two port model for virtual bilateral teleoperation, the type of components inside the system need to be defined. For such a bilateral teleoperation system, the role and character of the human user can be either in impedance or admittance mode. If a user manipulates the haptic device strongly, for example putting force on the device resulting in a velocity/ position change of the haptic device, it is admittance as the effort as input and flow as output. Alternatively, if a user follows the guidance or movement provided by the haptic device and changes the hand movement accordingly, then the operational mode is impedance as it takes flow as input and transfers to effort as output. Similarly, the environment can also be either impedance or admittance, according to its natural properties while coming into contact with the end effector of the robot. Most haptic devices, including the Phantom Desktop used in this study, are classified as impedance since they have low inertia and are highly back-drivable. While a user or environment causes position changes on the tip of haptic device, the device will

follow the command and move accordingly.

In this case study, the design method for the HARMP system is followed to design a haptic teleoperation system for remote manipulation. In this design, it is necessary to select an industrial robot available suitable for the required functions of the design specification. Therefore, based on the selection of the real robot Staubli, it is then necessary to add a real environment where the robot operates for embodiment design, subsequent demonstration and verification. Therefore a control method for haptic bilateral teleoperation including a real robot in the environment is proposed and developed as shown in Figure 7-3.

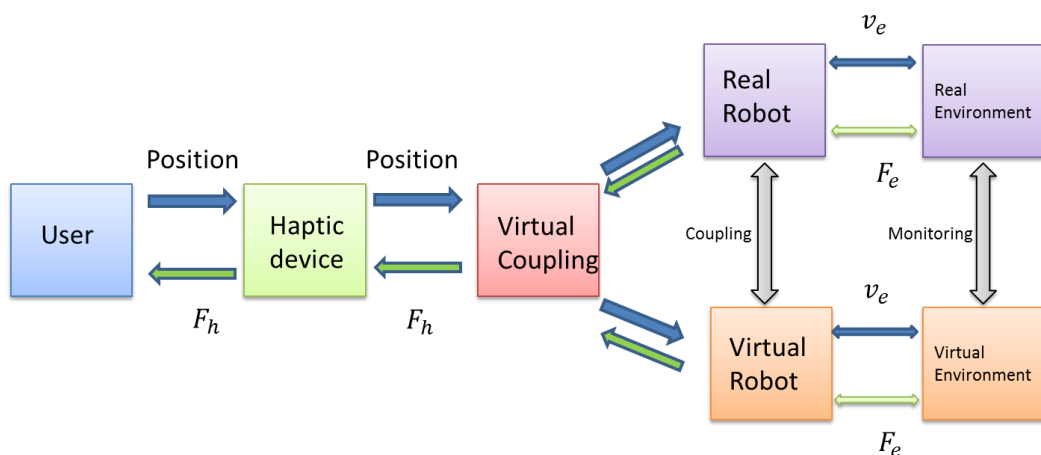


Figure 7-3. Modified bilateral control model

As shown in Figure 7-3, the real industrial robot and environment have been integrated into the control diagram parallel to the virtual robot and environment. In order to balance the interaction of the virtual robotic system with the physical robot, a virtual motion and haptic coordinates coupler is proposed and added after the haptic device. It is introduced as a mediator between the haptic device and robots, since the virtual and real robot may have different characteristics. The virtual coupler on one side deals with the command sent from the haptic device, calculates kinematics and mapping solution and then passes the command to two robots. On the other hand, the coupler processes the position information and force signals coming from the physical robot so that correct haptic feedback can be generated and realised in the user interface. The virtual robot, as designed earlier,

shows impedance characteristics as it is back-drivable while interacting with the virtual environment. It can take velocity and position changes from environment as inputs which results in force feedback from the physical real robotic to the haptic user interface system.

The real robot can be either impedance or admittance. A real robot is impedance, and able to react to influences in the environment, if it is another haptic device, or the robotic manipulator which has back-drivable joints and if it has delicate encoders or force sensors that can achieve force control. The virtual fixture for telepresence, such as contact with obstacles or engagement with frictional forces, can be directly input from the real environment and sent back to the haptic device to be detected by the user. The proposed approach is able to meet both of the above admittance and impedance requirements.

However, for most current industrial robots, they are not designed as a back-drivable device. Their stiffness and inertia is too high to be able to meet the accuracy and reliability requirements of manufacturing operations. Due to this restriction, the implementation of this case study only allows admittance control. The robot only uses commands generating torques in joints which leads to the velocity change in the environment. If it engages with obstacles, the obstacle will be moved otherwise it will cause damage to the joints or actuators of the robot. In this case, telepresence of the environment cannot be achieved directly. To solve this, a pseudo-impedance control method can be used. The real environment is being monitored in real time, and any change in the environment can be reconstructed in the virtual environment. The motion of real robot is coupled to the virtual robot while manipulating, in this way telepresence of the environment can still be achieved. The usability of this pseudo-impedance control depends on the accuracy of the sensing, detection and reconstruction of the real environment. The virtual environment may not be able to reflect the real environment correctly. So the real robot, the real environment, the virtual robot and the virtual environment should be monitored and compared by a user at all times during manipulating. In this way,

the user is supplied with the entire picture of the system in real time which can help with remote control. In case of any unexpected event, the user can make a decision and command the system according to human's judgement. This man-in-the-loop approach can ensure the safety of the system through full control by the user. In this way, the haptic bilateral control of the admittance industrial robot system can be achieved.

7.5 System Setup

7.5.1 Hardware Setup

Based on the system architecture and the selection of various key hardware components, a dedicated haptic system has been prototyped. The hardware setup of the system consists of the haptic device, industrial robot and its driver, robot controller, network connections and sensors in the environment.

7.5.2 Haptic Device

The haptic device Phantom Desktop is used as the master controller in this case study due to its availability and suitability. Its maximum output force is 7.9N. The movement is six DOF including position in Cartesian system by x, y, z axes, and orientation by roll, pitch and yaw joints. However, the force feedback it can provide is three DOF, only on x, y and z axes. Linear workspace is 160mm (W) x 120mm (H) x 120mm (D).

7.5.3 Industrial Robot

The real industrial robot selected from the three available Staubli robots in this case study is a Staubli TS80 SCARA shown in Figure 7-4. It is capable of four degrees of freedom manipulation. The SCARA configuration of the robot has features such as high speed and moderate capacity payload. It has four axes and four Degree of Freedom. The TS80 can reach to 800mm in its workspace with a maximum payload of 8 kg. It also features high speed that can achieve approximately 100 picks /minute. The robot is driven by its controller which comes with the robot. It is already installed in the laboratory at the University of Strathclyde for industrial and

research projects.



Figure 7-4. Staubli TS80 SCARA robot

7.5.4 Haptic Controller and its PC

Based on the requirements for haptic rendering and availability, a Dell Latitude E5540 with Intel i7-4500 and 16 GB RAM is used, on which the control of the haptic device and graphical interface is run. The system is 64-bit Windows 7 Professional, which is compatible for most engineering software needed in this study. The graphics card is a NVidia GeForce GT 720M.

7.5.5 Robot Controlling PC

The Staubli TS80 robot is normally controlled by a teach pendant or by Staubli's software UniVAL using the VAL3 language. However, in this haptic teleoperation system, it is not possible to use this mode of control of the robot to achieve the functionality specified. The real robot is controlled by the haptic device in order to enable haptic behaviour of the whole system. The haptic device is run on a Dell laptop with a Windows operating system. Sensors and other actuators in the working environment are integrated into the control system. The desired controller should be programmable, extendable and able to communicate with other systems.

Based on these requirements, the Beckhoff CX2020 Industrial PC shown in Figure 7-5 is selected to send commands to the robot and communicate with the haptic and sensing systems in this case study. The Beckhoff CX2020 has a 1.4 GHz Intel Celeron CPU and 2GB RAM. It ran on a Windows Embedded Compact 7 system and could be connected to four robot modules. Several bus terminals are connected as digital or analogue IO's, which can be used to control actuators in working scenarios and read signals for sensors in the environment. The industrial PC and IO's are communicating via EtherCAT that ensures high speed communication.



Figure 7-5. Beckhoff Industrial PC and IO's

7.5.6 IO's/ Sensing in the Environment

Other hardware installed in the system includes a conveyor belt, encoder, infrared sensors and a Scorpion 3D camera. The conveyor belt can be used to simulate the movement of an approaching target, while the speed and direction can be controlled through the bus terminal sent by the user. Infrared sensors are installed alongside the conveyor belt to detect the current position of the target object. These sensor signals are sent back to the system through the digital inputs on the

bus terminal. To identify and locate the object, a 3D camera from Scorpion is used in the system. The Scorpion 3D can identify the shape and 3D location of the moving object on a conveyor belt in real time. This information can be sent to the HARMF system to reconstruct the object model in a virtual environment.

7.5.7 Network Connection

The haptic control PC, Beckhoff industrial PC and the SCARA robot are communicating with each other through Ethernet. A network switch from Netgear is used to setup the communication between the haptic control PC and the Beckhoff industrial PC. The drive of the SCARA robot and the Beckhoff industrial PC are directly connected via an Ethernet cable. The speed of these communications reaches 100Mb/s which is adequate for the desired requirement.

7.5.8 Hardware System Structure of Bilateral Robot Control

The Hardware system structure of the bilateral robot control can be shown in Figure 7-6.

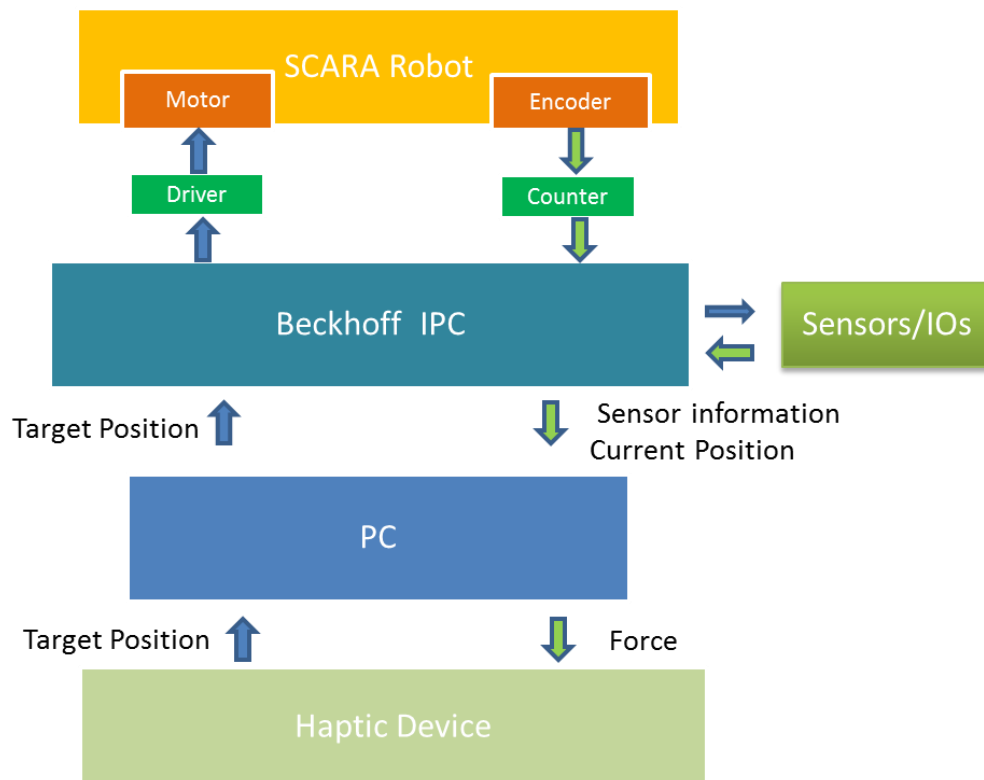


Figure 7-6 Overall HARMP hardware structure

A haptic device is manipulated by the user and sends position/velocity information to the haptic interface PC. This information is sent to the Beckhoff IPC. The SCARA robot driver can take these position/velocity commands and actuate robot motors for the desired motion. The real position of the SCARA robot can be read and calculated from the encoders integrated in the robot, and then sent back to the Beckhoff controller IPC. Meanwhile, the IO's and sensors in the environment can communicate with the Beckhoff controller IPC by sending the sensor information to it. The current position and velocity of the SCARA robot and sensor information are sent to the haptic interface PC for haptic modelling, which will be applied on the haptic device as haptic assist for a user.

7.5.9 Software Setup

7.5.10 Windows/ OpenHaptics

The haptic control runs on the master PC with Microsoft Visual Studio and OpenHaptics (the same HARMP system used for previous case studies). The

Scorpion 3D camera also runs on the PC with a 3D version of the Scorpion Vision Software.

7.5.11 Beckhoff TwinCAT 3 XAE

The software and control architecture is detailed in Figure 7-7. The Beckhoff industrial PC is running a Windows Embedded Compact 7 operating system. The control software from the Beckhoff TwinCAT 3 is selected for robotic control. TwinCAT is a Windows based software system that can achieve real-time PLC, NC and CNC control with compatible PCs. The version used in this study is the TwinCAT 3 XAE (eXtended Automation Engineering). It is integrated with Microsoft Visual Studio which makes it be able to program control automation in C/C++ languages. One of the features of the TwinCAT 3 XAE is the data generated by modules in TwinCAT 3 which can be exchanged with other systems regardless of the languages. This is done by its transport layer, ADS (The Automation Device Specification). TwinCAT 3 turns different individual software modules into independent devices. A real time ADS interface is in charge of data exchange amongst devices. The data and messages are managed and transferred inside the system via TCP/IP network. This ADS message router works for all TwinCAT PCs and Beckhoff Bus controllers. It can even communicate with Matlab applications. In this way, all devices with TwinCAT 3 in the system can be connected to exchange data which can be used to enable haptic interaction as shown in Figure 7-7.

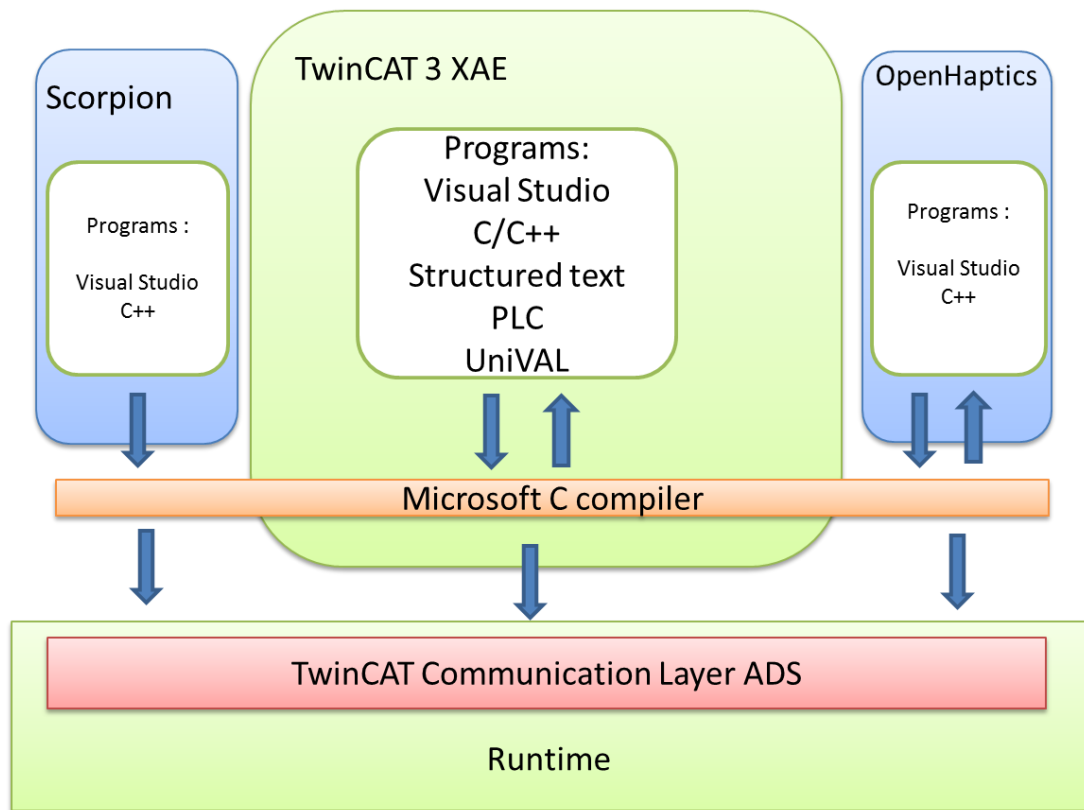


Figure 7-7 TwinCAT and ADS structure of communication in HARMP system

The TwinCAT 3 XAE, Scorpion 3D camera software and OpenHaptics can be all connected through Microsoft C compilers and communicate in the ADS layer. Programs and modules used to detect and identify the object, manipulate the haptic device, send commands to the industrial robot and feedback to the haptic device are all implemented with Microsoft Visual Studio on a Windows system. Data, messages and commands generated by these modules can be exchanged with each other to achieve the control and information loop inside the system.

There are several reasons Beckhoff TwinCAT 3 XAE was chosen for the industrial robot control system in this case study.

1. It is integrated with Microsoft Visual Studio and data can be exchanged with each module in the system. The programming of the HARMP system is based on OpenHaptics, which also runs on Visual Studio and a Windows system. To achieve teleoperation of the real industrial robot using the haptic device, the motion command data sent from the haptic device and feedback data from the real robot

need to be exchanged through the control system. This can be done directly by running the haptic control system and Beckhoff TwinCAT 3 on the same PC and connecting through a TwinCAT communication layer ADS in real-time. The real SCARA robot itself can be controlled by other solutions such as VAL3 by Staubli or the ROS system. However, although VAL3 is running on a windows system, it is not easy to communicate with the other modules. It is not open and programmable enough to read and use the command sent from the haptic system to control the real robot. ROS is another popular control system for robotics. It is highly programmable and flexible. However, it only runs on Linux systems that cannot communicate with the haptic control system directly. Therefore, using TwinCAT 3 is the most straight forward and compatible control solution in this instance.

2. TwinCAT 3 XAE (eXtended Automation Engineering) also integrates robotic Motion Control. With integrated UniVAL module developed by Staubli for Beckhoff control systems, TwinCAT 3 software provides a motion control solution for Staubli robots including point-to-point movements, manual motion and axis coupling.

3. The TwinCAT 3 turns a PC device to a PLC controller. For a PLC (Programmable Logic Controller), besides controlling the robot and its motors, it is also able to integrate other IO's and hardware into the control system. In this case, it includes sensors and conveyor belt controllers and encoders. These devices can be implemented using either Structured Text (ST) or function blocks, making the control system flexible and extendable.

7.6.1 Geometric Modelling

To build the geometric model of the TS80 SCARA robot in a virtual interface, the original CAD model of the robot needed to be built first. It can be acquired from the official Staubli resource which provides CAD libraries for Staubli robotic arm products. The models can be downloaded in formats including .STEP, .IGES in 3D and DXF in 2D. For this case study, the 3D STEP model of TS80 SCARA with 200mm z-axis stroke and flooring mounting is selected. The downloaded CAD file can be imported into 3DS Max for modification.

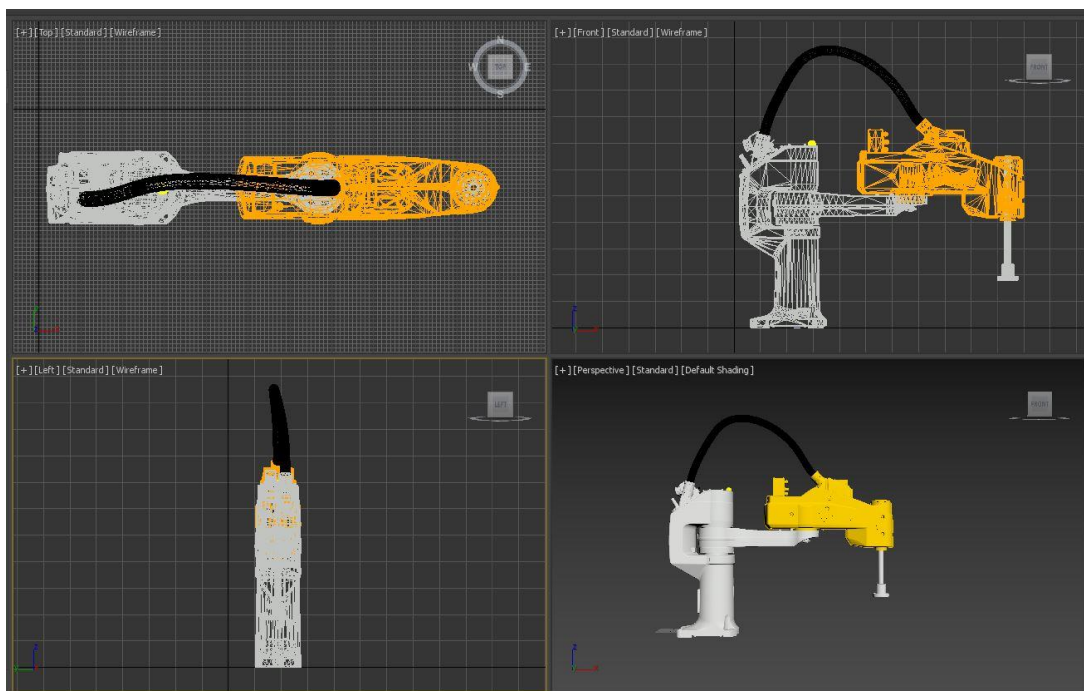


Figure 7-9 Imported TS80 CAD model in 3DS Max

As shown in Figure 7-9, the CAD model of the SCARA Robot includes several parts. These parts are assembled together to form the whole robot. To export the robot model in a format that is readable by the haptic interface, these parts should be saved and transformed separately. Therefore, four parts are selected to be saved separately and then exported to the OBJ file which is compatible in OpenHaptics. These four parts include the base, body arm, forearm and the end stroke. Each of the parts are saved in OBJ and imported to the graphical interface of the HARMF system. The parts are imported as draggable objects with haptic features that can be touched by a user using the haptic device. The material properties saved in the

material file for each part are also imported along with geometric CAD model so that they can be shown in the interface as well. The position and orientation of the imported model can be adjusted by calling functions as described in Chapter 6. For these four parts of the robot, the base part is fixed on the “floor”, while other parts can be moved and manipulated by the user. These parts form the geometric model of the SCARA robot in the haptic interface as shown in Figure 7-10.

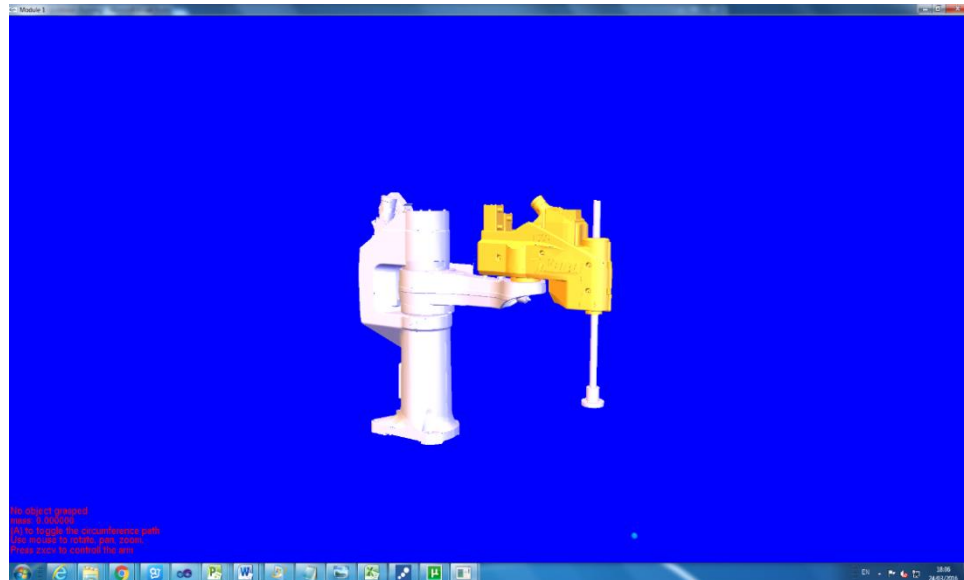


Figure 7-10 Geometric model in haptic interface

7.6.2 Kinematics Solutions

The next step is to calculate the forward and inverse kinetics solution for the TS80 SCARA robot to update the robot model in the haptic interface while being manipulated by the user. The procedure of solving the kinematic problem can follow the procedures described in Chapter 6. The TS80 SCARA robot has four axes and four degree of freedoms. The first, second and fourth joints are revolute joints and the third one is a prismatic (sliding) joint. The joint angles of the first and second links combining decide the x and y position of the end effector in the workspace. The third joint is prismatic that creates relative translation between links. It controls the z position of the end effector in the workspace. The last joint is revolute, leading to rotation of the end effector that can be used for different tasks.

Table 7-2 Link parameters

l	a_{i-1} (m)	α_{i-1}	d_i (m)	θ_i
1	0.33	0	0	θ_1
2	0.27	180	0	θ_2
3	0	0	d_3	0
4	0	0	0	θ_4

To determine the movement of the end effector and each link, the homogeneous transform matrix of the arms needs to be specified with the above four parameters. To construct transforms from frame 4 to frame 0, the kinematic problem is broken down to four sub-problems of a homogeneous transform matrix for each link that:

$${}^0_1T = \begin{bmatrix} \cos\theta_1 & -\sin\theta_1 & 0 & 0.33\cos\theta_1 \\ \sin\theta_1 & \cos\theta_1 & 0 & 0.33\sin\theta_1 \\ 0 & 0 & 1 & 0 \\ 0 & 0 & 0 & 1 \end{bmatrix}$$

$${}^1_2T = \begin{bmatrix} \cos\theta_2 & -\sin\theta_2 & 0 & 0.27\cos\theta_2 \\ \sin\theta_2 & \cos\theta_2 & 0 & 0.27\sin\theta_2 \\ 0 & 0 & 1 & 0 \\ 0 & 0 & 0 & 1 \end{bmatrix}$$

$${}^2_3T = \begin{bmatrix} 1 & 0 & 0 & 0 \\ 0 & 1 & 0 & 0 \\ 0 & 0 & 1 & d_3 \\ 0 & 0 & 0 & 1 \end{bmatrix}$$

$${}^3_4T = \begin{bmatrix} \cos\theta_4 & -\sin\theta_4 & 0 & 0 \\ \sin\theta_4 & \cos\theta_4 & 0 & 0 \\ 0 & 0 & 1 & 0 \\ 0 & 0 & 0 & 1 \end{bmatrix}$$

The total transform matrix from frame 4 to frame 0 is determined by these sub transform matrixes, given by

$${}^0_4T = {}^0_1T {}^1_2T {}^2_3T {}^3_4T \quad \text{Eq. 29}$$

$$= \begin{bmatrix} \cos(\theta_1 + \theta_2 + \theta_4) & -\sin(\theta_1 + \theta_2 + \theta_4) & 0 & 0.33\cos\theta_1 + 0.27\cos(\theta_1 + \theta_2) \\ \sin(\theta_1 + \theta_2 + \theta_4) & \cos(\theta_1 + \theta_2 + \theta_4) & 0 & 0.33\sin\theta_1 + 0.27\sin(\theta_1 + \theta_2) \\ 0 & 0 & 1 & -d_3 \\ 0 & 0 & 0 & 1 \end{bmatrix}$$

Then the inverse kinematic needs to be solved. Although the SCARA robot has four degree of freedom, the third and fourth joints can be controlled separately. Therefore, the inverse kinematic problem can be simplified to a planar manipulator with two links that only focuses on the first and second links of the SCARA robot as shown in Figure 7-11.

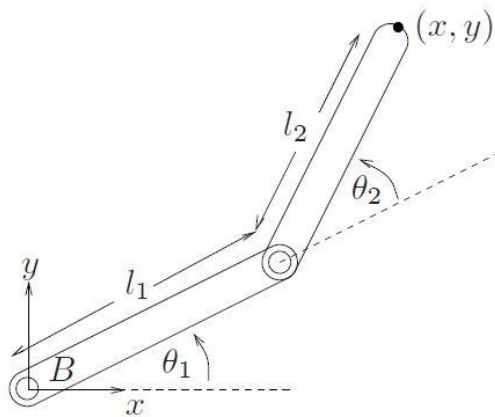


Figure 7-11 Two links planar manipulator

The target position of the end effector on the plane (x, y) can be determined by the mapped position (x, z) of the haptic device manipulated by the user. This is a simpler kinematic problem compared to the 3R manipulator in the last chapter. With the given x, y and links length l_1, l_2 , the joints angle θ_1, θ_2 can be solved as:

$$\theta_2 = \pm \cos^{-1}\left(\frac{l_1^2 + l_2^2 - (x^2 + y^2)}{2l_1 l_2}\right)$$

$$\theta_1 = \text{atan}(y, x) \pm \cos^{-1}\left(\frac{(x^2 + y^2) + l_1^2 - l_2^2}{2l_1 \sqrt{(x^2 + y^2)}}\right) \quad \text{Eq. 30}$$

For each given target position there are two solutions for inverse kinematics and the better solution can be determined by the current status. After solving the joint angles for the first and second angle, the position and orientation of these two parts can be updated. Position z of the end effector can be directly determined by the mapped position y of the haptic device. In this way, the inverse kinematics can be solved for the SCARA robot to update the geometric model in the haptic interface.

7.6.3 Mapping of Coordinate Systems

The structures of haptic controller and real robot might be kinematically different. This may result in a different work space volume, unit scales and reference frames. The coordinate system and reference frames of the Phantom Desktop and TS80 SCARA robot are shown in Figure 7-12.

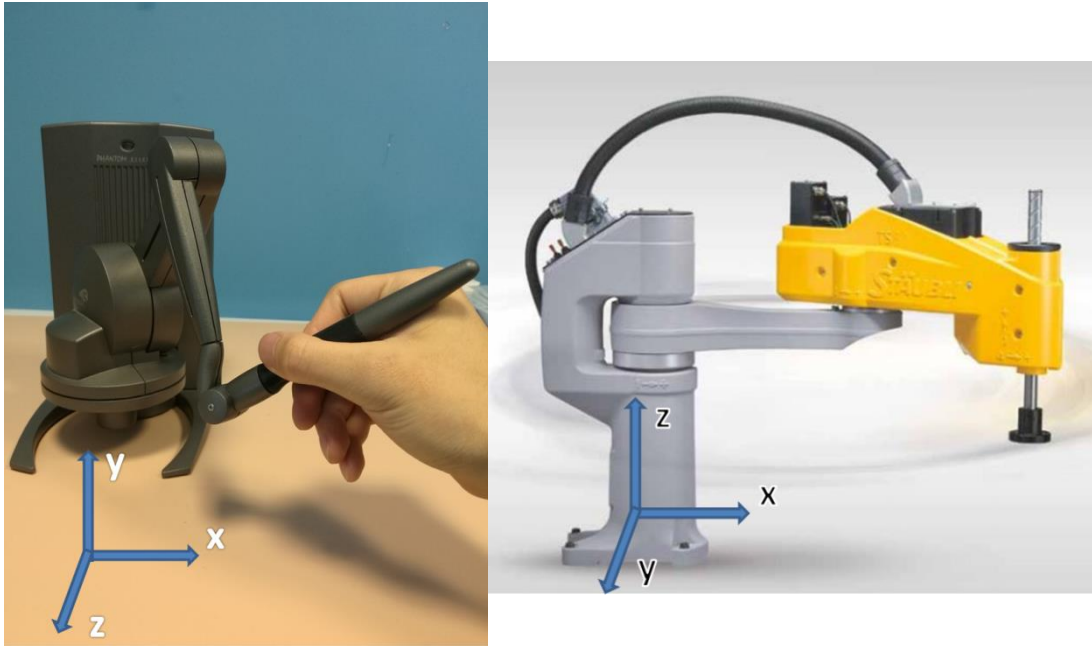


Figure 7-12 Comparison between coordinates of Phantom Desktop and TS80 SCARA

The reference frame of the real robot is based on the requirements of this case study and hence their parameters are pre-defined by its manufacturer that cannot be changed. To achieve bilateral manipulation using the haptic device, the position and velocity of the haptic device's tip should be scaled and transformed to fit the standard frame of the real robot. Also, as can be seen from the above figure, the haptic device and TS80 robot's frame has a different direction in the z and y axes in the workspace which should also be considered while mapping the movement of haptic devices to the real robot. The coordinates and position of haptic devices should firstly be transformed to the origin of the real robot's reference frame, and then multiplied by a scale factor to fit the workspace volume, and finally the y axis should be swapped with the z axis accordingly. The (x, y) coordinates of the target position of the end effector can be determined by the mapped position (x, z) of the

haptic device, and position, z , of the end effector can be determined by the mapped position, y , of the haptic. In this way the inverse kinematic and mapping between different devices' frame is complete.

7.7 Haptic Modelling

For the haptic modelling for bilateral robotic control, the HARMP system designed is followed. Again, the haptic features can be designed and implemented for three objectives: telepresence, constraints, and guidance.

7.7.1 Telepresence

Telepresence for bilateral control is the classic objective of the haptic teleoperation system. The bilateral control can be achieved while one of two systems' demands are determined from the measured outputs of the other. Ideally, while the real robot is being manipulated, the haptic controller device should provide the real or scaled force as the robot encounters its environment, allowing a user to haptically interact with the real environment. However, to achieve this telepresence and force control, it is required that the real robot should be an impedance type that is back-drivable and able to react to the force in the real environment. This bilateral force control can be implemented by two methods: For a robot system that has integrated force/ torque sensors built in, the force it encounters in the environment can be measured by sensors and sent back to the haptic device for haptic telepresence. Alternatively, it can be implemented using the impedance control. While being manipulated by the haptic controller, if the robot reaches any obstacles to disturb its movement, it will cause position and velocity errors compared to the target position and velocity commanded. The correcting force/torque can be generated according to this position and velocity error between these two systems and then sent back to the haptic device. As a result, the user can feel the same or scaled force/ torque in the environment.

However, for many industrial robots in the market, including the Staubli TS80 SCARA robot used in this case study, they don't have force/ torque sensors

integrated due to their specific uses and costing reasons. In addition, since these industrial robots are used for automation assembly tasks with high reliability and stiffness, most of them are not designed as back-drivable. If using the method that uses position/velocity errors to generate the force/ torque, while engaging with the obstacle, the robot will continue moving. The position/velocity error is hard to detect before it causes damage to the obstacle or even the robot itself. Therefore, alternative methods need to be investigated to achieve the haptic bilateral control.

In this case study, a method to implement this haptic telepresence by coupling the real and virtual robot is presented. As shown in the bilateral control model in Figure 7-3, the haptic controller device is commanding both the real and virtual robot. The virtual environment can be built and updated, similarly to the real environment. Virtual models of the obstacles and objects in the real environment are built and placed accordingly into the virtual environment, then the real environment is being monitored in real time. With the help of a Scorpion 3D camera and infrared trigger sensors, if the obstacles or target objects move in the environment, the position and velocity can be detected and then used to update the virtual model in the virtual environment in real time. In this way, the virtual haptic telepresence for the virtual robot can be implemented. By mapping and coupling the motion of the real robot to the virtual robot while manipulating, the telepresence of the environment can still be achieved.

7.7.2 Constraints

7.7.2.1 Natural Constraints

Natural constraints in haptic teleoperation are defined by the structure and mechanism of the robot. The motion of the virtual robot is kept inside the working envelope by introducing a spring damper model with high stiffness at the edge of its workspace. Since the motion of real robot is coupled with the virtual robot, the motion of real robot can also be limited inside the workspace to avoid collision with its structural body or going out of range to cause singularities.

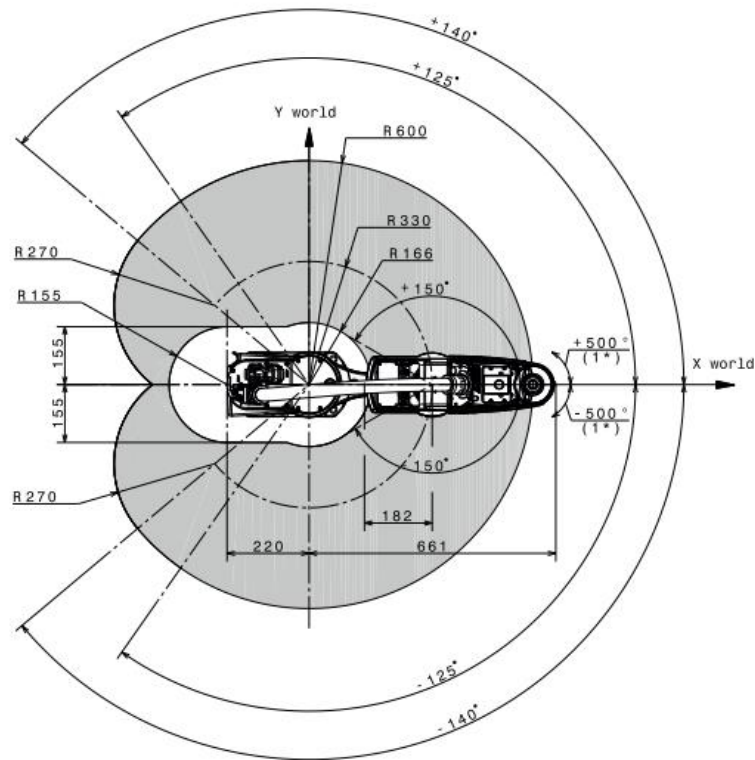


Figure 7-13 Working envelope of TS80 SCARA robot

The working envelope of the TS80 SCARA robot is shown in Figure 7-13. As can be seen, on the xy-plane there are outer limits and inner limits of the workspace demonstrated by the shadow area that the end effector of the robot should not surpass. These limits are ideally defined by the length of first and second links and the angle limit of each joint. On the z-axis, the workspace is limited by the motion range of the end stroke, which is 0-200mm depending on the length of the stroke. So the 3D geometry of the working envelop can be defined and the surface of this area can be haptically modelled by introducing a spring damper model with high stiffness. It can prevent a user surpassing the working envelope proving unsolvable for kinetics and motion control of the manipulator. While the control system sends motion command to the robot through UniVAL, the robot will start moving to the reach the target position without considering if the target is out of the working envelope. Therefore, the integration of these haptic constraints and coupling of the virtual and real robot will increase the safety and controllability of the teleoperation system.

7.7.3 Artificial Constraints and Guidance

The implementation for constraints and guidance follow the HARMP system. For artificial constraints, the manipulation will be strictly constrained by desired paths or movements. For example, if the end effector is required to move over the surface of a part to polish it, an artificial constraint that limits the movement of the robot can be placed on the surface. For virtual guidance, repulsion and attraction guidance can be introduced to assist the user's manipulation in tasks such as obstacle avoidance and target capture.

One of the features of haptic modelling in this case study is that constraints and guidance can be updated according to the information received from the sensing systems in the real environment. The sensing system includes a 3D camera, trigger sensors and the conveyor encoders. The shape, size, position and velocity information of the object in the real environment can be detected and sent back to the control system in real-time. This information will be used to update the haptic constraints and guidance, as well as the geometric model in the virtual environment. Additionally, the vision camera monitors the robot's environment and shows images to the user during teleoperation. While the constraints are dictatorial, the haptic guidance is suggestive and still allows the user full control. If a user detects any unexpected situation or errors between the real environment and virtual environment through the vision system, they can ignore the guidance and take full control reacting to the situation. The guidance will be overridden until the user decides to use guidance again. By coupling the motion of the real robot to the virtual robot, the integration of these haptic constraints and guidance will be able to provide assistance for haptic bilateral teleoperation of the robot.

7.8 Robotic Control System

With graphical and haptic modelling for the virtual robot and environment, the next step is to investigate a stable bilateral control of robotic system.

7.8.1 Control logic Flow

The control logic flow of the bilateral haptic teleoperation system is shown in Figure 7-14.

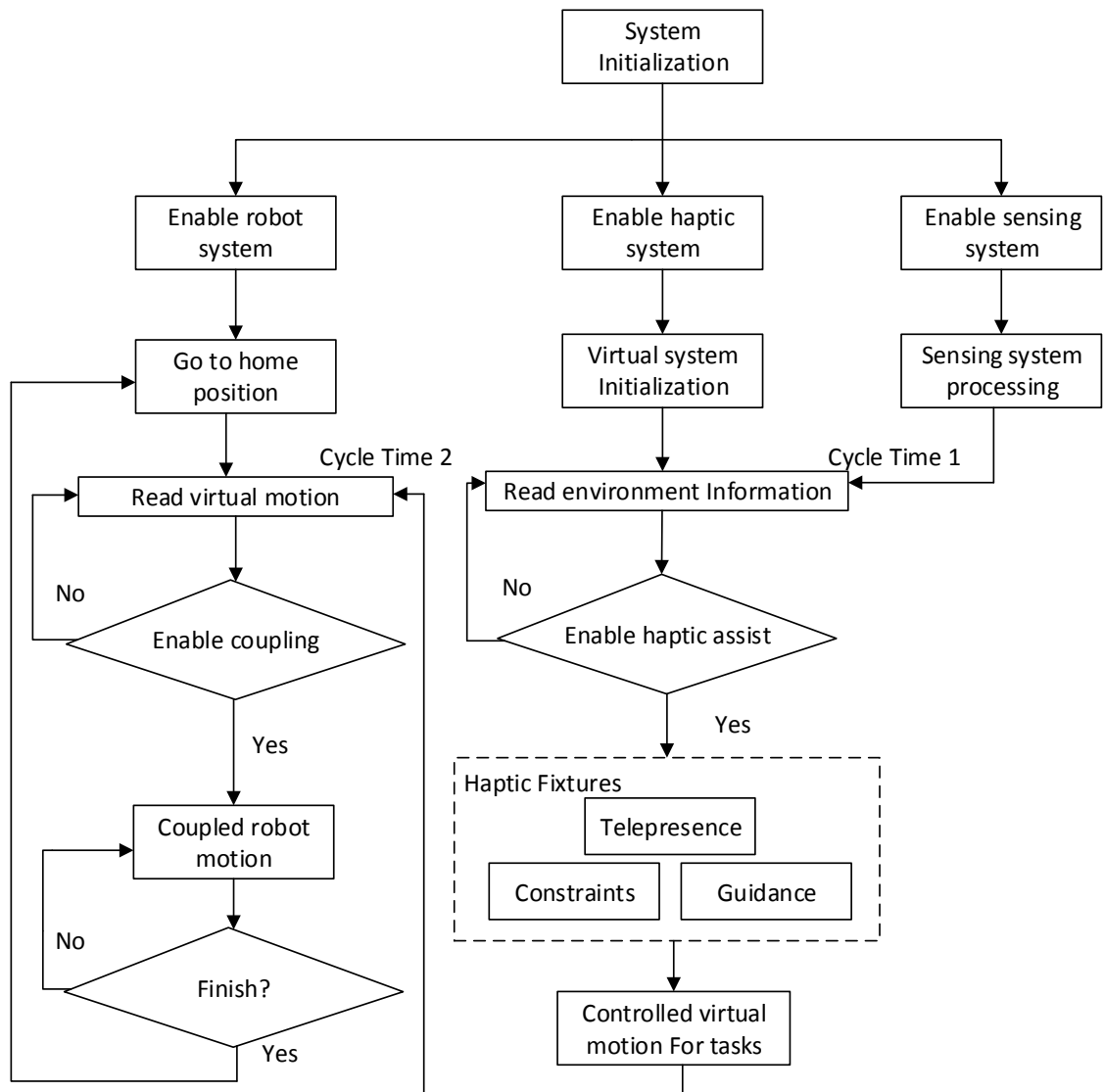


Figure 7-14 Control logic flow

Firstly, the whole system is initialized. The haptic interface, sensing system, robot system and control system are then enabled. The haptic device and interface starts running, the robot system is then powered on and goes to a safe home position awaiting further commands. The sensing system starts to scan the environment and process the data. The sensing system includes the Scorpion 3D camera, infrared trigger sensors and conveyor belt encoders. The shape, size and current position of

the target objects can be detected and calculated. This information is then sent through the communication layer and then read by the haptic system. The information about the target objects in the environment can be used to update the virtual environment of the haptic interface. Once the virtual environment is updated according to the real environment, it can be used for haptic modelling for telepresence. Then virtual constraints and guidance can also be modelled according to information received and the task requirements. The constraints and guidance can be enabled by a user according to task requirements. The manipulation of the virtual robot is then controlled by the haptic device enabled by haptic assistance models. Motion information from the virtual robot is then sent to the robot control system through the communication layer. If a user decides to enable the coupling of robot and it is safe and ready to do so, the coupling can be initiated. After being enabled, the motion of the real robot and virtual robot can be coupled to achieve bilateral control using the haptic device. This coupled motion continues until the task is accomplished. If the current task is finished, the robot goes back to its home position.

7.8.2 Bilateral Position/Velocity Control

A bilateral position and velocity control loop is developed for the robotic system with a haptic device and industrial robot. It includes position/velocity control of the haptic controller and the real robot with the mapping of the workspace between them as shown in Figure 7-15.

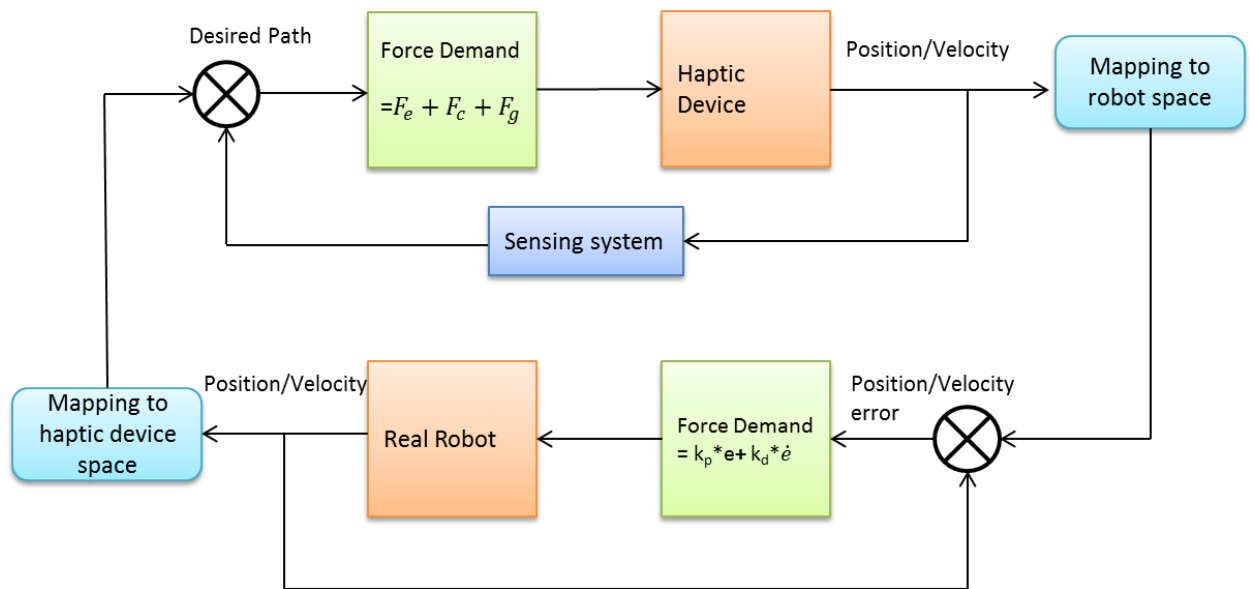


Figure 7-15. Bilateral position/velocity control loop

The haptic device can be manipulated by the user, outputting the position and velocity of its end effector in real time. This command of position/ velocity of the haptic device end effector are mapped into the workspace and coordinate system of the robot. This mapping includes the transformation and scaling of the coordinates. An admittance control is implemented for the robot. The position and velocity error can be acquired by the difference between the commanding position/velocity and current position/velocity. The force demand can be calculated as $f = k_p * e + k_d * \dot{e}$, it can be applied on the actuator on the real SCARA robot to achieve the desired motion. The output position/velocity is again sent back in the control flow to calculate the position/velocity error generating further force commands.

The output position/velocity of the robot is mapped back to the haptic device workspace and coordinates. By introducing the sensing system into the control loop, the environment information can be acquired and the real environment can be modelled virtually. The force demand for the haptic device can be updated with the haptic model including telepresence, constraints and guidance. In this way, the bilateral control and telepresence of the bilateral robotic system still can be

achieved.

7.9 Experiment Setup

A set of experiments have been undertaken to assess the haptic feedback provided by the HARMP system. The experimental environment was established in the robotics laboratory at the University of Strathclyde. The Phantom Desktop is manipulated by the user on a desk. A monitor on the desk shows the geometric model during the teleoperation. A video camera monitors the robot, and the real-time video is streamed to the same monitor for comparison to the geometric model. A Scorpion 3D camera is set above the conveyor belt to detect the position and size information of the incoming target. The experimental procedure is shown in Table 7-3. For robotic tasks, two teleoperation procedures were conducted. The first procedure uses haptic modelling of the environment and bilateral control, while the second procedure does not use haptic control as a comparison. The user must have basic experience with the use of a haptic device. The evaluation methods are updated for this case study, such that the performance of the haptic control of a robot in the real environment is evaluated by the user.

Table 7-3 Experiment set for the robotic manufacturing manipulations

	Experiment 1	Experiment 2
Part manipulating	With haptic modelling of environment and bilateral control	With only haptic modelling of environment/ without haptic bilateral control
Reaching constrained areas	With haptic modelling of environment and bilateral control	With only haptic modelling of environment/ without haptic bilateral control

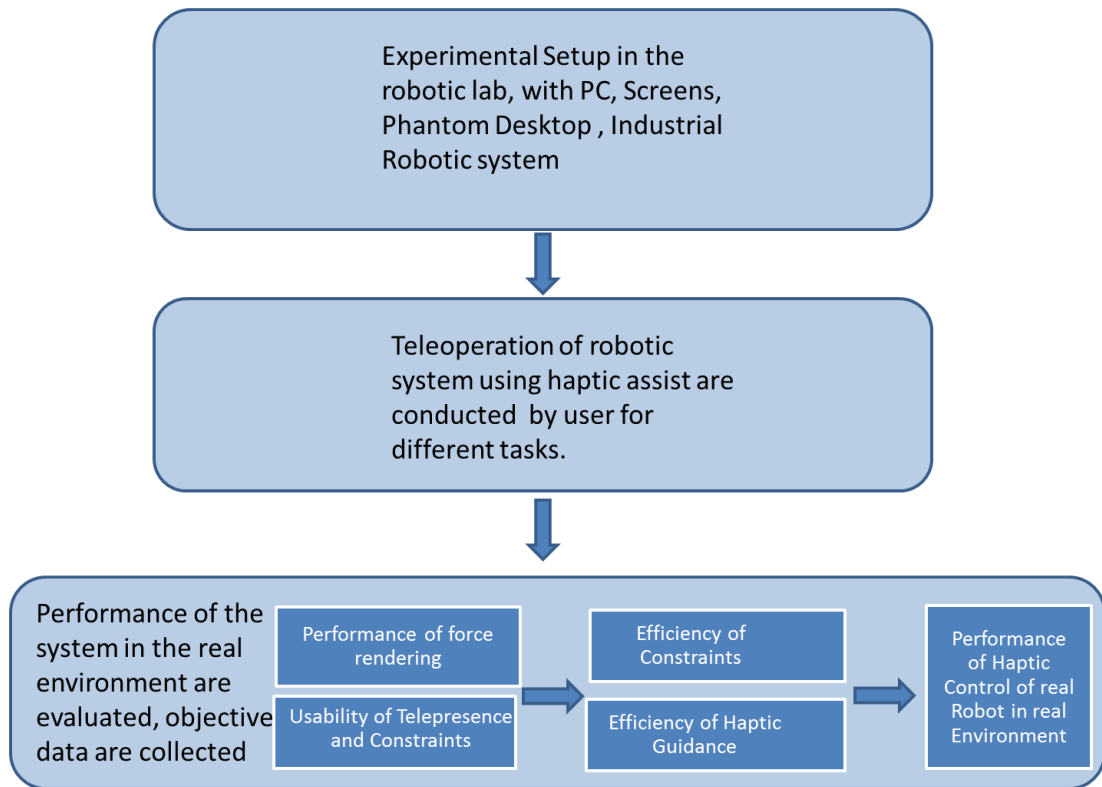


Figure 7-16 Updated evaluation method for Case Study 3.

7.10 Experimental Results

An image of the experiment during the teleoperation is shown in Figure 7-17. It can be seen that the user can monitor both the 3D robotic model and the real industrial robot whilst manipulating with the haptic master controller.

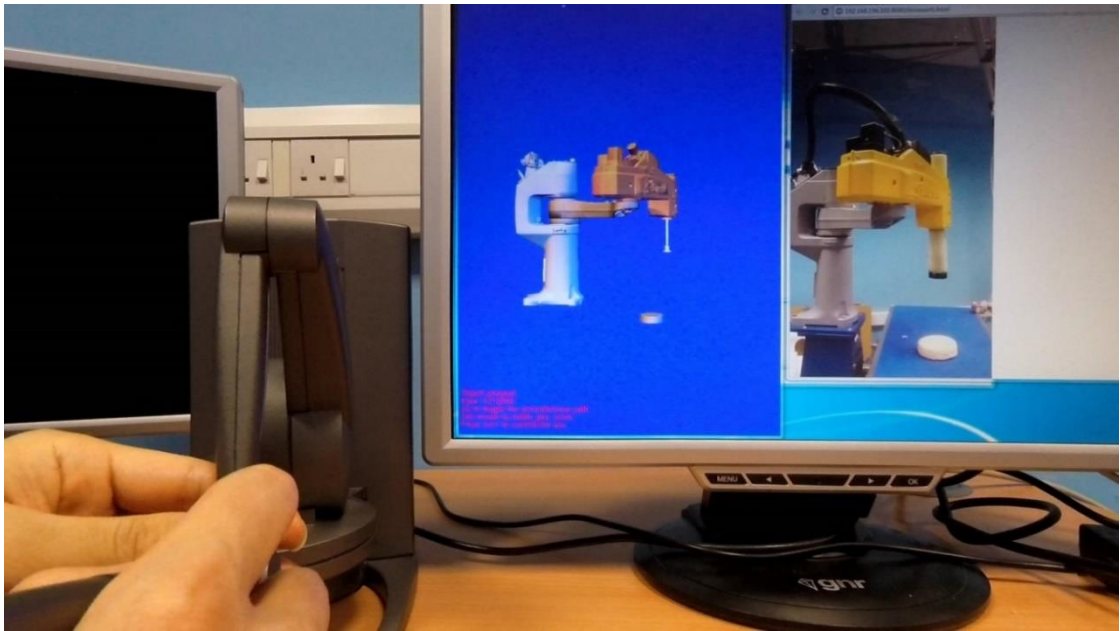


Figure 7-17 Experiment set up during tele operation

Figure 7-18 shows the plots of positions (x,y,z) of the virtual and real robot during the tele-manipulation in haptic bilateral control. It can be seen that the real robot follows the virtual robot's motion and path in x, y and z directions with a slight time lag. These exhibit good performance and usability of the robotic teleoperation system.

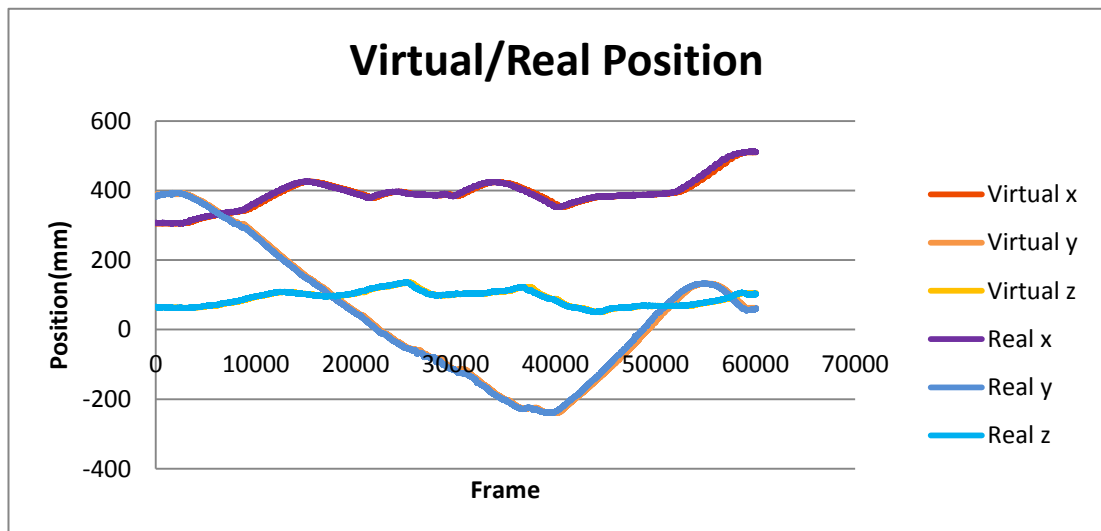


Figure 7-18 Virtual and real position with haptic bilateral control

Figure 7-19 and Figure 7-20 show the position error and bilateral forces between the virtual and real robot. It can be seen that the position error on the z-axis

remains small, while on the x-axis it reaches 25mm at the end of the manipulation. These position errors resulted in the bilateral force to be generated on the haptic controller to achieve bilateral control. It can be seen that the maximum generated force reaches 1.7N.

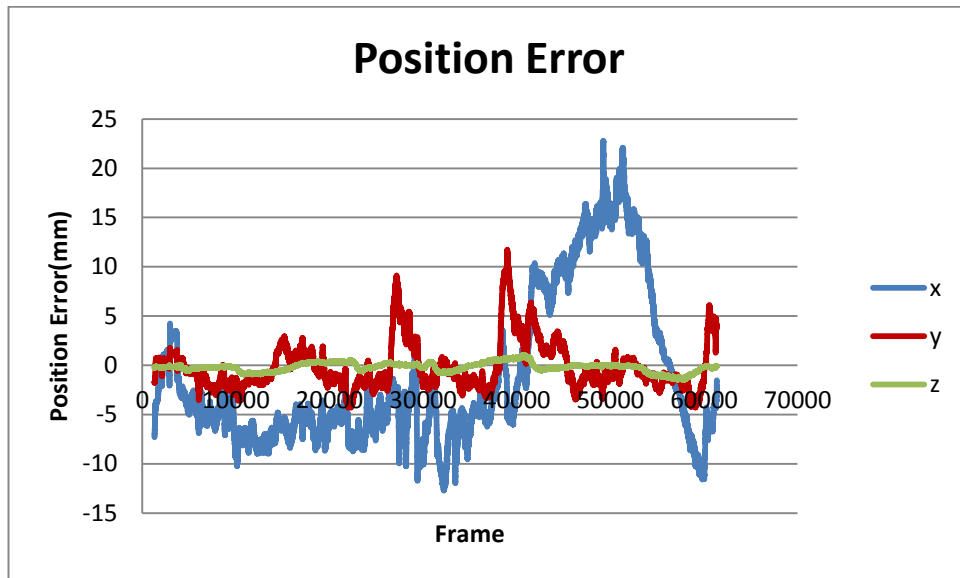


Figure 7-19 Position error with haptic bilateral control

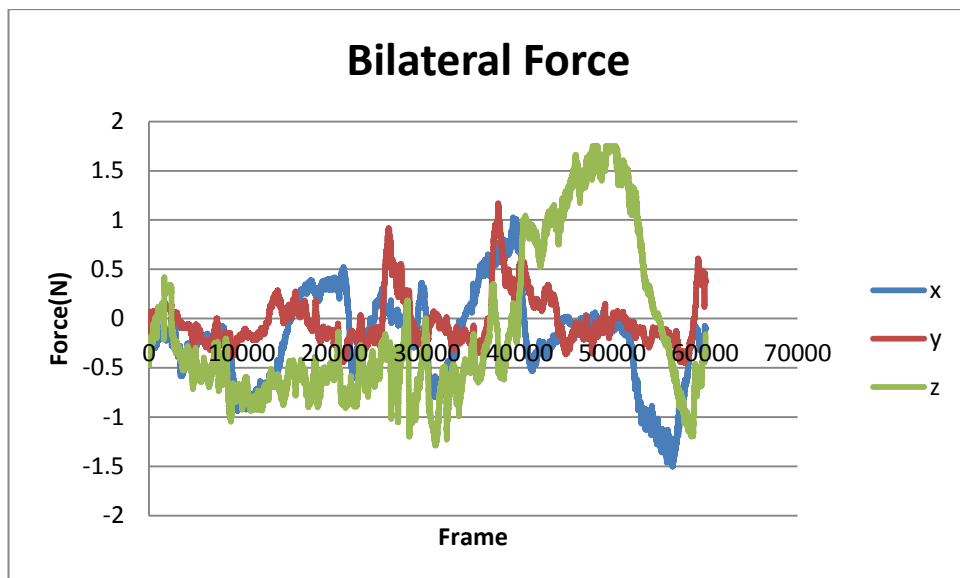


Figure 7-20 Bilateral Force during the manipulation

Figure 7-21 shows the plots of positions (x,y,z) of the virtual and real robot during teleoperation without haptic bilateral control. It can be seen that the real robot still follows the master position, however the time lag at some points is more significant

on the x, y and z axes compared to the time lag with bilateral control.

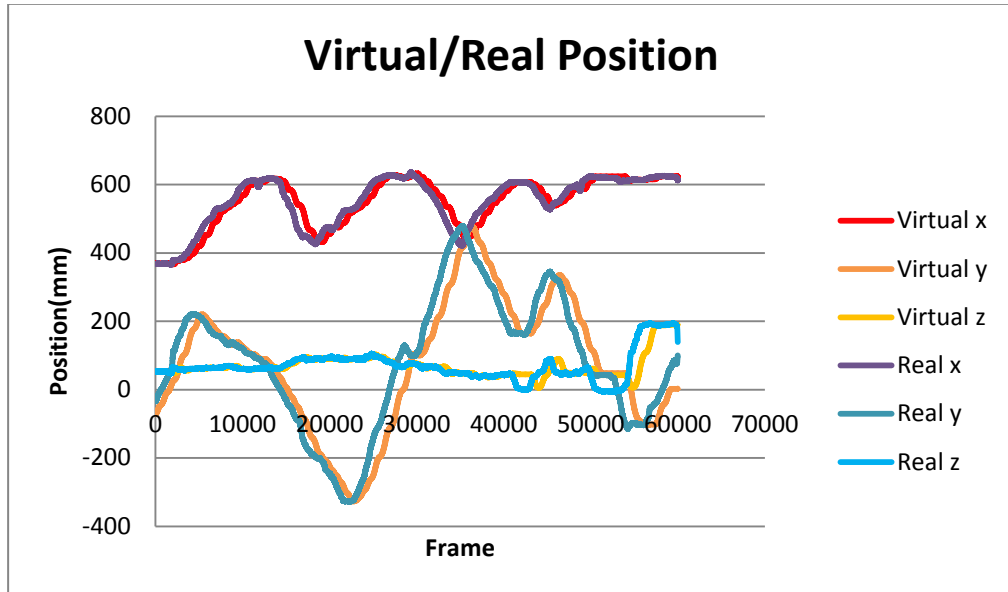


Figure 7-21 Virtual and real position without bilateral haptic control

Figure 7-22 shows the position error between the virtual and real robots during the teleoperation without the bilateral haptic control. It can be seen that real time position errors are relatively large compared with haptic bilateral control. The position errors reach 100mm, 150mm and 150mm respectively on the x, y and z axes, which are significant. Since this is not the haptic bilateral control, such position errors did not result in the bilateral force on the master controller. However, the constraint force is still applied while the end effector of the manipulator reaches the limits of the workspace to ensure safe operation.

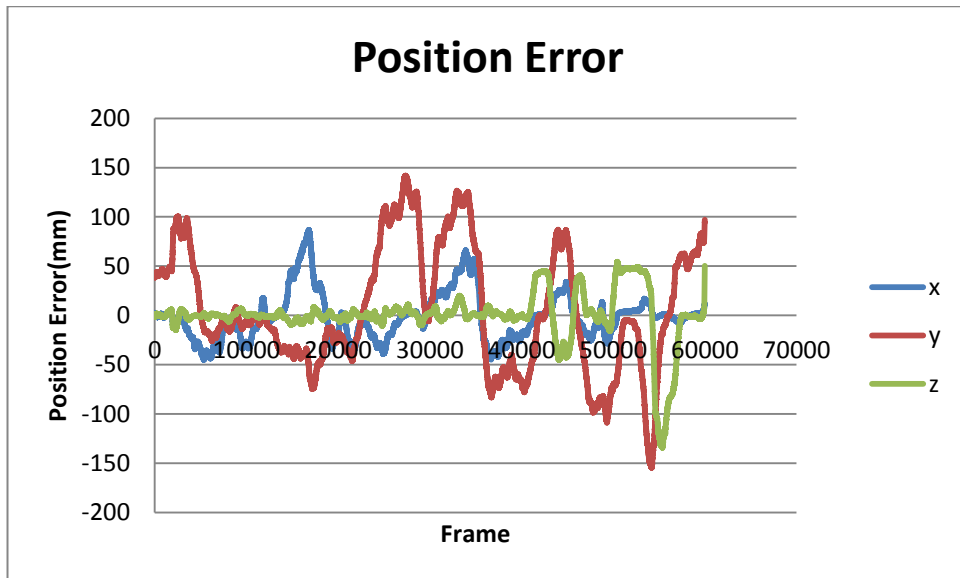


Figure 7-22 Position error without bilateral haptic control

Figure 7-23 shows the constraint force applied on the haptic controller. It can be seen that maximum constraint force reaches 1.75N on the x-axis and 1.5N on y and z axes. Comparing to the position shown in Figure 7-21, it can be seen that when the manipulator reaches its limit of workspace, the force generated increases in the relevant directions. More importantly, the constraint force informs a user of the situation and helps maintain control with allowable workspace.

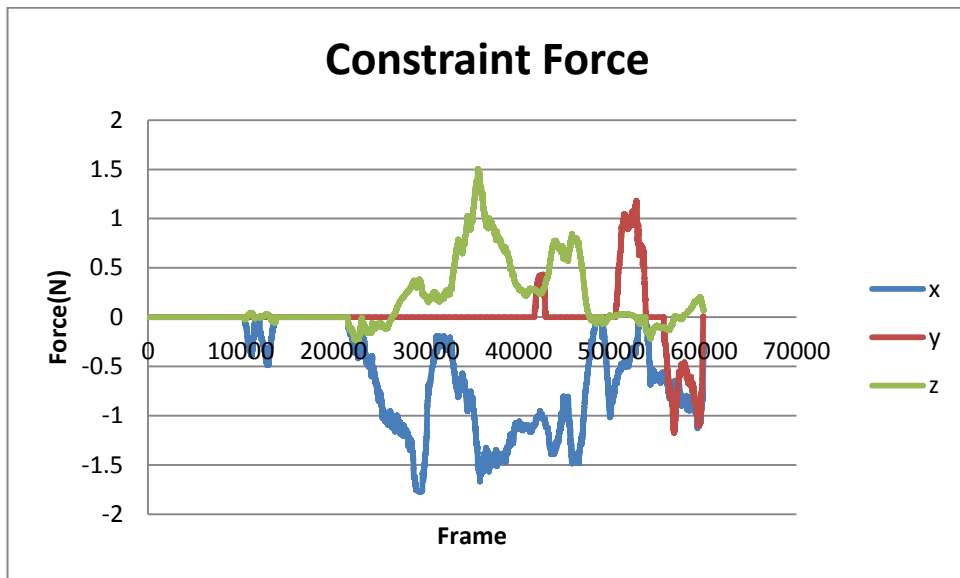


Figure 7-23 Constraint force without bilateral haptic control

Comparing Figure 7-18 and Figure 7-21, it can be seen that with haptic assistance

for bilateral control, the first system demonstrates significantly better performance. The position error and time lag are much smaller which means the usability and the efficiency of the robotic tele-manipulation system are improved with haptic bilateral control methods and the haptic system design model.

7.11 Chapter Summary

In this chapter, the HARMP design method is deployed in the design of the haptic control system of a haptic system required in manufacturing and other similar applications involving real robots. System requirements are identified for geometric and haptic modelling. Control diagrams including the master haptic controller, virtual robot and real robot are designed. Firstly, a haptic teleoperation system is formulated to control a virtual robot. Geometric models of the industrial robot are built and their kinematics are analysed. Haptic virtual fixtures are implemented for telepresence, constraints and guidance in the manipulation of a virtual robot. Communication is established between the haptic device and the real robot. Control logic flows are designed for the specific task, and a stable position/ velocity control of the end effector of the real robot is implemented. While a user manipulates the haptic device to control the virtual robot, the real robot will also follow commands for a desired motion. This teleoperation can be used for manipulation tasks that require the accuracy and strength of the robot but at the same time require full control by an operator. The haptic assistance provided during manipulation helps the user detect obstacles, obey the constraints and follow the desired motion. As a result, there will be an increase the safety, efficiency and usability of the robotic system.

Chapter 8 Discussion of the Results

8.1 Introduction

In this chapter the results and evaluation methods for the HARMP system used in the case studies are assessed and discussed. The specification templates of the HARMP system are enhanced and updated during the progress of the study. The design specification for the haptic system is completed and compared with other literature. Finally, original research questions are revisited and research objectives are reviewed.

Following a referenced work (Gediga, Hamborg and Düntsch, 2002), these questions are asked:

1. "Which is better?"

This question is answered in terms of the comparisons made between the uses of the haptic virtual fixtures. The virtual fixtures are classified as telepresence, constraints and guidance in the HARMP system. In case study of dental surgery simulation, two models of telepresence of cutting force are built and tested. The user experience and graphical results of the actuated force plots are compared to discover the relationship between force models and the quality of force rendering. By conducting cutting procedures with and without virtual constraints, the graphical results of the cutting paths are compared to verify the possible usability of virtual constraints. As for haptic guidance, in the case study of space robotic manipulation, two manipulation tasks were conducted using different guidance methods and approaches. The results are analysed and compared and the best method is identified. The results demonstrated that the haptic virtual fixtures developed for the HARMP system, in this study, proved to outperform other approaches that were suggested in literature.

2. "How good it is?"

This aims to verify the quality and usability of the system.

The quality of the geometric model and force rendering are evaluated based on both the experience and graphical plots of the result. For the evaluation of the force model with haptic virtual fixtures, generated quantitative results are analysed with statistical methods. In the case study of space robotic manipulation with haptic assistance, the usability of dynamic guidance specifically is evaluated. The quantitative results including impact velocity and MSE (mean squared error) of both position and velocity after capture are used. The standard variation from several repetitions is calculated to determine the stability and repeatability. The time and distance to accomplish the given task are collected as indicators of the efficiency. In this way, the usability of the haptic guidance in space manipulation tasks are evaluated and shown to be sufficient for the task undertaken.

3. "What are weaknesses?"

This aims to identify weaknesses in the system and propose suggestions for future development.

Several weaknesses of the HARMP system are identified.

The first one is the realism of the force model. The force model used in the dental surgery simulation is based on calculations taking into account the material properties of jaw bones. The proposed model may exhibit less realism compared to other approaches which build force models based on force data acquired from the real cutting experiment. This is due to the limit of the experimental devices and the accuracy of the environment. Although the model is less real than the experimental model, it can still be used to study the relationship between the force model and the quality of the force rendering.

The second one is the design of test cases. In the evaluation of usability of the haptic guidance in space capture tasks, a task scenario is built for an approaching target. The position and velocity of the target is predefined. However, this

predefined simulation is two dimensional with x and y axes. In the haptic interface and in the real working scenario, the movement of the target is three dimensional. Therefore, both the inverse kinematics solution for minimum reaction torque and haptic guidance methods need to be developed and tested in three dimensional environments.

The third weakness is the quality of force rendering. In this study the quality of force rendering of different force models are compared. However, there is still a need to modify a discontinuous force model to improve its quality. For a case where two or more haptic virtual fixtures are applied such as constraints and guidance, the usability of each type of virtual fixtures might be compromised. The relationship between haptic virtual fixtures utilised at the same time still needs further investigation.

8.2 Evaluation of Research Undertaken

This research aim is to derive a general design model of haptic system and formulate a HARMP system for high accuracy control for robotic manipulation and planning tasks. The research hypothesis was: "A general design model of a haptic system with virtual fixtures for high accuracy manipulation and planning tasks to provide useful and informative instruction for haptic system building". The research objectives were:

1. To develop a general design methodology of a haptic system with virtual fixtures for high accuracy manipulating and planning tasks, clarifying the design flow and necessary system components and specifications.
2. To build a Haptic Assisted Robotic Manipulating and Planning system (HARMP) that provides haptic interface and haptic assistance for robotic manipulation and planning tasks.
3. To classify the types of haptic virtual fixtures, including telepresence, constraints and guidance, and assign them to different tasks according to the task

requirements.

4. To validate the HARMP system design in control tasks for a real robot in a remote environment and integrating this with industrial hardware and sensing systems for environment modelling.

5. Develop an evaluation method to analyse and assess the usability of the haptic assistance provided as well as the performance of the system and sufficiency of the system design model.

The initial design of the Haptic Assisted Robotic Manipulating and Planning system (HARMP) is presented in Chapter 4. The system architecture including a haptic-user interaction system, haptic modelling environment and evaluation module is devised. Subsequently, in the case studies the HARMP system architecture is modified for tasks in surgical applications and robotic manipulation.

The types of haptic virtual fixtures are formulated from the literature review in Chapter 2. These virtual fixtures are classified into three categories according to their nature and use in Chapter 4. These include telepresence, constraints and guidance. In Chapter 5, the telepresence of cutting forces and virtual constraints are utilised for haptic dental surgical simulation. In Chapter 6, haptic guidance is used as the assistance in the space robotics manipulation tasks. In Chapter 7, the telepresence of the haptic force feedback is used to achieve bilateral control of a robot. In this way, haptic virtual fixtures are classified and assigned to different tasks according to the task requirements and research objective 3 is achieved. Also, in Chapter 7 the HARMP system design for robot control tasks is validated, with integration of industrial hardware and sensing system for environment modelling. This meets the requirement of objective 4.

In Chapter 5, Chapter 6 and Chapter 7 the performance of the system and usability of haptic virtual fixtures are evaluated. The results meet objective 5 and answered research question 4.

The design methodology of haptic systems with virtual fixtures for high accuracy manipulation and planning tasks is proposed in Chapter 4. The basic components and specification of a haptic system are concluded from the literature review. In Chapter 5 the system specification formulated for dental surgical simulation. In the case studies, the system specifications are modified and updated for haptic manipulation and planning tasks. The final system specification is shown in Table 8-1.

Table 8-1 Final system specification

Specification category	Category attributes	Design parameter	Developed	Actuated and tested
Geometric model	Manipulation target	CAD or Dicom model to be imported	√	√
		Robotic system model: imported from CAD model	√	√
		Modification: Kinematics are solved while manipulated	√	√
	Manipulator cursor	Indicating the supposed end effector/tool position	√	√
Force model	Telepresence	Touch of geometric model	√	√
		Cutting force	√	√
		Frictional forces	√	√
	Constraints	Natural constraint: Joints limit	√	√
		Artificial constraint: Desired path Singularities Forbidden areas	√	√
	Guidance	Attraction: Towards target Dynamic control Impedance control	√	√
		Repulsion: Avoid obstacles	√	
Force rendering	Force scaling	Scale matching	√	√
		Scale resolution		
	Force actuation	Actuating force model on haptic device	√	√
Stability		√	√	
Environment modelling	Lighting condition	Showing the lighting condition in working environment	√	

	Working scenario	Building objects models in the environment from the data acquired by sensing system	√	√
Integrated knowledge library	Task procedure planner	Surgical planning and training procedure	√	√
		Control of industrial robot.	√	√
		Communication between systems and platforms.	√	√
		Coupling of virtual and realistic robots, monitoring and updating the environment	√	

In this way objective 1 is realised. All research questions are answered and research objectives are realised.

8.3 Chapter Summary

In this chapter the results and evaluation methods of a HARMP system are assessed. The specifications of the HARMP system are developed and updated during the process of the study. A complete design specification for a haptic system is proposed and compared with literature. Finally, the research objectives are reviewed.

Chapter 9 Conclusion, Limitations and Future Work

9.1 Introduction

In this chapter, the work undertaken in this research study is summarised. Firstly a conclusion is made on the development of the research methodology, system specification, validation and evaluation. The contributions to knowledge are identified and summarized. Also, the limitations of the methodology and system devised are concluded. Finally, future work that could potentially improve the system's performance is proposed.

9.2 Conclusion

Based on the literature review, the knowledge gaps for the design of a generic haptic assisted systems are identified. This provides the basis of four research questions for this study. A novel design method is proposed as a generic design approach to support the design of mechatronic systems which require haptic force feedback during operation. Based on the proposed methodology, a new haptic system could be designed generating a solution. These systems are an example of the integration of professional knowledge and experience. These systems have different types of haptic virtual fixtures for manipulating and planning tasks which require extreme delicacy in operations in order to achieve desirable results. This knowledge and experience needs to be systematically captured through experiments, simulation and theoretical analysis of a physical model in a clearly defined environment. As an example, space robots in a microgravity environment is selected and modelled to demonstrate the haptic system design methodology. Force rendering models are generated based on the understanding of a physical system and its dynamic behaviour in relation to its performance and behaviour. A geometric model is also required and created to accurately represent the spatial boundaries of the haptic physical system in the virtual environment. These models are used to develop kinematic and dynamic models of the haptic system in order for the virtual world model to truly represent the actual system.

During the application of the HARMP design methodology, a number of intermediate results are generated. These include the initial system specification template used to fully define the “customer’s voice”. Required knowledge for the haptic system is illustrated in the robotic planning and manipulating tasks in Chapter 6. Haptic system models are proposed and implemented, including geometric model, kinematic model, force rendering model and path planning model, and the physical prototype systems on which these models can be applied. A haptic assisted robotic manipulating and planning (HARMP) system has been built for a given problem, for example, the dental surgical simulation and its planning system.

Based on the HARMP methodology, it is proposed that a system architecture is constructed with components including hardware (Haptic user interaction system) and software (Haptic modelling environment). The system specification template is derived from the geometric modelling, force modelling, force rendering, environment modelling and an integrated knowledge library. The haptic virtual fixtures are classified into three categories: telepresence, virtual constraints and guidance. In three case studies the task requirements are analysed to identify the specification and virtual fixtures required such that the HARMP system can be modified accordingly.

To evaluate the HARMP methodology, three case studies are conducted to assess its suitability and effectiveness. These case studies include a dental surgical simulation and its planning system, a space robotic simulation and path planning system and teleoperation of a manufacturing robotic system. For each case study an experiment is established and an evaluation method is designed. Throughout each case study data is collected and analysed. These results show that the HARMP design methodology addresses the overall design requirements for a new system which requires haptic interaction. It provides a structured approach in dealing with diverse haptic design requirements for different applications as demonstrated in the three case studies. Haptic technology can be utilised in varied situations from

relatively delicate manipulation with small forces, e.g. medical applications, to applications requiring large haptic feedback force, such as space manipulation tasks. The methodology also enables the accommodation of rendering requirements for different applications with different levels of haptic force feedback. The force feedback currently is three DOF on x, y and z axes. The approach also meets the requirements for the update rate of the system for force rendering to ensure sufficient usability and realism of the haptic force feedback for the human operator. The latency phenomenon, which has been experienced in space applications and in complex systems, depends on communications between sub-systems. This requires special design consideration of the real time haptic control systems in order to minimise the latency effect, by introducing methods such as predictive haptic interaction. This is a method could lead to further future work. In addition, human-robot system interaction can be considered in the process of designing a haptic system.

Finally, the performance of the HARMP system and the usability of system functions are evaluated. The quality of the force rendering in the system is shown to be sufficient for the required manipulation and planning tasks. The usability and efficiency of the proposed haptic telepresence, constraints and guidance are shown to offer great advantages with respect to other state of art methods in dental, space and manufacturing applications. The performance of the haptic bilateral control of real robots in manufacturing scenarios was tested and shown to meet design requirements.

9.3 Contributions to Knowledge

This research investigation addresses haptic feedback and human interaction with haptic system technology in dealing with a range of application requirements. The contribution to knowledge reflects this wide range of activities in broad haptic interactions, including a literature review, a new design methodology and validation of the proposed methodology through three case studies and finally the novel haptic systems formulated through these case studies.

The main research contributions of this study are summarised as follows:

1. Through a thorough literature and technology review, comparison tables are produced to demonstrate the functionalities and inadequacies of existing robotic systems in dealing with the required manipulation tasks. There are knowledge gaps in designing haptic systems for dental surgical students to learn the complex operations, and in utilising haptic virtual fixtures in space robotics system. There is also no system in manufacturing where existing robotic systems can be easily adapted for haptic control applications.
2. A novel design methodology entitled HARMP for haptic system design is proposed, fully formulated and evaluated, incorporating virtual fixtures for high accuracy manipulation and planning tasks. Furthermore, the HARMP methodology can be used to verify the design process and design activity flow in order to generate the necessary system specifications and components for the final haptic system for a given task.
3. Applying the HARMP methodology, a generic Haptic Assisted Robotic Manipulating and Planning system (HARMP) is proposed and investigated. The system provides a common haptic interface and haptic assistance for multiple applications such as robotic planning and manipulation tasks. The HARMP system has been proven to be effective in three different applications in dental training, space robotics and manufacturing. It is speculated that the HARMP system could be equally applicable in other applications.
4. A new categorisation for the types of haptic virtual fixtures are proposed, which includes telepresence, constraints and guidance, and their designation to different tasks according to the task requirements.
5. A novel haptic force rendering scheme is also investigated, that utilizes scaling and force thresholds to ensure the stability and usability of the modelled haptic virtual fixtures while actuating them on the haptic device.

6. An enhance to the HARMP design model is proposed to enable bilateral haptic interaction as a haptic coupler which enables a novel use of haptic system.

Through three case studies, the system structure and specification are modified, improved, updated and finalized. The performance of the HARMP system is shown to meet the task requirements in three chosen case studies. The HARMP system is extendable and compatible for a wide range of accurate haptic control tasks, and the design methodology for precision control with haptic systems is demonstrated to work.

The above knowledge and research enables the research aim of this study to be reached. A general design methodology is devised to support the design and building of haptic systems, and a Haptic Assisted Robotic Manipulating and Planning system (HARMP) is built and validated that can help the user gain experience and provide haptic assistance to improve performance in robotic manipulation tasks.

9.4 Limitations

In the evaluation sections of each case study and the final discussion of the results, several weaknesses and limitations of the HARMP and its design methodology have been identified.

The first limitation is the reality of the force modelling and its evaluation. This specifically refers to the build and performance of haptic force modelling for telepresence, comparing to the real force that the user or the end effector will experience in the realist operation and environment.

1. In the first case study, the force model used in the dental surgery simulation is built based on calculations that take into account the material properties of jaw bones. The proposed model may show less reality compared to other approaches which build force models based on force data acquired from real cutting experiments (Lin *et al.*, 2014). This is due to the limit of surgical experimental devices and environment. Although the developed model shows less reality than

the experimental model, it can still be used to study the relationship between force model and quality of the force rendering. Also, as extendable the HARMP system is, the experimental data can always be imported to the HARMP based on the user's requirement. The case study of dental surgical simulation in the HARMP system was supervised and approved by an experienced surgeon and Professor at the Glasgow Dental School. To get subjective evaluation for the usability and reality of the system, a group of dental school students were invited to trial the system. However, due to the strict rules of Glasgow Dental School regarding their students participating in external researches, the application and ethical approval that was submitted was rejected. Therefore, the evaluation was focused on the relationship between the force model and the quality of the force rendering, rather than evaluating the reality of the cutting force compared to the forces encountered in real dental surgeries.

2. In the third case study, the haptic virtual fixtures were used to achieve a pseudo-bilateral control of a remote industrial robot. A haptic force for telepresence was provided back to the user to allow the coupling of position and velocity between the master haptic controller and the real industrial robot. The objects in the real environment were detected by the sensing system and modelled in the HARMP virtual interface so that the telepresence through bilateral control can be achieved. However, the usability of this pseudo-bilateral highly depends on the accuracy of the sensing and modelling of the target objects. If the end effector of the real robot encounters an object which fails to be modelled in the virtual interface, it may not be able to provide force feedback to inform the user of the presence of the object. This is due to the limitation of the functional design of the industrial robot used in this study. The Staubli Ts80 robots, the most commonly used industrial robot, used in this study, are designed to be stiff and robust to have the ability to perform highly repetitive tasks that require reliability in position control. However, on the other hand, they are not able to conduct delicate current control which is required for the force control. Therefore, this limits their usability in the telepresence for real environments without the accurate assistance from the sensing system.

The second limitation is the design of working scenarios and test cases. For a general system design methodology for multiple manipulation tasks, variety of work scenarios and task cases need to be designed to prove the comprehensiveness of the system and design methodology. For example, in the evaluation of the usability of the haptic guidance in space capturing tasks, a task scenario is built with an approaching target. The position and velocity of the target is predefined, as in the Matlab simulation. However, the Matlab simulation is two dimensional with only x and y axes. In the haptic interface and in the real working scenario, the movement of target is most likely three dimensional. Therefore, both the inverse kinematics solution for minimum reaction torque and haptic guidance methods required developing and testing in three dimensional environments. There are a couple of test cases built as the working scenarios for each case study to validate and evaluate parts of the developed system functions.

The third limitation is the quality of force rendering. This study proposed a haptic force rendering scheme that utilizes scaling and force threshold to ensure the stability and usability of the modelled haptic virtual fixtures while actuating them on the haptic device. However,

1. Scaling down a built force model for haptic rendering still compromises the reality of the telepresence. The force models in case study 1 are scaled down with a ratio of 0.2 due to the limitation of the maximum force that can be provided by the haptic device Phantom desktop. Although, the plot and change of the force can be felt by the user proportionally, there is still a notable different between the scaled down force and the original force model. Actually, this issue commonly limits the work of researchers and designers. For many years there was no significant progress made on increasing the force ability of the desktop-level haptic devices. A few commercial haptic devices which can provide forces higher than 20N are very costly and require a large space to operate.

2. It is still difficult to modify a force model that has large and sudden force changes to increase its quality in force rendering. Also, for a given task where two or more

haptic virtual fixtures are applied at the same time, such as both constraints and guidance are provided, the usability of each type of virtual fixtures might be compromised. This compromise occurs in the dental simulations, when the cutting force is added to the device on the y axis, larger errors are caused on the x and y axis even with the same haptic constraints being applied on these two axes. The relationship between haptic virtual fixtures actuated at the same time requires further study.

9.5 Future Work

After identifying the limitations of conducted works, the suggestions for future work is improvement to the usability and performance of the system and design methodology can be made.

Further research work can be conducted to improve the reality of the force modelling and its evaluation. If conditions allow, the force modelling of telepresence can be built with data collected from the real experiment. For example, if a medical institution plans to use the HARMP system to build a surgical training system, a cutting experiment can be conducted to acquire force data. The force sensors can collect the force data while a surgical tool is operating on the sawbone (SAWBONES, 2018). Sawbone is an artificial bone material currently available on the market. It can simulate the physical properties and structures of real bones. After getting the real force data, the force model can be built with higher reality. To evaluate the reality of the force model, participants with the specific professional knowledge and experience should be invited to trial the system. Subjective results including their opinion of comparison with the real operation can be collected to evaluate the reality of the built force model. The force sensors can also be used on the real industrial robot to detect the interaction with the environment. Installing force sensors on one or more dimensions can achieve real bilateral control with telepresence of the remote environment.

Secondly, improvements can be made for force rendering. A novel method needs further investigation for the rendering of the force model that has large and sudden

force changes to increase its quality and stability. In addition, for a given task where two or more haptic virtual fixtures are applied at the same time, such as both constraints and guidance are provided, the relationship between haptic virtual fixtures and their effects on each other need to be further studied. Statistic tools such as ANOVA (Analysis of variance) might be able to provide some solution. Several experimental sets can be designed with the control of applied virtual fixtures as controlled variables. And by applying ANOVA on the results, the effects of each type of virtual fixture and their dependencies can be analysed and studied.

Thirdly, more comprehensive system functions in working scenarios and test cases can be implemented. The HARMP system is designed to be compatible and extendable. Therefore, it would be more usable if it can provide a variety of choices and solutions, such as a function that the user can select a cutting tool from several options in the dental surgery simulation. Also, validating the system with more test cases can help prove the integrity of the design and make the result more convincing. For example, in space capturing tasks, the target can be set approaching from more directions at different velocities to test the usability of the proposed haptic guidance methods.

To summarise, by overcoming the limitations of software/hardware and difficulties in the system design and validation, enriching the system functions, working scenarios and test cases, the usability of the design methodology for haptic assisted systems for accurate control task can be improved and become more beneficial as a haptic system design instruction.

Reference

- Abbott, J.J., Marayong, P. and Okamura, A.M. (2007) 'Haptic virtual fixtures for robot-assisted manipulation'. *Robotics Research*, 28 49-+.
- Adams, R.J. and Hannaford, B. (1999) 'Stable haptic interaction with virtual environments'. *Ieee Transactions on Robotics and Automation*, 15 (3), pp. 465-474.
- Adams, R.J. and Hannaford, B. (2002) 'Control law design for haptic interfaces to virtual reality'. *Ieee Transactions on Control Systems Technology*, 10 (1), pp. 3-13.
- Aggarwal, R. and Darzi, A. (2009) 'From scalpel to simulator: A surgical journey'. *Surgery*, 145 (1), pp. 1-4.
- Agus, M. et al. (2003) 'Real-time haptic and visual simulation of bone dissection'. *Presence-Teleoperators and Virtual Environments*, 12 (1), pp. 110-122.
- Anderson, R.J. and Spong, M.W. (1992) 'ASYMPTOTIC STABILITY FOR FORCE REFLECTING TELEOPERATORS WITH TIME-DELAY'. *International Journal of Robotics Research*, 11 (2), pp. 135-149.
- Arbabafti, M. et al. (2011) 'Physics-Based Haptic Simulation of Bone Machining'. *Ieee Transactions on Haptics*, 4 (1), pp. 39-50.
- Archer, L.B. (1971) *Technological Innovation - a Methodology*. Inforlink Limited for Science Policy Foundation Limited.
- Artigas, J. et al. (2016) Published. 'Teleoperation for On-Orbit Servicing Missions through the ASTRA Geostationary Satellite'. *IEEE Aerospace Conference*, Mar 05-12 2016 Big Sky, MT. NEW YORK: Ieee.
- Artigas, J. and Hirzinger, G. (2016) 'A Brief History of DLR's Space Telerobotics and Force-Feedback Teleoperation'. *Acta Polytechnica Hungarica*, 13 (1), pp. 239-249.
- Artusi, M. et al. (2011) 'Electroactive Elastomeric Actuators for the Implementation of a Deformable Spherical Rover'. *Ieee-Asme Transactions on Mechatronics*, 16 (1), pp. 50-57.
- Bakker, D. et al. (2010) 'Transfer of manual dexterity skills acquired in the Simodont, a dental haptic trainer with a virtual environment, to reality: a pilot study'. *Bio-Algorithms and Med-Systems*, 6 (11), pp. 21-24.
- Balcikonyte, E., Balcuniene, I. and Alekna, V. (2003) 'Bone mineral density and radiographic mandibular body height'. *Stomatologija Baltic Dental and Maxillofacial Journal*, 5 137-140.
- Basdogan, C. et al. (2007) 'VR-based simulators for training in minimally invasive surgery'. *Ieee Computer Graphics and Applications*, 27 (2), pp. 54-66.
- Baumann, R., Clavel, R. and Ieee (1998) Published. 'Haptic interface for virtual reality based minimally invasive surgery simulation'. *IEEE International Conference on Robotics and Automation*, May 16-20 1998 Katholieke Univ Leuven, Leuven, Belgium. NEW YORK: Ieee, pp.381-386.
- Beare, J.I. (1906) *Greek Theories of Elementary Cognition from Alcmaeon to Aristotle*. Clarendon Press.
- Bell, S.W. et al. (2016) 'Improved Accuracy of Component Positioning with Robotic-Assisted Unicompartamental Knee Arthroplasty'. *Journal of Bone and Joint Surgery-American Volume*, 98 (8), pp. 627-635.
- Boschert, S. and Rosen, R. (2016) 'Digital Twin—The Simulation Aspect'. In: Hehenberger, P. and Bradley, D. (eds.) *Mechatronic Futures: Challenges and Solutions for Mechatronic Systems and their Designers*. Cham: Springer International Publishing, pp. 59-74.

- Bowyer, S.A., Davies, B.L. and Baena, F.R.Y. (2014) 'Active Constraints/Virtual Fixtures: A Survey'. *Ieee Transactions on Robotics*, 30 (1), pp. 138-157.
- Bröhl, A.P. (1995) *Das V-Modell: der Standard für die Softwareentwicklung mit Praxisleitfaden*. Oldenbourg.
- Budynas, R. and Nisbett, K. (2010) *Shigley's Mechanical Engineering Design*. McGraw-Hill Education.
- Burdea, G. and Zhuang, J.C. (1991) 'DEXTEROUS TELEROBOTICS WITH FORCE FEEDBACK - AN OVERVIEW .2. CONTROL AND IMPLEMENTATION'. *Robotica*, 9 291-298.
- Bück-Rich, U. (1970) *Ernst Heinrich Weber (1795-1878): und der Anfang einer Physiologie der Hautsinne*. Juris Druck + Verlag.
- Caccavale, F. and Siciliano, B. (2001) 'Kinematic control of redundant free-floating robotic systems'. *Advanced Robotics*, 15 (4), pp. 429-448.
- Cheng, F.T., Chen, T.H. and Sun, Y.Y. (1994) 'RESOLVING MANIPULATOR REDUNDANCY UNDER INEQUALITY CONSTRAINTS'. *Ieee Transactions on Robotics and Automation*, 10 (1), pp. 65-71.
- Chiaradia, M., Cocuzza, S. and Debei, S. (2011) *Increased performance reaction control of multi degrees of freedom space manipulators*.
- Cocuzza, S. et al. (2005) Published. 'Free-flying robot 3D simulator validation by means of air-bearings table 2D tests - Test-bed design'. *56th International Astronautical Congress 2005*, 2005. pp.3472-3485.
- Cocuzza, S., Chiaradia, M. and Debei, S. (2011) Published. 'Base reaction control of hyper-redundant space manipulators'. *62nd International Astronautical Congress 2011*, 2011. pp.5571-5581.
- Cocuzza, S., Cuccato, D. and Debei, S. (2013) Published. 'Least-squares-based reactionless capture of a non-cooperative spacecraft with a space manipulator'. *64th International Astronautical Congress 2013*, 2013.
- Cocuzza, S., Li, M. and Yan, X. (2016) Published. 'Soft and minimum reactions robotic capture of non-cooperative spacecrafts'. *67th International Astronautical Congress 2016*, 2016. pp.3748.
- Cocuzza, S., Pretto, I. and Angrilli, F. (2008a) Published. 'Optimal kinematic control of redundant space robotic systems for orbital maintenance: Simulated microgravity tests'. *59th International Astronautical Congress 2008*, 2008a. IAC 2008, pp.601-614.
- Cocuzza, S., Pretto, I. and Angrilli, F. (2008b) Published. 'Optimal kinematic control of redundant space robotic systems for orbital maintenance: Simulated microgravity tests'. *59th International Astronautical Congress 2008*, 2008b. IAC 2008, pp.601-614.
- Cocuzza, S., Pretto, I. and Debei, S. (2012) 'Least-Squares-Based Reaction Control of Space Manipulators'. *Journal of Guidance Control and Dynamics*, 35 (3), pp. 976-986.
- Cocuzza, S. et al. (2007) 'Control Of Dynamic Attitude Disturbances On Spacecrafts Equipped With Robotic Systems For Orbital Maintenance'. *58th International Astronautical Congress 2007*.
- Coles, T.R., Meglan, D. and John, N.W. (2011) 'The Role of Haptics in Medical Training Simulators: A Survey of the State of the Art'. *Ieee Transactions on Haptics*, 4 (1), pp. 51-66.
- Craig, J.C. (1999) 'Somesthesis'. *Annual Review of Psychology*, 50 305-331.
- Craig, J.J. (2005) *Introduction to Robotics: Mechanics and Control*. Pearson/Prentice Hall.
- CyberGlove (2018a) *CyberForce*. Available at:
<http://www.cyberglovesystems.com/cyberforce/#overview>.

- CyberGlove (2018b) *CyberGrasp*. Available at: <http://www.cyberglovesystems.com/cybergrasp/>.
- Denavit, J. and Hartenberg, R.S. (1955) 'A kinematic notation for lower-pair mechanisms based on matrices'. *Trans. of the ASME. Journal of Applied Mechanics*, 22 215-221.
- Dubowsky, S. and Papadopoulos, E. (1993) 'THE KINEMATICS, DYNAMICS, AND CONTROL OF FREE-FLYING AND FREE-FLOATING SPACE ROBOTIC SYSTEMS'. *Ieee Transactions on Robotics and Automation*, 9 (5), pp. 531-543.
- Dubowsky, S., Torres, M.A. and Ieee (1991) 'PATH PLANNING FOR SPACE MANIPULATORS TO MINIMIZE SPACECRAFT ATTITUDE DISTURBANCES'. *1991 Ieee International Conference on Robotics and Automation, Vols 1-3*, 2522-2528.
- Duffy, A.H.B. and O'Donnell, F.J. (1999) 'A design research approach'. *Critical Enthusiasm*. pp. 33-40.
- Dym, C.L. and Little, P. (2000) *Engineering design: a project-based introduction*. John Wiley.
- Elson, L. et al. (2015) 'Precision of acetabular cup placement in robotic integrated total hip arthroplasty'. *Hip International*, 25 (6), pp. 531-536.
- Fahrner, W.R., Job, R. and Werner, M. (2001) 'Sensors and smart electronics in harsh environment applications'. *Microsystem Technologies-Micro-and Nanosystems-Information Storage and Processing Systems*, 7 (4), pp. 138-144.
- Forsyth, B.A.C. and MacLean, K.E. (2006) 'Predictive haptic guidance: intelligent user assistance for the control of dynamic tasks'. *Ieee Transactions on Visualization and Computer Graphics*, 12 (1), pp. 103-113.
- French, M.J. (1985) *Conceptual design for engineers*. Design Council.
- Gediga, G., Hamborg, K.-C. and Düntsch, I. (2002) *Evaluation of Software Systems*.
- Geomagic (2018a) *OpenHaptics Toolkit*. Available at: <https://www.3dsystems.com/haptics-devices/openhaptics>.
- Geomagic (2018b) *Touch X*. Available at: <https://www.3dsystems.com/haptics-devices/geomagic-touch-x>.
- Gradt, T. et al. (1998) 'Friction and wear at low temperatures'. *International Journal of Hydrogen Energy*, 23 (5), pp. 397-403.
- Grunwald, M. (2008) *Human Haptic Perception: Basics and Applications*. Birkhäuser Basel.
- Hannaford, B. (1989) 'A design framework for teleoperators with kinesthetic feedback'. *IEEE Transactions on Robotics and Automation*, 5 (4), pp. 426-434.
- Haption (2018a) *Virtuose™ 6D Desktop*. Available at: <https://www.haption.com/en/products-en/virtuose-6d-desktop-en.html>.
- Haption (2018b) *Virtuose™ 6D TAO*. Available at: <https://www.haption.com/en/products-en/virtuose-6d-tao-en.html>.
- He, X.J. and Chen, Y.H. (2008) 'Six-degree-of-freedom haptic rendering in virtual teleoperation'. *Ieee Transactions on Instrumentation and Measurement*, 57 (9), pp. 1866-1875.
- Hix, D. and Hartson, H.R. (1993) *Developing user interfaces: ensuring usability through product & process*. J. Wiley.
- Hogan, N. (1985) 'IMPEDANCE CONTROL - AN APPROACH TO MANIPULATION .1. THEORY'. *Journal of Dynamic Systems Measurement and Control-Transactions of the Asme*, 107 (1), pp. 1-7.
- Hsu, E. and Sima, Q. (2010) *Pulse Diagnosis in Early Chinese Medicine: The Telling Touch*. Cambridge University Press.
- Hu, J. et al. (2006) 'Effectiveness of Haptic Feedback in Open Surgery Simulation and Training Systems'. *Medicine Meets Virtual Reality 14*, 119 213-218.
- Hurst, K. (1999) *Engineering Design Principles*. Elsevier Science.

- Iwata, H. (1993) 'Pen-Based Haptic Virtual Environment'. *Ieee Virtual Reality Annual International Symposium*, 287-292.
- Jasinevicius, T.R. *et al.* (2004) 'An evaluation of two dental simulation systems: virtual reality versus contemporary non-computer-assisted'. *Journal of dental education*, 68 (11), pp. 1151-1162.
- Khatib, O. (1986) 'REAL-TIME OBSTACLE AVOIDANCE FOR MANIPULATORS AND MOBILE ROBOTS'. *International Journal of Robotics Research*, 5 (1), pp. 90-98.
- Krueger, T. and Schiele, A. (2015) 'Preparations for the Haptics-2 Space Experiment On-board the International Space Station'. 13th Symposium on Advanced Space Technologies for Robotics and Automation (ASTRA 2015).
- Kuang, A.B. *et al.* (2004) 'Assembling virtual fixtures for guidance in training environments'. *12th International Symposium on Haptic Interfaces for Virtual Environment and Teleoperator Systems, Proceedings*, 367-374.
- Kusumoto, N. *et al.* (2006) 'Application of virtual reality force feedback haptic device for oral implant surgery'. *Clinical Oral Implants Research*, 17 (6), pp. 708-713.
- Ladeveze, N., Fourquet, J.Y. and Puel, B. (2010) 'Interactive path planning for haptic assistance in assembly tasks'. *Computers & Graphics-Uk*, 34 (1), pp. 17-25.
- Lahav, O. and Mioduser, D. (2008) 'Haptic-feedback support for cognitive mapping of unknown spaces by people who are blind'. *International Journal of Human-Computer Studies*, 66 (1), pp. 23-35.
- Lin, Y. *et al.* (2014) 'Simulation and evaluation of a bone sawing procedure for orthognathic surgery based on an experimental force model'. *Journal of biomechanical engineering*, 136 (3), pp. 034501.
- Lindberg, R.E., Longman, R.W. and Zedd, M.F. (1990) 'KINEMATIC AND DYNAMIC PROPERTIES OF AN ELBOW MANIPULATOR MOUNTED ON A SATELLITE'. *Journal of the Astronautical Sciences*, 38 (4), pp. 397-421.
- Luciano, C., Banerjee, P. and DeFanti, T. (2009) 'Haptics-based virtual reality periodontal training simulator'. *Virtual Reality*, 13 (2), pp. 69-85.
- MacLean, K.E. (2008) 'Haptic Interaction Design for Everyday Interfaces'. *Reviews of Human Factors and Ergonomics*, 4 (1), pp. 149-194.
- McNeely, W.A. *et al.* (1999) 'Six degree-of-freedom haptic rendering using voxel sampling'. *Siggraph 99 Conference Proceedings*, 401-408.
- Melville, C., Yan, X.-T. and Gu, L. (2016) 'TiV-Model—An Attempt at Breaching the Industry Adoption Barrier for New Complex System Design Methodologies'. In: Hehenberger, P. and Bradley, D. (eds.) *Mechatronic Futures: Challenges and Solutions for Mechatronic Systems and their Designers*. Cham: Springer International Publishing, pp. 41-57.
- Moog (2018) *Haptic Technology in the Moog Simodont Dental Trainer*. Available at: <http://www.moog.com/markets/medical-dental-simulation/haptic-technology-in-the-moog-simodont-dental-trainer.html>.
- Muller, R.F.G. (1951) 'Principles of ancient Indic medicine'. *Acta historica scientiarum naturalium et medicinalium*, 8 1-163.
- Nahvi, A. *et al.* (1998) Published. 'Haptic manipulation of virtual mechanisms from mechanical CAD designs'. *IEEE International Conference on Robotics and Automation*, May 16-20 1998 Katholieke Univ Leuven, Leuven, Belgium. NEW YORK: Ieee, pp.375-380.
- NASA (2009) *What is Microgravity?* Available at: <https://www.nasa.gov/centers/glenn/shuttlestation/station/microgex.html>.

- Nenchev, D., Umetani, Y. and Yoshida, K. (1992) 'ANALYSIS OF A REDUNDANT FREE-FLYING SPACECRAFT MANIPULATOR SYSTEM'. *Ieee Transactions on Robotics and Automation*, 8 (1), pp. 1-6.
- Newman, W. and Hogan, N. (1987) Published. 'High speed robot control and obstacle avoidance using dynamic potential functions'. *Proceedings. 1987 IEEE International Conference on Robotics and Automation*, Mar 1987 1987. pp.14-24.
- Norman, G.R. and Neufeld, V. (1985) *Assessing clinical competence*. New York : Springer Pub. Co.
- Novint (2007) *Novint Falcon*. Available at:
<https://cs.stanford.edu/people/conti/falcon.html>.
- O'Neil, K.A. (2002) 'Divergence of linear acceleration-based redundancy resolution schemes'. *Ieee Transactions on Robotics and Automation*, 18 (4), pp. 625-631.
- Ogata, K. (1978) *System dynamics*. Prentice-Hall.
- Okutomi, M. and Mori, M. (1986) 'Decision of robot movement by means of a potential field'. *Advanced Robotics*, 1 (2), pp. 131-141.
- Oxford (2018) '*Oxford Dictionaries*'.
- Pahl, G. et al. (2013) *Engineering Design: A Systematic Approach*. Springer London.
- Park, J. et al. (2002) 'Characterization of instability of dynamic control for kinematically redundant manipulators'. *2002 Ieee International Conference on Robotics and Automation, Vols I-IV, Proceedings*, 2400-2405.
- Park, K.C. et al. (1998) Published. 'The enhanced compact QP method for redundant manipulators using practical inequality constraints'. *IEEE International Conference on Robotics and Automation*, May 16-20 1998 Katholieke Univ Leuven, Leuven, Belgium. NEW YORK: Ieee, pp.107-114.
- Payandeh, S. and Stanisic, Z. (2002) 'On application of virtual fixtures as an aid for telemanipulation and training'. *10th Symposium on Haptic Interfaces for Virtual Environment and Teleoperator Systems, Proceedings*, 18-23.
- Pretto, I. et al. (2008) 'A Point-Wise Model of Adhesion Suitable for Real-Time Applications of Bio-Inspired Climbing Robots'. *Journal of Bionic Engineering*, 5 98-105.
- Quinn, F. et al. (2003) 'A pilot study comparing the effectiveness of conventional training and virtual reality simulation in the skills acquisition of junior dental students'. *European journal of dental education : official journal of the Association for Dental Education in Europe*, 7 (1), pp. 13-19.
- Rebelo, J. et al. (2014) 'Bilateral Robot Teleoperation A Wearable Arm Exoskeleton Featuring an Intuitive User Interface'. *Ieee Robotics & Automation Magazine*, 21 (4), pp. 62-69.
- Rehman, F.U. (2006) *A framework for conceptual design decision support*. Thesis [Ph. D] -- University of Strathclyde, 2006.
- Roberts, E.W. (1990) 'Thin solid lubricant films in space'. *Tribology International*, 23 (2), pp. 95-104.
- Roozenburg, N.F.M. and Eekels, J. (1995) *Product design: fundamentals and methods*. Wiley.
- Rosenberg, L.B. (1993) 'VIRTUAL FIXTURES - PERCEPTUAL TOOLS FOR TELEROBOTIC MANIPULATION'. *Ieee Virtual Reality Annual International Symposium*, 76-82.
- SAWBONES (2018) *Sawbones Medical Education Models*. Available at:
<https://www.sawbones.com/models/materials-guide/>.
- Schiele, A. (2015) 'Preliminary Findings from the Haptics-1 Space Experiment'. *13th Symposium on Advanced Space Technologies for Robotics and Automation (ASTRA 2015)*.

- Schiele, A. *et al.* (2016a) 'Haptics-1: Preliminary Results from the First Stiffness JND Identification Experiment in Space'. *Haptics: Perception, Devices, Control, and Applications, Eurohaptics 2016, Pt I*, 9774 13-22.
- Schiele, A., Hirzinger, G. and Ieee (2011) Published. 'A New Generation of Ergonomic Exoskeletons - The High-Performance X-Arm-2 for Space Robotics Telepresence'. *IEEE/RSJ International Conference on Intelligent Robots and Systems*, Sep 25-30 2011 San Francisco, CA. NEW YORK: Ieee.
- Schiele, A. *et al.* (2016b) Published. 'Haptics-2-A system for bilateral control experiments from space to ground via geosynchronous satellites'. *IEEE International Conference on Systems, Man, and Cybernetics (SMC)*, Oct 09-12 2016b Budapest, HUNGARY. NEW YORK: Ieee, pp.892-897.
- Schultheis, M.T. and Rizzo, A.A. (2001) 'The application of virtual reality technology in rehabilitation'. *Rehabilitation Psychology*, 46 (3), pp. 296-311.
- Schwartz-Dabney, C. and Dechow, P. (2002) 'Edentulation alters material properties of cortical bone in the human mandible'. *Journal of Dental Research*, 81 (9), pp. 613-617.
- Schwartz-Dabney, C. and Dechow, P. (2003) 'Variations in cortical material properties throughout the human dentate mandible'. *American Journal of Physical Anthropology*, 120 (3), pp. 252-277.
- Selvaggio, M. *et al.* (2016) 'Vision Based Virtual Fixture Generation for Teleoperated Robotic Manipulation'. *Ieee Iccarm 2016 - 2016 International Conference on Advanced Robotics and Mechatronics (Iccarm)*, 190-195.
- Shafto, M. *et al.* (2012) 'Modeling, simulation, information technology & processing roadmap'. *National Aeronautics and Space Administration*.
- Sherrick, C.E. (1985) 'Touch as a Communicative Sense - Introduction'. *Journal of the Acoustical Society of America*, 77 (1), pp. 218-219.
- Smart, S. (2013) *Haptic Technology and its Application in Dental Deformity Surgical Training and Planning*. University of Strathclyde.
- Sohmura, T. *et al.* (2004) 'Prototype of simulation of orthognathic surgery using a virtual reality haptic device'. *International Journal of Oral and Maxillofacial Surgery*, 33 (8), pp. 740-750.
- Steele, M. and Gillespie, R.B. (2001) 'Shared Control between Human and Machine: Using a Haptic Steering Wheel to Aid in Land Vehicle Guidance'. *Proceedings of the Human Factors and Ergonomics Society Annual Meeting*, 45 (23), pp. 1671-1675.
- Steinberg, A.D. *et al.* (2007) 'Assessment of faculty perception of content validity of PerioSim (c), a haptic-3D virtual reality dental training simulator'. *Journal of Dental Education*, 71 (12), pp. 1574-1582.
- Stryker (2018) *Power tools*. Available at: <https://www.stryker.com/content/stryker/us/en/surgical/products/system-8.html.html>.
- Suh, N.P. (1990) *The Principles of Design*. Oxford University Press.
- Tamre, M. and Sell, R. (2005) *Integration of V-model and SysML for advanced mechatronics system design*.
- Teo, C.L. *et al.* (2002) 'A robotic teacher of Chinese handwriting'. *10th Symposium on Haptic Interfaces for Virtual Environment and Teleoperator Systems, Proceedings*, 335-341.
- Troulis, M.J. *et al.* (2002) 'Development of a three-dimensional treatment planning system based on computed tomographic data'. *International Journal of Oral and Maxillofacial Surgery*, 31 (4), pp. 349-357.

- Tse, B. *et al.* (2010) 'Design and Development of a Haptic Dental Training System - hapTEL'. *Haptics: Generating and Perceiving Tangible Sensations, Pt II, Proceedings*, 6192-101-+.
- Turro, N. *et al.* (2001) Published. 'Haptically augmented teleoperation'. *IEEE International Conference on Robotics and Automation*, May 21-26 2001 Seoul, South Korea. NEW YORK: Ieee, pp.386-392.
- Umetani, Y. and Yoshida, K. (1989) 'Resolved Motion Rate Control of Space Manipulators with Generalized Jacobian Matrix'. *Ieee Transactions on Robotics and Automation*, 5 (3), pp. 303-314.
- Vincent, H. *et al.* (2004) 'Haptic interfaces and devices'. *Sensor Review*, 24 (1), pp. 16-29.
- Wang, D. *et al.* (2005) 'Cutting on triangle mesh: Local model-based haptic display for dental preparation surgery simulation'. *Ieee Transactions on Visualization and Computer Graphics*, 11 (6), pp. 671-683.
- Wang, D.X. *et al.* (2003) 'Development of dental training system with haptic display'. *Roman 2003: 12th Ieee International Workshop on Robot and Human Interactive Communication, Proceedings*, 159-164.
- Wang, D.X. *et al.* (2012a) 'iDental: A Haptic-Based Dental Simulator and Its Preliminary User Evaluation'. *Ieee Transactions on Haptics*, 5 (4), pp. 332-343.
- Wang, Q. *et al.* (2012b) 'Real-Time Mandibular Angle Reduction Surgical Simulation With Haptic Rendering'. *Ieee Transactions on Information Technology in Biomedicine*, 16 (6), pp. 1105-1114.
- Warren, C.W. (1989) 'GLOBAL PATH PLANNING USING ARTIFICIAL POTENTIAL FIELDS'. *Proceedings - 1989 Ieee International Conference on Robotics and Automation, Vol 1-3*, 316-321.
- Wong, C. *et al.* (2018) 'Autonomous robots for harsh environments: a holistic overview of current solutions and ongoing challenges'. *Systems Science & Control Engineering*, 6 (1), pp. 213-219.
- Wu, F.L. *et al.* (2014) 'A virtual training system for maxillofacial surgery using advanced haptic feedback and immersive workbench'. *International Journal of Medical Robotics and Computer Assisted Surgery*, 10 (1), pp. 78-87.
- Xia, Y.S., Feng, G. and Wang, J. (2005) 'A primal-dual neural network for online resolving constrained kinematic redundancy in robot motion control'. *Ieee Transactions on Systems Man and Cybernetics Part B-Cybernetics*, 35 (1), pp. 54-64.
- Xu, J.X. and Wang, W. (2007) Published. 'Two optimization algorithm for solving robotics inverse kinematics with redundancy'. *IEEE International Conference on Control and Automation*, May 30-Jun 01 2007 Guangzhou, PEOPLES R CHINA. NEW YORK: Ieee, pp.1142-1149.
- Yan, X. *et al.* (2012) Published. 'A novel haptic model and environment for maxillofacial surgical operation planning and manipulation'. *Proceedings of the 37th International MATADOR Conference, 2012*. Springer Science & Business Media, pp.109.
- Yan, X.T. and Zante, R. (2010) 'A Mechatronic Design Process and Its Application'. In: Bradley, D. and Russell, D.W. (eds.) *Mechatronics in Action: Case Studies in Mechatronics - Applications and Education*. Godalming: Springer-Verlag London Ltd, pp. 55-70.
- Yoshida, K. (2003) 'Engineering Test Satellite VII flight experiments for space robot dynamics and control: Theories on laboratory test beds ten years ago, now in orbit'. *International Journal of Robotics Research*, 22 (5), pp. 321-335.
- Zhang, Y., Ge, S.S. and Lee, T.H. (2004) 'A unified quadratic-programming-based dynamical system approach to joint torque optimization of physically constrained redundant

- manipulators'. *Ieee Transactions on Systems Man and Cybernetics Part B-Cybernetics*, 34 (5), pp. 2126-2132.
- Zhang, Y.N. and Ma, S.G. (2007) 'Minimum-energy redundancy resolution of robot manipulators unified by quadratic programming and its online solution'. *2007 Ieee International Conference on Mechatronics and Automation, Vols I-V, Conference Proceedings*, 3232-3237.
- Zhang, Y.N. and Wang, J. (2002) 'A dual neural network for convex quadratic programming subject to linear equality and inequality constraints'. *Physics Letters A*, 298 (4), pp. 271-278.
- Zhang, Y.N., Wang, J. and Xia, Y.S. (2003) 'A dual neural network for redundancy resolution of kinematically redundant manipulators subject to joint limits and joint velocity limits'. *Ieee Transactions on Neural Networks*, 14 (3), pp. 658-667.
- Zhu, Y. and Li, X.R. (2007) 'Recursive Least Squares with Linear Constraints'. *Commun. Inf. Syst.*, 7 (3), pp. 287-312.

Appendix

Appendix 1. 1 3D Design of Space Station Model

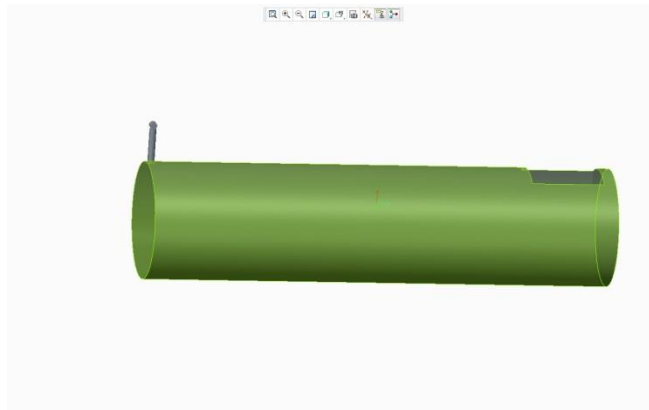
In the case study of haptic space manipulator control, a space station model is designed with nine bodies in total, including the station, 5 parts of robotic beam, and 3 joints, as shown in Appendix 1-3.



Appendix 1 Beams of the robotic arm



Appendix 2 Joints

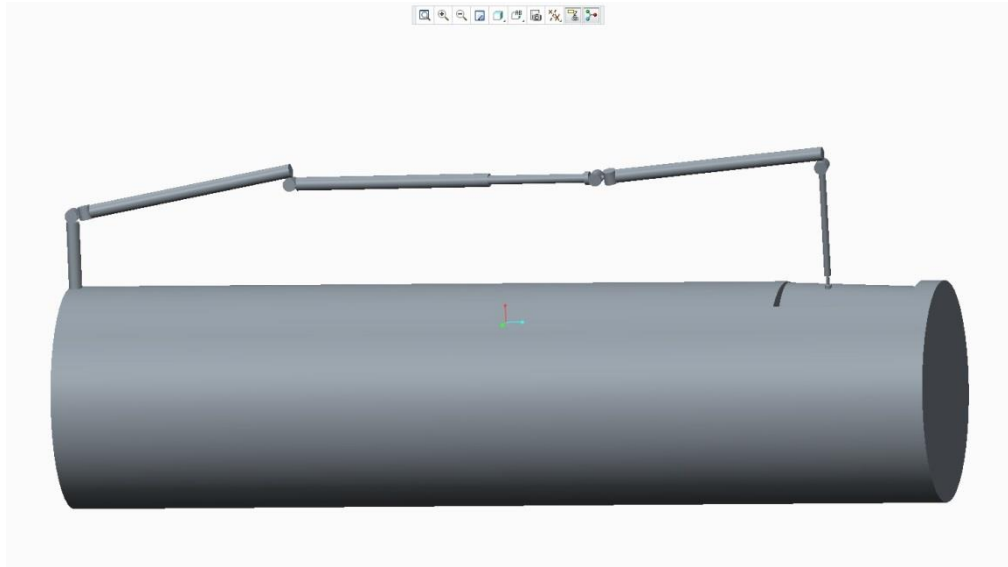


Appendix 3 Space station (Base)

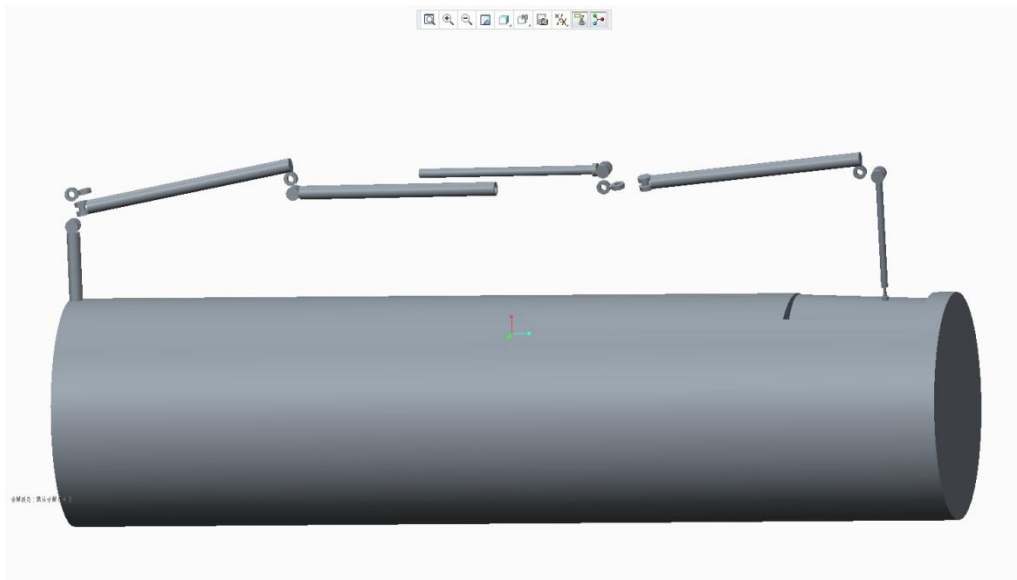
Appendix 1.2 Assembly Drawing Robotic System

To assemble these bodies several constraints are used depending on the mechanism relations between the connected bodies. There are mainly two types of constraints, co-axis and co-planar. Since pins are used as most of joints, the parts are assembled with the co-axis constraint to make them free to rotate. There is a cylinder in the design as an extension of the robotic arm, as shown in Appendix 4-6. It is assembled with constraints by a set of distances which allows a translational movement or freedom. More details of these connections will be presented in the

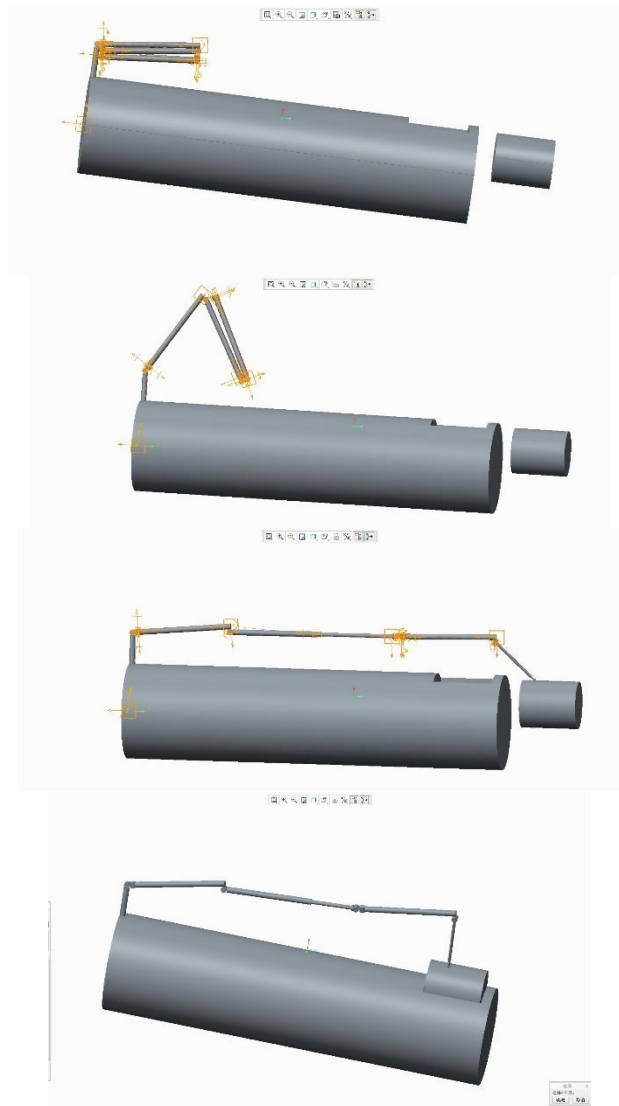
following mechanism part.



Appendix 4 Final view of design



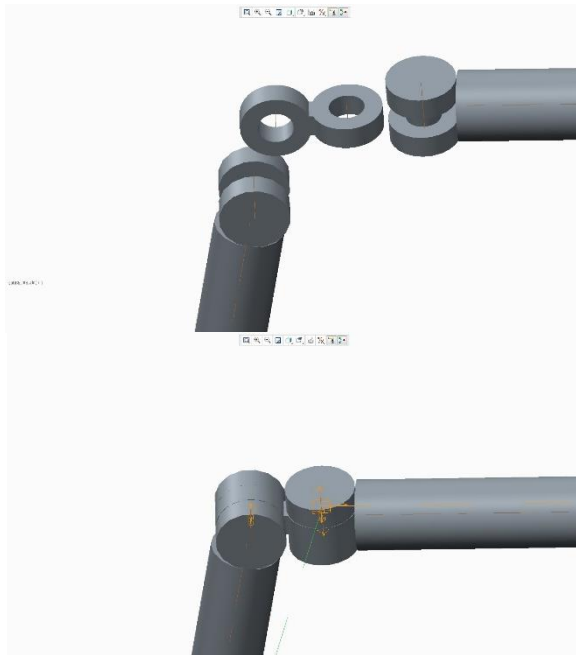
Appendix 5 Assembly view of design.



Appendix 6 Demonstration of the mechanism to transfer the capsule from parked status

Appendix 1.3 Mechanic Analysis

For the seven rotational DOF in the system, seven pin joints are used as shown in Appendix 7. In this way, the body's movement is restricted to rotation around the pin joint axes. Since there are seven DOF in this design in total, this robotic arm is very flexible and nimble and can reach around 23 meters in every direction. In every axis of these rotational joints, servo .DC motors are selected to enable and power the rotation and movement of the real space station mounted robotic arm.



Appendix 7 An example of rotational joints

Longer reachability is required for this space station mounted robotic system in order to reach every part of the space station for either docking operations or possible maintenance operations. To realise these functional requirements, a prismatic joint in the form of a cylinder is chosen to enable translational movement to allow an extension in the length of the overall robotic structure, as shown in Appendix 8. Each of this cylinders can be extended to almost 4 meters and has a translational DOF. Therefore, in this design, there are eight DOF in the system, namely 7 rotational and 1 translational degrees of freedom.



Appendix 8 Cylinder joint